UMONS
Université de Mons

Faculté de Médecine, Pharmacie et Sciences Biomédicales

health
Research Institute for Health Science and technology

Study of Adiponectin pathway in muscle deconditioning and its involvement in exercise rehabilitation.

Thesis submitted for the legal grade of PhD in Biomedical Sciences

by

Sébastien SZCZEPANSKI

Supervisor:	**Prof. Alexandra Tassin** Respiratory Physiology, Pathophysiology and Rehabilitation Unit, University of Mons, UMONS
Co-Supervisor:	**Prof. Anne-Emilie Declèves** Molecular and Metabolic Biochemistry Unit, UMONS
Jury Members:	**Prof. Caroline Cieniewski-Bernard**, Université de Lille **Prof. Michel Abou Samra**, UCLouvain **Prof. Denis Nonclercq**, UMONS **Prof Alexandre Legrand**, UMONS **Dr. Frédérique Coppée**, UMONS **Dr. Vanessa Tagliatti**, UMONS

Academic year 2024-2025

Acknowledgements

Since the majority of the individuals I wish to thank are French speakers, the following acknowledgements will be written in French to ensure they can fully appreciate my gratitude.

En premier lieu, je souhaite remercier le Prof. Alexandra Tassin d'avoir accepté d'être ma promotrice de thèse. Merci de m'avoir fait confiance et d'avoir tout rendu possible en portant ce magnifique projet au FNRS il y a 5 ans. Merci à toi pour tous tes conseils, ta rigueur, ton esprit critique, et ta redoutable intuition scientifique qui m'ont énormément appris au cours de ces dernières années. Merci d'avoir été présente au quotidien, de m'avoir écouté, guidé, parfois réveillé… mais surtout véritablement coaché avec sans cesse la même passion pour ce que tu fais. Merci d'avoir été une promotrice extraordinaire, d'avoir toujours cru en moi et de ne m'avoir jamais laissé tomber.

Je voudrais aussi remercier le Prof. Alexandre Legrand de m'avoir accueilli au sein de son laboratoire pour permettre la réalisation de cette thèse. Merci pour vos remarques et conseils tout au long de ce travail qui m'ont notamment appris à affiner ma manière d'aborder et d'interpréter les données.
Mes remerciements vont ensuite au Prof. Anne-Emilie Declèves pour avoir accepté d'être ma co-promotrice de thèse ainsi que pour m'avoir fourni de nombreux outils qui ont permis la réalisation de ce travail. Merci pour vos conseils pertinents et votre soutien.

Il me parait ensuite essentiel de remercier chacun des membres de mon comité d'accompagnement de thèse ainsi que chacun des membres du jury de thèse qui a évalué ce travail et contribué à son amélioration au travers de ses conseils et critiques.
Par ailleurs, je souhaite adresser mes remerciements au Fond National de Recherche Scientifique (FNRS) qui m'a financé au cours de mes 4 années de thèse ainsi qu'à l'Université de Mons qui m'a octroyé une bourse de 3 mois supplémentaire à la fin de celle-ci. Je tiens aussi à remercier les organismes ayant financé la recherche présentée dans ce travail comme le Fond de recherche médicale en Hainaut (FRMH) et l'association Belge contre les Maladies neuro-Musculaires (ABMM).
Je tiens également à remercier le Prof. Lionel Tafforeau et l'ensemble de son laboratoire de biologie cellulaire pour l'accès à ses équipements, ainsi que le Prof. Sylvain Gabriel et son laboratoire InFlux avec qui nous avons collaboré pour le développement des hydrogels de gélatine utilisés dans le volet *in vitro* de cette étude. De manière plus générale, je tiens à remercier l'UMons pour la mise à disposition de ses infrastructures ainsi que l'ensemble du personnel qui contribue à l'entretien des infrastructures et des locaux au quotidien.

Je souhaite ensuite remercier tout particulièrement l'ensemble des membres du laboratoire de Physiologie, Physiopathologie et Réadaptation respiratoire pour avoir été présents au quotidien tout au long de cette incroyable aventure :

Merci à Vincianne (Vivi), pour l'ensemble du travail que tu réalises au quotidien et qui nous permet de travailler efficacement et sereinement sans jamais manquer de rien. Merci pour tous tes coups de mains, ta technique incroyable, ton esprit logique qui m'a souvent décoincé et ton investissement sans faille dans tous nos projets. Merci aussi pour ton soutien au quotidien, ton écoute et tes conseils.

Merci également à Bernard (BB), pour ton aide dans la conception des cages HLUI et dans le développement du modèle EPS. Merci pour tes précieux conseils et dépannages informatiques, pour tes changements de bonbonnes dont toi seul a le secret, et bien évidement pour tes incroyables gaufres lardons qui ont changé définitivement ma vision des gaufres.

Merci à Aurélie (Panpan) pour ta bonne humeur au quotidien, ta spontanéité, et tes infos toujours croustillantes. Merci pour ton humour qui parviendra toujours à me faire rire, même dans les moments les plus stressants ! Merci aussi de m'avoir fait profiter de ton expérience et de tes conseils pour la suite.

Je tiens aussi à remercier mes collègues (et copains) doctorants Thuy-Hàng, Antoine, Maëlle et Lise avec qui j'ai eu la chance de partager ces années de thèse. Une dream team parfaite, au labo comme en congrès, toujours prête à jouer les 400 coups à notre BB adoré. Merci d'avoir été vous, d'avoir été drôles, présents et d'avoir été une inépuisable source de soutien ! Courage à vous pour la suite, vous me manquez déjà ! Je n'oublie pas de remercier le Dr Mélany Pierard qui m'a appris énormément au début de mon mémoire, j'ai continué d'appliquer tes conseils pendant toute ma thèse.

Je souhaite également remercier Sarah Hennuy et Jérôme Francq pour l'incroyable travail qu'ils réalisent au sein de l'animalerie de l'UMons. Merci pour votre aide au quotidien, vos conseils pratiques et votre vigilance avec les animaux présents à l'animalerie.
Je remercie aussi le Dv Sylviane Michel pour ses précieux conseils qui ont permis de raffiner nos protocoles d'expérimentation et de maximiser le bien-être des animaux dans cette étude.

Je tiens à remercier aussi l'ensemble des membres du laboratoire de biochimie métabolique et moléculaire. Merci pour votre accueil dans mon 2e labo, pour nos échanges sur nos galères communes, votre soutien et pour la bonne humeur de Biomol !

Un grand merci également aux étudiants qui ont participé et se sont impliqués dans ce projet pour leurs mémoires et stages respectifs. Merci à Lisa, à Victor et bien entendu à mes 2 étudiantes préférées, déjà citées plus haut, Maëlle et Lise.

Je souhaite désormais remercier chaleureusement ma famille ; mes parents, ma sœur, mon beau-frère, ma marraine, ma cousine et mes grand-mères pour m'avoir toujours soutenu avant et pendant ma thèse. Merci d'avoir été présents et compréhensifs, d'avoir sans cesse pris des nouvelles, de m'avoir écouté vous parler de choses incompréhensibles mais de m'avoir quand même toujours encouragé. Mention spéciale à Flore, ma filleule, te voir grandir et tes « câlins à Apain » sont ma plus grande source de motivation.

J'aimerai consacrer la fin de ces remerciements à mes amis qui me portent (ou supportent) au quotidien. Merci à Tristan, François et Millan d'être présents depuis tant d'années, de me comprendre, et d'être de véritables piliers sans failles sur lesquels je peux compter. Je tiens évidement à remercier aussi Justine pour ton amour, ta franchise mais surtout pour ton soutien inconditionnel ainsi que Vanille (le V) pour ton soutien et tes nombreuses visites « à t'mamy ». A vous 5, vous avez été véritablement l'équipe de première ligne qui m'a évité de nombreux craquage, et m'a porté jusqu'au bout de cette aventure.
Je remercie également mes amis Nicolas, Olivia et Pierre qui sont toujours présents aussi malgré leurs vies bien remplies.

Il m'est impensable de terminer ces remerciements sans avoir une pensée pour Luka, bien que tu ne sois plus là, merci d'avoir partagé un petit bout de cette thèse avec moi.

Finalement, merci à tous ceux qui ont contribué de près ou de loin à cette thèse et que j'aurai pu omettre malgré ces 2 pages déjà bien remplies …

Table of contents

Abstract

Skeletal muscle deconditioning leads to a **Disuse-mediated Muscle Atrophy (DMA)**. **Exercise training (ET)** as a treatment is often limited by persistent muscle weakness. A better understanding of processes underlying ET benefits is needed to develop pharmacological approaches. Molecules secreted by skeletal muscle (**myokines)** are involved in adaptations to ET. **Adiponectin (ApN),** an adipo/myokine, is an attractive therapeutic target for muscle disorders. Still, the effect of muscle disuse on ApN pathway components was poorly studied, as well as the therapeutic potential of ApN in this context.

In the first part of our study, we optimized a murine model of Hindlimb Unloading and Immobilization (HLUI) mimicking DMA and limiting body weight loss and stress as confounding factors. In this model, **we determine the role of fiber-type composition on the effect of muscle disuse (AIM#1)** and **concomitant variations of ApN pathway components (AIM #2).** Comparing the slow-twitch *Soleus* and the fast-twitch *TA* muscles, we showed that HLUI induces a fibre-type-dependent atrophy whose severity is likely also influenced by muscle positioning during immobilization. HLUI causes a type I/IIa myofiber switch characterized by a different kinetic according to muscle type. Concomitantly, an elevation of ApN plasmatic level, disturbances in oligomeric form proportion, and muscle-type dependent alterations in adiporeceptor expression were observed.

In the second part of the study, we **investigated whether the loss of ApN protective properties during muscle deconditioning may exacerbate DMA (AIM #3)** or **limit the benefits of muscle reconditioning (AIM#4).** In ApN KO *Soleus* mouse muscle submitted to HLUI, we showed an enhanced DMA severity and an increased proportion of type IIa myofibres. The latter is likely involved in the global CSA increase shown in ApN KO animals. HLUI also has a "pre-conditioning-like effect" increasing, during ET, the type IIa/I myofibre transition. Importantly, this effect is impaired in the absence of ApN, suggesting that the loss of ApN protective properties impairs muscle plasticity during rehabilitation.

Finally, since ApN is known for its antioxidant properties, the *Soleus* muscle redox status has been investigated. Globally, ApN KO does not exacerbate HLUI-mediated changes in pro-oxidant/ antioxidant indicators, suggesting that additional ApN properties may be involved in the increased DMA severity observed in these animals. However, in ApN KO mice, correlation analyses showed that myofibers of smaller diameters exhibited higher *Nox* expression, Sod1 protein levels, and lipid peroxidation, indicating that DMA occurring in the absence of ApN is associated with redox equilibrium perturbations. These modifications are, globally, no longer observed after ET, even in ApN KO mice, suggesting that additional ApN-independent processes underline ET effects.

In conclusion, our study highlights that DMA is associated with fiber-type dependent perturbations of ApN pathway. A decrease in ApN protective properties aggravates atrophy and impairs compensatory mechanisms taken place during DMA, particularly fiber-type switches. This has persistent consequences in muscle plasticity during rehabilitation. However, ApN-independent mechanisms are likely involved in HLUI-mediated redox status perturbations and in ET benefits.

Abbreviations table

4EBP1	4E-Binding protein 1
ACC	Acetyl-CoA Carboxylase
ACO	Acetyl-CoA oxidase
AIF	Apoptosis Inducing Factor
Akt	Protein Kinase B (PKB)
AMPK	AMP-activated kinase
ApN	Adiponectin
APPL1	Adaptor Protein Phospho-tyrosine with PH domain and Leucine zipper 1
ATP	Adenosine Triphosphate
BDNF	Brain derived neurotrophic factor
Bnip3	BCL2 interacting protein
CaCMK	Ca^{++} Calmodulin Complex
CaMKK β	Ca^{++}/Calmodulin-dependant protein kinase kinase Beta
CaN	Calcineurin
CPT1	Carnitine Palmitoyl transferase
CSA	Cross-sectional Area
CTRP	C1q TNFα Related Proteins
Cyt C	Cytochrome C
DGK ζ	Diacylglycerol kinase ζ
DMA	Disuse-mediated muscle atrophy
ECC	Excitation-contraction coupling
eEF2	Eukaryotic Elongation Factor 2
eEF2K	Eukaryotic Elongation Factor 2 kinase
eIF2B	Eukaryotic translation initiation Factor 2B
eIF4E	Eukaryotic translation initiation factor 4E
EET	Endurant exercise training
ET	Exercise training
ERK1/2	Extracellular Signal-Related kinase 1/2
FGF6	Fibroblast growth factor 6
FGF21	Fibroblast growth factor 21
FOXO	Forkhead box O family transcription factor
gAPN	Globular ApN form
GLUT4	Glucose Transporter 4
GPI	Glycosylphosphatidylinositol
GSK-β	Glycogen Synthase Kinase 3β
HGF	Hepatocyte Growth Factor
HLU	Hindlimb Unloading
HLUI	Hindlimb Unloading and Immobilization
HMW	High Molecular Weight ApN oligomers
HRP	Horse radish peroxidase
ICU-AW	Intensive Care Unit acquired weakness
IGF-1	Insulin like Growth Factor
IL-6	Interleukin-6

IL-15	Interleukin-15
IRS-1	Insulin Receptor Substrate 1
IR	Insulin Resistance
LAT1	L-type amino acid transporter 1
LC3	Microtubule-associated proteins 1A/1B light Chain 3b
LKB1	Liver kinase B1
LMW	Low Molecular Weight ApN trimers
LPS	Lipopolysaccharides
MFD	Minimum Feret's Diameter
MGF	Mechano-Growth Factor
MMW	Medium Molecular Weight ApN hexamers
MPB	Muscle Protein breakdown
MPS	Muscle Protein synthesis
mTOR	Mammalian Target of Rapamycin
MuRF1	Muscle Ring Finger potein 1
Myf5	Myogenic factor 5
MyHC	Myosin Heavy Chain
MyoD	Myoblast Determination protein
NFAT	Nuclear Factor of Activated T-cells
NF-κB	Nuclear Factor Kappa B
PA	Phosphatidic Acid
Pax 7	Paired box protein 7
PBS	Phosphate Buffer Saline
PDK1	Pyruvate dehydrogenase kinase isoform 1
PI3K	Phosphoinositide 3-Kinase
PGC1α	Peroxisome proliferator activated receptor gamma coactivator 1-alpha
PPAR	Peroxisome proliferator-activated receptor alpha
P38 MAPK	Mitogen-activated protein kinase
P70 S6K1	Ribosomal protein S6 kinase
RET	Resistance exercise training
Rheb	Ras Homolog enriched in brain
ROI	Region of Interest
ROS	Reactive Oxygen Species
S6	Ribosomal Protein S6
S6K1	Ribosomal S6 Kinase 1 protein
SCs	Satellite Cells
SOD1	Superoxide Dismutase 1
SOD2	Superoxide Dismutase 2
Sirt 1	Sirtuin 1
SR	Sarcoplasmic Reticulum
SRF	Serum Response Factor
TA	*Tibialis Anterior*
TSC	Tuberous Sclerosis Complex 1/2
Ub	Ubiquitin
UPP	Ubiquitin-Proteasome System

INTRODUCTION

Introduction

I. Overview of skeletal muscle structure

Skeletal muscle cells, also called myofibres, extend from tendon to tendon and are surrounded by a plasma membrane, the sarcolemma, which is enveloped by a connective tissue named endomysium. Myofibres are grouped in muscle facias (or bundles) delimited by the perimysium. Finally, muscle facias are maintained together by a connective sheath called epimysium (**Figure 1.a**) (1).

Myofibres are plurinucleate cells where nuclei are pushed to the periphery by the myofibrils, which consist of a succession of repetitive units allowing contraction, the sarcomeres. The sarcomere is composed of thin (actin, tropomyosin, and troponin) and thick (myosin) protein filaments (2). Sarcolemma depolarisation following motor neuron stimulation triggers Ca^{++} release by the sarcoplasmic reticulum (SR). In the cytosol, Ca^{++} binding to Troponin C shifts tropomyosin and permit contraction in the presence of Adenosine Triphosphate (ATP) (**Figure 1.a**) (1, 2).

Moreover, muscle progenitors (named Satellite Cells (SCs)) implicated in the muscle regeneration process are located in the niche between the sarcolemma and the basal lamina (**Figure 1.b**) (3, 4). SCs are maintained at a quiescent state via the expression of the transcription factor Pax 7 (Paired box protein 7) (3). Following muscle lesion and cytokines release, SCs are activated, proliferate, migrate, and differentiate to repair damaged myofibres (5, 6).

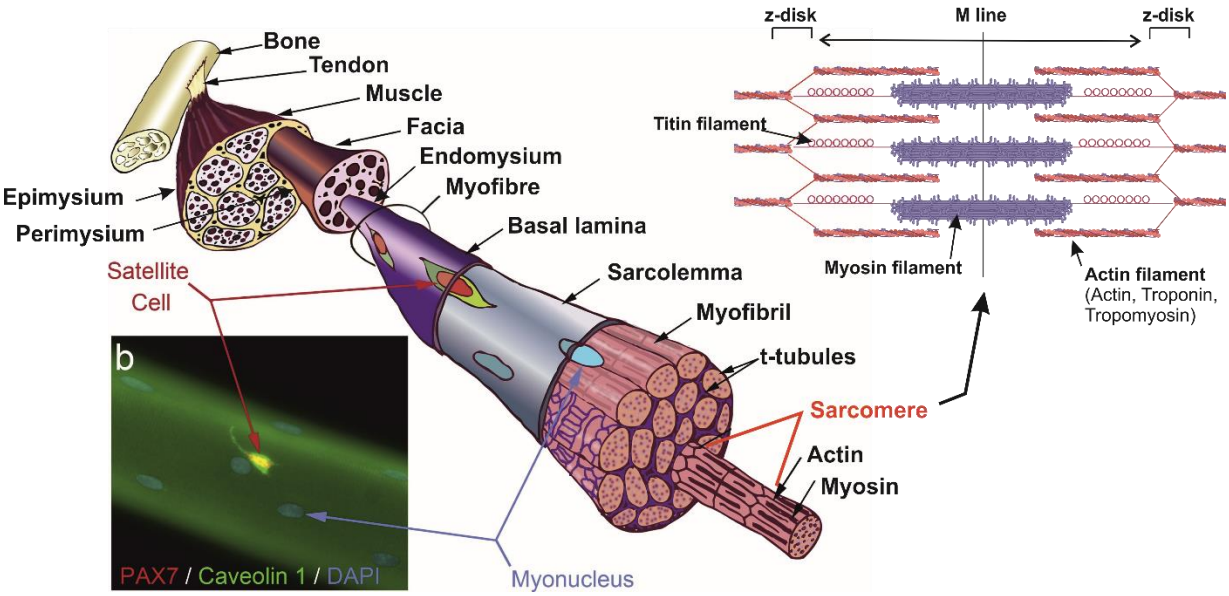

Figure 1. Schematic representation of skeletal muscle structure. *Modified from (6).*

II. Skeletal muscle plasticity

Skeletal muscle tissue has the remarkable ability to adapt to respond to various endogenous and exogenous stimuli, a property termed “muscle plasticity” (7, 8). Indeed, myofiber length, section, structure and metabolism are constantly influenced by external factors such as loading, neural stimulation or systemic hormones (1, 7, 9). Altogether, those factors are known to activate molecular pathways notably involved in myofiber hypo-/hyper- trophy and specialisation into myofiber subtypes (1, 7, 10). Furthermore, when injured, skeletal muscle tissue has the potential to initiate regeneration mechanisms that implicate SC.

1. Skeletal muscle hypo- and hyper-trophy

The principal component of muscle plasticity concerns changes in myofibre section (hypo- or hypertrophy) (11) generally associated with hypoactivity or Exercise Training (ET), respectively. It is commonly accepted that muscle activity, particularly when associated with mechanical constraints and a sufficient nutritional supply, leads to an increased muscle mass characterized by myofibre hypertrophy. However, skeletal muscle hypertrophy is also hormonal- and neuronal-dependant (12, 13).

Myofibre hypo- or hypertrophy are directly related to the balance between Muscle Protein Synthesis (MPS) and Muscle Protein Breakdown (MPB) which is highly regulated by internal and external factors (12). Although MPB in healthy muscle is rather stable and limited to protein turnover, variations in MPS are associated with muscle hypo- (in case of decreased MPS) and hypertrophy (in case of increased MPS) (12, 13).

a) Muscle Protein Synthesis (MPS)

In healthy skeletal muscle, MPS is mainly induced by the IGF-1/PI3K/Akt(PKB)/mTOR (Mammalian Target of Rapamycin) pathway that is activated by amino acids availability (indirectly via the Rag GTPases), Insulin-like Growth factor (IGF1) and insulin (14, 15).

In physiological conditions, the stimulation of the Insulin-like growth factor receptor (IGF1-R) induces PI3K (Phosphatidyl inositide-3 kinase) activation and subsequent phosphorylation and activation of Akt (also known as Protein kinase B, PKB) by PIP3 (Phosphatidylinositol Triphosphate) and PDK1 (pyruvate dehydrogenase kinase isoform 1) (12, 16). Fully activated Akt suppresses the inhibition of TSC (Tuberous Sclerosis Complex 1/2) on Rheb (Ras Homolog enriched in Brain), which activates in its turn the mTORC1 complex (12, 16). Once activated, the serine-threonine kinase activity of mTORC1 phosphorylates (**Figure 2.**):

- the ribosomal S6 Kinase 1 protein (S6K1), which then phosphorylate a component of the 40S ribosomal subunit, the ribosomal protein S6 (S6) (16–18). This S6 phosphorylation is partly implicated in the S6K1-mediated increase in ribosomal biogenesis (19, 20).
- the eukaryotic translation initiation factor 4E-Binding protein 1 (4EBP1), then preventing its sequestering-binding to the eukaryotic translation initiation factor 4E (eIF4E) protein, which is required to form the eIF4E cap-binding complex during mRNA translation initiation (16, 21, 22).

- the eukaryotic Elongation Factor 2 kinase (eEF2K) resulting in a hypo-phosphorylated eukaryotic elongation Factor 2 (eEF2) which is then able to bind ribosomes for the elongation process (23).

Altogether, those mTORC1-mediated phosphorylation cascades increase ribosomal biogenesis and mRNA translation (initiation and elongation) rates (12, 16). Additionally, the repression of the eukaryotic translation initiation Factor 2B (eIF2B) by the Glycogen Synthase Kinase 3β (GSK-3β) is also suppressed by an Akt-mediated GSK-3β phosphorylation, thus favouring the mRNA translation initiation step independently from mTORC1 (12, 24, 25).
Furthermore, mechanical loading *per se* was also identified as a mTOR complex activator. Indeed, the mTORC1 complex is also regulated by mechanical stimuli which are mediated through the production of endogenous phosphatidic acid (PA) by the Diacylglycerol kinase ζ (DGK ζ) , (12, 13, 26–28).

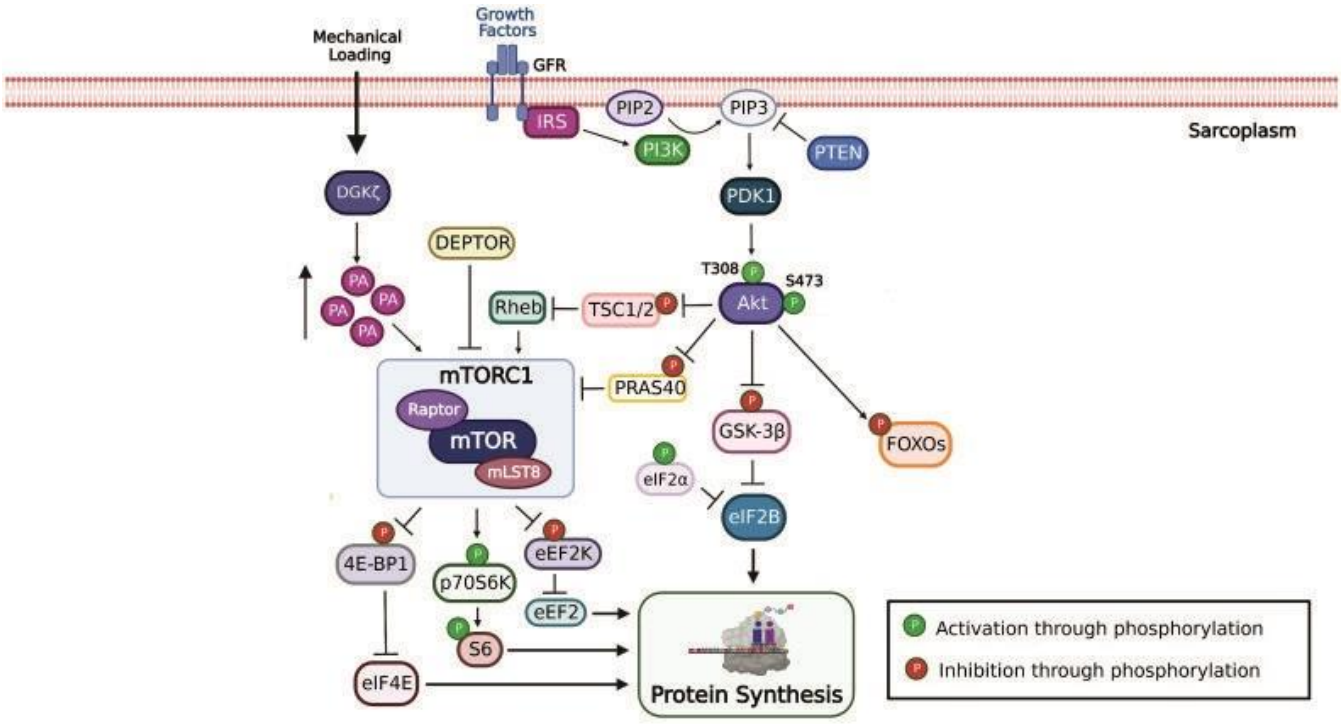

Figure 2. Schematic of the molecular pathways implicated in muscle protein synthesis activation by insulin, insulin-like growth factor (IGF1) and mechanical loading. *Modified from (24).*
Akt/PKB : Protein Kinase B ; 4E-BP1 : eukaryotic initiation factor 4E-Binding Protein ; eEF2K : eukaryotic Elongation Factor 2 Kinase; eEF2 : eukaryotic Elongation Factor 2 ; eIF2α : eukaryotic translation Initiation Factor 2α ; eIF2B : eukaryotic translation Initiation Factor 2B ; eIF4E : eukaryotic translation Initiation Factor 4E ; DEPTOR : DEP containing mTOR-interacting protein ; DGKζ : Diacylglycerol kinase ζ ; FOXOs : Forkhead box O ; GFR : Growth Factor Receptor ; GSK3β : Glycogen Synthase Kinase-3 beta ; IRS : Insulin Receptor Substrate ; mLST8 : mammalian lethal with sec-13 protein 8 ; mTORC1 : mammalian Target Of Rapamycin Complex 1 ; PDK1 : Pyruvate Dehydrogenase Kinase 1 ; PIP2 : PhosphatidylInositol bisphosphate ; PIP3 : PhosphatidylInositol trisphosphate ; PI3K : PhosphoInositide 3-Kinase ; PA : Phosphatidic acid ; PRAS40 : Prolin-rich Akt substrate of 40 kDa ; PTEN : Phosphatase and tensin homolog ; p70S6K : ribosomal protein S6 Kinase ; Raptor : Regulatory-associated protein of TOR ; Rheb : Ras Homolog Enriched in Brain ; S6 : ribosomal protein S6 ; TSC1/2 : Tuberous Sclerosis Complex 1/2

b) Muscle Protein Breakdown (MPB)

In physiological conditions, MPB is essentially implicated in muscle protein turnover which consists in removing and recycling damaged and old proteins (29–31). Several factors (hypercortisolaemia, prolonged fasting, inflammatory cytokines, etc.) induce muscle atrophy by over-activating MPB (32). In skeletal muscle, MPB results from the coordinated and consecutive actions of (**1**) caspase-3, (**2**) calpains, (**3**) autophagy, and (**4**) ubiquitin-proteasome proteolytic (UPP) systems (**Figure 3.**) (29, 33, 34):

- (**1**) Caspase-3 is a cysteine-aspartic protease whose activity is initiated by initiative caspases such as Caspase-9 and Caspase-12 (35). Indeed, pro-caspase 3 is activated in Caspase-3 which is in its turn implicated in myofilaments disassembling that occurs upstream of sarcomere protein degradation. Indeed, caspase-3 is an "executioner" caspase that can disrupt actomyosin complexes to make it available for the ubiquitin-proteasome system (31, 34, 36–38). Importantly, evidence has suggested that oxidized muscle contractile proteins are more susceptible to be targeted by caspase-3 and calpains (**Figure 3.**) (30, 31, 37, 39).
- (**2**) Calpains are calcium-dependant cysteine proteases that take part in the cytoskeleton (e.g. α-II-spectrin) and sarcomere (e.g. titin and nebulin) protein fragmentation before further degradation by other proteolytic systems (36, 40, 41). In humans, calpain 1 (CAPN1) and calpain 2 (CAPN2) (previously referred as μ-calpain and m-calpain respectively) are the calpains that contribute the most to MPB. Calpain activation is mediated by cytosolic increases in Ca^{++} that may result from disturbances in its sarcoplasmic handling in cases of excessive oxidative stress (**Figure 3.**) (33, 34, 39).
- (**3**) Autophagy is crucial for organelles (e.g. mitochondria) as well as for cytosolic protein turnover. Briefly, damaged and old organelles as well as cytosolic proteins and protein aggregates, are encircled in vesicles named autophagosome. The autophagosome content is then degraded by proteases (e.g. cathepsins) brought by the fusion with a lysosome (30, 34, 42). Similarly to calpains and caspases proteolytic systems, an excess in Reactive Oxygen Species (ROS) is known to enhance autophagy rates and expression of gene such as those encoding Bnip3 (BCL2 interacting protein) and LC3 (microtubule-associated proteins 1A/1B light chain 3b) (**Figure 3.**) (34, 39, 43).
- (**4**) Ubiquitin-proteasome system is widely implicated in MPB as the UPP takes place as a final step of proteolysis, occurring after myofilaments release by caspase-3 or calpains (36). The UPP system starts with 3 enzymatic complexes (E1 Ubiquitin (Ub) activating enzyme, E2 Ub-conjugating enzyme, and E3 ligase enzymes) which mediate subsequently the Ubiquitin (Ub) activation, conjugation and specific binding to the targeted protein (44). Poly-ubiquitylated proteins are then completely degraded in the 26S proteasome complex (composed of the major 20S catalytic subunit associated with 2 regulatory 19S subunits at each end) (**Figure 3.**) (45). Several E3 ligases have been described, notably the muscle specific atrogin-1/MAFbx (Atrogin-1) and the muscle ring finger protein 1 (MuRF1). Genes encoding those proteins (*FBXO32* and *TRIM63,* respectively) have been named *Atrogenes* due to their overexpression in different

models of skeletal muscle atrophy (15, 46). Atrogin-1 and MURF1 were then found to mediate light myosin isoforms and myosin heavy chain ubiquitination respectively (30, 47). Importantly, *FBXO32* and *TRIM63* expression are under the regulation of the Forkhead box O (FOXO) family of transcription factors (FoxO1, FoxO3 and FoxO4) that are sequestered in the cytosol through a Akt-mediated phosphorylation (48–50). This highlight Akt as a major regulator of the MPS/MPB balance as its activation in physiological condition support MPS while inhibiting MPB (24, 51).

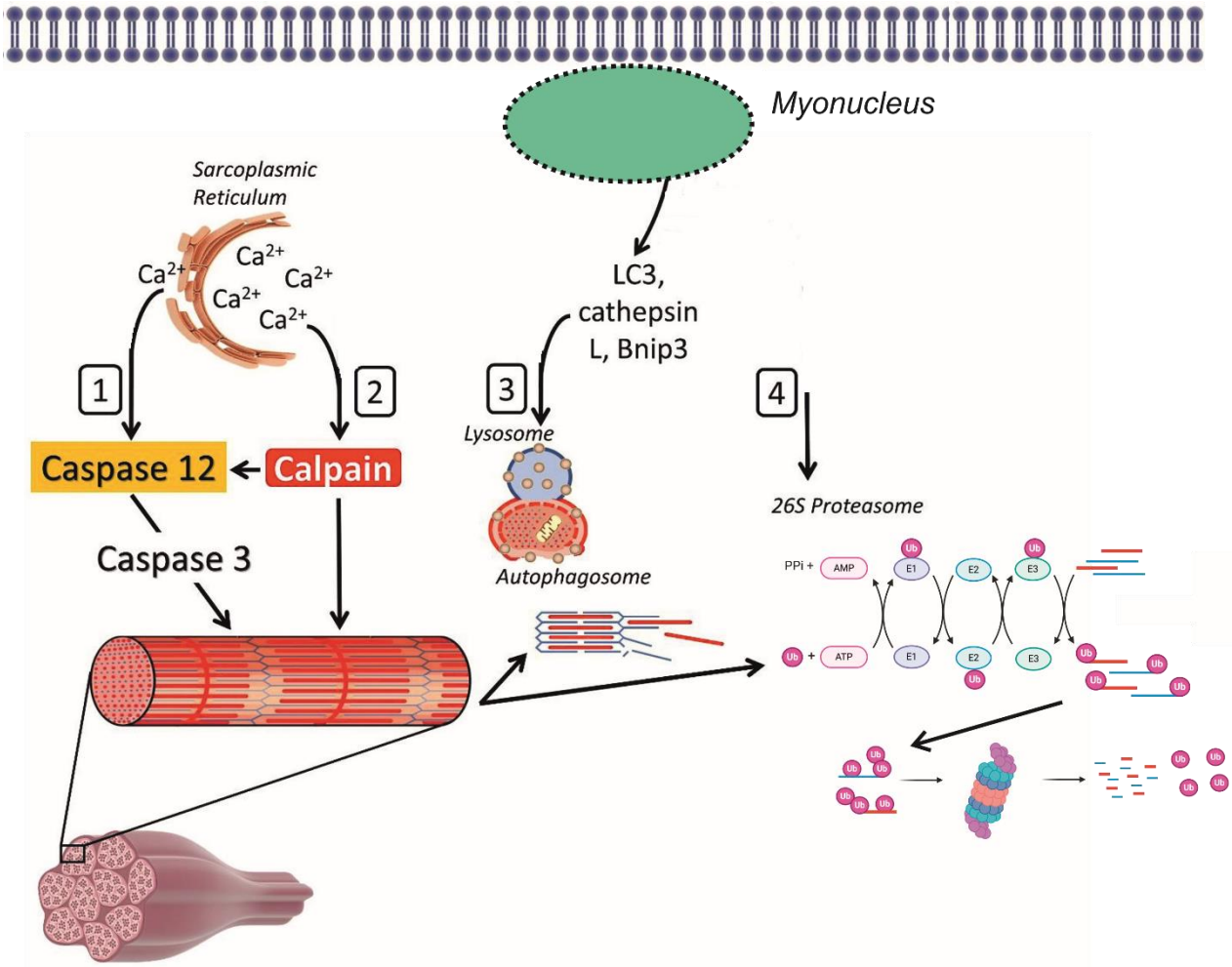

Figure 3. Schematic representation of proteolytic systems. *Modified from (30).*
In conditions associated with proteolysis, sarcoplasmic Ca^{++} leaks activate (1) the initiative Caspase-12 (which activates the executioner Caspase-3 implicated in sarcomere disassembling) and (2) Ca^{++}-dependant calpains. (3) The autophagy system is involved in the degradation of cytosolic protein, protein aggregates and organelles through the fusion of autophagosomes with lysosomes. (4) The Ubiquitin proteasome system takes place in the final step of proteolysis and catalyse the degradation of sarcomeric proteins released by processes (1) and (2).
AMP: Adenosine Monophosphate ; ATP: Adenosine Triphosphate ; Bnip3: BLC2 interacting protein ; E1: E1 Ubiquitin-activating enzyme ; E2: E2 Ubiquitin-conjugating enzyme ; E3: E3 ubiquitin-ligase enzyme ;LC3 : microtubule-associated proteins 1A/1B light chain 3b ; PPi: Diphosphate ; Ub: Ubiquitin.

2. Myofibres types in skeletal muscle

Human skeletal muscles present three main myofiber types (type I, IIa and IIx myofibers) whereas rodent skeletal muscles contain an additional type IIb myofiber type (7, 10). Each myofiber type can be identified by the Myosin Heavy Chain (MyHC) isoform expressed as follows:

- Type I myofibres express the MYH7 myosin heavy chain isoform and are generally described as "slow" myofibres. Type I myofibres are highly fatigue-resistant as they contain important amounts of myoglobin and mitochondria that support aerobic-oxidative metabolism. Those myofibres are generally described as smaller than other myofibre types, presumably allowing for efficient oxygen diffusion from the capillaries (6, 7, 52).
- Type IIa myofibres express the MYH2 myosin heavy chain isoform and are intermediate fibres able to use both glycolytic and oxidative metabolism in humans (while rodent type IIa myofibres use preferentially aerobic-oxidative metabolism). Those fibres are considered as fast myofibres that contain less mitochondria and are then less fatigue-resistant than type I myofibres (6, 7, 52, 53).
- Type IIx (MYH1 isoform) and type IIb (MYH4 isoform) myofibres are the largest myofibres. Those myofibres are characterized by lower amounts of mitochondria, high glycogen contents, and an "ultra" fast speed of contraction supported by anaerobic glycolytic metabolism (6, 7, 52, 53).

Skeletal muscle composition in myofibres types is directly related to the muscle position and physiological action. Indeed, postural muscles in hindlimbs that face gravitational constraints such as the *Soleus* muscle, are characterized by higher contents in endurant type I myofibres whereas forelimbs muscles used in motor tasks but not implicated in posture are mainly composed of fast IIa and IIx myofibres (7, 8, 54). However, adult skeletal muscles present heterogeneity in fibre types that allow for the selective recruitment of the most adapted myofibres populations to initiate a specific movement (11).

Additionally to those "pure" myofibres types, skeletal muscle is also composed of hybrid myofibres that express two or more MyHC isoforms (I/IIa, IIa/IIx, IIa/IIb and IIx/IIb) (10, 53, 55). Since their discovery in 1999 by Pette *et al.,* hybrid myofibres were suggested to fill the functional gap between pure fibres by providing a continuum of contractile functions and metabolism (8, 53, 56). Moreover, evidence demonstrated the hybrid myofiber role as intermediate during myofibre type transitions that occur in muscle development, ET, aging, or disuse (53). Depending on muscle activity, myofibres are able to optimize their metabolism and sarcomere macromolecules to specialize into sub-myofibre types characterized by distinct metabolic and contractile properties (13, 55).

The proportion of each myofiber subtype within the skeletal muscle is highly dynamic and depends on internal and external signals. Indeed, motor neuron activity, mechanical loading, and systemic hormones influence muscle myofibres composition by inducing myofiber-type

switches (11). Those transitions follow the rule of the "nearest neighbor" (I ↔ I/IIa ↔ IIa ↔ IIa/IIx ↔ IIx ↔ IIx/IIb ↔ IIb) and are generally described as "slow-to-fast switch" or "fast-to-slow switch (11, 53, 55).

Slow-to-fast switches are associated with muscle disuse (induced by microgravity in humans and hindlimb unloading in rodent models) and with hyperthyroidism (11, 24, 32, 57, 58). A slow-to-fast switch can also be induced experimentally with phasic high-frequency electrical stimulations that mimic the stimulation pattern of fast motor neurons (11).

On the other hand, fast-to-slow myofibers switch are rather attributed to muscle activity, overloading, ET, and hypothyroidism (11, 57, 59). Such a switch can be reproduced with chronic low-frequency electrical stimulation. The developmental (MyHC-emb) to adult fast MyHC switch is followed by fast MyHC-related gene expression until the beginning of slow nerve stimulation, thus suggesting that fast phenotypes are first expressed by default (7, 11).

At the molecular level, changes in myofiber type are mainly regulated by the increase in cytosolic Ca^{++} induced by the excitation-contraction coupling (ECC). Indeed, the Ca^{++} Calmodulin complex (CaCMK) activates the Calcineurin (CaN), a phosphatase that dephosphorylates the Nuclear Factor of Activated T-cells (NFAT) transcription factor which then translocates into the myonuclei to activate the transcription of type I related genes (**Figure 4.**) (54, 60–63). Furthermore, muscle contraction enhances Extracellular Signal-Related kinase 1/2 (ERK1/2) phosphorylation which in turn increases the phosphorylation of the transcriptional coactivator p300 and promotes myosin heavy chain I/β gene expression through NFAT (11, 64, 65).

In addition, other cellular pathways promote and support slow myofibre phenotypes such as the AMP-activated kinase (AMPK) pathway. Indeed, phosphorylated (and thus activated) AMPK is known to phosphorylate the Peroxisome proliferator-activated receptor gamma coactivator 1-alpha (PGC1α). Phosphorylated PGC1α is also deacetylated by Sirtuin 1 (Sirt1), allowing for its translocation into the myonucleus where it co-activates transcription factors that mediate oxidative metabolism and mitochondrial biogenesis (**Figure 4.**) (59, 66–70).

Interestingly, myofibre switches implicate an inversed regulation of fast- and slow-related genes. *Schiaffino* and *Reggiani* reported 3 possibles mechanisms involved in this simultaneous up- and down-regulation of fast or slow expression programs: 1) transcription factors that are both activators and repressors; 2) bidirectional promoters responsible for sense and antisense transcripts; and 3) the presence of miRNAs genes hosted in MyHC genes (7, 71).

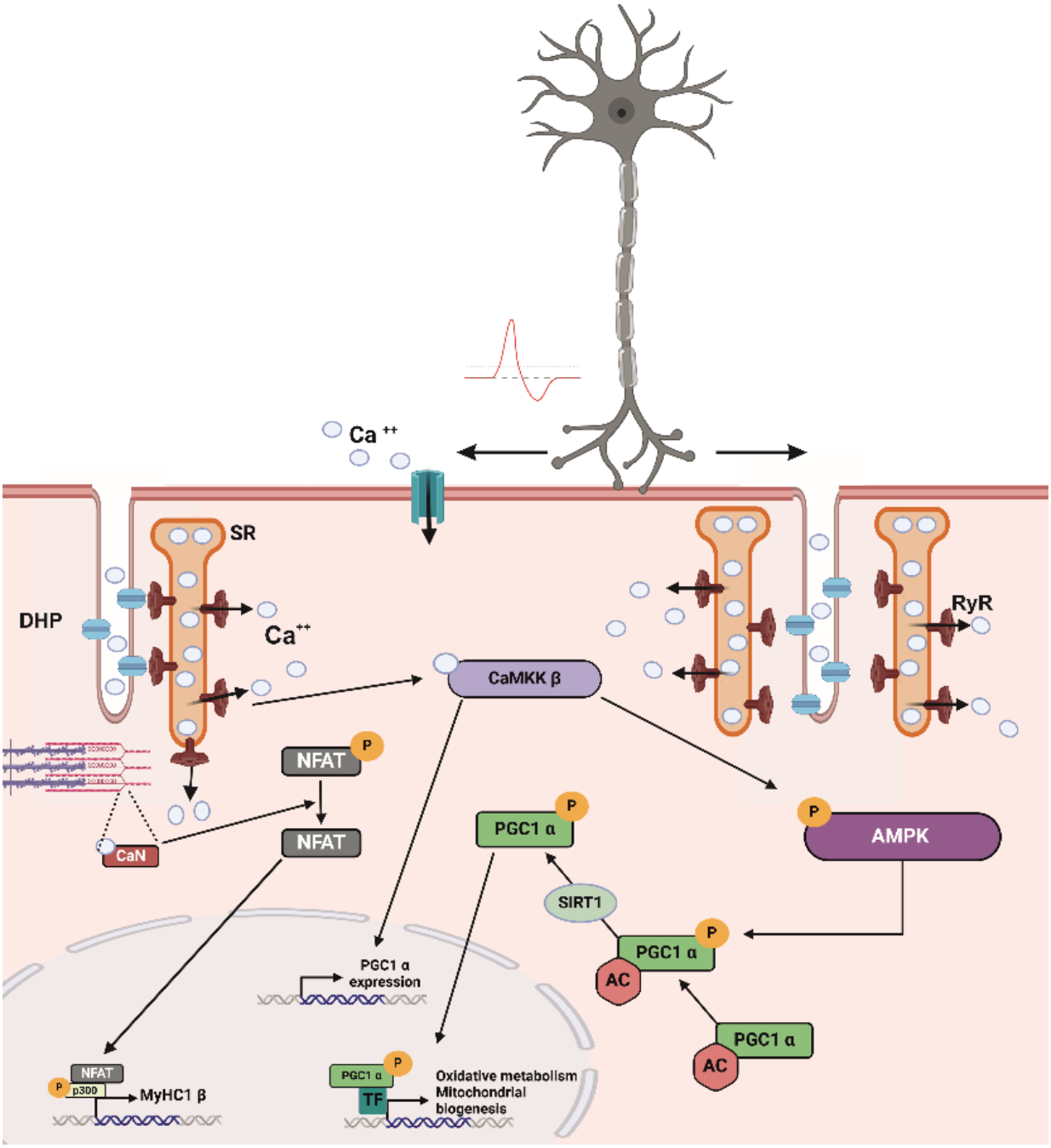

Figure 4. Schematic representation of the molecular pathways implicated in myofibres switch.

AC : Acetylation ; AMPK : AMP Activated Protein Kinase ; CaMKKß : Calmodulin/Ca^{++}-dependant protein kinase kinase beta ; CaN : Calcineurin ; DHP : Dihydropyridine channel ; NFAT : Nuclear Factor of Activated T-cells ; P : Phosphorylation ; p300 : Transcriptional coactivator p300 ; PGC1α : Peroxisome proliferator-activated receptor gamma coactivator 1-alpha ; RyR : Ryanodine receptors channel ; SIRT1 : Sirtuin 1 ; SR : Sarcoplasmic Reticulum ; TF : Transcription Factor. Original representation. Created with BioRender.

3. Muscle regeneration

Skeletal muscle has the ability to regenerate following injury (4, 6). Muscle regeneration (also named adult myogenesis) is a complex and highly coordinated process requiring an orchestrated expression of myogenic factors in muscle progenitor SCs (72–74). In healthy muscle, SCs are maintained in a quiescent state and express PAX7. In response to muscle damage, SCs activate and proliferate to provide myoblasts. Most of them down-regulate PAX7 and induce MyoD and then Myogenin to fuse, differentiate and repair damaged myofibers (**Figure 5.**). Others maintain Pax7 and return to a quiescent-like state allowing for self-renewal. Similar mechanisms are involved in exercise training-mediated muscle plasticity. Indeed, some training modalities are associated with myofibre micro-lesions that trigger SC activation and fusion with myofibres (72, 75). Such mechanism is notably driven by the production of Mechano Growth Factor (MGF), a spliced IGF-1 isoform reported to activate SCs following myofibre micro-lesion while supporting MPS with its IGF receptor binding-domain (76). This mechanism may contribute to muscle hypertrophy mediated by resistance exercise training, notably by providing additional myonuclei to support myofibre hypertrophy (75).

Importantly, growth factors such as IGF-1, fibroblast growth factor 6 (FGF6) or hepatocyte growth factor (HGF) are also implicated in muscle regeneration by promoting myoblasts mitosis, SCs number regulation and inflammation regulation respectively (77).

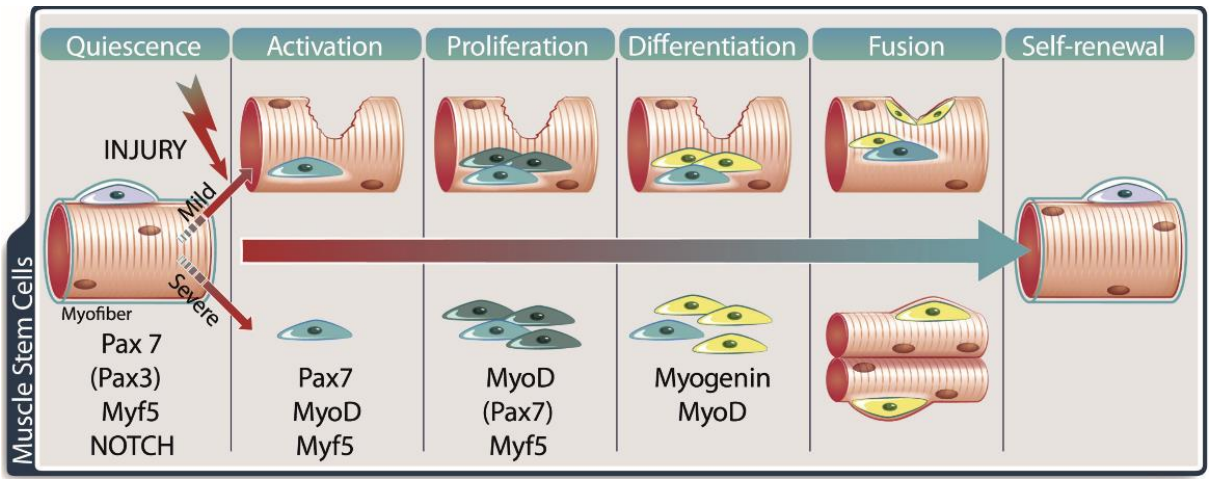

Figure 5. Schematic of muscle regeneration processes in mild and severe damages. *From (5).*
Following muscle lesion, quiescent satellites cells (SC, blue) are activated and differentiate into myoblasts (yellow). This highly coordinated process is mediated by the orchestrated expression of myogenic factors. PAX7 and the *Myf5* transcript are present at the quiescent state. Proliferating myoblast expressing MyoD and Myf5 differentiate and then express specific makers such as Myogenin, to finally fuse with damaged myofibres. In more severe lesions where myofibers are destroyed, myoblasts fuse together in new myofibres.

4. Muscle length adaptations.

Skeletal muscle responds to passive stretching or eccentric training by longitudinal muscle growth involving sarcomerogenesis (78) and extracellular matrix remodelling (79). Indeed, the strain notably exerted on titin, integrin, and SC induces mechanosensor transduction signals regulating sarcomerogenesis (80), a process consisting of the serial addition of new sarcomeres. This process allows gradual muscle re-positioning to maintain muscle optimal length (78). Although not completely understood, the sarcomerogenesis process is reported to involve PI3K-Akt-mTOR, IGF-1, Follistatin-Myostatin signalling pathways as well as the Serum response factor (SRF) that activates the transcription of genes encoding actin and actin-binding proteins (80).

III. Skeletal muscle deconditioning

1. Generalities

Skeletal muscle deconditioning concerns a wide range of patients as it can result directly from a pathological condition itself (cancer, metabolic disorders, trauma, muscular dystrophies, …) or be secondary to consecutive factors associated with hypo- or in-activity (bed rest, immobilization, wheelchair dependence, microgravity, …) (32, 81). Moreover, numerous pathological conditions are characterized by a systemic inflammation (such as traumas, cancers, sepsis or infections) that exacerbate skeletal muscle deconditioning (81, 82).

At the tissue level, prolonged skeletal muscle hypoactivity (characterized by a reduction in neural stimulation and/or a decrease in mechanical constraints) leads to the development of a disuse-mediated muscle atrophy (DMA) (83). DMA is associated with a reduction in muscle mass and a decreased myofibres Cross-Sectional Area (CSA)) (24, 83). These structural alterations are concomitant with metabolic disturbances accompanied by a switch from type I oxidative myofibers through type II glycolytic myofibres (54, 57). Altogether, disuse-mediated structural and metabolic alterations contribute to functional impairments such as a reduction in muscle strength and endurance that impair patient mobility and physical autonomy (81, 84, 85).

At the molecular level, skeletal muscle disuse is commonly reported as caused by an imbalance between MPS and MPB (32, 83). Furthermore, DMA is associated with mitochondrial dysfunctions that impair oxidative metabolism and result in excessive ROS production (30, 34). Those alterations will be discussed in detail in the following section entitled “Molecular mechanisms underlying DMA”.

Muscle mobilization, electrostimulation, and exercise training (ET) remain the only effective treatments against DMA. However, an important group of patients present ET intolerance and muscle weakness can persist even after muscle reconditioning program. When this persistent weakness occurs following prolonged bed rest, this syndrome is often referred to as “ICU-AW” (Intensive-Care Unit acquired weakness) (86–88) (**Figure 6.**).

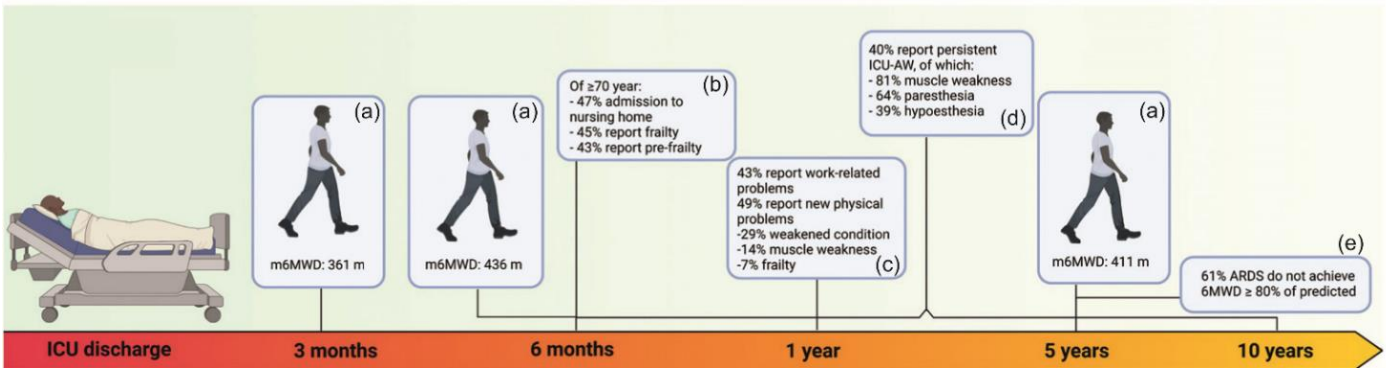

Figure 6. Summary of the prevalence and incidence of muscle functional disorders following Intensive-Care Unit (ICU) discharge.

(a) Systematic review and meta-analysis including 16 studies and 1755 ICU survivors *(89)*. (b) Prospective cohort study including 266 ICU survivors ≥ 70 years old *(90)*. (c) Prospective multicenter cohort study including 2345 adult ICU-survivors *(91)*. (d) Prospective multicentre cohort study including 301 COVID-19 ICU survivors of which 246 analyzed at one year *(92)*. (e) Single centre cohort study including 109 ARDS ICU survivors of which 94 were analysed at 5 years *(93)*.

m6MWD : Mean Six Minute Walking Distance. *Modified from* (86).

2. Molecular mechanisms underlying DMA

It is commonly reported that disuse-mediated muscle atrophy results from an imbalance between MPS and MPB. However, discrepancies remain regarding the contribution of these processes in the development of muscle alterations. As well, excessive oxidative stress and mitochondrial dysfunctions constitute other hallmarks of DMA that must be considered to fully describe pathophysiological mechanisms underlying DMA.

a) Muscle protein synthesis is reduced in disuse

It is now clear that disuse-mediated muscle atrophy in humans and rodents mainly results from MPS reduction (83, 94–98). Indeed, several groups reported that muscle disuse induced with immobilization decreases MPS up to 50%-60% in fasting and fed conditions in adult humans. Such a decrease in MPS was attributed to an anabolic resistance that impairs the hyper aminoacidemia-mediated MPS activation (81, 95, 97, 99).

At the molecular level, this disuse-mediated anabolic resistance remains poorly understood although it was suggested that disuse may alter the protein level of amino acid transporters (e.g. L-type amino acid transporter 1 (LAT1)) (100).

It is important to note that the disuse-mediated decline in MPS is consistent with the loss of muscle mass described in human studies, reinforcing the hypothesis that disuse-mediated anabolic resistance and the resulting MPS reduction are sufficient to explain the extent of muscle mass loss in DMA (81, 98, 99).

b) *Muscle protein breakdown pathways*

Conversely, the contribution of MPB in the development of disuse-mediated muscle alterations in healthy human muscles is still discussed. However, systemic inflammation and oxidative stress in ICU patient were clearly identified as MPB activators that trigger the upregulation of the UPP system and dysregulations in the autophagy proteolytic system (86, 101, 102).

More recently, it was shown that muscle inactivity *per se* also increases oxidative stress levels during prolonged bedrest and muscle immobilization in healthy patients (30, 34). Moreover, although muscle disuse was not thought to induce inflammation, RNA-sequencing analyses in unloaded rats *Soleus* indicate an up-regulation of genes related to inflammation and oxidative stress responses (103).

c) *Oxidative stress and mitochondrial dysfunction*

In the last decades, mitochondrial dysfunctions in DMA has been largely investigated as those alterations appear to be highly implicated in disuse-mediated MPS/ MPB imbalance (30, 34). Actually, the mitochondrial decline in respiratory capacities, volume, as well as morphological changes (e.g. increased fission) were identified as major contributors to the increased ROS production associated with prolonged muscle inactivity (30). Consequently, the unbalanced excess in ROS triggers the expression of proteins implicated in MPB and causes intracellular damages (e.g. myofibrillar protein oxidation) (48, 104). In addition, mitochondrial alterations are associated with the release of mitochondrial molecules in the cytosol such as the Apoptosis Inducing Factor (AIF) and the Cytochrome C (CytC) that notably activate caspase-3 (30).

Although the mechanisms linking muscle disuse and mitochondrial alterations remain incompletely understood, it seems that the disuse-mediated hyperglycaemia may contribute to mitochondrial alterations (86). Indeed, hyperglycaemia blunt the insulin-mediated glucose uptake and it was shown that 7 days of complete bedrest in young individuals reduce the whole body insulin sensitivity (105–107).

Nevertheless, it remains unclear whether Insulin Resistance (IR) is the cause or the consequence of mitochondrial alterations observed in disused muscles as other factors such as muscle hypoperfusion and the resulting impairment in O_2 delivery may also contribute to mitochondrial dysfunctions (86).

Importantly, prolonged skeletal muscle inactivity was also reported to decrease PGC1α expression and activity, thus preventing its beneficial effects on mitochondrial biogenesis and fatty acids oxidation. Interestingly, PGC1α overexpression was shown to protect mitochondria during rodent limb immobilization or HLU and to mitigate muscle alterations in those models of disuse (108, 109).

d) Satellite cell depletion and dysfunction

An increasing number of studies report the persistence of muscle weaknesses in patients following Intensive-Care Unit (ICU) discharge (86, 87, 110). Notably, a reduction in muscle SC content was described to contribute to the persistence of muscle functional alterations (87). It was suggested that the systemic inflammation associated with ICU may be responsible for SC activation and depletion that further impairs muscle regeneration processes (86, 87). Muscle disuse *per se* could also contribute to SC depletion but it currently remains a lack of evidence supporting this hypothesis as well as underlying mechanisms.

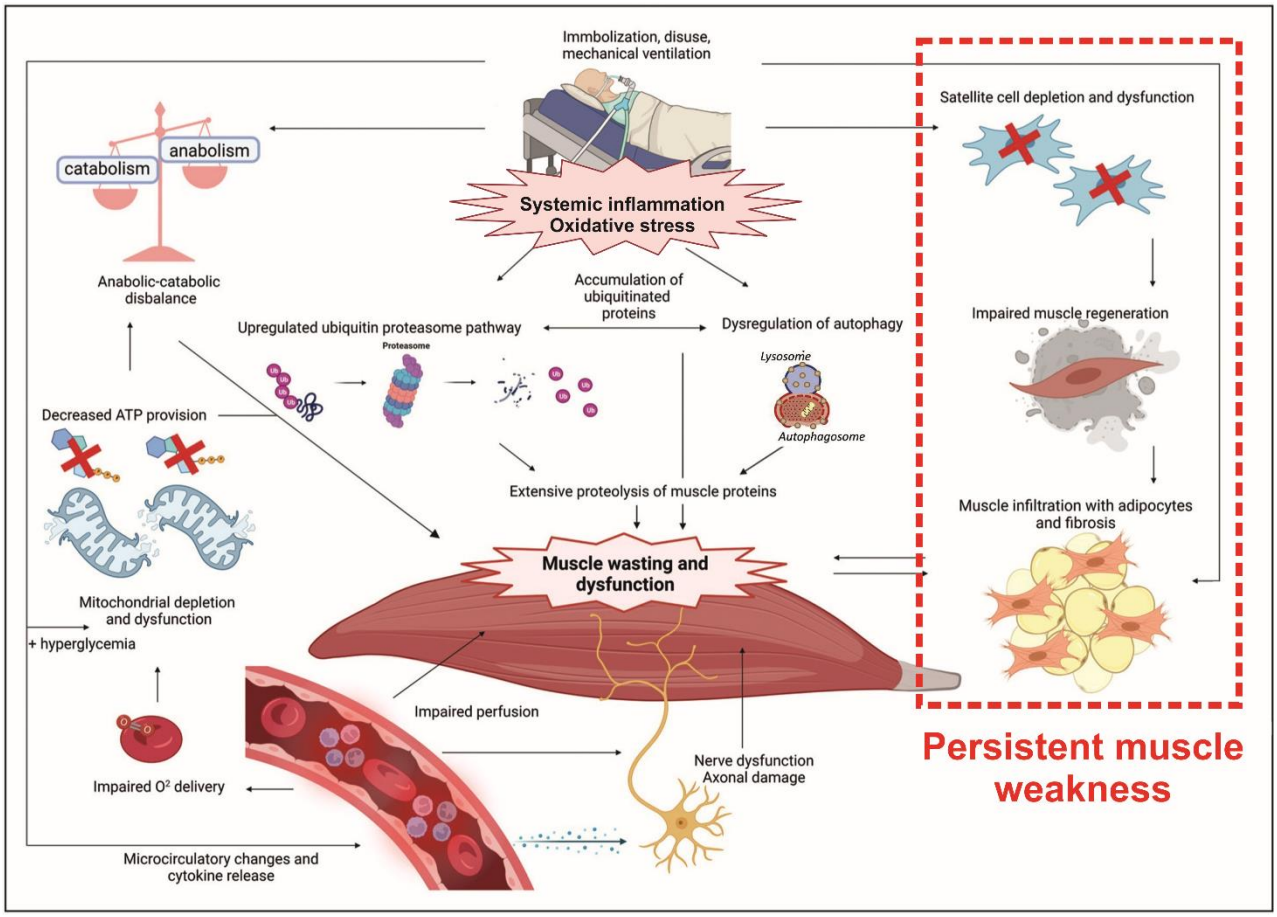

Figure 7. Schematic representation of pathophysiological mechanisms involved in the DMA associated with Intensive-Care Unit-Acquired weakness (ICU-AW). *Modified from (86).*

Prolonged immobilization and resulting muscle disuse are associated with excessive oxidative stress and inflammation which alter anabolic/catabolic balance. Indeed, the disuse-mediated hyperglycaemia and the impairments in muscle O_2 delivery contribute to mitochondrial alterations that lead to the development of anabolic resistance, an over-activation of the Ubiquitin Proteasome pathway, and dysregulated autophagic processes. Furthermore, systemic inflammation (exacerbated by mechanical ventilation) induces microcirculatory changes and cytokine release that can damage motoneurons. Importantly, in some cases, those conditions can result in persistent muscle weakness attributed to satellite cell depletion or dysfunction that impairs muscle regeneration and can provoke muscle infiltration with adipocytes or fibrosis.

3. Disuse muscle atrophy preclinical models

Numerous DMA models were developed in rodents and humans to investigate potential mechanisms or therapeutic approaches against skeletal muscle deconditioning. Indeed, using reductionist models, avoiding confounding factors found in patients, is a powerful tool to specifically study consequences of skeletal muscle disuse by isolating this component of numerous pathologies.

The most common models are denervation, immobilization, and hindlimbs suspension (Hindlimb unloading (HLU)) in rodents whereas human studies generally use bedrest, foot-step reduction, and limb immobilization models to induce DMA (81).

Regarding preclinical models in rodents, denervation is described to induce the more severe atrophy by preventing any neuronal stimulation while the atrophy generated by joint immobilization (cast, Velcro, …) is highly dependent on muscle position during the immobilization (stretched versus shortened) (32, 83, 85).

Hindlimb unloading models stand out from the precited models as it (i) allows prevention of mechanical loading in hindlimb muscles without modifying neuronal stimulation (83) and (ii) can be easily reversed to investigate muscle reconditioning by a reloading period. Unloading-mediated disuse was shown to affect preferentially anti-gravitational muscles in HLU mice and rat model (83), highlighting the importance of muscle physiological function (and thus myofibre type composition) in the development of DMA.

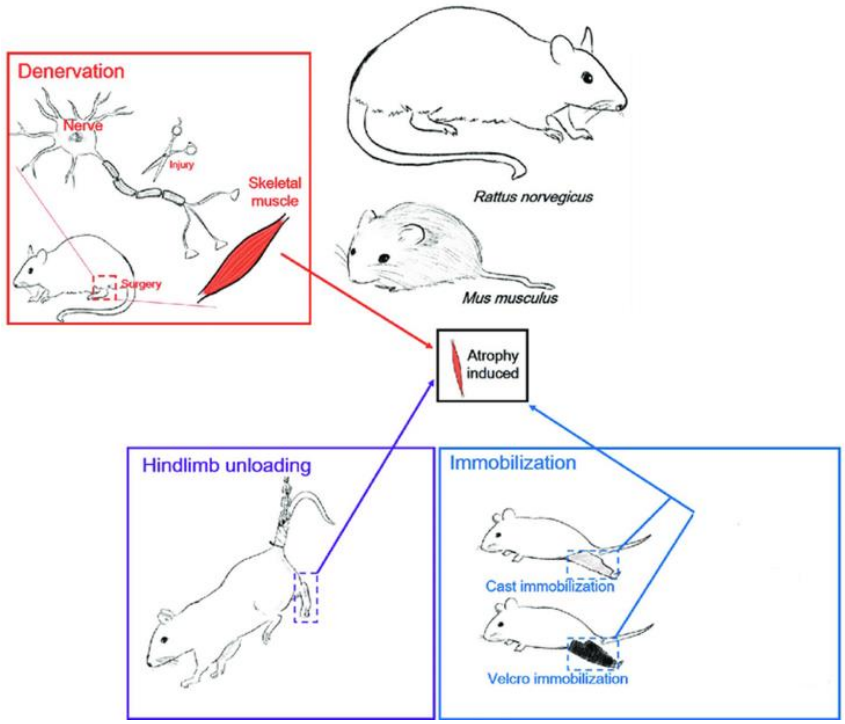

Figure 8. Schematic of the most common DMA models in rodents. *Modified from (111).*

IV. Exercise training and skeletal muscle reconditioning

a) Endurant aerobic and resistant anaerobic exercise training

Exercise training (ET), notably known for its several beneficial effects on whole-body metabolism, is recommended as a therapeutic approach to prevent and/or counteract several non-communicable diseases (112, 113) , and particularly, muscle deconditioning (114). Among the huge variety of ET modalities, we generally decipher:

- Endurant aerobic ET (EET) (e.g. Jogging, cycling or swimming) in which energy required for muscle contraction is provided by glucose metabolism in aerobic conditions. At the systemic level, EET has insulin-sensitizing effects and is associated with cardiovascular and respiratory system adaptations (e.g. increase in VO_2 max). In skeletal muscle, EET results in higher capillary density and type I myofiber proportions that enhance muscle endurance to ET (115–117).

  At the molecular level, EET promotes (i) glucose uptake, oxidative metabolism and mitochondrial biogenesis in muscle, mainly via the activation of the AMPK/PGC1α/SIRT1 axis (118), (ii) muscle mass maintenance through the sensibilisation of myofibers to different anabolic signals (e.g. IGF-1, Insulin, mechano-transduction signals, etc.) (116, 119) and (iii) muscle regeneration potential following lesions by increasing notably SC content as well as macrophages transition from M1 (proinflammatory) to M2 (anti-inflammatory) phenotype (116, 120–122).
- Resistance anaerobic ET (RET) (e.g. weightlifting with short periods of high intensity) in which energy is provided in anaerobic condition. RET leads to increased muscle strength and is more likely to induce muscle hypertrophy, particularly in type II myofibers through an increase in myofibrillar protein contents for instance (116, 123). This later is attributed at the molecular level to an mTOR-mediated increase of MPS rate (124, 125). However, it was demonstrated that myofiber hypertrophy occurring with RET also requires SCs activation and fusion with pre-existing myofibers in a load-dependant mechanism named myonuclear accretion (122, 126).

Although EET and RET remains widely used to describe ET modalities, the huge variety of ET possibilities conducted *Furrer* and *Handschin* to propose a “continuum of exercise” (**Figure 9**). Indeed, these authors notified that several sport disciplines demand both muscle strength and endurance and suggested that muscle response to EET or RET overlaps and that power output, intensity or duration in ET determine muscle plastic changes (123).

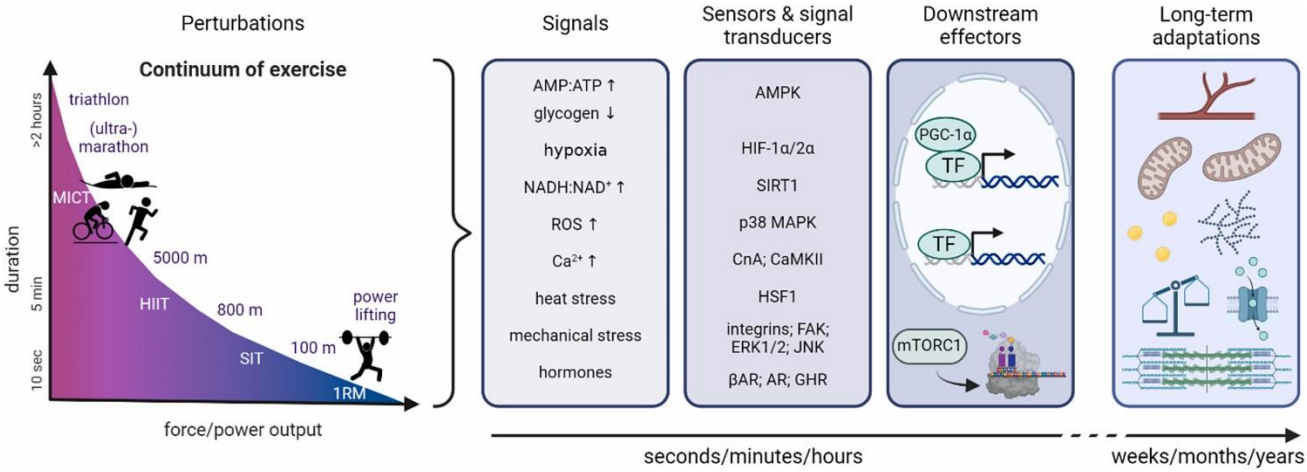

Figure 9. Schematic representation of the Continuum of exercise training, associated signals, signal transducers and downstream effectors that mediate ET long-term adaptations. From *(123).*

Furrer and Handschin proposed 'the continuum of ET' that highlights the large overlap between endurance ET and resistance ET modalities. In skeletal muscle, ET-mediated perturbations trigger specific intracellular signals. Those signals are detected and relayed by corresponding sensors and signal transducers which then regulate downstream effector activity to alter gene expression, protein translation, enzymatic activities and other cellular processes. The repetition of ET sessions over weeks, months or years initiate muscle adaptations to ET such as the increase in capillary density, mitochondrial content, and substrate uptake/ consumption (123).

MICT: moderate-intensity continuous training; HIIT: high-intensity interval training; SIT: sprint interval training; 1RM: one repetition maximum; ROS: reactive oxygen species; AMPK: AMP-activated protein kinase; HIF-1α/2α: hypoxia-inducible factor 1α/2α; SIRT1: sirtuin 1; can: calcineurin A ;CaMKII: Ca^{++} /calmodulin-activated kinase II; HSF1: heat shock factor 1; MAPK: mitogen-activated protein kinases; FAK: focal adhesion kinase; ERK1/2, extracellular-regulated kinase 1/2; JNK: c-jun NH2-terminal kinase; βAR: β-adrenergic receptor; AR: androgen receptor; GHR: growth hormone receptor; PGC-1α: peroxisome proliferator-activated receptor γ coactivator 1α; TF: transcription factor; mTORC1: mammalian target of rapamycin complex 1.

b) Myokines and exerkines

In addition to its roles in movement and metabolism homeostasis, skeletal muscle is an endocrine tissue which produces and secretes myokines (i.e. signalling molecules such as peptides, cytokines and metabolites) (127–129). Those myokines exert autocrine, paracrine, and endocrine effects and are thus crucially involved in the crosstalk between skeletal muscle and other tissues (127, 128, 130). Indeed, numerous myokines have been identified in the last decade (e.g. IL-6, Apelin, Irisin, Adiponectin, etc.) and most of them regulate key molecular processes in several target tissues such as liver, adipose tissue or pancreas (**Figure 10**). (127, 131, 132).

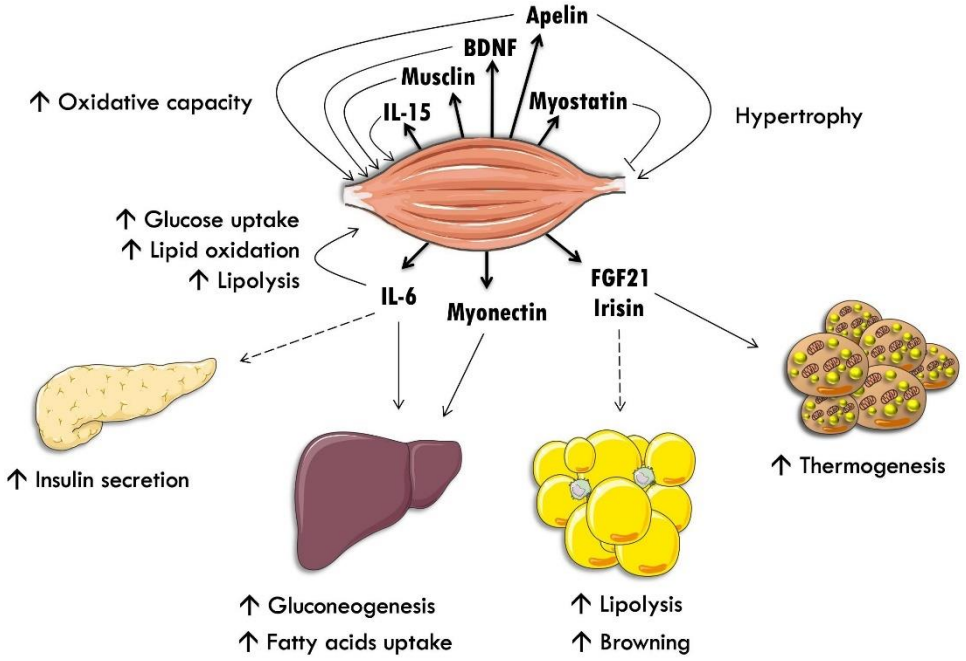

Figure 10. Schematic representation of skeletal muscle myokines and associated effects on target tissues. *From (127).* BDNF: Brain derived neurotrophic factor; IL-6: Interleukin-6; IL-15: Interleukin-15; FGF21: Fibroblast growth factor.

Furthermore, the release of some myokines (IL-6, IL-8, IL-15, Irisin, etc.) is directly induced by muscle contraction, those myokines are therefore referred as "exerkines" (127, 128, 133). Nevertheless, it should be noted that the term "exerkine" also includes the circulating factors produced and secreted by any tissue in response to ET (134, 135). For instance, growth hormone (GH), IGF-1, and testosterone plasmatic levels are all increased after ET and promote anabolic pathways resulting in an increased MPS (117, 123).

Due to their crucial implication in organ communications, those exerkines are particularly of interest in research studies investigating ET benefits in healthy and diseased individuals (135, 136).

V. Adiponectin pathway

1. Generalities

Adiponectin (ApN), also known as Adipocyte complement-related protein of 30 kDa (Acrp30), belongs to the C1q TNFα Related Proteins (CTRP) family. This family is composed of 15 other hormones which share, except CTRP4, similar structure and biological functions (inflammation regulation, energy metabolism, insulin signalling, …) (137, 138). Among those, ApN is an adipo/myokine secreted by adipose tissue and skeletal muscle (139) but also to a lesser extent by other tissues such as osteoblasts, bone marrow, placenta, and hypophysis (140, 141). At the plasmatic level, ApN is one of the most abundant adipokine with circulating ranges comprised between 5 and 30 µg/ml in humans (142, 143). After its discovery in mice and humans by 4 independent groups in 1995 (144–147), ApN was especially studied in obesity-related pathologies for its roles in metabolic processes such as fatty acid β-oxidation, glucose uptake, and insulin sensitivity (148, 149). However, ApN pathway has now been demonstrated to be a promising therapeutic candidate in several other pathological contexts.

2. Adiponectin and its circulating forms

Adiponectin, encoded by the *Adipoq* gene (MGI:106675) (145), is a polypeptide hormone synthetized as a 30kDa monomer composed of a N-terminal signal peptide, a short variable region, a collagenous stalk and a C-terminal globular domain (145–147). ApN monomers are further modified by post-translational modifications and multimerize to form ApN circulating oligomers (**Figure 10**)(150);

- Low Molecular Weight ApN Trimers (LMW), result from the homotrimerization of 3 monomers due to hydrophobic interactions between ApN globular domains and are stabilized by interactions of the collagenous stalks (150, 151). Proline residues hydroxylation appears to be involved in the collagenous stalk interactions and hydroxylation inhibition prevents trimer formation (152).
- Medium Molecular Weight ApN Hexamers (MMW), are composed of 2 ApN trimers linked by their collagen stalks in a Y-like shape (150, 153). The formation of disulphide bonds between Cys36 in humans (and Cys39 in mice) has been reported as essential for the oligomerization in MMW forms (150, 154).
- High Molecular Weight ApN oligomers (HMW) consist of 18 ApN monomers or more (150, 153). Successive post-translational modifications are implicated in the formation of HMW circulating forms, such as glycosylation, hydroxylation, and disulphide bonds (**Figure 11**) (152, 153). Importantly, HMW ApN forms were identified as the circulating form that exerts the most potent insulin-sensitizing effects (22, 155, 156).

Moreover, in inflammatory conditions, ApN can be cleaved by leukocyte elastases in a globular ApN form (gApN) (157). Globular ApN actions will be described in “ApN myoprotective effects on skeletal muscle” section.

In humans, LMW, MMW and HMW ApN represent 25%, 25-35% and 40-45% of the total ApN in plasma (158, 159). Importantly, several factors affect those proportions (sex, age, obesity, …), explaining a high inter-individual variability. Finally, it is important to notice that circulating forms do not interconvert into the plasma (142).

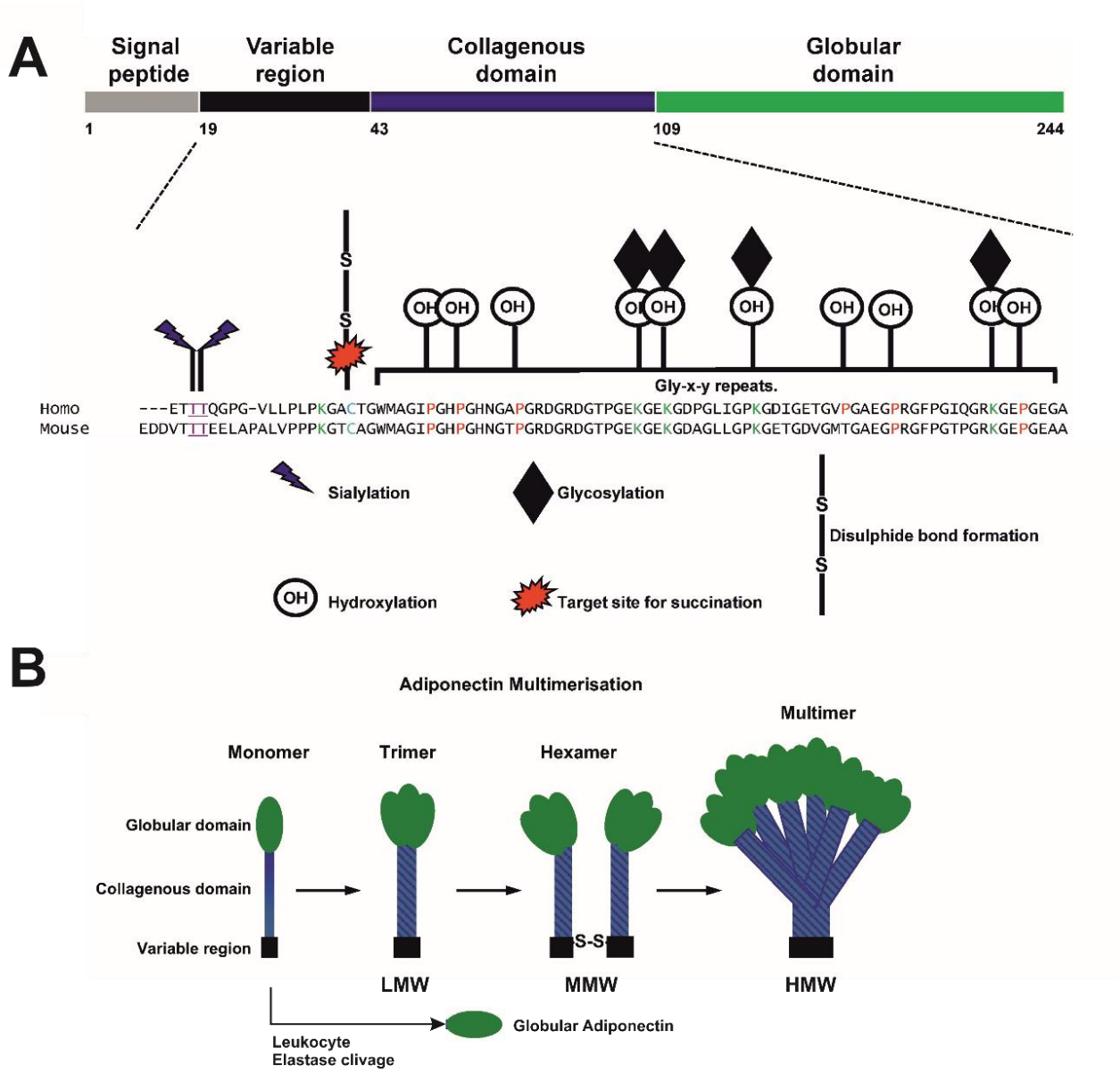

Figure 11. Schematic representation of Adiponectin (ApN) structural domains, post-translational modifications, amino acids sequence alignment, and multimerization. *Modified from (153). (A) Structural domains of a human ApN monomer and post-translational modifications involved in ApN multimerization. Human and mouse amino acid sequences are also aligned. Sialylation and succination sites are indicated as those modifications are known to reduce ApN clearance and multimerization, respectively. (B) ApN multimerization. ApN cleavage by leukocyte elastases into globular ApN (gApN) is also represented.*

3. Adiponectin receptors and co-receptors

ApN exerts its effects through 2 adiporeceptors, ADIPOR1 and ADIPOR2 that are encoded by *ADIPOR1* and *ADIPOR2* genes in humans and *Adipor1* (MGI:1919924) and *Adipor2* (MGI:93830) genes in mice (160–165). Those adiporeceptors share 66,7% of amino acids and are composed of 7 transmembrane domains (similar to G-coupled protein receptors but with an inversed topology (N-terminal extremity is internal and C-terminal extremity is external) (**Figure 12.**) (164, 166).

ADIPOR1 and *ADIPOR2* are ubiquitously expressed in the body although *ADIPOR1* is predominantly expressed in skeletal muscle, liver and macrophages whereas *ADIPOR2* is

preferentially expressed in liver and adipose tissue (164, 166). The full length ApN and gApN have a higher affinity for ADIPOR1 than ADIPOR2. ADIPOR1 and ADIPOR2 activate the AMPK/PGC1α pathway and PPARs signalling, respectively (165, 166).

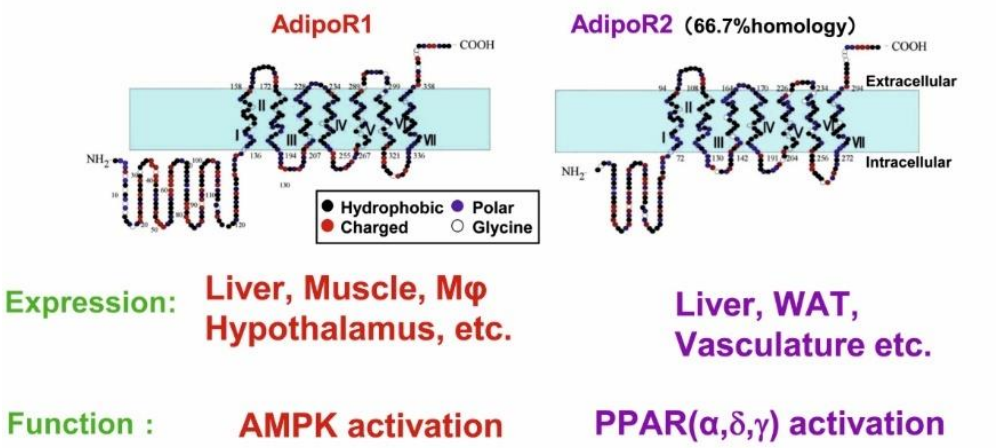

***Figure** 12. **Schematic of the Adiponectin receptors 1 and 2 structure, expression and function.** Modified from (166).*

More recently, t-cadherin (encoded by *Cdh13* (MGI:99551)) was identified as a Ca^{++}-dependant ApN co-receptor (167). T-cadherin is structurally different from the other members of the cadherin family. Indeed, t-cadherin is synthetized with an N-terminal pro-peptide and contains five Ca++-binding domains (EC1-EC5) but t-cadherin is maintained at the plasma membrane via with a GPI (Glycosylphosphatidylinositol) -anchor instead of an intracellular domain (**Figure 13.**) (168). T-cadherin extracellular domains EC1 and EC2 are essential for MMW and HMW ApN binding, whereas LMW and gApN are not able to interact with t-cadherin. Moreover, the presence of the N-terminal pro-peptide is also known to enhance ApN binding to this co-receptor (169). On the other hand, it has been shown that ApN increases t-cadherin protein level (but not *Cdh13* mRNA) in endothelial cells *in vivo* and *in vitro* by suppressing the plasma levels of GPI phospholipase D (170).

Evidences suggest that t-cadherin is required for ApN accumulation at the plasma membrane, thus promoting its interactions with AdipoR1 and AdipoR2 (170, 171). Moreover, t-cadherin was reported as essential for muscle regeneration process as its suppression prevents ApN regenerative properties (171).

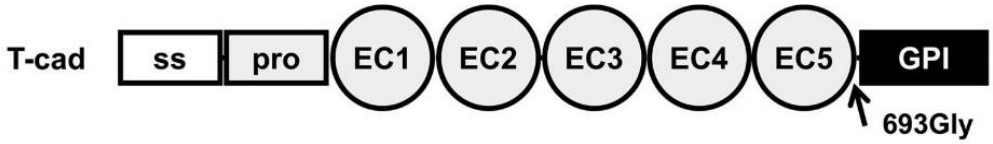

***Figure 13. Schematic of t-cadherin co-receptor structure.** From (169).*
EC: Extracellular repeat ; GPI : glycosylphosphatidylinositol-anchoring domain ; pro : prodomain ; ss : signal sequence.

4. Adiponectin signalling pathways in skeletal muscle

In skeletal muscle, ApN binding to AdipoR1 induce (i) a Ca^{++} influx that triggers CaMKKβ (Ca^{++} /Calmodulin-dependant protein Kinase Kinase Beta) activity and (ii) the recruitment of the APPL1 (Adaptor Protein Phospho-tyrosine with PH domain and Leucine zipper 1) that retains the Liver Kinase B1 (LKB1) in the cytosol (67, 172). The CaMKKβ and LKB1-mediated phosphorylation of AMPK on Thr172 residue results in the activation of the AMPK/SIRT1/ PGC1α axis (67, 172). Indeed, activated AMPK phosphorylates the PGC1α co-activator (P-PGC1 α) which is then fully activated by subsequent deacetylation meditated by Sirt 1, resulting in its translocation into the nucleus (Review in (68)). In the nucleus, P- PGC1α:

- associate with Sirt 1 to repress the Nuclear factor kappa B (NF-κB) transcription factor, involved in the transcription of pro-inflammatory genes (68, 173). More recently, *miR711* was identified as another intermediate by which ApN mediates NF-κB repression (174).
- coactivate the transcription of genes controlled by the Peroxisome proliferator-activated receptor alpha (PPARα) such as the Carnitine palmitoyltransferase 1 (*CPT1*) and the Acetyl-CoA oxidase (*ACO*). CPT1 and ACO proteins are respectively involved in fatty-acids entry and oxidation into mitochondria (68).
- coactivate the transcription of genes implicated in antioxidant response (e.g. Superoxide dismutase-2 (*SOD2*)), mitochondrial biogenesis, and oxidative metabolism.

Altogether, those ApN downstream signaling pathways therefore mediate the ApN anti-inflammatory, antioxidant and pro-oxidative properties (**Figure 14.**).

Furthermore, ApN binding to AdipoR1 is also responsible of insulino-sensitizing effects by stimulating glucose uptake in skeletal muscle. Indeed, APPL1 (Adaptor protein, Phosphotyrosine interacting with PH domain and Leucine Zipper 1) recruits the Insulin receptor substrate 1 (IRS-1) and maintains it close to the Insulin receptor (IR), thus favouring insulin signal transduction (68). In parallel, activated AMPK reduces (i) p70S6K1 inhibition on IRS-1 and with APPL1, enhances p38 MAPK signalling to increase GLUT4 translocation at the muscle membrane for glucose uptake, and (ii) the activity acetyl-CoA carboxylase (ACC) which mediate fatty-acid synthesis and stockage (68) (**Figure 14.**).

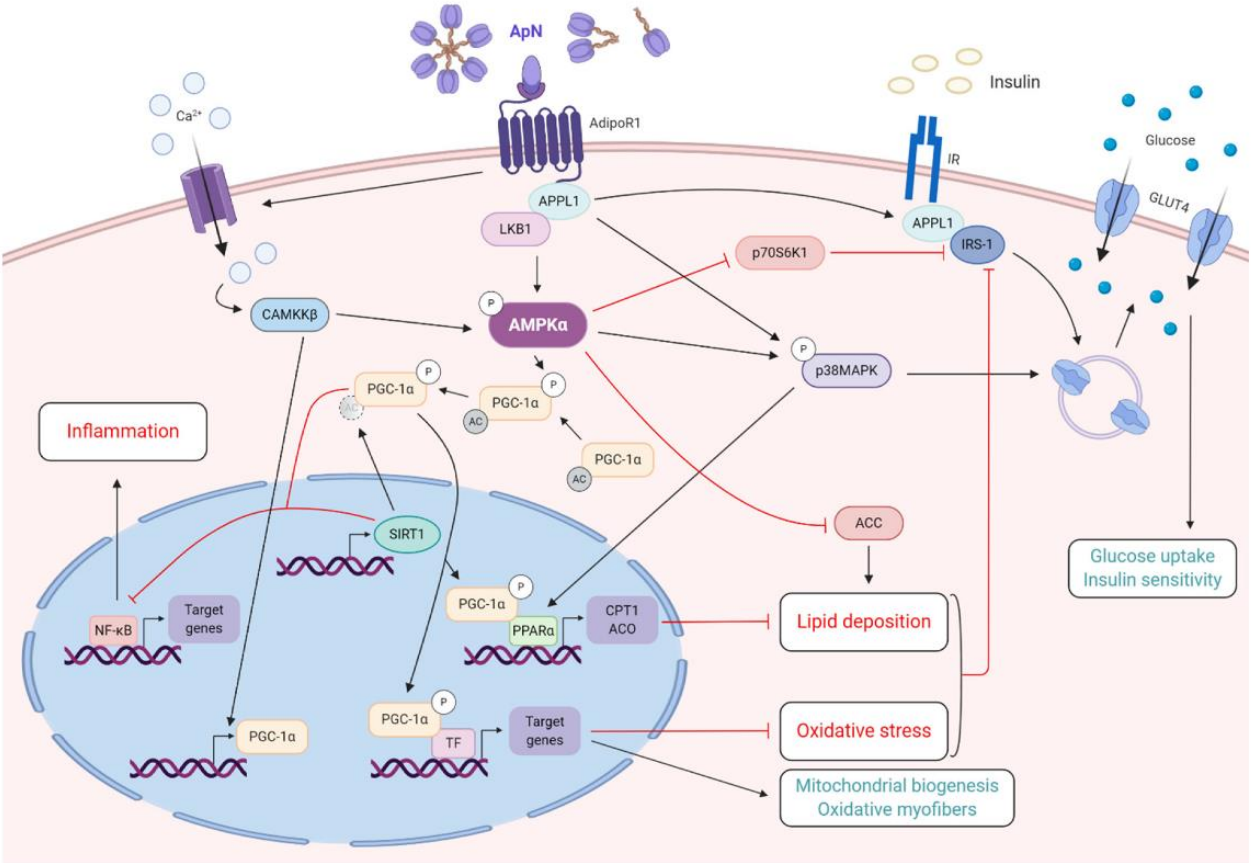

***Figure** 14. **ApN pathway beneficial effects in healthy skeletal muscle.** From (68).*
AC : Acetylation ; ACC : Acetyl-CoA carboxylase ; ACO : Acetyl-CoA Oxidase ; AMPK : AMP Activated Protein Kinase ; APPL1 : Adaptor protein, Phosphotyrosine interacting with PH domain and Leucine Zipper 1 ; CaMKKß : Calmodulin/Ca^{++}-dependant protein kinase kinase bαeta ; CaN : Calcineurin ; CPT1 : Carnitine palmitoyltransferase 1 ; GLUT4 : Glucose Transporter type 4 ; IR : Insulin receptor ; IRS-1 : Insulin receptor substrate 1 ; LKB1 : Liver Kinase B1 ; NFAT : Nuclear Factor of Activated T-cells ; NF- κB : Nuclear Factor kappa B ; P : Phosphorylation ; PGC1α : Peroxisome proliferator-activated receptor gamma coactivator 1-alpha ; PPARα : Peroxisome proliferator-activated receptor alpha ; p38MAPK : mitogen-activated protein kinase ; p70S6K1 : Ribosomal Protein S6K1 ; SIRT1 : Sirtuin 1 ; TF : Transcription Factor.

VI. ApN myoprotective effects on skeletal muscle

As described in the previous section, ApN has several beneficial effects on skeletal muscle, and an increasing number of studies describe the contribution of ApN in muscle homeostasis (Review by (68, 143)). Moreover, gain- and loss-of-function experiments demonstrated that ApN has myoprotective properties that make of ApN an interesting therapeutic candidate in several muscle disorders.

1. ApN counteract insulino-resistance

Several metabolic disorders are associated with the development of insulin-resistance (IR). Particularly, obesity, type II diabetes and sedentary behaviours are known to alter glucose uptake and insulin signalling in skeletal muscle (175).
Evidence of ApN insulin-sensitive properties was first found in IR obese mice and humans that present significantly lower *Adipoq* expression in adipose tissue than their matching controls

(145, 176). On the other hand, the administration of ApN by intraperitoneal injection was then shown to rescue insulin resistance in *ob/ob* mice (177) and AdipoR agonists such as AdipoRON enhanced both glucose uptake and metabolism (175).
Since those discoveries, the molecular mechanisms underlying those effects were dissected (See "Adiponectin signalling pathways in skeletal muscle" section) and loss-of-function experiments further demonstrated that ApN is essential in skeletal muscle to support insulin signalling (149, 178). Indeed, ApN-KO mice are more susceptible to develop IR when fed with high-fat-diet as compared to WT mice. As well, muscle-specific Adipor1-knockout mice (Adipor1-KO) also develop IR through IRS-1 repression by inhibitory phosphorylation on Serine residues (67, 149, 178).

2. ApN support the oxidative metabolism

In an elegant study led on muscle-specific Adipor1-KO mice, Iwabu *et al*., demonstrated that the Adipor1/AMPK/SIRT1/PGC1α axis is crucial to maintain type I oxidative myofibres and muscle ET endurance, notably by promoting oxidative metabolism and mitochondrial biogenesis (67). Indeed, muscle-specific Adipor1-KO prevents ApN-mediated Ca^{++} influx, reduces the activity of key ApN pathway effectors (e.g. CaMMK, AMPK, PGC1α), and results in mitochondrial alterations (e.g. decrease in mitochondrial content and in ROS detoxifying enzymes) (67).
Furthermore, the use of AdipoRON, in *mdx* (a model of Duchenne Muscular Dystrophy) and aged mice confirmed that pharmacological ApN pathway activation in muscle disorders rescues muscle strength and endurance by inducing a switch towards oxidative myofibres that is mediated by the AMPK and PGC1α (179, 180).

3. ApN mediates inflammation and oxidative stress regulation

In addition to its metabolic effects, ApN is known to have anti-inflammatory and antioxidant properties mediated by the Adipor1/AMPK/SIRT1/PGC1α axis. Interestingly, inflammatory stress induced by lipopolysaccharides (LPS) injection *in vivo* or pro-inflammatory cytokines *in vitro* was shown to up-regulate *Adipoq* mRNA expression. Therefore, the authors hypothesize that muscular inflammatory stress induces a local protective mechanism through ApN (181). Similarly, *Adipoq* expression is induced by oxidative stress (182) and ApN pathway activation protects against excessive ROS production through P-PGC1α which supports mitochondrial biogenesis and coactivates the expression of ROS detoxifying enzymes (e.g. SOD1/2, catalase, glutathione peroxidase) (143). Accordingly, ApN-KO mice appeared more sensitive to inflammatory and oxidative stress challenges (149, 183) but this was reversed by *Adipoq* gene electrotransfer in skeletal muscle (183, 184). More recently, ApN overexpression was shown to counteract both inflammation and oxidative stress in *mdx* mice (185). Those effects were also recapitulated in *mdx* mice treated with AdipoRON (179).

4. ApN has promyogenic effects

As described previously, the regeneration process in damaged skeletal muscle requires SC. However, processes taking place from SC activation to its fusion with the damaged myofibre are highly controlled and involve multiple cell types, notably macrophages and fibroadipogenic progenitors (4). Importantly, ApN pathway was shown to enhance the regeneration processes at several levels (Reviewed by (68)). Indeed, leucocyte elastases secreted by pro-inflammatory macrophages M1 are known to cleave full-length ApN into gApN which (i) promotes the resolution of inflammation by inducing M1 macrophages conversion into M2 anti-inflammatory macrophages and (ii) regulates SC activation, myoblasts fusion and differentiation (68, 186) (**Figure 15.**). Indeed, as concerns point (ii):

-Firstly, gApN enhances SC activation through the expression of *Myf5* transcription factor (187). Activated SC are then able to secret ApN in autocrine and paracrine manners, reinforcing the M1 to M2 macrophage switch as well as the proliferation and migration (by stimulating the expression of metalloproteinases (e.g. MMP-2)) of the activated SCs (68, 157, 186, 188).

-Secondly at the lesion site, gApN is implicated in SC differentiation into myoblast as well as myoblasts proliferation through the upregulation of the myoblast determination protein (MyoD) (68, 187).

-Finally, myoblast differentiation and fusion steps are also promoted by gApN. Indeed, it was shown that ApN-overexpression in *mdx* mice enhances the expression of gene encoding Myogenin and Mrf4 transcription factors (68, 187).

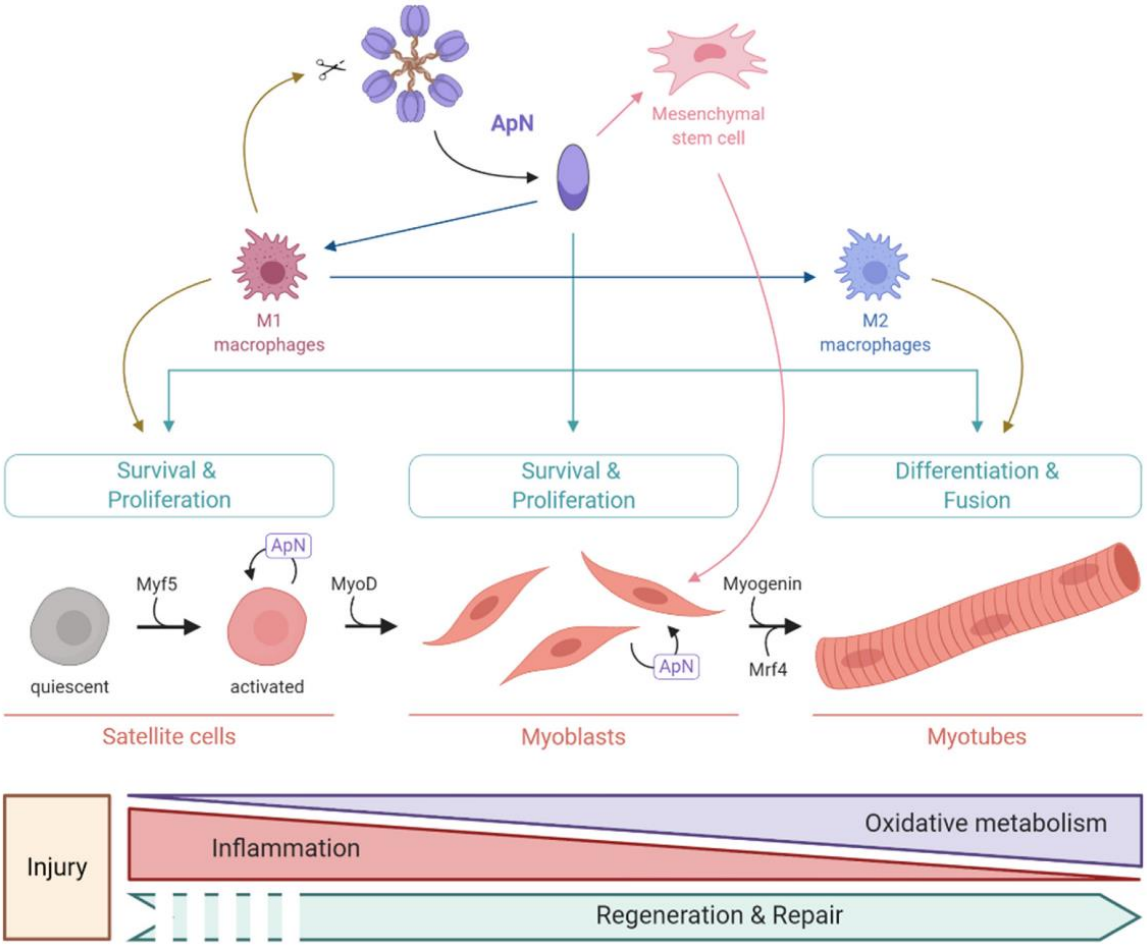

Figure 15. ApN promyogenic and regenerative properties.
Local pro-inflammatory cytokines release during damage recruits M1 macrophages that secrete elastases responsible for ApN clivage into globular ApN (gApN). gApN promotes (i) M1 macrophages shift into M2 macrophages implicated in inflammation resolution phase and (ii) mesangioblasts chemoattraction and differentiation toward the skeletal muscle lineage. In addition, gApN has direct promyogenic properties by stimulating myogenic transcription factors expression in satellite cells (SC). Finally, gApN promotes energy supply for regeneration by stimulating the oxidative metabolism. *From* (68).

VII. ApN pathway in muscle disuse and reconditioning

Altogether, the myoprotective effects of ApN presented in the previous section highlight the therapeutic potential of ApN pathway activation in muscle disorders particularly when associated with inflammation, oxidative stress, metabolic alterations, and regeneration defects (143). However, ApN pathway response to disuse in skeletal muscle should be interrogated before considering the use of AdipoR agonist to counteract disuse-mediated muscle alterations.

1. ApN pathway in muscle disuse

ApN pathway response to muscle disuse is almost completely unknown. Actually, only one study interrogated ApN pathway in a context of muscle deconditioning. In this study, Goto *et al.* reported a down-regulation of *Adipor1* but not *Adipor2* mRNA levels in the *Soleus* muscle of HLU mice and a positive relation between the muscle weight and *Adipor1* mRNA in a suspension-recovery experiment, suggesting that mechanical loading might regulate the expression of ApN pathway molecular actors (189). Nevertheless, potential changes in AdipoR1 and AdipoR2 protein levels were not addressed by the authors. Moreover, given metabolic roles of ApN pathway, its response to disuse needs to be better characterized both in slow- and fast-twitch muscles. This point is particularly of interest when considering that many muscle disorders are associated to fibre-type specific changes (10, 190).

2. ApN pathway in muscle reconditioning

Skeletal muscle ET is the only effective treatment to initiate muscle reconditioning following disuse (86, 191). However, ET as a therapeutic approach is often constrained by persistent skeletal muscle weakness and ET intolerance (191). Therefore, it appears essential to develop complementary approaches aiming to restore ET benefits in those patients.

Since ApN pathway and ET share common intracellular signalling such as the AMPK-SIRT1-PGC1α axis as well as p38 MAPK and P3K-Akt pathways (116, 143), ET benefits were suggested to be partly mediated by the AdipoR1 axis (192).

Furthermore, several studies reported that ET positively modulates ApN pathway. For instance, chronic ET protocols were reported to increase ADIPOR1 expression in rodents and human muscles (192–195) and our group further demonstrated that chronic ET on treadmill increase AdipoR1 protein level in the *Gastrocnemius* muscle (196).

However, the huge variety of experimental ET training protocols (and the potential associated body weight loss) may explain discrepancies regarding the observed ApN pathway responses, particularly when addressing plasmatic ApN and circulating forms (68, 143).

VIII. ApN KO mice

1. *Adipoq*$^{tm1/ChanJ}$ mice generation

In 2002, *Lawrence Chan*'s group used a replacement-type targeting vector to generate mice lacking ApN. Briefly, the targeting vector was designed from a mouse 129Sv strain bacterial artificial chromosome genomic clone that was composed of a *pMC1-TK-poly(A)* cassette at the 5' extremity followed by a *PGKneobpA* cassette (Neo) addressed to replace exon 2 (which include the start codon) in the *Adipoq* gene (**Figure 16.**). Mice embryonic stem cells (R1 ES cell line) were then transfected with the targeting vector to induce homologous DNA recombination, resulting in a loss-of-function mutation in the targeted *Adipoq* gene. Transfected ES clones were selected by Neomycin treatment and injected into blastocysts of C57BL/6J mice. Resulting chimeric mice were finally mated with C57BL/6J mice (197).

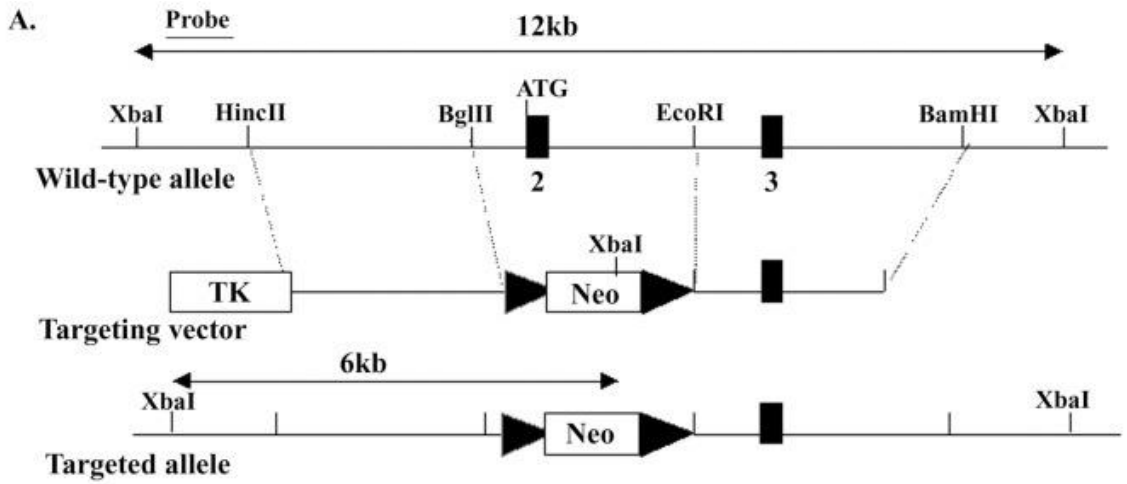

Figure 16. Representation of the replacement targeting vector used by* Ke Ma *et al., to generate ApN KO mice. *From (197).* The targeting vector was designed from a mouse 129Sv strain bacterial artificial chromosome genomic clone that was composed of a *pMC1-TK-poly(A)* cassette at the 5' extremity followed by a *PGKneobpA* cassette (Neo) addressed to replace exon 2 (which include the start codon) in the *Adipoq* gene *(197)*.

2. *Adipoq*$^{tm1/ChanJ}$ mice phenotype

Adipoq$^{tm1/ChanJ}$ mice were shown to have undetectable ApN plasmatic levels (198). However, the lack of ApN in those mice alter body weight evolution and glucose homeostasis but, more surprisingly, enhanced fatty acid β-oxidation in muscle and liver cells as compared to WT mice (197). In skeletal muscle, it was reported that *Adipoq*$^{tm1/ChanJ}$ mice present increased type IIb myofibre area and higher intramyocellular lipids content as compared to WT mice (143). Regarding the cardiovascular system, leukocyte rolling velocity was found decreased whereas thier adhesion to vascular endothelium is increased when compared to WT (198). Importantly, we have to underline here the relatively small amount of available data regarding *Adipoq*$^{tm1/ChanJ}$ mice phenotype in comparison with WT mice. More exactly, a complete characterization of mice carrying the *Adipoq*$^{tm1/ChanJ}$ mutation is complexified by different internal breading strategies between studies, diversifying therefore genetic backgrounds and phenotypes.

AIMS

AIMS

Skeletal muscle deconditioning leads to **Disuse-mediated Muscle Atrophy (DMA)**, frequently accompanied by a slow-to-fast fiber-type shift and persistent muscle weakness. **Exercise training (ET)** as a therapeutical strategy is often constrained by exercise intolerance. To develop new pharmacological approaches, a better understanding of molecular processes underlying ET benefits is therefore needed. The adaptive response to training includes complex molecular mechanisms with a widespread regulation of metabolic, stress response, and mitochondrial pathways. Among those processes, secreted molecules known as exercise-induced **myokines** are thought to promote many of the favourable adaptations to ET.

Adiponectin (ApN), an adipo/myokine, was suggested to be involved in ET benefits at the muscle level. As well, ApN receptor agonists constitute attractive candidates for the development of new therapeutic strategies in muscle disorders. However, the effect of muscle deconditioning on ApN pathway components was poorly studied and therefore, ApN agonists have never been considered to limit consequences of muscle deconditioning. Only one study interrogates ApN pathway in a reversible murine model of skeletal muscle disuse consisting in hindlimb unloading in mice. In this model, a down-regulation of *AdipoR1* was highlighted at the mRNA level in the *Soleus* muscle. However, protein levels were not addressed in this study. Furthermore, considering ApN metabolic effects, it is essential to examine muscle type-specific impacts of disuse in relation to ApN pathway response.

The objectives of the first part our study are therefore:

- **to determine the role of skeletal muscle fiber-type composition on the effect of muscle disuse**, comparing the slow-twitch *Soleus* and the fast-twitch *TA* muscles **(AIM#1)**
- **to decipher concomitant variations of ApN plasmatic level, oligomeric form proportion, and ApN (co-)receptor expression (AIM #2)**

To this aim, a murine model of Hindlimb Unloading and Immobilization (HLUI) will be optimized to limit confounding factors such as body weight loss and stress.

In the second part of the study, our objective is **to investigate whether the loss of ApN myoprotective properties during muscle deconditioning may exacerbate DMA (AIM #3).** To this aim, loss-of-function experiments will be performed by using ApN KO mice.

Finally, we aim **to determine whether the absence of ApN may limit the benefits of muscle reconditioning (AIM#4).** Since ApN is well known for its antioxidant properties, parameters indicative of skeletal muscle redox status will be particularly assessed to better understand mechanisms underlying ApN roles in muscle deconditioning and rehabilitation.

RESULTS

Results

IX. PART1: Adiponectin pathway characterization in a murine model of moderated muscle disuse.

Preface

This part concerns the investigation of the role of fiber-type composition on the effect of muscle disuse (**AIM#1**). To this aim, a murine model of Hindlimb Unloading and Immobilization (HLUI) has been optimized to limit confounding factors. In the same model, we also further deciphered concomitant variations of ApN plasmatic level, oligomeric form proportion, and ApN (co-)receptor expression (**AIM #2**)

Results have been included in a publication currently under revision in ***Physiological Reports***.

RUNNING HEAD: Myofiber type and adiponectin modifications in disused muscle

Muscle-type specific alterations and Adiponectin pathway characterization in a murine model of muscle disuse.

Szczepanski Sébastien[1], Limpens Maëlle[1], Jenart Vincianne[1], Declèves Anne-Emilie[2], Legrand Alexandre[1], Tassin Alexandra[1]

[1] Laboratory of Respiratory Physiology, Pathophysiology and Rehabilitation, Research Institute for Health Sciences and Technology, University of Mons, 7000 Mons, Belgium.
[2] Department of Metabolic and Molecular Biochemistry, Research Institute for Health Sciences and Technology, University of Mons, 7000 Mons, Belgium.

Correspondence: *Tassin Alexandra: alexandra.tassin@umons.ac.be*

ABSTRACT

Disuse-mediated Muscle Atrophy (DMA) is associated with a slow-to-fast fiber-type shift and persistent muscle weakness. While Exercise training (ET) reconditioning is constrained by exercise intolerance, Adiponectin (ApN) was suggested as a therapeutic candidate in muscle disorders. However, the effect of DMA on ApN pathway components was poorly studied. Furthermore, considering ApN metabolic effects, it is essential to examine ApN pathway response to disuse in relation with muscle type.

Therefore, effects of HindLimb Unloading and Immobilization (HLUI) were studied in the slow-twitch Soleus and the fast-twitch Tibialis Anterior (TA) muscles.

The Soleus muscle present a moderated atrophy in type IIa myofibers. The TA muscle is more severely affected and exhibits a type I to IIa switch. HLUI increased the hybrid I/IIa myofibers proportions in both muscles, suggesting an ongoing myofiber switch that is delayed in the Soleus muscle. Concomitantly, we highlighted higher ApN plasmatic level and modifications in oligomeric forms proportions. HLUI also downregulates Adiporeceptors in the Soleus but not in the TA muscle.

In conclusion, HLUI in mice induces a fibre type-dependent atrophy and a type I/IIa myofiber switch occurring concomitantly with an elevation of ApN plasmatic level, disturbances in oligomeric forms proportions, and muscle-type dependent alterations in adiporeceptor expression.

Are ApN pathway response to disuse and DMA severity fiber-type specific ?

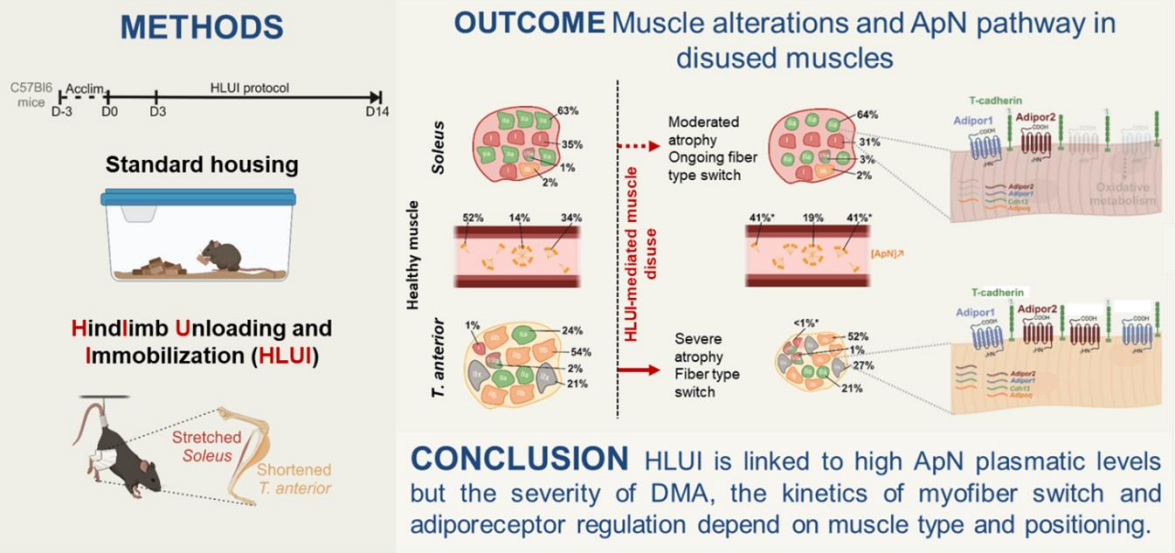

NEW & NOTEWORTHY

Disuse-mediated Muscle Atrophy (DMA) is associated to persistent muscle weakness impairing reconditioning. Adiponectin (ApN) is a candidate for therapeutic strategies in muscle disorders but ApN pathway variations in DMA remain unclear.

In a murine model of hindlimb unloading and immobilization (HLUI), we highlighted a muscle-type dependant atrophy accompanied by a type I/IIa switch. Concomitantly, we notice an elevation of ApN plasmatic level, disturbances in oligomeric form proportion and muscle-type dependent alterations in adiporeceptor expression.

Keywords: Adiponectin pathway/Myofiber-type/Skeletal muscle deconditioning.

INTRODUCTION

Skeletal muscle deconditioning can directly result from a pathological condition by itself (cancer, metabolic disorders, traumas, and hereditary muscular dystrophies), or be secondary to the associated hypo- or in-activity, notably due to prolonged bed rest, limb immobilization, mechanical ventilation, or wheelchair dependence (1–3). At the tissue level, skeletal muscle deconditioning is associated with the development of a Disuse Muscle Atrophy (DMA) mainly characterized by a decrease in myofibers cross-sectional area (CSA) and a slow-to-fast myofiber type switch (4–7). At the molecular level, DMA is associated with a protein synthesis/degradation imbalance, abnormal oxidative stress, and mitochondrial dysfunction (4, 5, 7–10). Importantly, morphological alterations are associated with functional impairments. In an important group of patients, muscle weakness can persist even after muscle reconditioning programs (11–13). Moreover, DMA was suggested to be associated with impaired adult myogenesis that could limit the effect of muscle reconditioning as well as muscle regeneration in case of injury (11, 14).

Several studies aimed to counteract the development of DMA, mostly by suggesting nutritional supplementation with antioxidant cocktails. Unfortunately, such strategies failed in human studies, and the only effective treatments remain mobilization, electrostimulation, and exercise training (ET) (11, 15). Unfortunately, patient intolerance to ET often limits muscle reconditioning, thus stressing the need for the development of pharmacological approaches to protect muscles in this frequent pathological context (11).

At the physiological state, skeletal muscle is at the center of a crosstalk involving Adiponectin (ApN), an adipo/myokine with auto-, para- and endocrine actions (16–18). ApN post-translational modifications result in multimeric forms found in the plasma and classified as Low (LMW), Medium (MMW), and high molecular weight (HMW) (19). Those circulating forms target tissues via ADIPOR1 and ADIPOR2 receptors, predominantly expressed in skeletal muscle and liver, and activating AMPK and PPARα pathways, respectively (16, 20, 21). More recently, t-cadherin was identified as an ApN co-receptor required to maintain ApN at the tissue membrane (22–24).

In addition to its well-described anti-diabetic, anti-apoptotic, and anti-oxidative properties (25–27), ApN exerts myoprotective effects, notably by activating the ADIPOR1/AMPK/SIRT1/PGC1α axis allowing for reduced inflammatory and oxidative stress and an enhanced oxidative metabolism (21, 28–30). Those discoveries are mainly based on studies in mice demonstrating that ApN-KO muscles are more sensitive to oxidative stress, inflammation and apoptosis (26) and that muscle-specific Adipor1-KO mice show reduced endurance, type-I fiber number, mitochondrial content and oxidative stress-detoxifying enzymes (21). Furthermore, ApN was reported to have pro-myogenic effects (reviewed by (28)). Notably, elastases produced by M1 macrophages at the lesion site cleave ApN into its globular form (gApN) (31) which regulates satellite cells (SC) activation and later regeneration steps (32–35). The t-cadherin receptor (23, 36) and AdipoR1 (21) are also reported as key actors in ApN-mediated muscle regeneration.

However, discrepancies remain about ApN roles in skeletal muscle. Indeed, in elderly patients, muscle mass loss was associated with elevated ApN circulating levels, a concept named “ApN paradox” (37, 38).

On the other hand, the therapeutic potential of ApN agonists was assessed in different models of muscle disorders e.g. *mdx* mice (a model of Duchenne Muscular Dystrophy) (30), aged mice (39), and dexamethasone-induced atrophy (40). In those studies, ApN pathway activation limited oxidative stress and inflammation in *mdx* mice, promoted oxidative metabolism in both aged and *mdx* mice (30, 39) and reduced atrophy induced by dexamethasone *in vivo* (40). These data support the therapeutic potential of ApN pathway activators in muscle diseases, particularly when associated with oxidative stress and metabolic alterations. However, ApN agonists have never been considered in the pathological context of muscle deconditioning. Moreover, it is still unclear whether muscle disuse can affect ApN pathway components as only one study interrogates this pathway in Hindlimb Unloaded (HLU) mice, a model of muscle disuse. In this model, *Goto et al*. highlighted a down-regulation of *Adipor1* but not *Adipor2* mRNA levels in the *Soleus* muscle and a positive relation between the muscle weight and *Adipor1* mRNA in a suspension-recovery experiment, suggesting that mechanical loading might regulate the expression of ApN pathway molecular actors (41). However, potential changes in ADIPOR1 and ADIPOR2 protein levels were not addressed in this study. Moreover, given metabolic roles of ApN pathway, its response to disuse needs to be better characterized both in slow- and fast-twitch muscles. This point is particularly of interest when considering that many muscle disorders are associated to fibre-type specific changes (42, 43).

In this study, we optimized a murine model of Hindlimb Unloading and Immobilization to determine the role of fiber-type composition on the effect of muscle disuse, comparing the slow-twitch *Soleus* and the fast-twitch *TA* muscles. Concomitantly, we decipher variations of ApN plasmatic level, oligomeric form proportion, and ApN (co-)receptor expression at the mRNA and protein levels.

MATERIALS AND METHODS

Animals

All animal experiments met the Belgian national standard requirements regarding animal care and were conducted in accordance with the Ethics and Welfare Committee of the University of Mons (LE023/03).

At 12 weeks of age, male C57BL/6 mice (RRID: MGI:2159769, *Charles River*, France) were housed in large rat cages (58x40x20cm) equipped (HLUI group) or not (CTL group) with a device allowing hindlimb unloading through tail suspension. HLUI mice were connected to this device for a 3-day acclimatization period but kept at floor level to allow movements with both forelimbs and hindlimbs (from D-3 to D0). Mice of the HLUI group were then tail-suspended and hindlimbs immobilized for 3 (D3) or 14 days (D14). (Fig 1*A*). Relative humidity was maintained at 35-40% with a constant room temperature (21°C) and a 12h/12h day/night light cycle. Animals had access to food and water *ad libidum*.

Hindlimb Unloading and immobilization (HLUI)

The HLU device, adapted from Marzuca-Nassr *et al.* (44), is composed of a rod fixed to the top of the cage, a pulley with a hook, and a small chain to connect the hook to a paperclip fixed on the mouse tail by using medical tapes (Leukosilk®; 1,5 x 0,5 cm). Hindlimb muscles were immobilized in an extended position from the ankle (which is in a dorsiflexion position) to the upper hip using medical band-aids (Nepenthes; 16 x 1 cm) (Fig 1*B*). This system allows mice to be suspended at a 30° angle by maintaining mouse movement with their forelimbs in the rod axis (Fig 1*C-D*). Two mice were housed in a cage to allow social interactions.

Muscle collection and preparation

After 3 or 14 days of protocol, mice were anesthetised and euthanised (Euthanimal 20%, *Alfasan*) and the *Soleus* and *Tibialis Anterior* (*TA*) muscles were collected to perform morphometrical analyses and molecular investigations (RT-qPCR and Western blots). Morphometrical analyses required muscle embedding in OCT cryo-compound (ImmunoLogic, 1620-C) frozen in isopentane cooled with liquid nitrogen. Cryosections (8 µm) were performed with a cryotome (Leica 1950). Contralateral muscles were snap-frozen in liquid nitrogen to allow molecular investigations. Blood was collected and centrifugated (13500 rpm, 15 minutes) to isolate plasma for ELISA assays.

Morphometrical analyses in hindlimb muscles

Myofiber type immunofluorescence staining

Soleus and *Tibialis Anterior* muscles cryosections were blocked for 1 hour at room temperature with 10% Goat-serum/PBS (VWR, S2000-100) before being incubated for 2 hours at room temperature with a primary antibody cocktail directed against MyHC7 (type I fibers), MyHC2 (type IIa fibers), MyHC4 (type IIb fibers) and laminin (Supplemental Table S*1*). Slides were washed 3 times in PBS and incubated for 1 hour with the secondary antibodies cocktail. (Supplemental Table S*1*). Slides were washed 3 times in PBS and mounted with ProLong™ Gold Antifade Mountant (P36934, Invitrogen). Images were then captured to cover the whole muscle section with a Nikon Eclipse i80 microscope (10x magnification).

Images processing and measurements

Each capture was processed with *QuPath-0.5* software to subtract the background fluorescence signal and provide DAPI/Cy5, DAPI/FITC, and DAPI/TRITC images. Processed individual images were then stitched with *Image Composite Editor* software to reconstitute the whole muscle section in the 3 precited channel combination without pixel down-sampling. Reconstituted muscle sections were then

segmented thanks to the *Cellpose v2.2.3* software (CPx pre-trained model) (45, 46) to determine the Regions Of Interest (ROIs) corresponding to positive myofibers in the channel combination of interest. Since *Cellpose v2.2.3* allows to export ROI as a mask.PNG image, we used the LabelsToRoi plugin (47) to transpose myofibers segmentation in the *Fiji* software for ROI measurements. Each myofiber CSA was finally obtained after conversion of the corresponding ROI (in pixel) in µm² with the pixel/µm ratio. Myofibers were then classified in clusters according to their area (<120 μm^2, 120-300 μm^2, and every 300 μm^2 until 3900 μm^2 in the *Soleus* muscle and 6000 μm^2 in the *TA* muscle) to evaluate changes in myofibers CSA distribution. Minimum Feret's diameter (MFD), a geometrical parameter used for morphometric analysis, was also measured from the segmented ROIs as it is less affected by the orientation of the muscle section (48).
Double positive ($MyH7^+/MyH2^+$) myofibers were identified by overlapping DAPI/Cy5 images Cellpose segmentation (corresponding to type I fibers) on DAPI/FITC images (corresponding to type IIa fibers) with the LabelsToROI plugin of *Fiji.* The percentage of double-positive myofibers was expressed as the percentage of $MyH7^+$ myofibers that are also $MyH2^+$.

RT-qPCR analyses

Total RNAs were extracted from *Soleus* and *TA* muscles with Trizol reagent (Invitrogen) according to the manufacturer guidance before being treated with DNAse I (ThermoFischer). cDNAs were synthetized from 1µg of RNA using Maxima First Strand cDNA synthesis kit (ThermoFischer). RT-qPCRs were performed in triplicate for each primer (Eurogentec) (Supplemental Table *S2*) with the SYBR Green FastStart Essential DNA Green Master (Roche) and by using the LightCycler®96 (Roche) device (cycling conditions: initial denaturation step at 95°C for 10 min, followed by 40 cycles of 15s at 95°C and 60s at primer Tm). Raw data were analysed with the LightCycler®96 software (technical replicates with CT > 0.2 were removed from the analyses) and quantified by using $2^{-\Delta\Delta Ct}$ method (*Rplp0* as housekeeping gene).

ApN plasmatic components

ApN plasmatic concentrations were measured by using the Adiponectin/Acrp Quantikine ELISA kit (R&D) according to the manufacturer's instructions. Relative amounts of LMW, MMW and HMW ApN circulating forms were determined using a non-denaturating SDS-PAGE electrophoresis followed by a Western blot. Based on ApN plasmatic concentrations provided by ELISA assay, 10µg of ApN were separated onto an 8% polyacrylamide gel (125V; 2h20) before being transferred onto a nitrocellulose membrane (Amersham). Membranes were then stained with Ponceau Red, washed 3 times in TBS-Tween (0.2%), and blocked 1 hour in 5% non-fat dry milk diluted in TBS-T. Primary antibodies directed against ApN (1:1000, Rb IgG Ab85827, Abcam, RRID:AB_10675534) as well as corresponding secondary HRP conjugated antibodies (Donkey anti-Rb IgG, VWR, NA934) were diluted in 1% non-fat dry milk TBS-T for incubation for 2 hours at 4°C and for 1 hour at room temperature respectively. The HRP signal was visualized using Supersignal West Femto Max Sensitivity Kit (Thermo Fisher Scientific). Densitometry was performed using *Fiji* software. The densitometry signal was normalized to the total proteins stained by Ponceau Red. The signal corresponding to LMW, MMW and HMW ApN forms were then normalized on the total ApN signal and therefore expressed as a percentage. S_A Index, a relevant indicator of insulin sensitivity corresponds to the ratio HMW/(LMW+MMW+HMW) (49).

Western Blot analyses

Soleus and *TA* muscles were homogenized in lysis buffer (CelLytic, Sigma, C3228; Protease Inhibitor Cocktail, Sigma, P8340; Phosphatase Inhibitor Cocktail, Millipore, 524632). Equal protein amounts were then separated on a 12% SDS-PAGE gel (100V; 3h30) before being transferred onto a nitrocellulose membrane (Amersham) by using the Trans-Blot Turbo Transfer System (Biorad™). Membranes were then stained with Ponceau Red, washed 3 times in TBS-Tween (0.2%), and blocked 1 hour in 5% non-fat dry milk diluted in TBS-T. Primary antibodies directed against Adipor1 (1:1000, Rb

IgG, Gentaur, ADIPOR12-A), AdipoR2 (1:1000, Rb IgG, Gentaur, ADIPOR22A) and t-cadherin (1:1000, R&D, AF3264) as well as corresponding secondary HRP conjugated antibodies (Donkey anti-Rb IgG, VWR, NA934) and (Rabbit anti-goat IgG, Abcam, ab6741)) were diluted in 1% non-fat dry milk TBS-T for incubation overnight at 4°C and 1 hour at room temperature respectively. The HRP signal was visualized using Supersignal West Femto Max Sensitivity Kit (Thermo Fisher Scientific) and the Fusion FX7 spectra (Vilber, France). Densitometry was performed using *Fiji* software. The densitometry signal was normalized to the total proteins stained by Ponceau Red.

Statistical analysis

Statistical analyses were done using *SigmaPlot* software, version 14. Data were expressed as mean ± SD and represented as histograms (mean ± SD) or boxplots (5 and 95th percentile). For comparison, depending on normality and equal variance tests, we used : **(i)** a Student's t-test (plasmatic ApN and ApN oligomers, *AdipoQ* and *Fbxo32* in the *Soleus*, adipo(co)receptor mRNA and protein levels; myofiber CSA, proportion and MFD as indicated in figure legends), or **(ii)** a Welch's t-test (*Adipoq* mRNA, type IIx CSA and MFD in the *TA* muscle), or **(iii)** the non-parametric Mann-Whitney Rank Sum test (Type I myofiber CSA and type IIb myofiber proportion in the *Soleus* muscle), and **(iv)** Chi-square test (myofiber CSA distribution in the *Soleus* and *TA* muscles). B.w. were expressed as a percentage of the baseline b.w (D0) and compared with a Two-way Analysis of Variance Repeated measure statistical test. B.w evolution during the protocol was also evaluated using linear regression, calculation of slope coefficients, and mean comparison between HLUI and CTL mice with a Student's t-test.

RESULTS

Optimization of a model of moderate muscle disuse

To study the impact of muscle disuse on ApN pathway, we used a murine model of Hindlimb Unloading (HLU). The model, adapted from (44), allowed to limit mouse stress by maintaining social interactions and movements. Here, we added an acclimatization period of 3 days and combined the HLU suspension technique with a hindlimb immobilization procedure (HLUI) (Fig 1, *A-D*).

HLUI mouse b.w was similar to CTL at baseline (D0, Fig 1*E*). We observed a slight decrease in b.w. the day before euthanasia (D13) (b.w. variation between D0 and D13 in CTL: +4,5% ± 4.6% and HLUI: -1.8% ± 4.4 %, Fig 1*F*). B.w. evolution in the CTL group showed a slight gain during the protocol with an evolution slope of 0.7 ± 1.1% (Fig 1*G*). B.w. evolution in the HLUI group was relatively stable but we can notice a slope value slightly negative (-0.5 ± 0.85 %) and significantly different to the CTL group at a statistical level (p=0.012, student's *t*-test) (Fig 1*G*). Regarding mean food consumption, no differences were found between HLUI and CTL groups (Supplemental Fig. S*1*).

To further characterize the HLUI model, we also investigated the expression of *Fbxo32 (*encoding Atrogin-1), an early marker of DMA development in rodents. We showed that 3 days of HLUI successfully induced *Fbxo32* upregulation in the *Soleus* and the *TA* muscles (Supplemental Fig. S*2*).

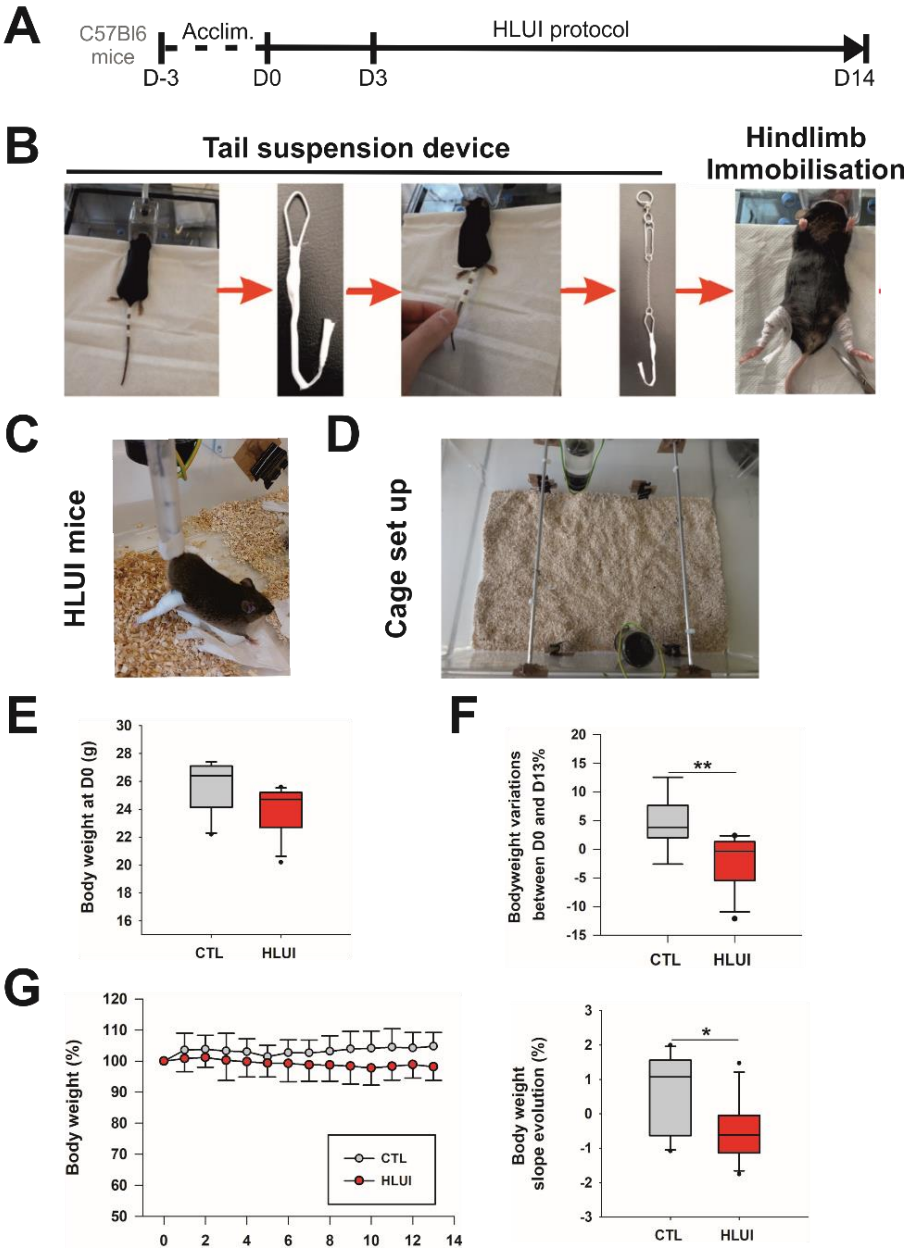

Figure 1. Murine model of Hindlimb Unloading and Immobilisation (HLUI). (A) Timeline. Mice were first submitted to an acclimatization period (acclim.) of 3 days during which they were attached to the tail-suspension system and kept at floor level to allow the use of both forelimbs and hindlimbs (from D-3 to D0). This step was followed by 3 (D3) or 14 days (D14) of HLUI protocol. **(B) HLUI procedure.** Three bands of medical tape were fixed to the tail. A paperclip was modified to form a hook attached to the tail by using 3 bands of medical tape. The hook was connected to a metal chain ending in a ring. Hindlimbs were immobilized in extension position (ankle was fixed in dorsiflexion position) with medical tape. HLUI mice were then suspended with a 30° angle. **(C) HLUI mice. (D) Cage set up.** Large rat cages were converted by adding a rod fixed to the top of the cage. For tail suspension, the chain was attached to the rod via the ring therefore allowing a sliding mechanism. Mice were thus able to move with their forelimbs in the rod axis. Two mice were housed per cage to allow social interactions. **(E) B.w at D0.** Data represented as boxplots; *CTL(n=10) vs HLUI(n=11),* Mann-Whitney Rank Sum test, NS. **(F) Body weight variations between D0 and D13.** Data represented as boxplots; **: p<0.01, *CTL(n=10) vs HLUI(n=11),* Student's t-test. **(G) Body weight (b.w) evolution and slope comparison.** B.w was measured daily and the first day of protocol (D0) was defined as a 100% baseline. Data represented as mean ± SEM, *CTL(n=10) vs HLUI(n=11)*. B.w slope evolution was determined from D1 to D13 of the protocol. Data represented as boxplots; *: p<0.05, *CTL(n=10) vs HLUI(n=11),* Student's t-test.

Effects of moderate muscle disuse in mice are fibre-type dependent

Soleus slow-twitch muscle

Myosin heavy chain (MyHC) immunodetection on *Soleus* muscle cryosections allowed the detection of type I, type IIa and type IIb myofibers in CTL and HLUI mice (Fig. 2*A*). When all myofiber cross-sectional areas (CSA) were measured in the whole muscle, we observed that the HLUI protocol did not affect *Soleus* myofiber mean CSA. However, the analysis of myofiber CSA distribution showed an increased proportion of myofibers in smaller area clusters (<1200 µm²) in HLUI mice when compared with CTL myofibers CSA distribution ($p<0.001$, Chi-square) (Fig. 2*B*). To minimize potential risks of bias linked to sectioning angle orientation, the MFD was also measured, but no modification was observed when considering the whole muscle section.

Fiber-type-specific myofiber morphometrical analyses revealed that HLUI-induced muscle disuse was associated with fiber-type-dependent alterations. Indeed, HLUI had no impact on type I myofiber CSA (Fig. 2*C*) but type IIa myofiber CSA distribution showed a switch towards fibers with smaller CSA (<1200 µm²) in the HLUI groups compared to CTL mice ($p<0.05$, Chi-square). Type IIa myofiber mean MFD was also reduced in HLUI mice as compared to CTL mice ($p<0.05$, Student's t-test) (Fig. 2*D*). Type IIb myofibers were only detected on 3 to 5 CTL and HLUI *Soleus* muscles. When present, type IIb myofiber CSA appeared not affected by HLUI but a significative reduction of the MFD was observed in HLUI *Soleus* muscles ($p<0.05$, Student's t-test) (Supplemental Fig. S*3*).

Since DMA is commonly described as characterized by a myofiber type switch (4, 6), we interrogated this feature in the HLUI model. In the *Soleus* muscle, the percentage of type I, type IIa, and type IIb myofibers were 35.3 ± 8.2 %; 63.1 ± 6.2%, and 1.6 ± 2.5%, respectively. These proportions were not significantly modified in the *Soleus* muscle of HLUI mice (Fig. 2*F,* Supplemental Table S*3*). However, morphometrical analyses revealed the presence of $MyH7^{+}$(Cy5)/$MyH2^{+}$(FITC) double positives myofibers generally named hybrid I/IIa (or switching) myofibers. The proportion of type I ($MyH7^{+}$) myofibers that are also type IIa ($MyH2^{+}$) myofibers was found to increase in HLUI *Soleus* muscles (8.4 ± 3.3%) as compared to CTL (3.7 ± 2.3%) ($p<0.05$, Student's t-test) (Fig. 2*H-G*), suggesting an ongoing slow-to-fast myofiber transition in the *Soleus* muscle upon HLUI.

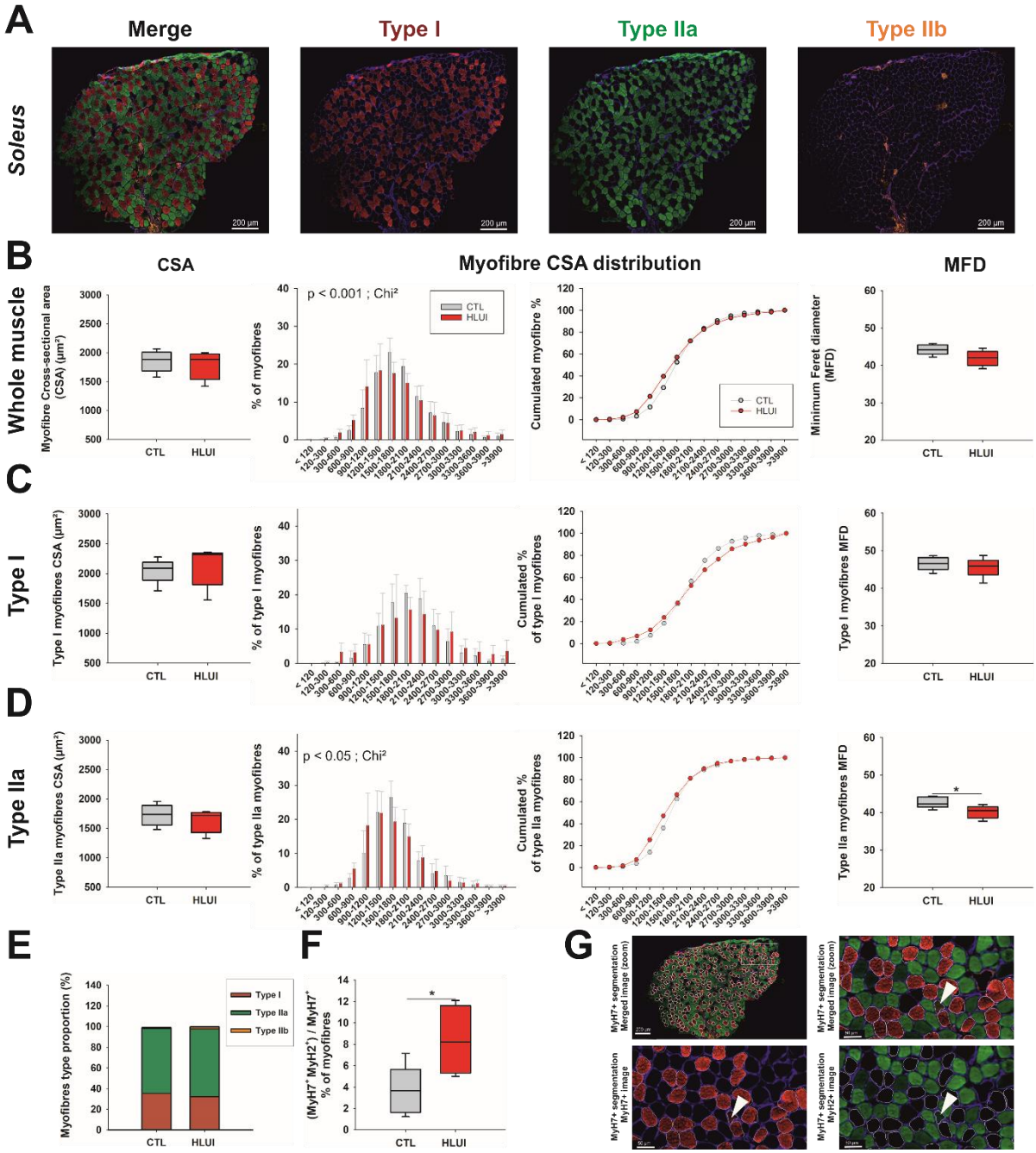

Figure 2. Effects of HLUI-mediated muscle disuse in mice *Soleus* are fiber-type dependant. Cross-sectional Area (CSA), myofiber CSA distribution and Feret's diameter were measured following type I, IIa and IIb immunofluorescence detection and morphometrical analysis were performed with *Cellpose* and *Image J* softwares. **(A) Representative fields**. **(Left)** CSA was measured in all fibers **(B)**, in type I **(C)** and in type IIa myofibers **(D)**. Data represented as boxplot. *CTL(n=5) vs HLUI(n=5)*, Student's t-test, NS. **(Center)** Myofibers were classified in clusters according to their CSA (µm²). All fibers **(B)**, type I fibers **(C)** and in type IIa myofibers **(D)**. Data represented as mean ± SD, *CTL(n=5) vs HLUI(n=5)*, Chi-square. Cumulative percentages of myofibers in CSA clusters in, all fibers **(B)**, in type I **(C)**, in type IIa **(D)** and in type IIb fibers. **(Right)** Minimim Feret's diameter (MFD) was measured in all fibers **(B)**, in type I **(C)** and in type IIa myofibers **(D)**. Data represented as boxplot; *: p<0.05, *CTL(n=5) vs HLUI(n=5)*, Student's t-test. **(E) Myofibers type proportions**. Data represented as stacked bars; Student's t-test, NS. **(F) Percentage of type I myofibers also positive for IIa myofibers markers**. Data represented as boxplot; *: p<0.05, *CTL(n=5) vs HLUI(n=5)*, Student's t-test. **(G) Representative field showing hybrid (I/IIa) myofiber detection.** White arrow: Hybrid (I/IIa) myofibers.

Tibialis Anterior fast-twitch muscle:

MyHC immunodetection in *Tibialis Anterior* (TA) muscle cryosection allowed the detection of type I, type IIa and type IIb myofibers in CTL and HLUI mice (Fig. 3*A*). We also observed unstained myofibers that likely correspond to IIx myofibers (Supplemental Fig. *S4*) as described in (50). HLUI-induced disuse decreased the whole *TA* muscle myofiber CSA, with a mean CSA of 2484 ± 328 µm² in HLUI mice, and of 3147 ± 435 µm² in the CTL group ($p<0.05$, Student's t-test) (Fig. 3*B*). Moreover, myofiber CSA distribution analyses indicated that HLUI mice *TA* muscles present higher percentages of myofibers in clusters corresponding to small/intermediate CSA (<2700µm²) as compared to CTL *TA* muscles ($p<0.001$, Chi-square). MFD measurements are also in agreement with a reduced myofiber CSA in HLUI *TA* muscle ($p<0.01$, Student's t-test) (Fig. 3*B*).

Regarding fiber-type-specific changes in the *TA* muscle, HLUI mainly affected type IIa and type IIb myofibers. Indeed, type IIa myofibers CSA was reduced in HLUI mice (1852 ± 343 µm²) as compared to CTL (2342 ± 367 µm²) ($p<0.05$, Student's t-test) (Fig. 3*C*). Moreover, HLUI mice also presented changes in type IIa myofibers CSA distribution in favor of smaller CSA clusters (<1800 µm²) ($p<0.05$, Chi-square) (Fig. 3*C*). Similarly, type IIb myofibers CSA was decreased in HLUI mouse *TA* (2864 ± 474 µm²) as compared to CTL (3724 ± 555 µm²) ($p<0.05$, Student's t-test) (Fig. 3*D*) and type IIb myofibers CSA distribution in HLUI mice shifted towards small and intermediate clusters (<3000 µm²) ($p<0.001$, Chi-square) (Fig. 3*D*). HLUI did not impact significantly type I and unstained myofibers CSA but we highlighted changes in unstained fibers CSA distribution ($p<0.001$, Chi-square) (Supplemental Fig. *S4*)

As concerns myofibers type proportion, CTL *TA* muscle present 1.3 ± 0.8% of type I, 24.4 ± 5.3 % of type IIa, 53.6 ± 9 % of type IIb and 20.6 ± 9 % of unstained (IIx) myofibers. Importantly, type I myofiber percentage was found significantly reduced in HLUI mice *TA* muscles (0.4 ± 0.4 %) ($p<0.05$, Student's t-test) whereas type IIa (20.5 ± 10.6 %), type IIb (52.5 ± 11.8 %) and type IIx (26.6 ± 8.8%) myofibers proportions were unchanged (Fig. 3*E*, Supplemental. Table *S3*). This is consistent with the analysis of double positive fibers that showed that almost the totality of $MyH7^+$ (Cy5-stained, type I myofibers) in the *TA* muscle of HLUI mice (94.7 ± 11.9%) are also $MyH2^+$ (FITC-stained, type IIa myofibers). In the CTL group, the corresponding mean percentage was only of 67.2 ± 18.7% ($p<0.05$, Student's t-test) (Fig. 3*F*). Those results suggest that HLUI is accompanied by a slow-to-fast myofiber transition induced by HLUI in the *TA* muscle.

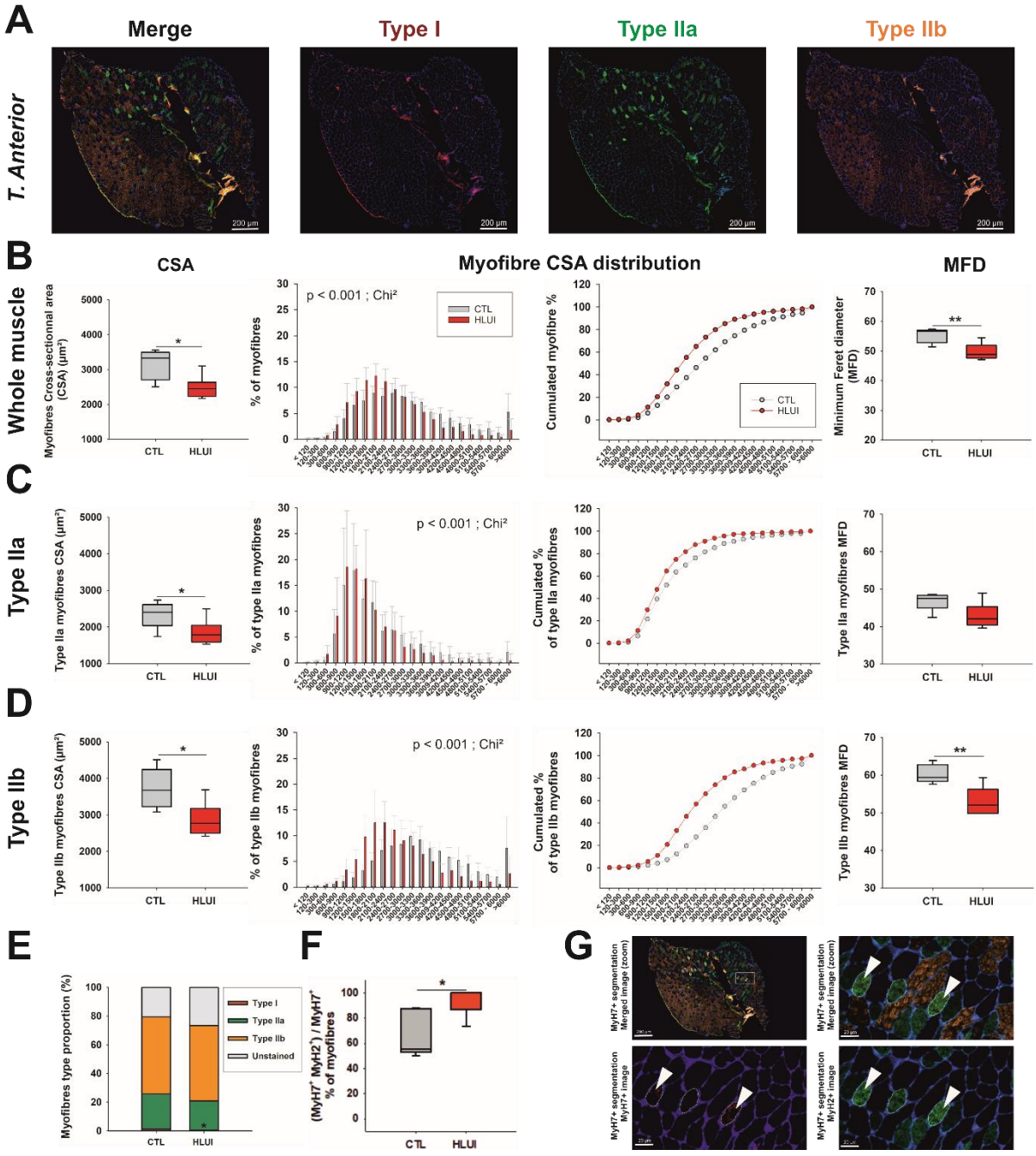

Figure 3. Effects of HLUI-mediated muscle disuse in mice *Tibialis Anterior* are fiber-type dependant.

Cross-sectional Area (CSA), myofiber CSA distribution and Feret's diameter were measured following type I, IIa and IIb immunofluorescence detection and morphometrical analysis were performed with *Cellpose* and *Image J* softwares. **(A) Representative fields**. **(Left)** CSA was measured in all fibers **(B)**, in type IIa **(C)**, and in type IIb fibers **(D)**. Data represented as boxplot; *: p<0.05, *CTL(n=5) vs HLUI(n=5)*, Student's t-test. **(Center)** Myofibers were classified in clusters according to their CSA (µm²). All fibers **(B)**, type IIa fibers **(C)**, and in type IIb fibers **(D)**. Data represented as mean ± SD. *CTL(n=5) vs HLUI(n=5)*, Chi-square. Cumulative percentages of myofibers in clusters in all fibers **(B)**, in type IIa **(C)**, and in type IIb fibers **(D). (Right)** Minimim Feret's diameter (MFD) was measured in all fibers **(B)**, in type IIa **(C)**, and in type IIb fibers **(D).** Data represented as boxplot; **: p<0.01, *CTL(n=5) vs HLUI(n=5)*, Student's t-test. **(E) Myofibers type proportions**. Data represented as stacked bars; *: p<0.05 Student's t-test. **(F) Percentage of type I myofibers also positive for IIa myofibers markers.** Data represented as boxplot; *: p<0.05, *CTL(n=5) vs HLUI(n=5)*, Student's t-test. **(G) Representative field showing hybrid (I/IIa) myofiber detection.** White arrow: Hybrid (I/IIa) myofibers.

Moderate muscle disuse in mice modifies plasmatic ApN oligomer distribution.

The expression of *Adipoq* (encoding ApN) was not significantly modified by HLUI, either in the *Soleus* or the *TA* muscles. However, we noticed that *Adipoq* expression tends to be higher but also more variable in HLUI *TA* muscles than in the CTL group (Fig. 4*A*).

Interestingly, ApN plasmatic level was increased in HLUI mice (11.73 ± 1.73 µg/ml) as compared to CTL (10.02 ± 1.70 µg/ml) ($p<0.05$, Student's t-test) (Fig. 4*B*). This increase is associated with modifications in ApN oligomer distribution in the plasma (Fig 4*C-E*). Indeed, although the SA Index (Fig. 4*C*) and HMW ApN circulating forms were not significantly modified by HLUI (Fig. 4*E)*, the proportion of LMW circulating forms was reduced in HLUI mice (40.52 ± 6.87%) as compared to CTL (50.79 ± 3.36%) ($p<0.05$, Student's t-test) (Fig. 4*E*). In contrast, the proportion of MMW ApN forms was increased (40.71 ± 3.77%) when compared with CTL (34.23 ± 4.27%) ($p<0.05$, Student's t-test) (Fig. 4*E*).

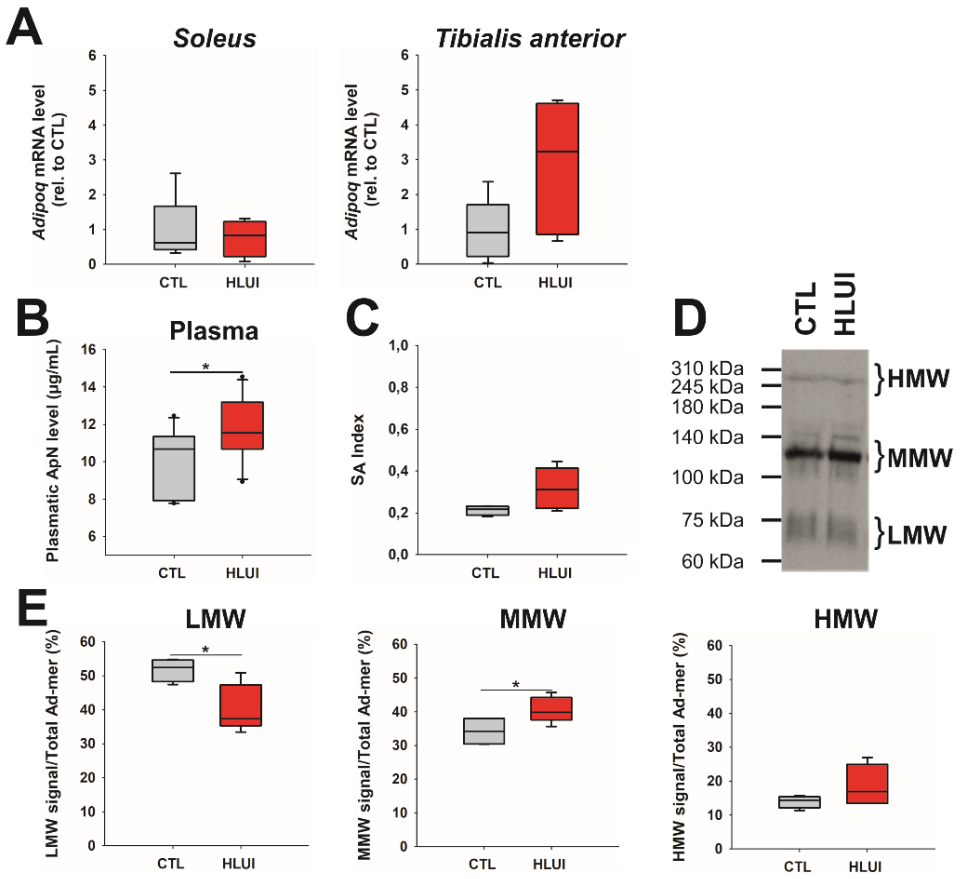

Figure 4. HLUI-mediated muscle disuse in mice modify plasmatic ApN oligomer distribution.

(A) *Adipoq* mRNA levels were assessed in *Soleus* and *Tibialis Anterior* hindlimb muscles of CTL and HLUI mice by RTqPCR with ΔΔCt method (housekeeping gene: *Rplp0*; data normalized to CTL). Data represented as boxplot, *CTL(n=6) vs HLUI(n=5)*, Student's t-test: NS. **(B) Plasmatic ApN levels** were measured by ELISA in the plasma of CTL and HLUI mice. Data represented as boxplot; *: $p<0.05$, *CTL(n=10) vs HLUI(n=11)*, Student's t-test. **(C-E) Plasmatic ApN oligomers.** The proportion of high (HMW), Medium (MMW) and Low (LMW) molecular weight ApN oligomers were determined using non-denaturant PAGE-SDS followed by a western blot **(C) SA Index** corresponds to the ratio HMW/(LMW+MMW+HMW). Data represented as boxplot; *CTL(n=4) vs HLUI(n=5)*, Student's t-test: NS. **(D) Representative blot. (E) ApN oligomers distribution.** Densitometric analyses were performed with *Image J* software. Each ApN form signal was normalized on the Ponceau Red signal and then reported as a percentage of the total ApN signal. Data represented as boxplot; *: $p<0.05$, *CTL(n=4) vs HLUI(n=5)*, Student's t-test.

The effect of muscle disuse on ApN (co)receptors expression depends on muscle type.

Here, we investigated ApN pathway (co)receptors expression at the mRNA and protein levels in HLUI-induced disused muscles. Globally, the data indicate that the effect of muscle disuse differs in slow-twitch *Soleus* (Fig. 5*A-B*) and fast-twitch *TA* muscles (Fig. 5*C-D*). Indeed, HLUI in mouse *Soleus* was associated with a decrease in *Adipor1* (0.47 ± 0.14), *Adipor2* (0.38 ± 0.11) and *Cdh13* (0.53 ± 0.17) mRNA levels as compared to CTL ($p<0.01$, Student's t-test) (Fig. 5*A*). At the protein level, the decreased Adipor1 protein level was not statistically significant in the *Soleus* of HLUI mice (24.25 ± 23.32) as compared to CTL (38.65 ± 11.42) (Student's t-test) and we observed relatively high variability in the HLUI group. *Adipor2* expression decline is consistent with the significant decrease of Adipor2 protein level (30.11 ± 7.13) as compared to CTL mice (49.30 ± 13.50) ($p<0.05$, Student's t-test) (Fig. 5*B*). As concerns the co-receptor t-cadherin, the immunodetection on Western blot allowed us to detect two bands corresponding to t-cadherin with (130kDa) and without (100kDa) its prodomain, as described in (23, 51). Densitometric analysis indicated that the total amount of t-cadherin was increased in disused *Soleus* muscles (28.50 ± 9.51) as compared to CTL (18.34 ± 5.33) ($p<0.05$, Student's t-test) (Fig. 5*B*). This difference was observed for the 100kDa form ($p<0.05$, Student's t-test) and was at the limit of statistical significance for the 130kDa form ($p=0.057$, Student's t-test) (Supplemental Fig. S*5*).

Contrary to data obtained in the *Soleus* muscle, HLUI in mouse *TA* is not associated with modifications of ApN (co)receptor expression, neither at the mRNA, nor at protein levels (Fig. 5*C-D* and Supplemental Fig. S*6*).

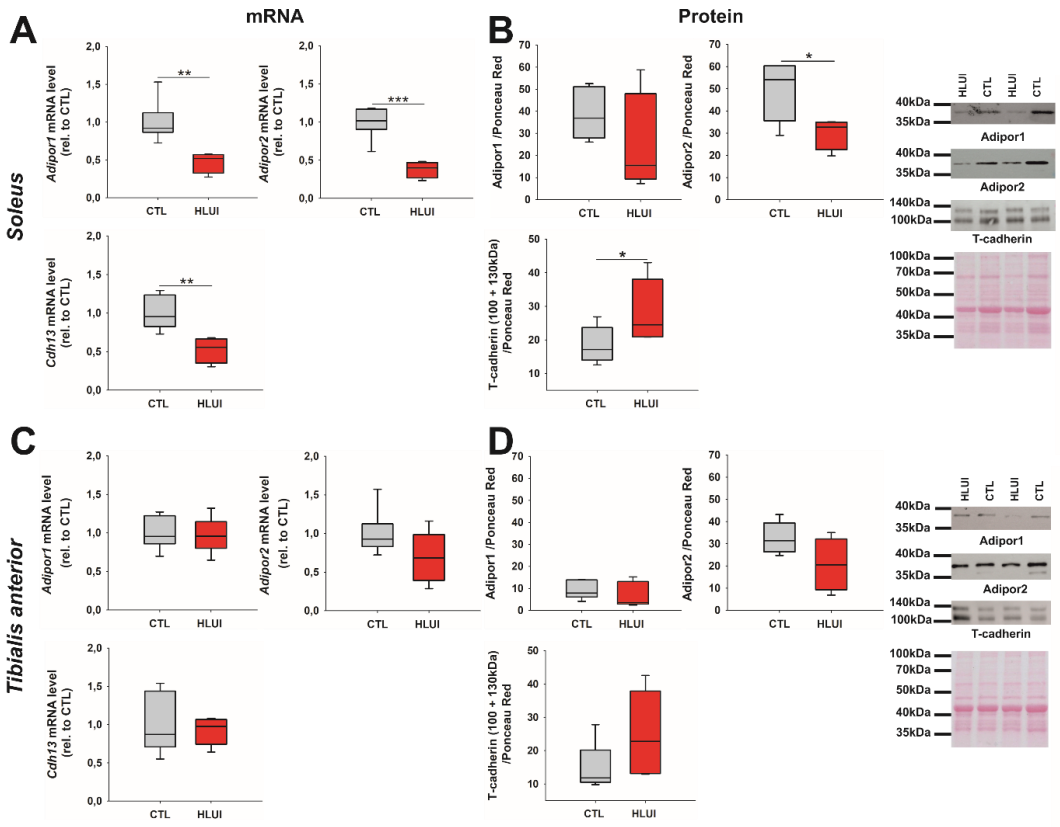

Figure 5. The protein level of AdipoR in skeletal muscle is affected by DMA but this effect depends on muscle type. Adiporeceptors mRNA **(A-C)** and protein levels **(B-D)** were assessed in **(A-B)** the *Soleus* slow-twitch muscle and **(C-D)** the *Tibialis Anterior* fast-twitch muscle. **(A-C)** *Adipor1, Adipor2* and *Cdh13* mRNA levels were *assessed* by RTqPCR with ΔΔCt method (housekeeping gene: *Rplp0*; data normalized to CTL). Data represented as boxplot; **: $p<0.01$, ***: $p<0.001$, *CTL(n=6) vs HLUI(n=5)*, Student's t-test. **(B-D)** Adipor1, Adipor2 and T-cadherin protein levels were determined using denaturant PAGE-SDS followed by a western blot. Densitometric analyses were performed with the *Image J* software. Signal was normalized on Ponceau Red. Data represented as boxplot; *: $p<0.05$, *CTL(n=7) vs HLUI(n=5)*, Student's t-test **Right,** representative blots.

DISCUSSION

Hindlimb Unloading models are widely used to mimic muscle disuse in rodents (4, 44, 52). Here, this model was coupled with hindlimb immobilization and optimized to reduce mouse stress (acclimatization period, social interactions, displacement with forelimbs, …) thus permitting to minimize bias in assessing disuse-mediated muscle effects. These optimizations successfully limited b.w. loss in HLUI mice as compared to other studies in hindlimb unloading rodent models (53, 54). B.w parameter being important to control throughout HLUI experiments to avoid confounding factors. Indeed, b. w. loss is known to be associated with an activation of muscle proteolysis pathways (55, 56) and to modify ApN pathway components.

Evaluation of the disuse-mediated alterations in hindlimb muscles indicates that 14 days of HLUI affect differently the slow twitch *Soleus* muscle and the fast twitch *TA* muscle.
In the *Soleus* muscle, HLUI has a moderate effect, mostly affecting type IIa myofiber distribution by a shift towards smaller CSA. Since the disuse-mediated slow-to fast myofiber switch has been largely described (4, 5, 7, 19), we investigated myofiber-type proportions and found that this parameter was unchanged in the *Soleus* muscle of HLUI mice. However, we observed an increased proportion of type I fibers that are also positive for the type IIa marker. Since these hybrid I/IIa myofibers are known to be implicated in fiber-type transitioning (57, 58), this suggests an ongoing switch from type I to type IIa myofibers in the HLUI *Soleus* muscle. It is commonly reported that 14 days of Hindlimb Unloading (HLU) provoke a significative decrease in myofibers CSA associated with a slow-to-fast transition in the antigravitational *Soleus* muscle (4, 6, 59). Here, the moderated effect of disuse in the *Soleus* muscle could be explained by the positioning of the *Soleus* during immobilization. Indeed, in our experimental condition, mouse ankles are in a neutral position, close to the dorsiflexed position, the plantarflexion being commonly considered “unnatural”. Ankle joint immobilization in the dorsiflexal position stretches the *Soleus* muscle, a condition associated with less severe atrophy than shortened muscles, due to persistent isometric contractions (60–62). This could contribute to a delayed slow-to-fast myofiber switch in the *Soleus* muscle upon HLUI, this muscle being likely in a transitioning state.
In the *TA* muscle, HLUI has a stronger effect, and affects both type IIa and type IIb myofibers CSA. HLUI *TA* muscles also present evidence of a slow-to-fast myofibers switch. Indeed, the proportion of type I myofibers is clearly reduced by disuse, and the majority of type I myofibers in HLUI *TA* muscles are also positive for the type IIa marker. Conversely to the *Soleus*, ankle joint immobilization in HLUI mice shortened the *TA* muscle, a position known to maximize atrophy development (62).

Given the myoprotective effects of ApN (21, 28–30), we investigated whether muscle deconditioning is accompanied by alterations of its plasmatic level, circulating forms proportions and muscular receptor expression.
At a systemic level, we observed increased levels of ApN in the plasma of HLUI mice as well as disturbances of LMW and MMW circulating form proportions. Increased ApN plasmatic levels were suggested to be implicated in sarcopenia-mediated muscle wasting as higher ApN plasmatic levels are associated with low skeletal muscle mass and higher mortality in elderly people (37, 63). However, this hypothesis was rejected by C. Walowski *et al.*, who suggested that muscle mass loss is not causally related to ApN in old adults. The authors attribute “the ApN paradox” to an age-related decrease of Insulin-like Growth Factor (IGF-1), negatively associated to ApN plasmatic level (38). Conversely, plasmatic ApN is decreased in *mdx* mice (a model of Duchenne Muscular Dystrophy (DMD)) (64). Here, several factors may contribute to the increased ApN plasmatic levels, but *Adipoq* expression levels are not significantly modified in the disused muscles, suggesting a modification of its secretion by other secretory organs such as adipose tissue. Potential modifications in *Adipoq* post-transcriptional processes in HLUI mouse muscles cannot be excluded. Since ApN circulating forms do not interconvert

in plasma (65), the observed decrease in LMW proportion in favor of MMW in HLUI plasma is probably the result of variations of ApN post-translational modifications upon disuse.

Even if ApN plasmatic level increases upon disuse, our results suggest an ApN resistance in the *Soleus* muscle. Indeed, *Adipor1, Adipor2* and *Cdh13* expressions are downregulated in HLUI *Soleus* muscle as compared to controls. Accordingly, Goto *et al.* observed a similar decline in *Adipor1* but not in *Adipor2* mRNA levels in the *Soleus* muscle after 14 days of HLU without immobilization (41). Moreover, they demonstrated that functional overloading and muscle regrowth following HLU is accompanied by an upregulation of *Adipor1* mRNA levels, thus highlighting a link between mechanical loading and ApN pathway regulation (41). On the other hand, *Adipor1* and *Adipor2* mRNA down-regulation may also result from a disuse-mediated hyperinsulinemia (66–69) as *Adipor1* and *Adipor2* mRNA expression were reported inversely regulated by insulin in physiological conditions, via Phosphoinositide 3-kinase/Foxo1 dependent pathways (70). However, *Adipor1, Adipor2* and *Cdh13* expressions were found unchanged in HLUI mice *TA* muscles. Although hyperinsulinemia was not directly assessed in our study, we can reasonably assume that if present, such hyperinsulinemia would have affected *Adipor1, Adipor2* and *Cdh13* mRNA levels in the *TA* muscle.

Moreover, the HLUI-mediated adiporeceptor down-regulation is associated with decreased levels of Adipor2 protein level in the *Soleus* muscle. Adipor1 protein level also tends to decrease with HLUI but we notice a higher inter-individual variability. Such alterations in AdipoR protein level can prevent ApN biological activities. Indeed, the Adipor1/AMPK/SIRT1/PGC1α axis (71) was reported as essential for the maintenance of type I myofibers and oxidative metabolism (21). Consequently, this suggests that this decreased adiporeceptor protein level is involved in the slow-to-fast myofiber switch occurring in the *Soleus* muscle of HLUI mice. Furthermore, the resulting disuse-mediated PGC1α hypoactivation may limit its repressive action on FoxO3, a transcription factor that promotes the expression of the MAFbx Ubiquitines Ligases (Atrogin 1) implicated in myofiber atrophy (4, 42, 72). The consequences of a downregulation of AdipoR2 are unclear as this receptor has been poorly studied in skeletal muscle due to its reduced abundance in this tissue compared to AdipoR1. However, AdipoR2 activation by ApN is known to activate the expression of PPARs ligands, thus stimulating glucose and lipid homeostasis (20, 73, 74). AdipoR2 protein level reduction in HLUI *Soleus* muscles could thus have consequences at the metabolic level. Interestingly, despite *Cdh13* mRNA decrease by disuse, t-cadherin protein level appears increased in the *Soleus* muscle. Such an increase in t-cadherin protein level is consistent with the elevated ApN plasmatic level as t-cadherin protein, but not *Cdh13* mRNA, is known to be increased by ApN in endothelial cells *in vivo* and *in vitro* via the suppression of an endogenous GPI phospholipase D implicated in t-cadherin cleavage (24). It is now well established that t-cadherin acts locally to maintain ApN at the myofiber membrane. However, t-cadherin has no transmembrane domain and is then unable to activate intracellular pathways by itself (23, 51).

Contrary to the *Soleus*, Adipor1, Adipor2 and t-cadherin protein levels appear unaffected by the disuse in the *TA* muscle. Such results are consistent with the absence of modifications in ApN (co)receptors expression in this muscle. Disuse-mediated ApN pathway alterations are thus rather muscle-type dependent than related to the severity of muscle atrophy. Our data therefore highlight the necessity to better understand fiber-type specific alterations of adiporeceptors in muscle disuse. In prospect of our study, potential change in adiporeceptors membrane location, internalization rate and recycling (75, 76), as well as the presence of AdipoR homo- and hetero-dimers (77, 78) have also to be better deciphered in this pathological context as factors influencing ApN effects (75–78).

Conclusions

In conclusion, HLUI in mice induces a fiber-type-dependent atrophy accompanied by a type I/IIa myofiber switch. Muscle activity in physiological conditions (anti-gravity *vs* running) and positioning during immobilization (stretched *vs* shortened) constitute additional factors influencing the kinetics of disuse consequences. Muscle alterations occur concomitantly with an elevation of ApN plasmatic level,

disturbances in oligomeric form proportion, and muscle-type dependent alterations in adiporeceptor expression. Further studies are now needed to determine whether the observed ApN pathway changes upon disuse participates to a vicious cycle reinforcing muscle dysfunction in this pathological context.

DATA AVAILABILITY

All data supporting the findings of this study are available within the article and its Supplementary Material.

SUPPLEMENTAL MATERIAL

Table 1. Primary and secondary antibody cocktails used in myofiber type immunofluorescence staining.

Table 2. Mouse primers used in RTqPCR analysis.

Table 3. Effect of the HLUI-mediated disuse on myofiber-type proportions in the slow twitch *Soleus* and the fast twitch *TA* muscles.

Suppl. Fig 1. Food consumption assessment in CTL and HLUI mice.

Suppl. Fig 2. Early effects of HLUI on *Fbxo 32* expression.

Suppl. Fig 3. Effects of moderate muscle disuse in mice *Soleus* type IIb fibers.

Suppl. Fig 4. Effects of moderate muscle disuse in mice *TA* type I and unstained fibers.

Suppl. Fig 5. Mature (100kDa) and pro-domain bearing (130kDa) t-cadherin protein levels and corresponding western blot immunodetection and Red Ponceau in the *Soleus* muscle.

Suppl. Fig 6. Mature (100kDa) and pro-domain bearing (130kDa) t-cadherin protein level and corresponding western blot immunodetection and Red Ponceau in the *TA* muscle.

Suppl. Fig 7. Early effects of HLUI on bodyweight evolution and *Fbxo 32* expression.

Suppl. Fig 8. Adiponectin circulating forms western blot immunodetection and corresponding Red Ponceau.

Suppl. Fig 9. Adipor1 western blot immunodetection and corresponding Red Ponceau in (A) *Soleus* and (B) *Tibialis Anterior* muscles.

Suppl. Fig 10. Adipor1 western blot immunodetection and corresponding Red Ponceau in (A) *Soleus* and (B) *Tibialis Anterior* muscles.

ACKNOWLEDGMENTS

We thank Bernard Blairon for his technical assistance during the conception and the optimization of the Hindlimb Unloading setup. We also thank Sarah Hennuy, Jérôme Francq and the Dv Sylviane Michel for their precious advice and suggestions regarding animal welfare during the optimization of the HLUI model and all through the protocols.

GRANTS

S.S., holds a FRIA doctoral fellowship (FC 41735) from the National Fund for Scientific Research (F.R.S-F.N.R. S), Belgium. The authors acknowledge funding from FRMH (Fonds pour la Recherche Médicale en Hainaut (Grant call 2015) and ABMM-téléthon (Grant call 2015).

DISCLOSURES

The authors declare they have no conflict of interest, financial or otherwise.

AUTHOR CONTRIBUTIONS

A.T., A.L., A.E.D., and S.S., conceived and designed research; S.S., M.L., and V.J., performed the experiments; S.S., analyzed data; A.T., and S.S., interpreted results of experiments; A.T., and S.S., prepared figures; A.T., and S.S drafted the manuscript; A.T., S.S., A.L., A.E.D., M.L., and V.J., edited and revised manuscript; A.T., S.S., A.L., A.E.D., M.L., and V.J., approved final version of manuscript.

REFERENCES

1. **Atherton PJ**, **Greenhaff PL**, **Phillips SM**, **Bodine SC**, **Adams CM**, **Lang CH**. Control of skeletal muscle atrophy in response to disuse: clinical/preclinical contentions and fallacies of evidence. *Am J Physiol Endocrinol Metab* 311: E594-604, 2016. doi: 10.1152/ajpendo.00257.2016.

2. **Nunes EA**, **Stokes T**, **McKendry J**, **Currier BS**, **Phillips SM**. Disuse-induced skeletal muscle atrophy in disease and nondisease states in humans: mechanisms, prevention, and recovery strategies. *American Journal of Physiology-Cell Physiology* 322: C1068–C1084, 2022. doi: 10.1152/ajpcell.00425.2021.

3. **Gao Y**, **Arfat Y**, **Wang H**, **Goswami N**. Muscle Atrophy Induced by Mechanical Unloading: Mechanisms and Potential Countermeasures. *Front Physiol* 9: 235, 2018. doi: 10.3389/fphys.2018.00235.

4. **Bodine SC**. Disuse-induced muscle wasting. *The International Journal of Biochemistry & Cell Biology* 45: 2200–2208, 2013. doi: 10.1016/j.biocel.2013.06.011.

5. **Shenkman BS**. From Slow to Fast: Hypogravity-Induced Remodeling of Muscle Fiber Myosin Phenotype. *Acta Naturae* 8: 47–59, 2016.

6. **Wang J**, **Wang F**, **Zhang P**, **Liu H**, **He J**, **Zhang C**, **Fan M**, **Chen X**. PGC-1α over-expression suppresses the skeletal muscle atrophy and myofiber-type composition during hindlimb unloading. *Bioscience, Biotechnology, and Biochemistry* 81: 500–513, 2017. doi: 10.1080/09168451.2016.1254531.

7. **Baehr LM**, **Hughes DC**, **Waddell DS**, **Bodine SC**. SnapShot: Skeletal muscle atrophy. *Cell* 185: 1618-1618.e1, 2022. doi: 10.1016/j.cell.2022.03.028.

8. **Vilchinskaya N**, **Krivoi I**, **Shenkman B**. AMP-Activated Protein Kinase as a Key Trigger for the Disuse-Induced Skeletal Muscle Remodeling. *IJMS* 19: 3558, 2018. doi: 10.3390/ijms19113558.

9. **Baldwin KM**, **Haddad F**, **Pandorf CE**, **Roy RR**, **Edgerton VR**. Alterations in muscle mass and contractile phenotype in response to unloading models: role of transcriptional/pretranslational mechanisms. *Front Physiol* 4, 2013. doi: 10.3389/fphys.2013.00284.

10. **Puthucheary Z**, **Harridge S**, **Hart N**. Skeletal muscle dysfunction in critical care: Wasting, weakness, and rehabilitation strategies: *Critical Care Medicine* 38: S676–S682, 2010. doi: 10.1097/CCM.0b013e3181f2458d.

11. **Boelens YFN**, **Melchers M**, **van Zanten ARH**. Poor physical recovery after critical illness: incidence, features, risk factors, pathophysiology, and evidence-based therapies. *Current Opinion in Critical Care* 28: 409–416, 2022. doi: 10.1097/MCC.0000000000000955.

12. **Dos Santos C**, **Hussain SNA**, **Mathur S**, **Picard M**, **Herridge M**, **Correa J**, **Bain A**, **Guo Y**, **Advani A**, **Advani SL**, **Tomlinson G**, **Katzberg H**, **Streutker CJ**, **Cameron JI**, **Schols A**, **Gosker HR**, **Batt J**. Mechanisms of Chronic Muscle Wasting and Dysfunction after an Intensive Care Unit Stay. A Pilot Study. *Am J Respir Crit Care Med* 194: 821–830, 2016. doi: 10.1164/rccm.201512-2344OC.

13. **Cuthbertson BH**, **Roughton S**, **Jenkinson D**, **MacLennan G**, **Vale L**. Quality of life in the five years after intensive care: a cohort study. *Crit Care* 14: R6, 2010. doi: 10.1186/cc8848.

14. **Matsuba Y**, **Goto K**, **Morioka S**, **Naito T**, **Akema T**, **Hashimoto N**, **Sugiura T**, **Ohira Y**, **Beppu M**, **Yoshioka T**. Gravitational unloading inhibits the regenerative potential of atrophied soleus muscle in mice. *Acta Physiologica* 196: 329–339, 2009. doi: 10.1111/j.1748-1716.2008.01943.x.

15. **Arc-Chagnaud C**, **Py G**, **Fovet T**, **Roumanille R**, **Demangel R**, **Pagano AF**, **Delobel P**, **Blanc S**, **Jasmin BJ**, **Blottner D**, **Salanova M**, **Gomez-Cabrera M-C**, **Viña J**, **Brioche T**, **Chopard A**. Evaluation of an Antioxidant and Anti-inflammatory Cocktail Against Human Hypoactivity-Induced Skeletal Muscle Deconditioning. *Front Physiol* 11: 71, 2020. doi: 10.3389/fphys.2020.00071.

16. **Krause MP**, **Liu Y**, **Vu V**, **Chan L**, **Xu A**, **Riddell MC**, **Sweeney G**, **Hawke TJ**. Adiponectin is expressed by skeletal muscle fibers and influences muscle phenotype and function. *American Journal of Physiology-Cell Physiology* 295: C203–C212, 2008. doi: 10.1152/ajpcell.00030.2008.

17. **Krause M**, **Milne K**, **Hawke T**. Adiponectin—Consideration for its Role in Skeletal Muscle Health. *IJMS* 20: 1528, 2019. doi: 10.3390/ijms20071528.

18. **Amin RH**, **Mathews ST**, **Camp HS**, **Ding L**, **Leff T**. Selective activation of PPARγ in skeletal muscle induces endogenous production of adiponectin and protects mice from diet-induced insulin resistance. *American Journal of Physiology-Endocrinology and Metabolism* 298: E28–E37, 2010. doi: 10.1152/ajpendo.00446.2009.

19. **Wang Y**, **Lam KSL**, **Yau M**, **Xu A**. Post-translational modifications of adiponectin: mechanisms and functional implications. *Biochem J* 409: 623–633, 2008. doi: 10.1042/BJ20071492.

20. **Yamauchi T**, **Iwabu M**, **Okada-Iwabu M**, **Kadowaki T**. Adiponectin receptors: A review of their structure, function and how they work. *Best Practice & Research Clinical Endocrinology & Metabolism* 28: 15–23, 2014. doi: 10.1016/j.beem.2013.09.003.

21. **Iwabu M**, **Yamauchi T**, **Okada-Iwabu M**, **Sato K**, **Nakagawa T**, **Funata M**, **Yamaguchi M**, **Namiki S**, **Nakayama R**, **Tabata M**, **Ogata H**, **Kubota N**, **Takamoto I**, **Hayashi YK**, **Yamauchi N**, **Waki H**, **Fukayama M**, **Nishino I**, **Tokuyama K**, **Ueki K**, **Oike Y**, **Ishii S**, **Hirose K**, **Shimizu T**, **Touhara K**, **Kadowaki T**. Adiponectin and AdipoR1 regulate PGC-1α and mitochondria by Ca2+ and AMPK/SIRT1. *Nature* 464: 1313–1319, 2010. doi: 10.1038/nature08991.

22. **Denzel MS**, **Scimia M-C**, **Zumstein PM**, **Walsh K**, **Ruiz-Lozano P**, **Ranscht B**. T-cadherin is critical for adiponectin-mediated cardioprotection in mice. *J Clin Invest* 120: 4342–4352, 2010. doi: 10.1172/JCI43464.

23. **Tanaka Y**, **Kita S**, **Nishizawa H**, **Fukuda S**, **Fujishima Y**, **Obata Y**, **Nagao H**, **Masuda S**, **Nakamura Y**, **Shimizu Y**, **Mineo R**, **Natsukawa T**, **Funahashi T**, **Ranscht B**, **Fukada S**, **Maeda N**, **Shimomura I**. Adiponectin promotes muscle regeneration through binding to T-cadherin. *Sci Rep* 9: 16, 2019. doi: 10.1038/s41598-018-37115-3.

24. **Matsuda K**, **Fujishima Y**, **Maeda N**, **Mori T**, **Hirata A**, **Sekimoto R**, **Tsushima Y**, **Masuda S**, **Yamaoka M**, **Inoue K**, **Nishizawa H**, **Kita S**, **Ranscht B**, **Funahashi T**, **Shimomura I**. Positive Feedback Regulation Between Adiponectin and T-Cadherin Impacts Adiponectin Levels in Tissue and Plasma of Male Mice. *Endocrinology* 156: 934–946, 2015. doi: 10.1210/en.2014-1618.

25. **Kadowaki T**, **Yamauchi T**, **Kubota N**, **Hara K**, **Ueki K**, **Tobe K**. Adiponectin and adiponectin receptors in insulin resistance, diabetes, and the metabolic syndrome. *J Clin Invest* 116: 1784–1792, 2006. doi: 10.1172/JCI29126.

26. **Liu Y**, **Palanivel R**, **Rai E**, **Park M**, **Gabor TV**, **Scheid MP**, **Xu A**, **Sweeney G**. Adiponectin Stimulates Autophagy and Reduces Oxidative Stress to Enhance Insulin Sensitivity During High-Fat Diet Feeding in Mice. *Diabetes* 64: 36–48, 2015. doi: 10.2337/db14-0267.

27. **Tian L**, **Luo N**, **Zhu X**, **Chung B-H**, **Garvey WT**, **Fu Y**. Adiponectin-AdipoR1/2-APPL1 signaling axis suppresses human foam cell formation: Differential ability of AdipoR1 and AdipoR2 to regulate inflammatory cytokine responses. *Atherosclerosis* 221: 66–75, 2012. doi: 10.1016/j.atherosclerosis.2011.12.014.

28. **Abou-Samra M**, **Selvais CM**, **Dubuisson N**, **Brichard SM**. Adiponectin and Its Mimics on Skeletal Muscle: Insulin Sensitizers, Fat Burners, Exercise Mimickers, Muscling Pills … or Everything Together? *IJMS* 21: 2620, 2020. doi: 10.3390/ijms21072620.

29. **Jiang Q**, **Cheng X**, **Cui Y**, **Xia Q**, **Yan X**, **Zhang M**, **Lan G**, **Liu J**, **Shan T**, **Huang Y**. Resveratrol regulates skeletal muscle fibers switching through the AdipoR1-AMPK-PGC-1α pathway. *Food Funct* 10: 3334–3343, 2019. doi: 10.1039/c8fo02518e.

30. **Abou-Samra M**, **Selvais CM**, **Boursereau R**, **Lecompte S**, **Noel L**, **Brichard SM**. ADIPORON , a new therapeutic prospect for Duchenne muscular dystrophy. *Journal of Cachexia, Sarcopenia and Muscle* 11: 518–533, 2020. doi: 10.1002/jcsm.12531.

31. **Waki H**, **Yamauchi T**, **Kamon J**, **Kita S**, **Ito Y**, **Hada Y**, **Uchida S**, **Tsuchida A**, **Takekawa S**, **Kadowaki T**. Generation of Globular Fragment of Adiponectin by Leukocyte Elastase Secreted by Monocytic Cell Line THP-1. *Endocrinology* 146: 790–796, 2005. doi: 10.1210/en.2004-1096.

32. **Fiaschi T**, **Giannoni E**, **Taddei ML**, **Chiarugi P**. Globular Adiponectin Activates Motility and Regenerative Traits of Muscle Satellite Cells. *PLoS ONE* 7: e34782, 2012. doi: 10.1371/journal.pone.0034782.

33. **Fiaschi T**, **Cirelli D**, **Comito G**, **Gelmini S**, **Ramponi G**, **Serio M**, **Chiarugi P**. Globular adiponectin induces differentiation and fusion of skeletal muscle cells. *Cell Res* 19: 584–597, 2009. doi: 10.1038/cr.2009.39.

34. **Fiaschi T**, **Magherini F**, **Gamberi T**, **Modesti PA**, **Modesti A**. Adiponectin as a tissue regenerating hormone: more than a metabolic function. *Cell Mol Life Sci* 71: 1917–1925, 2014. doi: 10.1007/s00018-013-1537-4.

35. **Gamberi T**, **Modesti A**, **Magherini F**, **D'Souza DM**, **Hawke T**, **Fiaschi T**. Activation of autophagy by globular adiponectin is required for muscle differentiation. *Biochimica et Biophysica Acta (BBA) - Molecular Cell Research* 1863: 694–702, 2016. doi: 10.1016/j.bbamcr.2016.01.016.

36. **Obata Y**, **Kita S**, **Koyama Y**, **Fukuda S**, **Takeda H**, **Takahashi M**, **Fujishima Y**, **Nagao H**, **Masuda S**, **Tanaka Y**, **Nakamura Y**, **Nishizawa H**, **Funahashi T**, **Ranscht B**, **Izumi Y**, **Bamba T**, **Fukusaki E**, **Hanayama R**, **Shimada S**, **Maeda N**, **Shimomura I**. Adiponectin/T-cadherin system enhances exosome biogenesis and decreases cellular ceramides by exosomal release. *JCI Insight* 3: e99680, 2018. doi: 10.1172/jci.insight.99680.

37. **Baker JF**, **Newman AB**, **Kanaya A**, **Leonard MB**, **Zemel B**, **Miljkovic I**, **Long J**, **Weber D**, **Harris TB**. The Adiponectin Paradox in the Elderly: Associations With Body Composition, Physical Functioning, and Mortality. *The Journals of Gerontology: Series A* 74: 247–253, 2019. doi: 10.1093/gerona/gly017.

38. **Walowski CO**, **Herpich C**, **Enderle J**, **Braun W**, **Both M**, **Hasler M**, **Müller MJ**, **Norman K**, **Bosy-Westphal A**. Analysis of the adiponectin paradox in healthy older people. *J cachexia sarcopenia muscle* 14: 270–278, 2023. doi: 10.1002/jcsm.13127.

39. **Balasubramanian P**, **Schaar AE**, **Gustafson GE**, **Smith AB**, **Howell PR**, **Greenman A**, **Baum S**, **Colman RJ**, **Lamming DW**, **Diffee GM**, **Anderson RM**. Adiponectin receptor agonist AdipoRon improves skeletal muscle function in aged mice. *eLife* 11: e71282, 2022. doi: 10.7554/eLife.71282.

40. **Singh AK**, **Shree S**, **Chattopadhyay S**, **Kumar S**, **Gurjar A**, **Kushwaha S**, **Kumar H**, **Trivedi AK**, **Chattopadhyay N**, **Maurya R**, **Ramachandran R**, **Sanyal S**. Small molecule adiponectin receptor agonist GTDF protects against skeletal muscle atrophy. *Molecular and Cellular Endocrinology* 439: 273–285, 2017. doi: 10.1016/j.mce.2016.09.013.

41. **Goto A**, **Ohno Y**, **Ikuta A**, **Suzuki M**, **Ohira T**, **Egawa T**, **Sugiura T**, **Yoshioka T**, **Ohira Y**, **Goto K**. Up-Regulation of Adiponectin Expression in Antigravitational Soleus Muscle in Response to Unloading Followed by Reloading, and Functional Overloading in Mice. *PLoS ONE* 8: e81929, 2013. doi: 10.1371/journal.pone.0081929.

42. **Ciciliot S**, **Rossi AC**, **Dyar KA**, **Blaauw B**, **Schiaffino S**. Muscle type and fiber type specificity in muscle wasting. *The International Journal of Biochemistry & Cell Biology* 45: 2191–2199, 2013. doi: 10.1016/j.biocel.2013.05.016.

43. **Tobias IS**, **Galpin AJ**. Moving human muscle physiology research forward: an evaluation of fiber type-specific protein research methodologies. *American Journal of Physiology-Cell Physiology* 319: C858–C876, 2020. doi: 10.1152/ajpcell.00107.2020.

44. **Marzuca-Nassr GN**, **Vitzel KF**, **Murata GM**, **Márquez JL**, **Curi R**. Experimental Model of HindLimb Suspension-Induced Skeletal Muscle Atrophy in Rodents. *Methods Mol Biol* 1916: 167–176, 2019. doi: 10.1007/978-1-4939-8994-2_16.

45. **Stringer C**, **Wang T**, **Michaelos M**, **Pachitariu M**. Cellpose: a generalist algorithm for cellular segmentation. *Nat Methods* 18: 100–106, 2021. doi: 10.1038/s41592-020-01018-x.

46. **Pachitariu M**, **Stringer C**. Cellpose 2.0: how to train your own model. *Nat Methods* 19: 1634–1641, 2022. doi: 10.1038/s41592-022-01663-4.

47. **Waisman A**, **Norris AM**, **Elías Costa M**, **Kopinke D**. Automatic and unbiased segmentation and quantification of myofibers in skeletal muscle. *Sci Rep* 11: 11793, 2021. doi: 10.1038/s41598-021-91191-6.

48. **Briguet A**, **Courdier-Fruh I**, **Foster M**, **Meier T**, **Magyar JP**. Histological parameters for the quantitative assessment of muscular dystrophy in the mdx-mouse. *Neuromuscular Disorders* 14: 675–682, 2004. doi: 10.1016/j.nmd.2004.06.008.

49. **Pajvani UB**, **Du X**, **Combs TP**, **Berg AH**, **Rajala MW**, **Schulthess T**, **Engel J**, **Brownlee M**, **Scherer PE**. Structure-Function Studies of the Adipocyte-secreted Hormone Acrp30/Adiponectin: IMPLICATIONS FOR METABOLIC REGULATION AND BIOACTIVITY. *J Biol Chem* 278: 9073–9085, 2003. doi: 10.1074/jbc.M207198200.

50. **Bloemberg D**, **Quadrilatero J**. Rapid Determination of Myosin Heavy Chain Expression in Rat, Mouse, and Human Skeletal Muscle Using Multicolor Immunofluorescence Analysis. *PLoS ONE* 7: e35273, 2012. doi: 10.1371/journal.pone.0035273.

51. **Fukuda S**, **Kita S**, **Obata Y**, **Fujishima Y**, **Nagao H**, **Masuda S**, **Tanaka Y**, **Nishizawa H**, **Funahashi T**, **Takagi J**, **Maeda N**, **Shimomura I**. The unique prodomain of T-cadherin plays a key role in adiponectin binding with the essential extracellular cadherin repeats 1 and 2. *Journal of Biological Chemistry* 292: 7840–7849, 2017. doi: 10.1074/jbc.M117.780734.

52. **Morey-Holton E**, **Globus RK**, **Kaplansky A**, **Durnova G**. The hindlimb unloading rat model: literature overview, technique update and comparison with space flight data. *Adv Space Biol Med* 10: 7–40, 2005.

53. **Tousen Y**, **Ichimaru R**, **Kondo T**, **Inada M**, **Miyaura C**, **Ishimi Y**. The Combination of Soy Isoflavones and Resveratrol Preserve Bone Mineral Density in Hindlimb-Unloaded Mice. *Nutrients* 12: 2043, 2020. doi: 10.3390/nu12072043.

54. **Moustafa A**. Hindlimb unloading-induced reproductive suppression via Downregulation of hypothalamic Kiss-1 expression in adult male rats. *Reprod Biol Endocrinol* 19: 37, 2021. doi: 10.1186/s12958-021-00694-4.

55. **Kangalgil M**, **Küçük AO**, **Ulusoy H**, **Özçelik AÖ**. Nutrition determinants of acute skeletal muscle loss in critically ill patients: A prospective observational cohort study. *Nut in Clin Prac* 39: 579–588, 2024. doi: 10.1002/ncp.11086.

56. **Kvedaras M**, **Minderis P**, **Krusnauskas R**, **Ratkevicius A**. Effects of ten-week 30% caloric restriction on metabolic health and skeletal muscles of adult and old C57BL/6J mice. *Mechanisms of Ageing and Development* 190: 111320, 2020. doi: 10.1016/j.mad.2020.111320.

57. **Medler S**. Mixing it up: the biological significance of hybrid skeletal muscle fibers. *Journal of Experimental Biology* 222: jeb200832, 2019. doi: 10.1242/jeb.200832.

58. **Blottner D**, **Hastermann M**, **Weber R**, **Lenz R**, **Gambara G**, **Limper U**, **Rittweger J**, **Bosutti A**, **Degens H**, **Salanova M**. Reactive Jumps Preserve Skeletal Muscle Structure, Phenotype, and Myofiber Oxidative Capacity in Bed Rest. *Front Physiol* 10: 1527, 2020. doi: 10.3389/fphys.2019.01527.

59. **Marzuca-Nassr GN**, **Murata GM**, **Martins AR**, **Vitzel KF**, **Crisma AR**, **Torres RP**, **Mancini-Filho J**, **Kang JX**, **Curi R**. Balanced Diet-Fed Fat-1 Transgenic Mice Exhibit Lower Hindlimb Suspension-Induced Soleus Muscle Atrophy. *Nutrients* 9: 1100, 2017. doi: 10.3390/nu9101100.

60. **Baker JH**, **Matsumoto DE**. Adaptation of skeletal muscle to immobilization in a shortened position. *Muscle and Nerve* 11: 231–244, 1988. doi: 10.1002/mus.880110308.

61. **Goldspink DF**. The influence of immobilization and stretch on protein turnover of rat skeletal muscle. *The Journal of Physiology* 264: 267–282, 1977. doi: 10.1113/jphysiol.1977.sp011667.

62. **Fujita N**, **Fujimoto T**, **Tasaki H**, **Arakawa T**, **Matsubara T**, **Miki A**. Influence of muscle length on muscle atrophy in the mouse tibialis anterior and soleus muscles. *Biomed Res* 30: 39–45, 2009. doi: 10.2220/biomedres.30.39.

63. **Menzaghi C**, **Trischitta V**. The Adiponectin Paradox for All-Cause and Cardiovascular Mortality. *Diabetes* 67: 12–22, 2018. doi: 10.2337/dbi17-0016.

64. **Abou-Samra M**, **Lecompte S**, **Schakman O**, **Noel L**, **Many MC**, **Gailly P**, **Brichard SM**. Involvement of adiponectin in the pathogenesis of dystrophinopathy. *Skeletal Muscle* 5: 25, 2015. doi: 10.1186/s13395-015-0051-9.

65. **Peake PW**, **Kriketos AD**, **Campbell LV**, **Shen Y**, **Charlesworth JA**. The metabolism of isoforms of human adiponectin: studies in human subjects and in experimental animals. *eur j endocrinol* 153: 409–417, 2005. doi: 10.1530/eje.1.01978.

66. **Kakehi S**, **Tamura Y**, **Ikeda S**, **Kaga N**, **Taka H**, **Ueno N**, **Shiuchi T**, **Kubota A**, **Sakuraba K**, **Kawamori R**, **Watada H**. Short-term physical inactivity induces diacylglycerol accumulation and insulin resistance in muscle via lipin1 activation. *American Journal of Physiology-Endocrinology and Metabolism* 321: E766–E781, 2021. doi: 10.1152/ajpendo.00254.2020.

67. **Hamburg NM**, **McMackin CJ**, **Huang AL**, **Shenouda SM**, **Widlansky ME**, **Schulz E**, **Gokce N**, **Ruderman NB**, **Keaney JF**, **Vita JA**. Physical inactivity rapidly induces insulin resistance and microvascular dysfunction in healthy volunteers. *Arterioscler Thromb Vasc Biol* 27: 2650–2656, 2007. doi: 10.1161/ATVBAHA.107.153288.

68. **Mondon CE**, **Rodnick KJ**, **Dolkas CB**, **Azhar S**, **Reaven GM**. Alterations in glucose and protein metabolism in animals subjected to simulated microgravity. *Advances in Space Research* 12: 169–177, 1992. doi: 10.1016/0273-1177(92)90105-7.

69. **Hirose M**, **Kaneki M**, **Sugita H**, **Yasuhara S**, **Martyn JAJ**. Immobilization depresses insulin signaling in skeletal muscle. *American Journal of Physiology-Endocrinology and Metabolism* 279: E1235–E1241, 2000. doi: 10.1152/ajpendo.2000.279.6.E1235.

70. **Tsuchida A**, **Yamauchi T**, **Ito Y**, **Hada Y**, **Maki T**, **Takekawa S**, **Kamon J**, **Kobayashi M**, **Suzuki R**, **Hara K**, **Kubota N**, **Terauchi Y**, **Froguel P**, **Nakae J**, **Kasuga M**, **Accili D**, **Tobe K**, **Ueki K**, **Nagai R**, **Kadowaki T**. Insulin/Foxo1 Pathway Regulates Expression Levels of Adiponectin Receptors and Adiponectin Sensitivity. *J Biol Chem* 279: 30817–30822, 2004. doi: 10.1074/jbc.M402367200.

71. **Yamauchi T**, **Nio Y**, **Maki T**, **Kobayashi M**, **Takazawa T**, **Iwabu M**, **Okada-Iwabu M**, **Kawamoto S**, **Kubota N**, **Kubota T**, **Ito Y**, **Kamon J**, **Tsuchida A**, **Kumagai K**, **Kozono H**, **Hada Y**, **Ogata H**, **Tokuyama K**, **Tsunoda M**, **Ide T**, **Murakami K**, **Awazawa M**, **Takamoto I**, **Froguel P**, **Hara K**, **Tobe K**, **Nagai R**, **Ueki K**, **Kadowaki T**. Targeted

disruption of AdipoR1 and AdipoR2 causes abrogation of adiponectin binding and metabolic actions. *Nat Med* 13: 332–339, 2007. doi: 10.1038/nm1557.

72. **Sandri M**, **Sandri C**, **Gilbert A**, **Skurk C**, **Calabria E**, **Picard A**, **Walsh K**, **Schiaffino S**, **Lecker SH**, **Goldberg AL**. Foxo transcription factors induce the atrophy-related ubiquitin ligase atrogin-1 and cause skeletal muscle atrophy. *Cell* 117: 399–412, 2004. doi: 10.1016/s0092-8674(04)00400-3.

73. **Yamauchi T**, **Kamon J**, **Ito Y**, **Tsuchida A**, **Yokomizo T**, **Kita S**, **Sugiyama T**, **Miyagishi M**, **Hara K**, **Tsunoda M**, **Murakami K**, **Ohteki T**, **Uchida S**, **Takekawa S**, **Waki H**, **Tsuno NH**, **Shibata Y**, **Terauchi Y**, **Froguel P**, **Tobe K**, **Koyasu S**, **Taira K**, **Kitamura T**, **Shimizu T**, **Nagai R**, **Kadowaki T**. Cloning of adiponectin receptors that mediate antidiabetic metabolic effects. *Nature* 423: 762–769, 2003. doi: 10.1038/nature01705.

74. **Yamauchi T**, **Kadowaki T**. Adiponectin Receptor as a Key Player in Healthy Longevity and Obesity-Related Diseases. *Cell Metabolism* 17: 185–196, 2013. doi: 10.1016/j.cmet.2013.01.001.

75. **Buechler C**, **Wanninger J**, **Neumeier M**. Adiponectin receptor binding proteins – recent advances in elucidating adiponectin signalling pathways. *FEBS Letters* 584: 4280–4286, 2010. doi: 10.1016/j.febslet.2010.09.035.

76. **Ding Q**, **Wang Z**, **Chen Y**. Endocytosis of adiponectin receptor 1 through a clathrin- and Rab5-dependent pathway. *Cell Res* 19: 317–327, 2009. doi: 10.1038/cr.2008.299.

77. **Kosel D**, **Heiker JT**, **Juhl C**, **Wottawah CM**, **Blüher M**, **Mörl K**, **Beck-Sickinger AG**. Dimerization of adiponectin receptor 1 is inhibited by adiponectin. *Journal of Cell Science* 123: 1320–1328, 2010. doi: 10.1242/jcs.057919.

78. **Almabouada F**, **Diaz-Ruiz A**, **Rabanal-Ruiz Y**, **Peinado JR**, **Vazquez-Martinez R**, **Malagon MM**. Adiponectin Receptors Form Homomers and Heteromers Exhibiting Distinct Ligand Binding and Intracellular Signaling Properties. *Journal of Biological Chemistry* 288: 3112–3125, 2013. doi: 10.1074/jbc.M112.404624.

Supplemental material

Table 1. Primary and secondary antibody cocktails used in myofiber type immunofluorescence staining.

Primary antibody cocktail				
	Antigen	**Host species/Isotype**	**Dilution**	**RRID**
ab 11575, Abcam	Laminin	Rabbit, IgG	1:50	RRID: AB_298179
BA-D5, DSHB	MyHC 7	Mouse, IgG2b	1:50	RRID: AB_2235587
SC-71, DSHB	MyHC2	Mouse, IgG1	1:100	RRID: AB_2147165
BF-F3, DSHB	MyHC4	Mouse, IgM	1:10	RRID: AB_2266724
Secondary antibody cocktail				
	Antigen	**Host species**	**Dilution**	**RRID**
Alexa 405, (ab175652) Abcam	Rabbit IgG	Goat	1:50	/
Alexa 647, (A-21242) Thermofisher	Mouse IgG2b	Goat	1:100	/
Alexa 488, (A-21121) Thermofisher	Mouse IgG1	Goat	1:100	/
Alexa 555, (A-21426) Thermofisher	Mouse IgM	Goat	1:50	/

Table 2. Mouse primers used in RTqPCR analysis.

Gene	**Sequence**	**Tm**
Rplp0	Fw: GGA-CCC-GAG-AAG-ACC-TCC-TT Rv: GCA-CAT-CAC-TCA-GAA-TTT-CAA-TGG	60°C
Adipoq	Fw: GTT-GCA-AGC-TCT-CCT-GTT-CC Rv: TCT-CCA-GGA-GTG-CCA-TCT-CT	58°C
Adipor1	Fw: TCT-TCG-GGA-TGT-TCT-TCC-TGG Rv: TTT-GGA-AAA-AGT-CCG-AGA-GAC-C	62°C
Adipor2	Fw: CCT-TTC-GGG-CCT-GTT-TTA-AGA Rv: GAG-TGG-CAG-TAC-ACC-GTG-TG	62°C
Cdh13	Fw: GCC-CTC-GTG-AGC-CTT-CTT-C Rv: CAC-CCT-GAG-GTC-CGT-GAT-GT	58°C
Fbxo32	Fw:GCA-AAC-ACT-GCC-ACA-TTC-TCT-C Rv: CTT-GAG-GGG-AAA-GTG-AGA-CG	60°C

Table 3. Effect of the HLUI-mediated disuse on myofiber-type proportions in the slow twitch *Soleus* and the fast twitch *TA* muscles.

	Soleus			**TA**		
	Myofibers proportion (%)		***P* Value**	**Myofibers proportion (%)**		***P* Value**
	CTL	**HLUI**		**CTL**	**HLUI**	
All myofibers	/	/	/	/	/	/
Type I myofibers	35.34 ± 8.24	32.23 ± 4.43	0.48	1.31 ± 0.81	0.39 ± 0.38	0.04*
Type IIa myofibers	63.05 ± 6.21	65.58 ± 4.27	0.46	24.44 ± 5.30	20.52 ± 10.57	0.47
Type IIb myofibers	1.61 ± 2.54	2.19 ± 2.61	0.69	53.61 ± 8.96	52.50 ± 11.75	0.87
Unstained myofibers	/	/	/	20.64 ± 9.03	26.59 ± 8.76	0.29
Hybrid I/IIa myofibers	1.19 ± 0.55	2.83 ± 1.40	0.41	1.84± 0.87	1.30 ± 1.02	0.43

Values are means ± SD; CTL (n=5), HLUI (n=5); (Except in the *Soleus* for type IIb where n=3). CSA, Cross-sectional Area; MFD, Minimum Feret's Diameter; Comparisons made HLUI vs CTL by Student's *t* test or Mann-Whitney Rank Sum test according to the normality assay result.

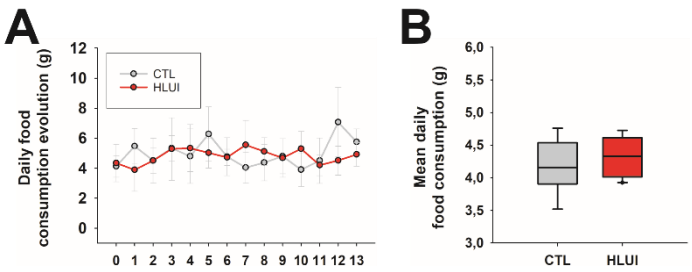

Suppl. Fig 1. Food consumption assessment in CTL and HLUI mice. (A) Food consumption was measured daily. Data plotted as mean ± SD, *CTL(n=10) vs HLUI(n=11)*, ***: p<0.001, Two-way ANOVA repeated measures. **(B)** Mean daily food consumption. Data represented as boxplots; *CTL(n=10) vs HLUI(n=11)*, Student's t-test, NS.

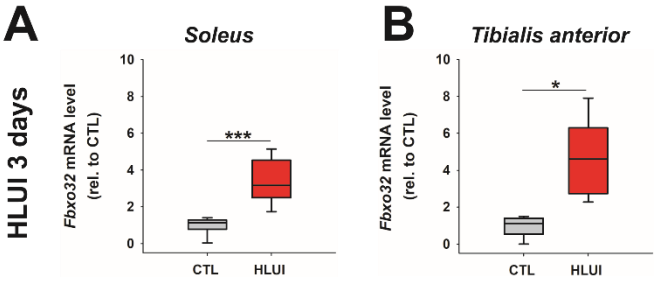

Suppl Fig 2. Early effects of HLUI on *Fbxo 32* expression. *Fbxo 32* mRNA level was assessed in **(A)** the *Soleus* and **(B)** the *Tibialis Anterior* muscles by RTqPCR with ΔΔCt method (housekeeping gene: *Rplp0*; data normalized to CTL). Data represented as boxplot; *: p<0.05; ***: p<0.001; Student's t-test.

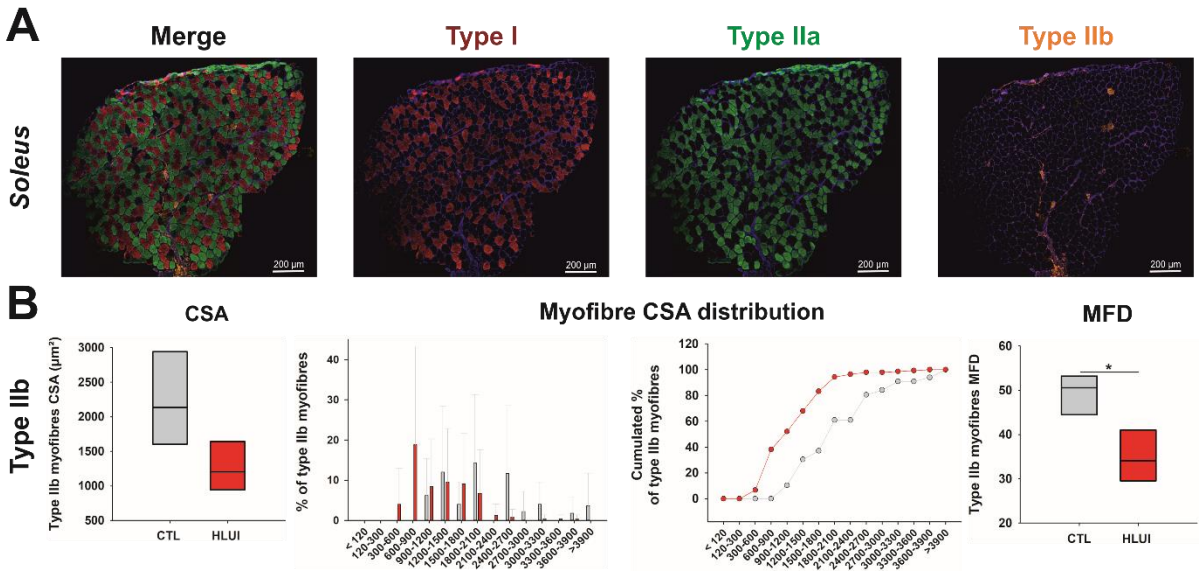

Suppl. Fig 3. Effects of HLUI-mediated muscle disuse in mice *Soleus* type IIb fibers. Cross-sectional Area (CSA), myofiber CSA distribution and Feret's diameter were measured following type I, IIa, and IIb immunofluorescence detection and morphometrical analysis were performed with *Cellpose* and *Image J* software. **(A) Representative fields**. **(B)** CSA was measured in type IIb fibers. Data represented as boxplot, *CTL(n=5) vs HLUI(n=5)*, Student's t-test, NS. **(C)** Type IIb myofibers were classified in clusters according to their CSA (µm²). Data represented as mean ± SD, *CTL(n=5) vs HLUI(n=5)*. Statistical tests have not been performed because of the low number of type IIb fibers in the *soleus* muscle, the Chi-square requiring a minimal number of observations in each cluster. **(D)** Cumulative percentages of type IIb myofibers in CSA clusters. **(E)** Minimum Feret's diameter (MFD) was measured in type IIb fibers. Data represented as boxplot; *: $p<0.05$, *CTL(n=5) vs HLUI(n=5)*, Student's t-test.

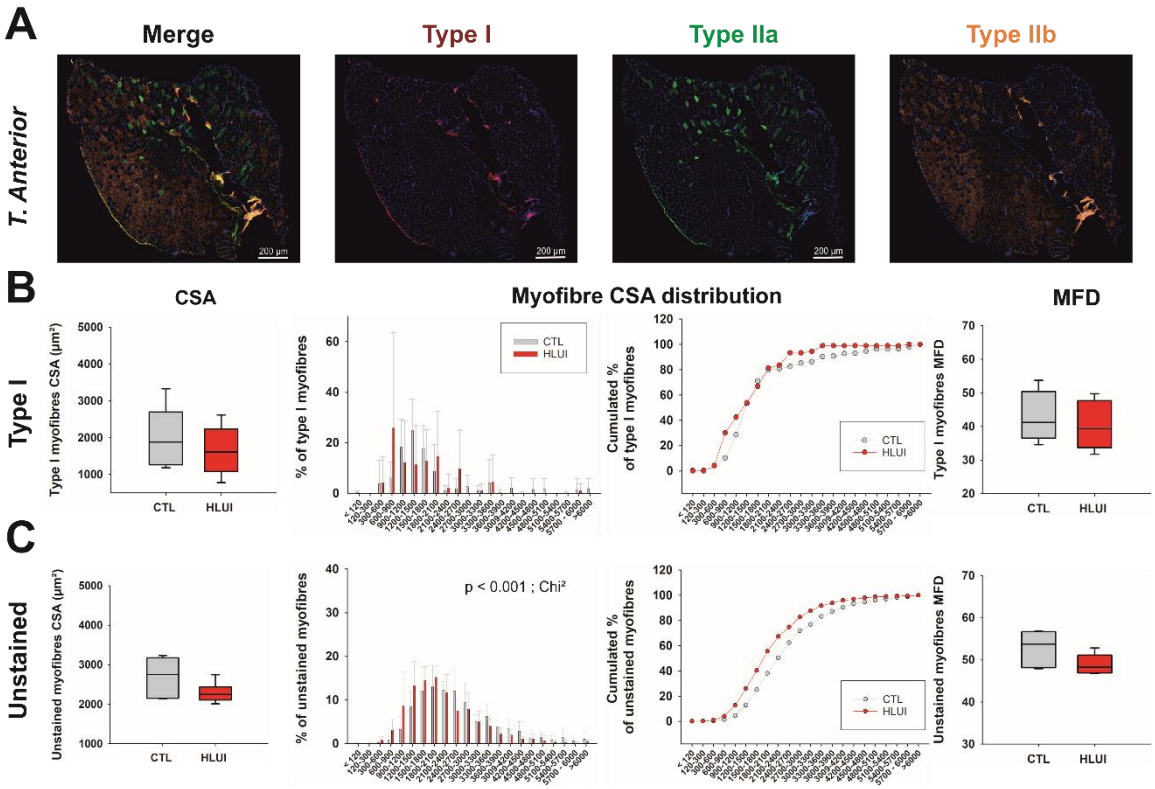

Suppl. Fig 4. Effects of HLUI-mediated muscle disuse in mice *TA* type I and unstained fibers. Cross-sectional Area (CSA), myofiber CSA distribution and Feret's diameter were measured following type I, IIa and IIb immunofluorescence detection and morphometrical analysis were performed with *Cellpose* and *Image J* softwares. **(A) Representative fields**. **(Left)** CSA was measured in type I fibers **(B)** and in unstained fibers **(C)**. Data represented as boxplot, *CTL(n=5) vs HLUI(n=5)*, Student's t-test in type I, Welch's t-test in unstained, NS. **(Center)** Myofibers were classified in clusters according to their CSA (µm²). Type I **(B)** and unstained fibers **(C)**. Data represented as mean ± SD, *CTL(n=5) vs HLUI(n=5)*, Chi-square. Cumulative percentages of myofibers in type I fibers **(B)** and in unstained fibers **(C)**. **(Right)** Minimim Feret's diameter (MFD) was measured in type I fibers **(B)** and in unstained fibers **(C)**. Data represented as boxplot, *CTL(n=5) vs HLUI(n=5)*, Student's t-test in type I, Welch's t-test in unstained, NS.

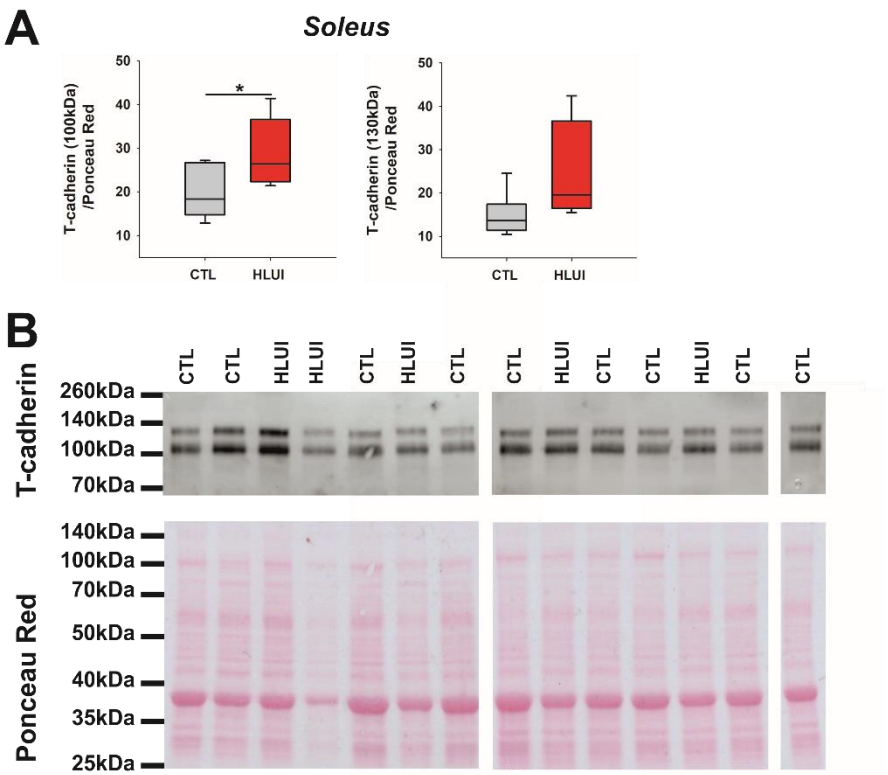

Suppl. Fig 5. (A) Mature (100kDa) and pro-domain bearing (130kDa) T-cadherin protein levels and (B) corresponding western blot immunodetection and Red Ponceau in the *Soleus* muscle. T-cadherin protein levels were determined using denaturant PAGE-SDS followed by a western blot. Densitometric analyses were performed with *Image J* software. Signal was normalized on Ponceau Red. Data represented as boxplot; *: p<0.05, *CTL(n=7) vs HLUI(n=5)*, Student's t-test. **Right,** representative blots.

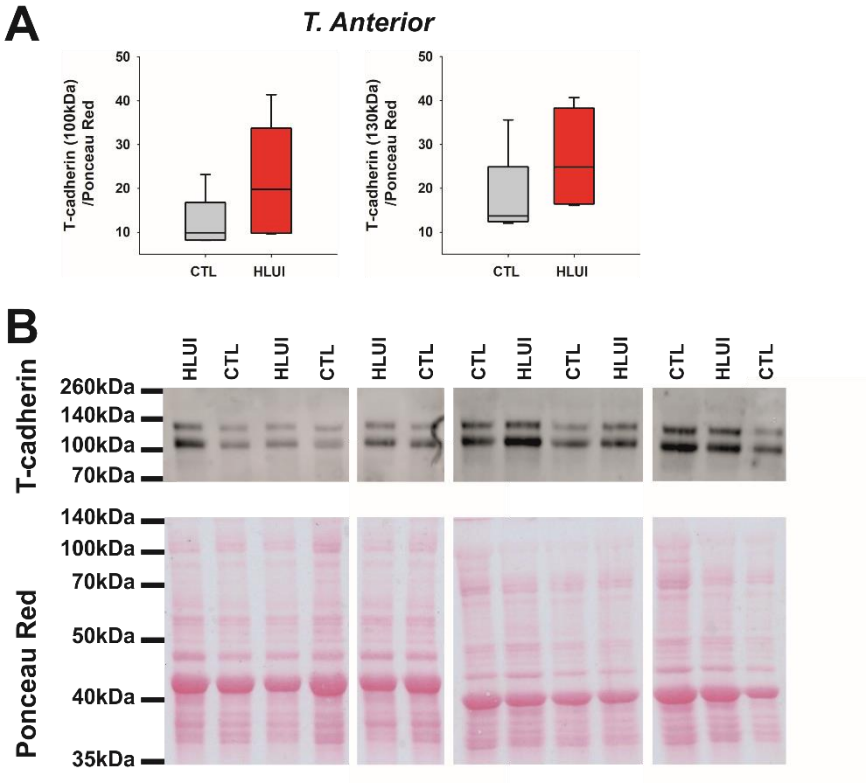

Suppl. Fig 6. (A) Mature (100kDa) and pro-domain bearing (130kDa) T-cadherin protein level and (B) corresponding western blot immunodetection and Red Ponceau in *Tibialis Anterior muscle*. T-cadherin protein levels were determined using denaturant PAGE-SDS followed by a western blot. Densitometric analyses were performed with *Image J* software. The signal was normalized on Ponceau Red. Data represented as boxplot; *: p<0.05, *CTL(n=7) vs HLUI(n=5)*, Student's t-test. **Right,** representative blots.

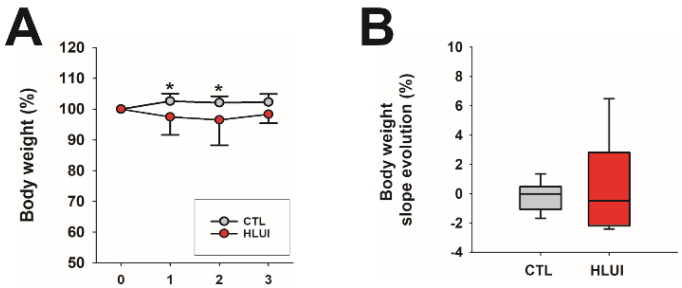

Suppl. Fig 7. Early effects of HLUI on bodyweight evolution. (A) B.w was measured daily and the first day of protocol (D0) was defined as a 100% baseline. Data represented as mean ± SD, *: p<05, *CTL(n=6) vs HLUI(n=6)*, Two-way ANOVA repeated measures. **(B)** Slope comparison. B.w slope evolution was determined between D1 and D3 of the protocol. Data represented as boxplots; *CTL(n=6) vs HLUI(n=6)*, Student's t-test, NS.

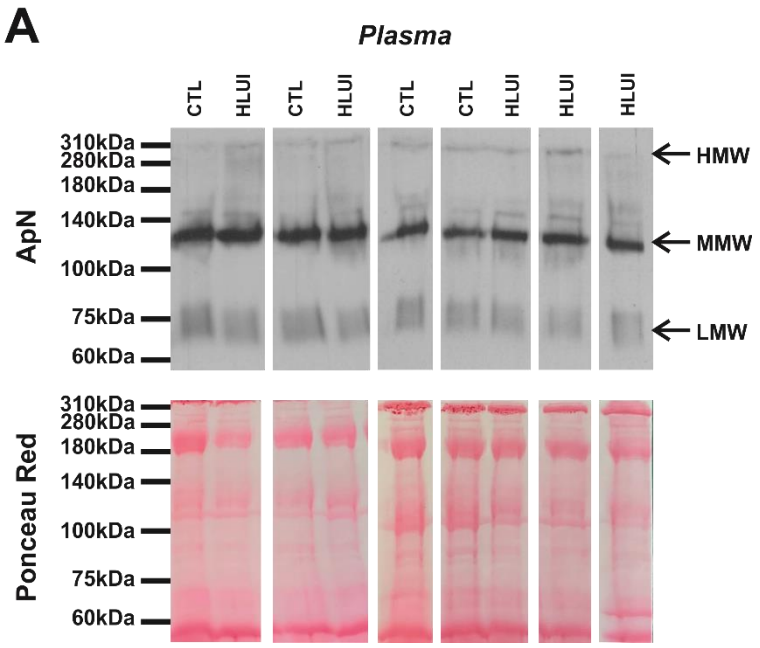

Suppl. Fig 8. Adiponectin circulating forms western blot immunodetection and corresponding Red Ponceau.

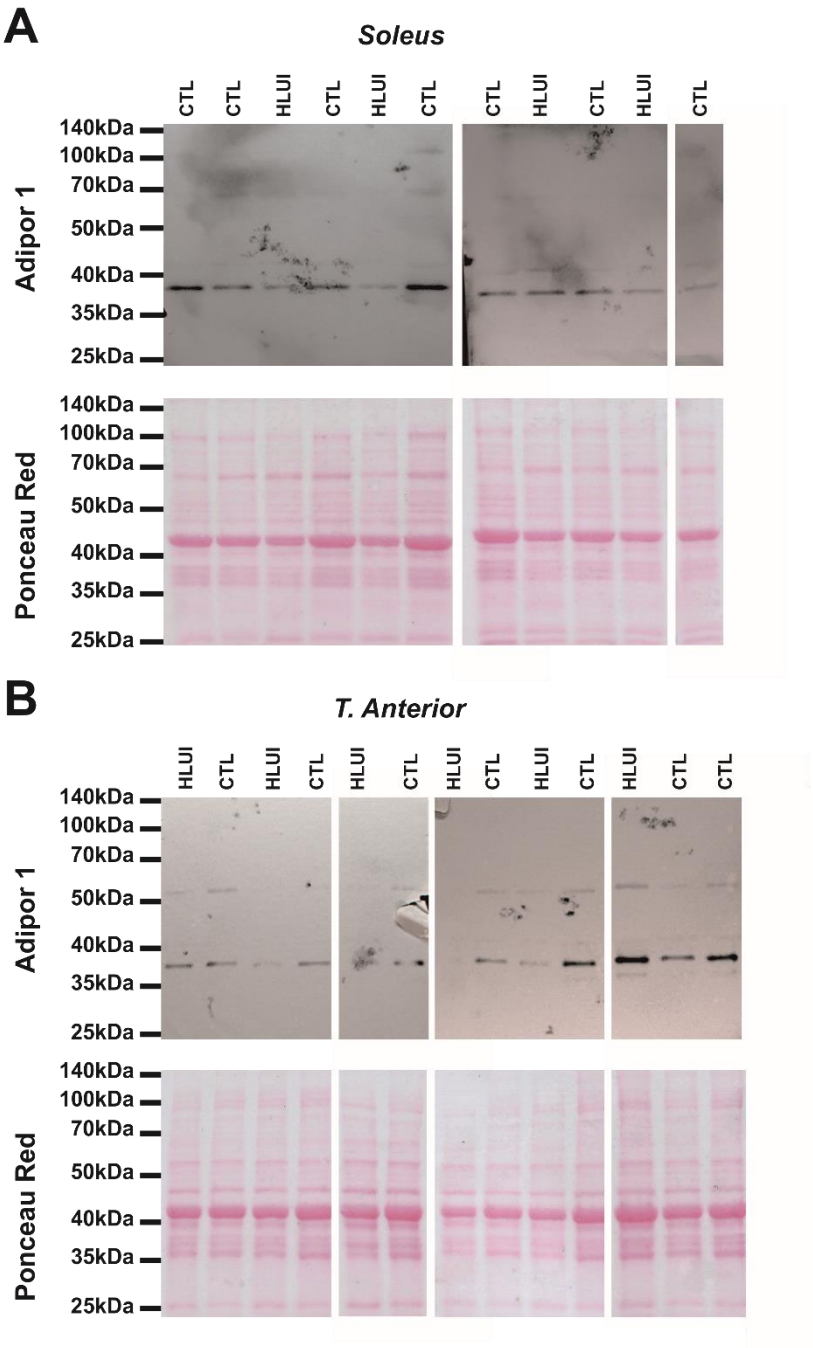

Suppl. Fig 9. Adipor1 western blot immunodetection and corresponding Red Ponceau in (A) *Soleus* and (B) *Tibialis Anterior* muscles.

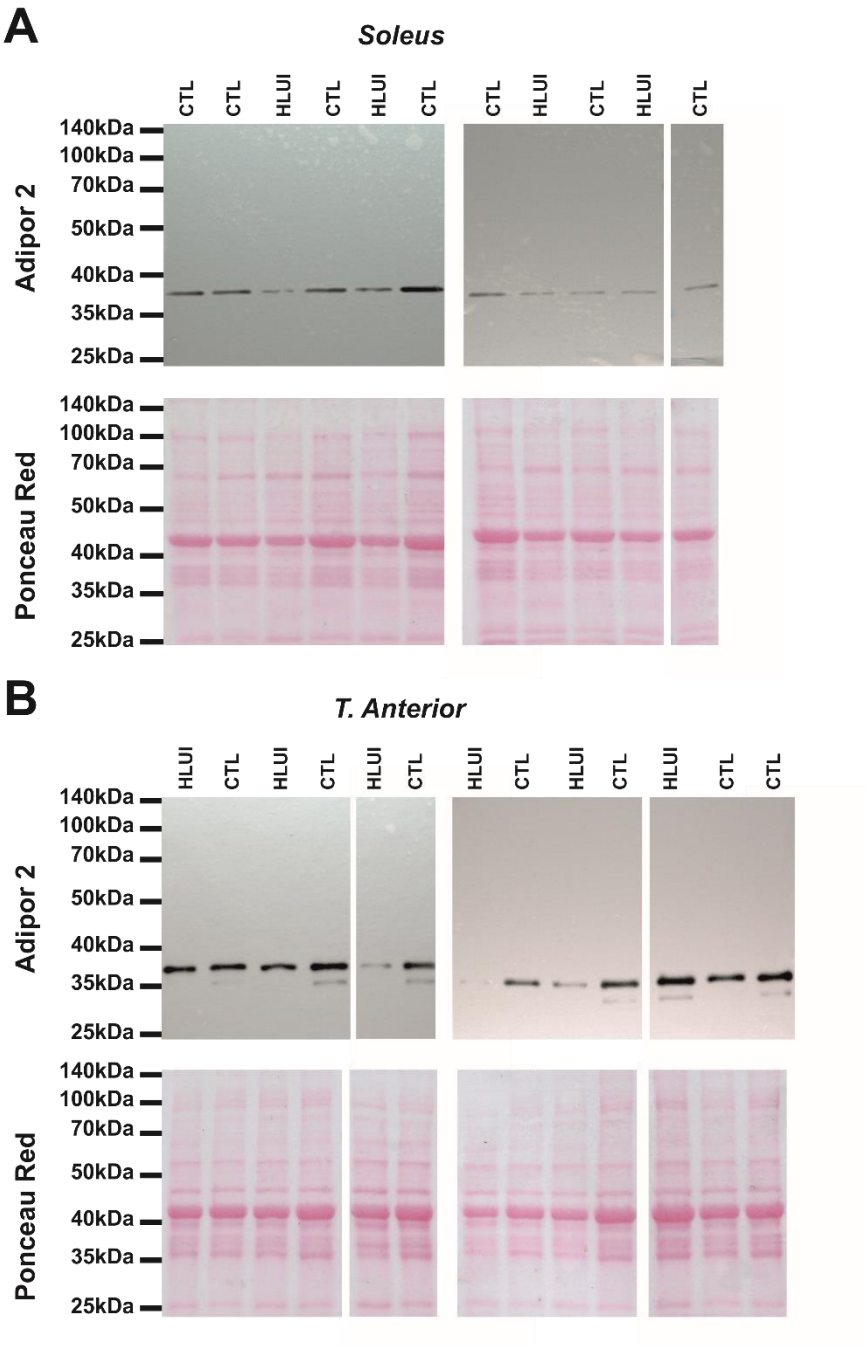

Suppl. Fig 10. Adipor1 western blot immunodetection and corresponding Red Ponceau in (A) *Soleus* and (B) *Tibialis Anterior* muscles.

X. PART2: Effect of Adiponectin knockout in a context of skeletal muscle deconditioning and reconditioning in mice.

Preface

In this part of the study, we investigated whether the loss of ApN protective properties during muscle deconditioning may exacerbate DMA **(AIM #3).** To this aim, loss-of-function experiments have been performed by using ApN KO mice. Moreover, we determined whether the absence of ApN may limit the benefits of muscle reconditioning **(AIM#4).**

Since ApN is well known for its antioxidant properties, parameters indicative of skeletal muscle redox status have been particularly assessed to better understand mechanisms underlying ApN roles in muscle deconditioning and rehabilitation.

Results have been included in a publication that will be submitted in the ***American Journal of Applied Physiology***.

Effect of Adiponectin knockout in a context of skeletal muscle deconditioning and reconditioning in mice.

Szczepanski Sébastien[1], Victor Blommaert[1], Jenart Vincianne[1], Declèves Anne-Emilie[2], Legrand Alexandre[1], Tassin Alexandra[1]

[1] Laboratory of Respiratory Physiology, Pathophysiology and Rehabilitation, Research Institute for Health Sciences and Technology, University of Mons, 7000 Mons, Belgium.
[2] Department of Metabolic and Molecular Biochemistry, Research Institute for Health Sciences and Technology, University of Mons, 7000 Mons, Belgium.

Correspondence: *Tassin Alexandra:* *alexandra.tassin@umons.ac.be*

ABSTRACT

Skeletal muscle deconditioning leads to a Disuse-mediated Muscle Atrophy (DMA) and a persistent muscle weakness impairing rehabilitation. To develop pharmacological therapeutical approaches, molecular mechanism underlying exercise training (ET) benefits have to be clarified. Adiponectin (ApN) is an adipo/myokin suggested to be involved in ET benefits. We previously demonstrated alteration of its pathway in a murine model of muscle disuse consisting in hindlimb unloading and immobilization (HLUI) in mice

Here, we investigated whether the loss of ApN protective properties during muscle deconditioning may exacerbate DMA or limit the benefits of muscle reconditioning.

The *Soleus* muscle of ApN-KO HLUI mice exhibited a more pronounced DMA severity and an increased proportion of type IIa myofibres as compared to WT. HLUI was also shown to have a “pre-conditioning-like effect” increasing the ET-mediated type IIa/I myofibre transition. This effect is prevented in the absence of ApN, suggesting impaired muscle plasticity during rehabilitation. Given ApN antioxidant properties, the *Soleus* muscle redox status has been investigated. ApN knockout does not exacerbate HLUI-mediated changes in pro-oxidant/ antioxidant indicators, suggesting that additional ApN properties may be involved in the increased DMA severity observed in these animals. However, in ApN KO mice, correlation analyses showed that myofibers with smaller cross-sectional area (CSA) exhibited higher *Nox* expression, Sod1 protein levels, and lipid peroxidation, therefore indicating that the atrophy occurring in the absence of ApN is associated with redox equilibrium perturbations. Most of these modifications are no longer observed after ET, even in ApN KO mice, suggesting that additional ApN-independent processes underline ET effects.

In conclusion, our study highlights that the loss of ApN protective properties aggravates atrophy and impairs compensatory mechanisms initiated during DMA, particularly fiber-type switches. This has persistent consequences in muscle plasticity during rehabilitation. However, ApN-independent mechanisms are likely involved in HLUI-mediated redox status perturbations and in ET benefits.

Keywords: Adiponectin, Exercise Training, Muscle deconditioning

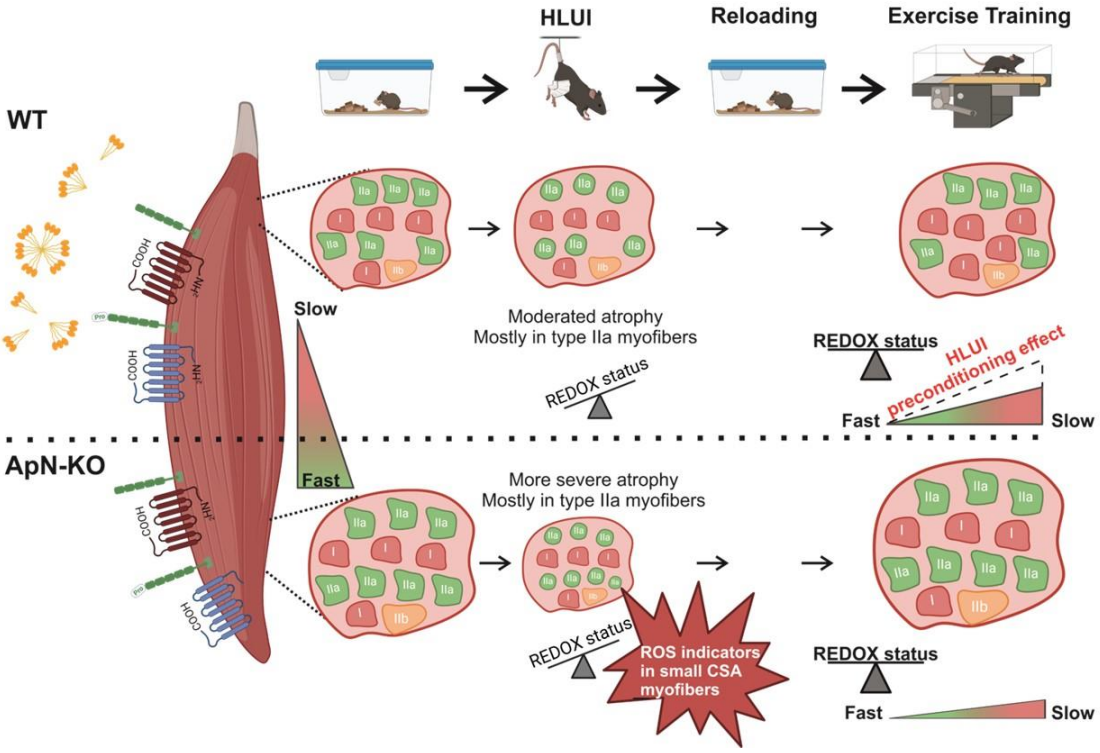

INTRODUCTION

Skeletal muscle deconditioning is associated to various pathological conditions e.g. sedentarity, chronic pathologies, hypogravity, bed rest or limb immobilization. At the tissue level, this leads to a Disuse-mediated Muscle Atrophy (DMA) characterized by muscle mass loss, myofibre atrophy, slow-to-fast fibre shift, and associated functional alterations (1, 2). Reductionist murine models of DMA, avoiding confounding factors found in patients, are useful for studying the specific effect of muscle disuse. Among those, the Hindlimb Unloading procedure (HLU) mimics numerous DMA characteristics. In such models, a protein synthesis/degradation imbalance, excessive oxidative stress, mitochondrial dysfunction, and an altered regeneration process were reported (1, 3–6).

As concerns current treatment against muscle deconditioning, exercise training (ET) remains the more potent. However, the effectiveness of ET as a therapeutic approach is often constrained by persistent muscle weakness inducing exercise intolerance (7, 8). Rehabilitation is particularly challenging in patients with pre-existing chronic pathologies affecting skeletal muscle. To develop new pharmacological approaches, a better understanding of molecular processes underlying ET benefits is needed. Recent advances in multiomics in rodent models revealed an adaptive response to endurance training that includes widespread regulation of immune, metabolic, stress response, and mitochondrial pathways (9).

Importantly, secreted molecules known as exercise-induced myokines are thought to promote many of the favorable adaptations to ET through auto-, para-, and endocrine actions (10). Skeletal muscle secretome includes protein hormones (e.g. Adiponectin (ApN), IL6, Irisin, and cathepsin B) and metabolites (e.g. L-lactate) (11) (12). Adiponectin (ApN), is an adipokine and a myokine well known for its anti-diabetic and hypolipidemic properties because of key roles in metabolic processes such as fatty acid β-oxidation, glucose uptake, and insulin sensitivity (13, 14). In addition, ApN also presents anti-inflammatory, anti-apoptotic, and antioxidant properties (13–15). ApN metabolic functions are mainly mediated by AdipoR1 and AdipoR2 receptors, predominantly expressed in skeletal muscle and liver,

respectively (16, 17). AdipoR1 signals through the AMPK pathway, whereas AdipoR2 initiates PPAR-α intracellular cascades (16, 18).

An increasing number of studies demonstrate the beneficial effects of ApN pathway activation on skeletal muscle. Indeed, ApN-KO mice present intra-muscular lipid accumulation, an increased type IIb myofiber area as well as a reduced peak contractile force (12). ApN-KO muscles are more sensitive to oxidative stress, inflammation and apoptosis (13). The essential role of the AdipoR1/AMPK/SIRT1/PGC1α axis in skeletal muscle is supported by the reduced endurance, type I fiber number, mitochondrial content, and oxidative stress-detoxifying enzymes observed in muscle-specific AdipoR1-KO mice (19). ApN pro-myogenic effects and their roles in muscle regeneration were reviewed in (20). Elastases produced by M1 macrophages at the lesion site cleave ApN into its globular form (gAd) (21) which regulates satellite cell activation and later regeneration steps in a auto and para-crine manner (22). The t-cadherin ApN co-receptor (T-cad) seems implicated in ApN-mediated regeneration (23), as well as p38MAPK and AMPK signaling pathways (24–26). T-cad was suggested to increase ApN abundance at the sarcolemma (23, 27, 28). Furthermore, ApN regulates mesangioblast differentiation (non-resident precursor cells with myogenic propriety) and M1/M2 macrophage switch (involved in inflammation resolution) (30). Finaly, ApN also induces PGC1α activity through AdipoR1, and this pathway enhances oxidative metabolism to supply energy for regeneration (31).

Interestingly, ApN plasmatic level (ApN_{pl}) was found to increase with ET in murine models (20). Our group also demonstrated that ET in mice increased (i) AdipoR1 protein abundance in the *Gastrocnemius* muscle and (ii) ApN plasmatic level reported by fat mass unit (32). ET benefits were suggested to be mediated by the AdipoR1 axis (33). The therapeutic value of AdipoR activation was therefore considered for muscle disorders (20, 34). However, this strategy has never been tested in the context of muscle deconditioning. Indeed, little is known regarding the contribution of ApN in DMA. Interestingly, one study reported that Adipor1 expression was downregulated in the *Soleus* muscle in a murine HLU model (35). Moreover, our group showed that Hindlimb Unloading and Immobilisation (HLUI) in mice induces a fiber-type-dependent atrophy occurring concomitantly with an elevation of ApN plasmatic level, disturbances in oligomeric form proportion, and muscle-type dependent alterations in adiporeceptor expression (at the mRNA and protein level). Given the myoprotective properties of ApN, we hypothesized that such deregulation could reinforce DMA but further studies were needed to determine whether ApN pathway changes upon disuse participates to a vicious cycle reinforcing muscle atrophy in this pathological context.

Here, we investigated whether the absence of ApN biological effects in mice may exacerbate the impact of HLUI-mediated muscle disuse and limit the benefice of muscle rehabilitation. Given (i) that ApN has antioxidant properties, (ii) that oxidative stress constitutes a hallmark of DMA, (iii) that ET is accompanied by beneficial changes in skeletal muscle redox status; indicative outcomes of ROS production and antioxidant processes have been particularly investigated as a first step towards a better understanding of mechanisms underlying ApN roles in muscle deconditioning and rehabilitation.

MATERIALS AND METHODS

Animals

All animal experiments met the Belgian national standard requirements regarding animal care and were conducted in accordance with the Ethics and Welfare Committee of the University of Mons (LE023/03). At 12 weeks of age, male ApN-KO (-KO) mice (B6; 129-*Adipoq*^{tm1Chan}/J, RRID: IMSR_JAX:008195, Charles River, France) and matching controls (-WT) (B6129SF2/J, RRID: ISMR_JAX:101045, Charles River, France) were housed in large rat cages (58x40x20cm) equipped (HLUI groups) or not (CTL groups) with a device allowing hindlimb unloading through tail suspension. HLUI groups (WT-HLUI and KO-HLUI mice) were connected to this device for a 3-day acclimatization period but kept at floor level to allow movements with both forelimbs and hindlimbs (from D-3 to D0). Mice of HLUI groups were then tail-suspended and hindlimbs immobilized for 14 days (D14) while CTL groups (WT-CTL and KO-CTL mice) were maintained in standard housing conditions. Following the HLUI protocol, mice were either euthanatized for tissue collection (-CTL and -HLUI groups) or reloaded (R) for 2 weeks before undergoing a 8 week of endurance exercise training (ET) protocol (-CRET and -HRET groups). Relative humidity was maintained at 35-40% with a constant room temperature (21°C) and a 12h/12h day/night light cycle. Animals had access to food and water *ad libidum*.

Hindlimb Unloading and immobilization (HLUI)

HLU device as well as hindlimb suspension and immobilization procedures were performed as described previously in (36). Briefly, -HLUI mice were connected to the HLU device for a 3-day acclimatization period but kept at floor level from D-3 to D0. Mice of the HLUI groups were then tail-suspended with hindlimbs immobilized in an extended position from the ankle (in a dorsiflexion position) to the upper hip with medical tape (Nepenthes; 16 x 1 cm). Two mice were housed in a cage to allow social interactions.

Reloading and exercise training (ET)

At the end of the HLUI protocol (W2), WT-HLUI and KO-HLUI mice were reloaded by removing the HLU device and immobilization tapes. Mice were then allowed to move freely in cages for 2 weeks of self-ambulatory recovery before the beginning of the 8-weeks ET protocol that was realized on treadmills. Briefly, mice were acclimatized for 10 minutes to the treadmill room and the device (Treadmill Control LE8700, Panlab apparatus®, Barcelona, Spain) during the 2nd week of reloading (W4). Then, the speed treadmill belt speed was fixed at 5cm/s during the first week of ET (W5). In the 2nd week of ET (W6), the treadmill started at 10cm/s with a gradual speed increase of 2cm/s every 2 min for 15 minutes. At the beginning of the 3rd week of ET (W7), a Maximum Running Velocity (MRV) Test was performed. From the 3rd week of ET (W7) to the last week of ET (W12), the belt speed during training was set at 70% of the maximal running velocity, and exercise duration was increased by 10 min per week until a maximum of 60 min was reached.

Maximum Running Velocity (MRV) test

Mice started the MRV test with an initial running speed of 18cm/s and the treadmill speed gradually increased by 2cm/s every 2 minutes. For each mouse, running velocity was considered maximal, and the test was interrupted, when the animal was unable to continue running at the belt speed despite receiving four electric stimulations in one minute.

Muscle collection and preparation

At W2 or W12, mice were anesthetised and euthanised (Euthanimal 20%, *Alfasan*) and *Soleus* muscles were collected to perform morphometrical analyses and molecular investigations (RT-qPCR and Western blots). Morphometrical analyses required muscle embedding in OCT cryo-compound (ImmunoLogic, 1620-C) frozen in isopentane cooled with liquid nitrogen. Cryosections (8 µm) were performed with a cryotome (Leica 1950). Contralateral muscles were snap-frozen in liquid nitrogen to allow molecular investigations. Blood was collected and centrifugated (13500 rpm, 15 minutes) to isolate plasma for ELISA assays.

Morphometrical analyses in hindlimb muscles

Myofiber-type immunofluorescence staining

The *Soleus* muscle cryosections were blocked for 1 hour at room temperature with 10% Goat-serum/PBS (VWR, S2000-100) before being incubated for 2 hours at room temperature with a primary antibody cocktail directed against MyHC7 (type I fibers), MyHC2 (type IIa fibers), MyHC4 (type IIb fibers) and laminin (Supplemental Table S*1*). Slides were washed 3 times in PBS and incubated for 1 hour with the secondary antibodies cocktail (Supplemental Table S*1*). Slides were washed 3 times in PBS and mounted with ProLong™ Gold Antifade Mountant (P36934, Invitrogen). Images were then captured to cover the whole muscle section with a Nikon Eclipse i80 microscope (10x magnification).

Images processing and measurements

Each capture was processed with *Image J* software to subtract the background fluorescence signal and provide DAPI/Cy5, DAPI/FITC, and DAPI/TRITC images. Processed images were then manually analyzed to determine the Regions Of Interest (ROIs) corresponding to positive myofibers in the channel combination of interest. *Image J* was then used to analyze ROI areas. Each myofiber CSA was finally obtained after conversion of the corresponding ROI (in pixel) in µm² with the pixel/µm ratio. Myofibers were then classified in clusters according to their area (<120 μm^2, 120-300 μm^2, and every 300 μm^2 until 3300 μm^2) to evaluate changes in myofibers CSA distribution.

RT-qPCR analyses

Total RNAs were extracted from *Soleus* muscle with Trizol reagent (Invitrogen) according to the manufacturer guidance before being treated with DNAse I (ThermoFischer). cDNAs were synthetized from 0.8µg of RNA using Maxima First Strand cDNA synthesis kit (ThermoFischer). RT-qPCRs were performed in triplicate for each primer (Eurogentec) (**Supplemental Table S1**) with the SYBR Green FastStart Essential DNA Green Master (Roche) and by using the LightCycler®96 (Roche) device (cycling conditions: initial denaturation step at 95°C for 10 min, followed by 40 cycles of 15s at 95°C and 60s at primer Tm). Raw data were analyzed with the LightCycler®96 software (technical replicates with CT > 0.2 were removed from the analyses) and quantified by using $2^{-\Delta\Delta Ct}$ method (*Rplp0* as housekeeping gene).

ELISA

ApN plasmatic concentrations were measured by using the Adiponectin/Acrp Quantikine ELISA kit (R&D) according to the manufacturer's instructions.

Western Blot analyses

The *Soleus* muscle was homogenized in lysis buffer (CelLytic, Sigma, C3228; Protease Inhibitor Cocktail, Sigma, P8340; Phosphatase Inhibitor Cocktail, Millipore, 524632). Equal protein amounts were then separated on a 12% SDS-PAGE gel (100V; 2h) before being transferred onto a nitrocellulose membrane (Amersham) by using the PowerPac HV power supply (Biorad™). Membranes were then stained with Ponceau Red, washed 3 times in TBS-Tween (0.2%), and blocked 1 hour in 5% non-fat dry milk diluted in TBS-T. Primary antibodies directed against Sod1 (1:1000, Rb polyclonal IgG, Abcam, ab16831), Sod2 (1:1000, Rb polyclonal IgG, NovusBio, NB1001992) and 4-HNE (1:1000, Rb polyclonal IgG, Abcam, Ab46545) as well as corresponding secondary HRP conjugated antibodies (Donkey anti-Rb IgG, VWR, NA934) and (Rabbit anti-goat IgG, Abcam, ab6741)) were diluted in 1% non-fat dry milk TBS-T for incubation overnight at 4°C and 1 hour at room temperature respectively. The HRP signal was visualized using Supersignal West Femto Max Sensitivity Kit (Thermo Fisher Scientific) and the Fusion FX7 spectra (Vilber, France). Densitometry was performed using *Fiji* software. The densitometry signal was normalized to the total proteins stained by Ponceau Red.

Statistical analysis

Statistical analyses were done using *SigmaPlot* software, version 14. Data were expressed as mean ± SD and represented as histograms (mean ± SD) or boxplots (5 and 95th percentile). For comparison, depending on normality and equal variance tests, we used : **(i)** Two way Analyses of variance with All pairwise Multiple Comparison Procedure (Holm-Sidak-method) (Global, type I and type IIa myofibers CSA; Myofiber proportions; *Adipoq*, Adipor1, Adipor2, Cdh13, *Sod1, Sod2, Nox2, Nox4* and *Nrf2* mRNA expression; B.w evolution slope from D0 to W2 and from W2 to W4; Sod1 and Sod2 protein levels and 4HNE levels), or **(ii)** Kruskal-Wallis One Way Analysis of Variance on Ranks (B.w evolution slope from W4 to W12), and **(iii)** Chi-square test (Global, type I and type IIa myofiber CSA distribution in the *Soleus* muscles). B.w were expressed as a percentage of the baseline b.w (D0) and compared at D-3, D0, W2, W4 and W12. B.w evolution during the protocol was also evaluated using linear regression, calculation of slope coefficients, and mean comparison between our experimental groups as described above.

RESULTS

ApN KO mice in disuse, reloading and reconditioning: body weight variations and knock-out validation.

To study the impact of ApN-KO in the context of muscle disuse, we used a murine model of Hindlimb Unloading and Immobilization (HLUI). The model, adapted from (37), allowed to limit mouse stress by maintaining social interactions and movements. Importantly, animal food was adapted to avoid the excess in antioxidant commonly found in standard diets. The HLUI protocol includes an acclimatation period of 3 days (D-3 to D0) and 2 weeks of HLUI (DO to W2) **(Figure 1*A*)**. This procedure was followed by a period of reloading (W2 to W4) and muscle reconditioning (ET; W4 to W12) **(Figure 1*B*)**.

Concerning body weight (b.w) evolution during the protocol, we did not observe any significant difference between HLUI and CTL groups excepted at W2 **(Figure 1*C*).** Indeed, b.w. slope evolution between D0 and D14 showed a slight gain in CTL mice which is not observed in the HLUI groups **(Supplementary Figure S1)**. We also observed that mouse b.w. is lower in ApN-KO mice than in WT mice **(Figure 1*C*)**. However, b.w. slope evolution showed a weight regain during the reloading period following HLUI, and a stabilization during the ET protocol, both in WT and ApN KO animals **(Supplementary Figure S2)**.

As expected, *AdipoQ* expression is abolished in ApN-KO mice. Also, we cannot observe any variation in its expression in WT-HLUI mice as compared to the corresponding control group **(Figure 1*D*)**. Fitting with anterior studies, *Adipor1* expression is altered by the HLUI protocol in the *Soleus* muscle **(Figure 1*E*).** Interestingly, ApN-KO mouse *Soleus* muscle also exhibited a lower *Adipor1* mRNA level than the WT group **(Figure 1*E*).** Finally, at the end of the ET protocol, the plasmatic ApN level was not significantly modified by the previous HLUI and as expected, ApN was undetectable in ApN-KO mouse plasma **(Figure 1*F*)**. At this timepoint, (W12), adiporeceptor expression was not significantly different between experimental groups in the *gastrocnemius* muscle **(Supplementary Figure S3)**.

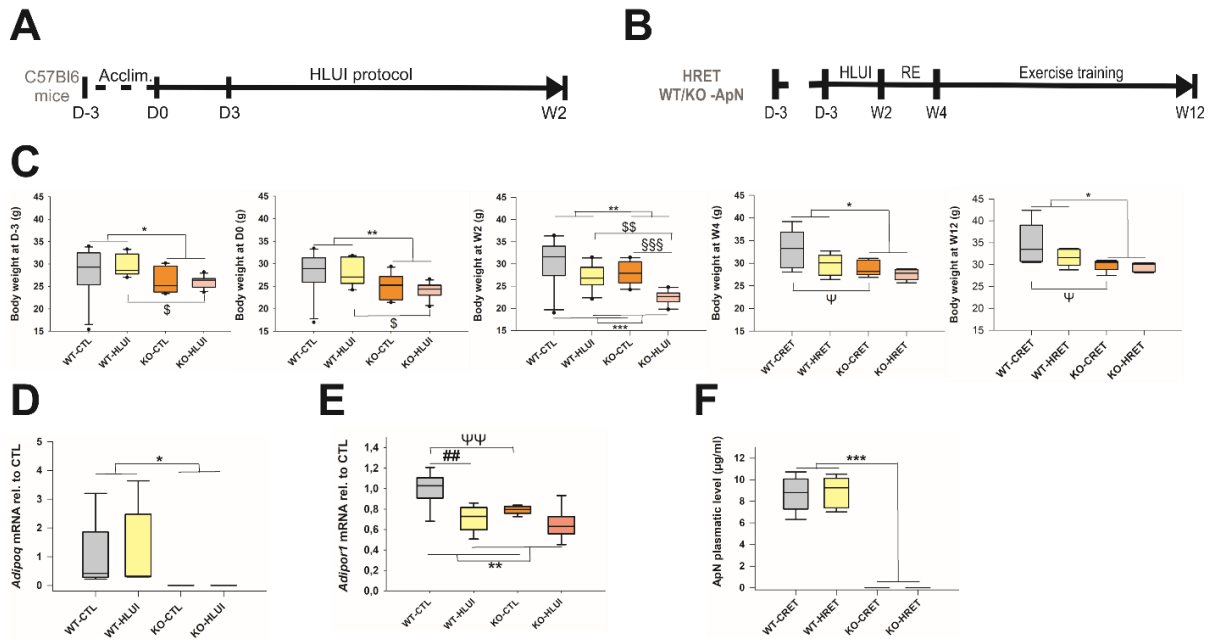

Fig 1. Body weight variations and knock out validation. (A) HLUI protocol timeline. (B) HLUI – Reloading and ET protocol timeline. (C) Body weight (b.w) at D-3, D0, W2, W4 and W12. B.w was measured daily and the first day of protocol (D0) was defined as a 100% baseline. Data represented as boxplots, $ p<0.05, $$ p<0.01 (KO-HLUI vs WT-HLUI), §§§ p<0.001 (KO-HLUI vs KO-CTL), Ψ p<0.05 (KO-CRET vs WT-CRET), * p<0.05, ** p<0.01 (KO- vs WT-, genotype effect), *** p<0.001 (HLUI- vs CTL-, protocol effect), Two-way ANOVA , All Pairwise Multiple Comparison, Holm-Sidak method. ***Adipoq* (D)** and ***Adipor1* (E) mRNA expression.** *Adipoq* and *Adipor1* mRNA levels were assessed by RTqPCR with ΔΔCt method (housekeeping gene: *Rplp0*; data normalized to CTL). Data represented as boxplot; ## p<0.01 (WT-HRET vs WT-CRET), ΨΨ p<0.01 (KO-CRET vs WT-CRET), ** p<0.01 (KO- vs WT-, protocole effect), Two-way ANOVA, All Pairwise Multiple Comparison, Holm-Sidak method. **(F) ApN plasmatic level** were measured by ELISA. *** p<0.001 (KO- vs WT-, protocol effect), Two-way ANOVA.

ApN knockout in mice increases the proportion of type IIa myofibres and exacerbates atrophy in the disused *Soleus* muscle.

After 2 weeks of hindlimb unloading in WT and ApN-KO mice **(Figure 2*A*)**, Myosin heavy chain (MyHC) isoforms were firstly immunolabeled on *Soleus* muscle cryosections **(Figure 2*B*)** to determine the proportion of type I, type IIa, and type IIb myofibers. We observed that the absence of ApN increased the proposition of type IIa myofibers at the expense of type I fibers ($p<0.01$, ApN-KO vs WT, Two-Way ANOVA, **Figure. 2*C*)**.

We then measured all myofibers cross-sectional area (CSA) in the whole muscle **(Figure 2*D*)**, and as expected, showed that the HLUI procedure causes a decreased in mean CSA whatever mouse genotype ($p<0.05$, HLUI vs CTL, Two-Way ANOVA). Importantly, this effect is more severe in the absence of ApN ($p<0.05$, KO-HLUI vs KO-CTL) than in WT mice (WT-HLUI vs WT-CTL, NS) (Two-Way ANOVA, all pairwise comparisons, **Figure 2*D*)**.

Concerning the fiber-type specificity of the observed effects **(Figure 2*E-F*)**, mean type I fiber CSA comparisons did not highlight any significant difference between experimental groups **(Figure 2*E*)**. However, a negative effect of HLUI is present in type IIa myofibers since they exhibit a significantly decreased mean CSA ($p<0.01$, HLUI vs CTL, two-way ANOVA). This effect is again more severe in ApN-KO mice ($p<0.05$, KO-HLUI vs KO-CTL) than in WT (WT-HLUI vs KO-CTL, NS) (Two-Way ANOVA, all pairwise comparisons, **Figure 2*F***).

Regarding fiber size clustering analyses **(Figure 2*G-I*)**, according to results obtained for mean CSA, global **(Figure 2*G*)** and type IIa **(Figure 2*I*)** myofiber size distribution showed an increased number of myofibers with smaller CSA in HLUI ApN KO animals as compared to corresponding CTL (§§§, $p<0.001$, KO-HLUI vs KO-CTL, Chi-square). This effect is also detectable for type I myofibers **(Figure 2*H*)** even if mean CSA were not statistically different (**Figure 2*E*)**. Moreover, this analysis highlighted that, at baseline in animals having not encountered muscle deconditioning, the number of myofibers in higher CSA clusters is increased in ApN-KO animals as compared to WT (^{Ψ}, KO-CTL vs WT-CTL, Chi-Square test, **Figure 2*G-I***). This is particularly the case of type I fibers (^{ΨΨΨ} $p<0.001$, KO-CTL vs WT-CTL, Chi-Square test, **Figure 2*H***). Furthermore, HLUI-mediated disuse also shifted type IIa myofibers CSA distribution towards clusters of small myofibers CSA in WT animals ($^{\#\#}p<0.01$, WT-CTL vs WT-HLUI, Chi-square test **(Figure 2*I*)**.

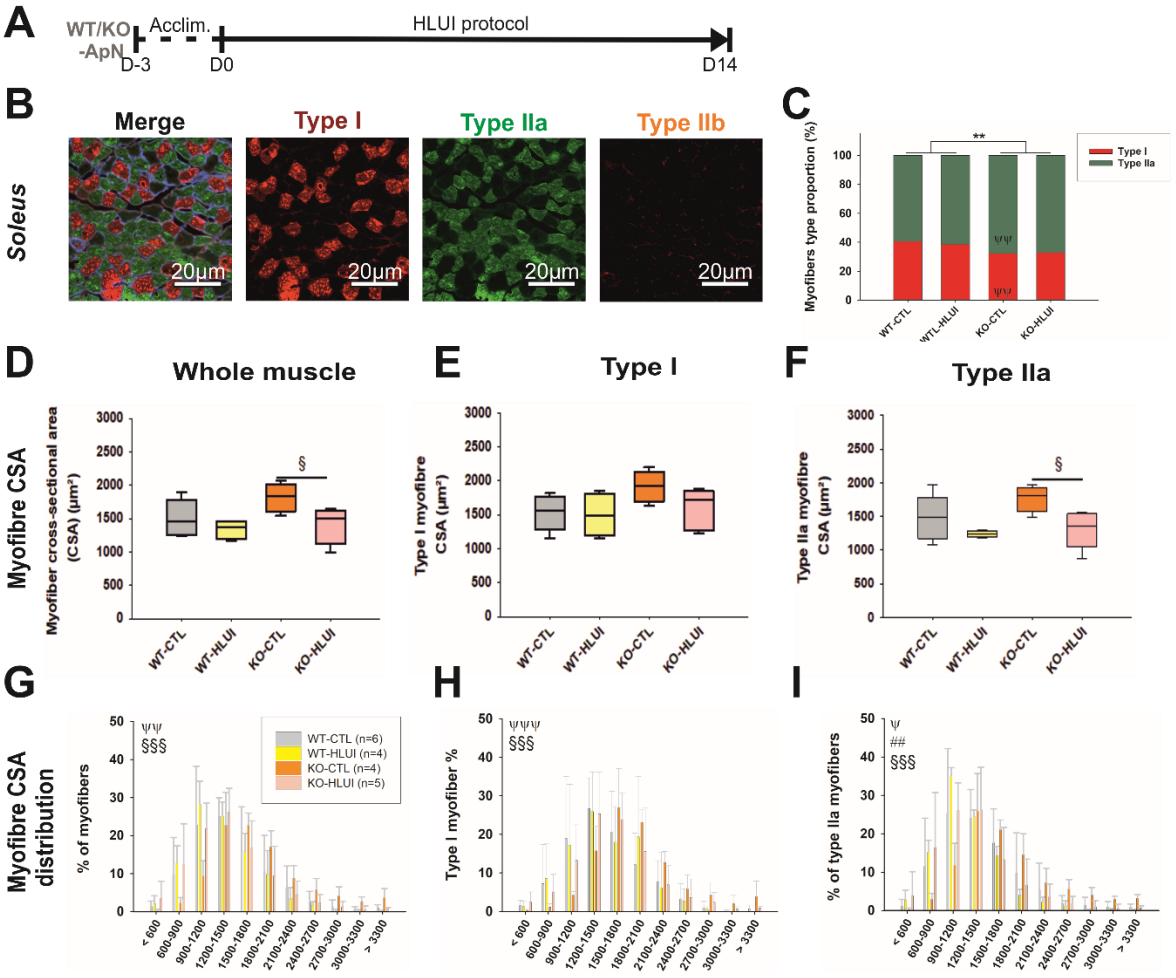

Fig 2. Cross-sectional Area (CSA) and myofiber CSA distribution were measured in *Soleus* muscle following type I, IIa and IIb immunofluorescence detection and morphometrical analysis were performed with *Image J* softwares. **(A) Timeline. (B) Representative fields**. **(C) Myofiber type proportion**. Data represented as stacked bars; **p<0.01 (Genotype effect), ΨΨ p<0.01 (WT-CTL vs KO-CTL), Two-way ANOVA, all pairwise comparison, Holm-Sidak method.

(D-F) CSA was measured in all fibers **(D)**, in type I **(E)** and in type IIa myofibers **(F)**. Data represented as boxplot. §, p<0,05 (KO-CTL vs KO-HLUI), Two-way ANOVA, all pairwise comparison, Holm-Sidak method. **(G-I)** Myofibers were classified in clusters according to their area (µm²). All fibers **(G)**, type I fibers **(H)** and type IIa fibers **(I).** Data represented as mean ± SD. ΨΨ p<0.01 (WT-CTL vs KO-CTL), §§§ p<0.001 (KO-CTL vs KO-HLUI), Chi-square.

HLUI-mediated disuse has a preconditioning-like effect on fast-to-slow myofiber transition during reconditioning, but this effect is lost in the absence of ApN

To study the impact of the absence of ApN in the context of reconditioning, we applied an aerobic exercise training protocol (ET) in ApN-KO and WT animals that had either undergone previous muscle deconditioning through HLUI (HRET) or not (CRET) **(Figure 3*A*)**. At the end of the protocol, Myosin heavy chain (MyHC) isoforms were immunolabeled on *Soleus* muscle cryosections **(Figure 3*B*).**

Concerning variations of type I, type IIa, and type IIb myofiber proportions between experimental groups **(Figure 3*C*)**, we first highlighted a higher percentage of type IIa myofibers in ApN-KO as compared to WT animals, at the expense of oxidative type I fibers (*, $p<0.01$, KO vs WT, Two-Way ANOVA). Interestingly, in WT animals submitted to a deconditioning period before ET (WT-HRET), an increased percentage of type I fiber is highlighted at the end of ET protocol when compared to WT animals that have not encountered muscle deconditioning before ET (CRET) ($^{\#\#}$, $p<0.01$, WT-HRET vs WT-CRET, Two Way ANOVA, all pairwise comparison). Importantly, this effect was not observed in the absence of ApN (KO-HRET vs KO-CRET: NS, Two Way ANOVA, all pairwise comparison).

Concerning myofiber mean CSA in the whole muscle, we showed that at the end of the ET protocol, myofiber mean CSA is greater in ApN-KO mice than in WT animals **(Figure 3*D*)**. This effect is not fiber-type specific since it can be observed both in type I **(Figure 3*E*)** and type IIa myofibers **(Figure 3*F*)**. This effect is likely to be discussed with the increased percentage of IIa myofiber also observed in ApN-KO mice as compared to WT (**Figure. 2*C***), those fibers being characterized by a higher CSA as compared to type I fibers. Fiber size clustering analyses are in agreement with mean CSA data, since we observed in ApN-KO animals, an elevation of the proportion of myofiber in clusters characterized by a higher CSA ($<1800\mu m^2$) in the whole muscle as well as in type I and type IIa myofibers analyzed independently **(Figure 3*G-I*)**.

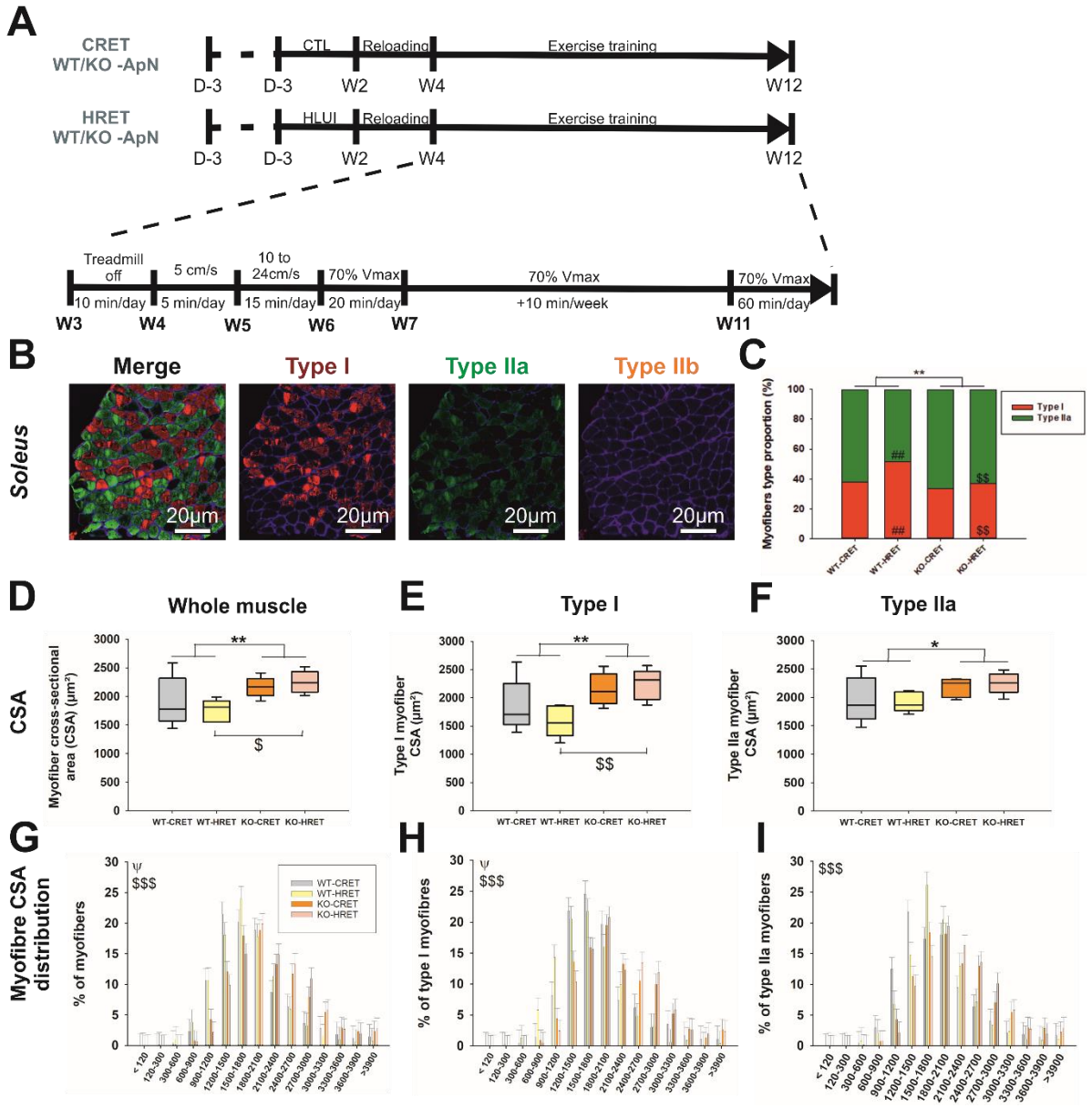

Fig 3. Cross-sectional Area (CSA) and myofiber CSA distribution were measured in *Soleus* muscle following type I, IIa and IIb immunofluorescence detection and morphometrical analysis were performed with *Image J* software. **(A) Timeline. (B) Representative fields**. **(C) Myofiber type proportion**. Data represented as stacked bars; **p<0.01 (Genotype effect), ##, p<0.01 (WT-HLUI vs WT-CTL), $$, p<0.01 (KO-HRET vs WT-HRET), Two-way ANOV, all pairwise comparison, Holm-Sidak method. **(D-F)** CSA was measured in all fibers **(D)**, in type I **(E)** and in type IIa myofibers **(F)**. Data represented as boxplot. $, p<0.05 (KO-HRET vs WT-HRET), Two-way ANOVA, all pairwise comparison, Holm-Sidak method. **(G-I)** Myofibers were classified in clusters according to their area (µm²). All fibers **(G)**, type I fibers **(H)** and type IIa fibers **(I).** Data represented as mean ± SD. Ψ p<0.05 (KO-CRET vs WT-CRET), $$$, p<0.001 (KO-HRET vs WT-HRET), Chi-square.

Disuse-mediated *Nox* over-expression is not exacerbated by ApN KO but reverted after 8 weeks of muscle reconditioning.

Since oxidative stress is a hallmark of muscle disuse, we investigated whether the loss of ApN antioxidant properties could influence key indicators of muscle redox status upon disuse and reconditioning **(Figure 4-6)**. Nicotinamide Adenine Dinucleotide Phosphate (NAD(P)H) oxidases (Nox) are well-known as significant actors in the cellular redox state (38, 39). Firstly, we thus investigated the expression of *Nox2* and *Nox4* typically expressed by skeletal muscle (40). As expected, *Nox2* and *Nox4* are overexpressed after the two weeks of HLUI, both in WT mice and in ApN-KO animals **(Figure 4*B*)**. This difference is no longer observed after ET which allows a return to the baseline of *Nox* expression level **(Figure 4*C*)**. However, the expression of the gene encoding NOX2, but not NOX4, is downregulated in ApN-KO animals **(Figure 4*B*)**, and this difference is maintained even after ET **(Figure 4*C*)**. As expected, *Nox2* and *Nox4* expression are positively correlated (r=0.82 p<0.001, Pearson Product Moment Correlation, **Figure 4*D*** and **Supplementary Figure S4**) but this association is lost after ET (**Figure 4*E*** and **Supplementary Figure S**).

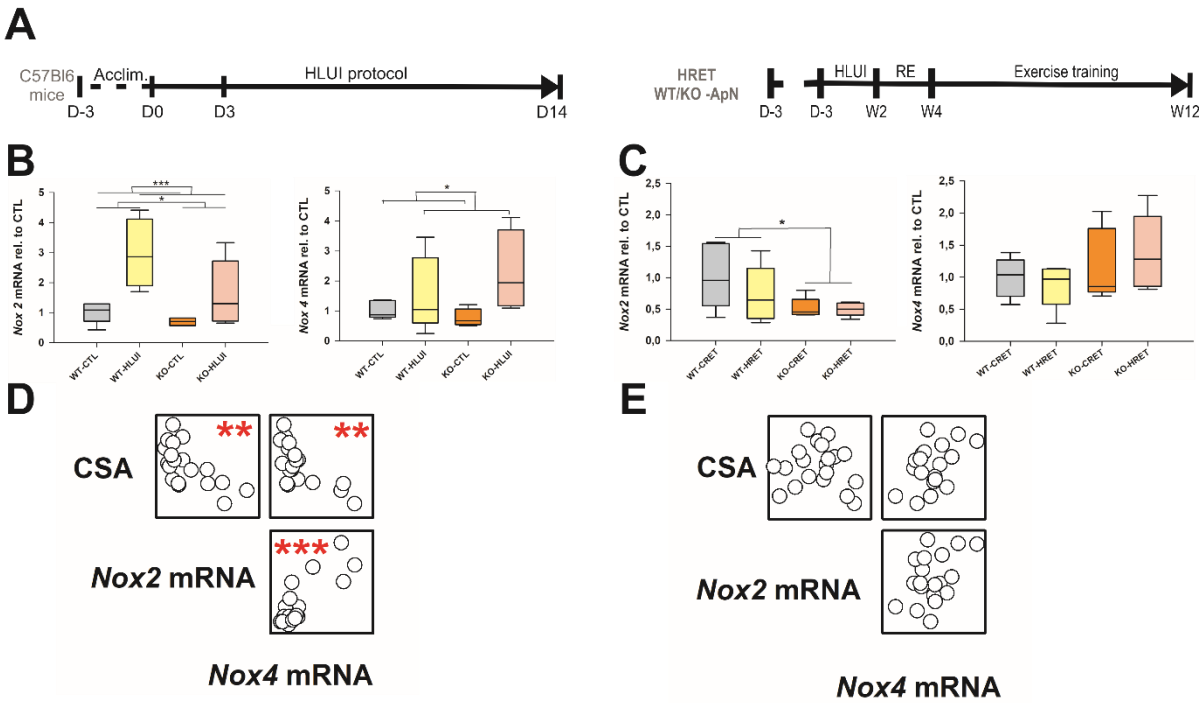

Fig 4. *Nox2* and *Nox4* mRNA response to disuse and reconditioning in ApN-KO mice muscles. (A) Timelines. *Nox 2* and *Nox 4* mRNA levels were assessed following disuse **(B)** or reconditioning protocol **(C)** by RTqPCR with ΔΔCt method (housekeeping gene: *Rplp0*; data normalized to CTL). Data represented as boxplot; * p<0.05, *** p<0.001, Two-way ANOVA. **(D-E)** Associations between mean CSA, *Nox2* and *Nox4* mRNA were assessed with Pearson Product Moment correlation test following disuse **(D)** or reconditioning protocol **(E).** Correlations were considered as statistically significant with *p-values <0.05, ** p<0.01.

ApN KO causes a decreased *Sod2* expression at baseline but does not modify *Sod* downregulation upon disuse or the effect of reconditioning.

To investigate the impact of the lack of ApN on the antioxidant response upon disuse and reconditioning, we evaluated the expression and the protein abundance of the two Superoxide Dismutase (SOD) isoforms: SOD1, mostly cytoplasmic, and the mitochondrial SOD2. The expression of *Nrf2* encoding the nuclear factor erythroid 2-related factor was also evaluated as an important regulator of the antioxidant response, notably upon ET (41).

As concerns *Sod* expression level in WT mice (**Figure 5*A-B*)**, HLUI caused both *Sod1* and *Sod2* downregulations ($^{\#}$, p<0.01, WT-HLUI vs WT-CTL, Two-Way ANOVA, all pairwise comparison). In ApN KO mice, *Sod* expression at baseline tends to be lower as compared to WT mice, particularly *Sod2* ($^{\Psi}$, p<0.05, KO-CTL vs WT-CTL, Two-Way ANOVA, all pairwise comparison, **Figure 5*B***) but the effect of HLUI is not exacerbated in the absence of ApN as compared to WT (**Figure 5*A-B*)**. After exercise training **(Figure 5*C-D*)**, *Sod1* is still downregulated in WT animals that have previously encountered HLUI ($^{\#}$, p<0,01, WT-HRET vs WT-CRET, Two-Way ANOVA, all pairwise comparison). *Sod1* is also downregulated in ApN-KO mice as compared to WT ($^{\Psi\,\Psi}$, p<0.01, KO-CRET vs WT-CRET, Two-Way ANOVA, all pairwise comparison) **(Figure 5*C*)**. However, ET attenuated HLUI-mediated *Sod2* downregulation, even in the absence of ApN (Two-Way ANOVA: NS **Figure 5*D***).

As concerns SOD1 and SOD2 protein levels **(Figure 5*E-H*),** and *Nrf2* expression **(Figure 5*I-J*)**, we did not observe any differences between experimental groups either after HLUI or after ET (Two-Way ANOVA: NS, **Figure 5*E-H***). However, in ApN-KO mice (among which KO-HLUI mice previously shown to exhibit a DMA**, Figure 2*D***), a negative correlation between myofiber CSA and SOD1 protein level was observed (r=-0.76 ; p<0.05, **Figure 5*L***) . Interestingly, this relation was not observed in WT mice (**Figure 5*K***). As expected, *Nrf2* and *Sod1* mRNA levels are positively correlated both in WT (r=0.74; p≤0.01, **Figure 5*M***) and ApN KO (r=0.85; p≤0.01, **Figure 5*N***) animals.

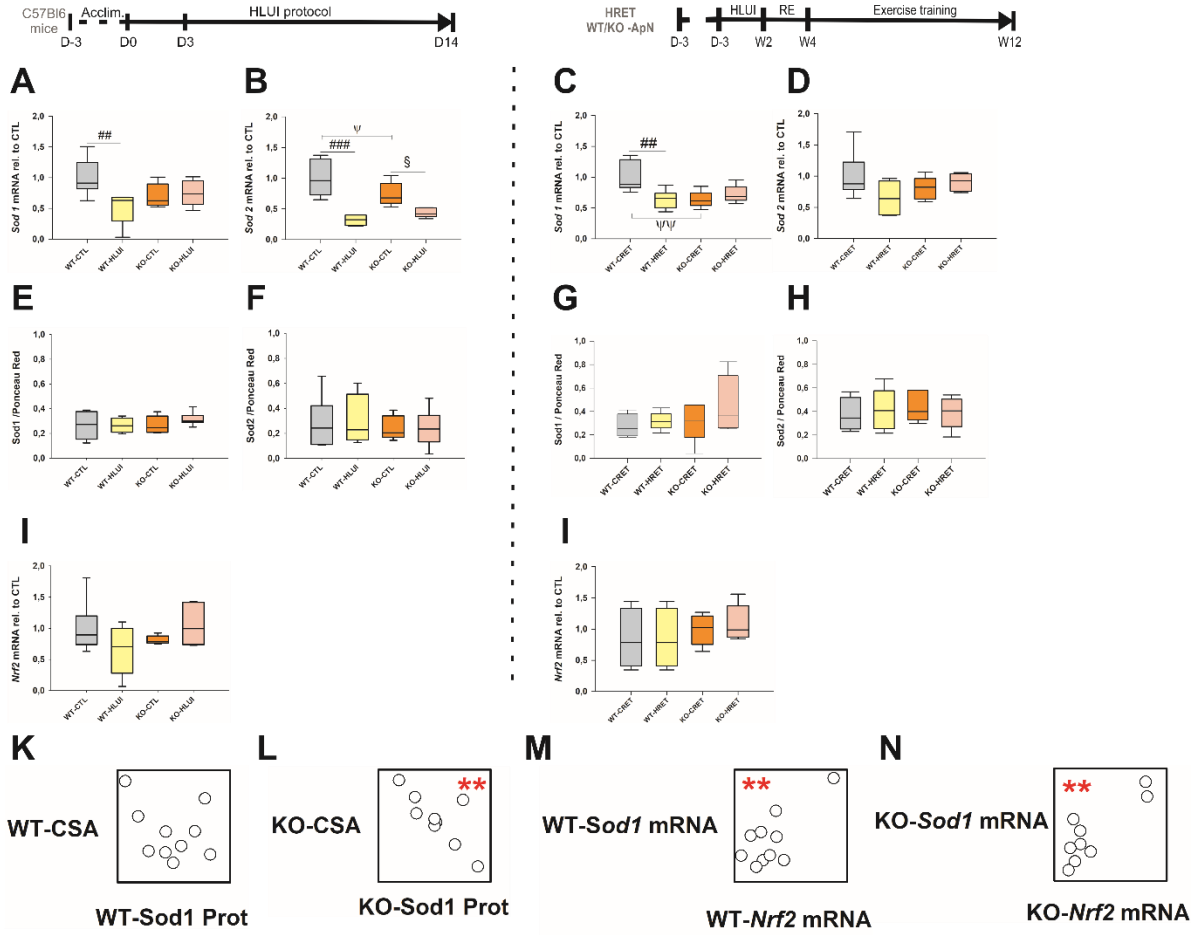

Fig 5. Sod1, Sod2 and *Nrf2* response to disuse and reconditioning in ApN-KO mice muscles. (A-D) *Sod1* and *Sod2* mRNA levels were assessed following disuse **(A-B)** or reconditioning protocol **(C-D)** by RTqPCR with ΔΔCt method (housekeeping gene: *Rplp0*; data normalized to CTL). Data represented as boxplot; ##, p<0.01 (WT-HLUI vs WT-CTL), $^{\Psi}$, p<0.05, (KO-CRET vs WT-CRET), §, p<0.05(KO-HLUI vs KO-CTL), ##, p<0.01 (WT-HRET vs WT-CRET), Two-way ANOVA, All Pairwise Multiple Comparison, Holm Sidak method. **(E-H)** Sod1 and Sod2 protein levels were determined using denaturant PAGE-SDS followed by a western blot. Densitometric analyses were performed with the *Image J* software. Signal was normalized on Ponceau Red. Data represented as boxplot; Two Way ANOVA, NS. **(K-N)** Associations between **(K-L)** mean CSA and Sod1 protein level, and between **(M-N)** *Sod1* and *Nrf2* mRNA were assessed with Pearson Product Moment correlation test following disuse in ApN-KO and WT animals. Correlations were considered as statistically significant with *p-values <0.05, ** p<0.01.

Finally, the consequences of a potential oxidant/antioxidant imbalance were evaluated by using 4HNE immunodetection on Western blot as an indicator of lipid peroxidation **(Figure 6)**. When comparing mean 4HNE levels between experimental groups, we did not observe any significant differences either after the HLUI procedure **(Figure 6*A*)**, or after reconditioning **(Figure 6*B*)**. However, 4HNE in the *Soleus* muscle is negatively correlated with myofiber mean CSA in ApN-KO mice (r=-0.67; p≤0.05) but not in WT (r=0.05; NS) **(Figure 6*A*)**. This relationship is no longer observed after ET **(Figure 6*B*)**. Moreover, the positive association between 4-HNE and SOD1 found in WT mice at W2 (r=0.69 ; p≤0.05) is lost in the absence of ApN **(Figure 6*A*)**, and according to previous results, after ET **(Figure 6*B*)**.

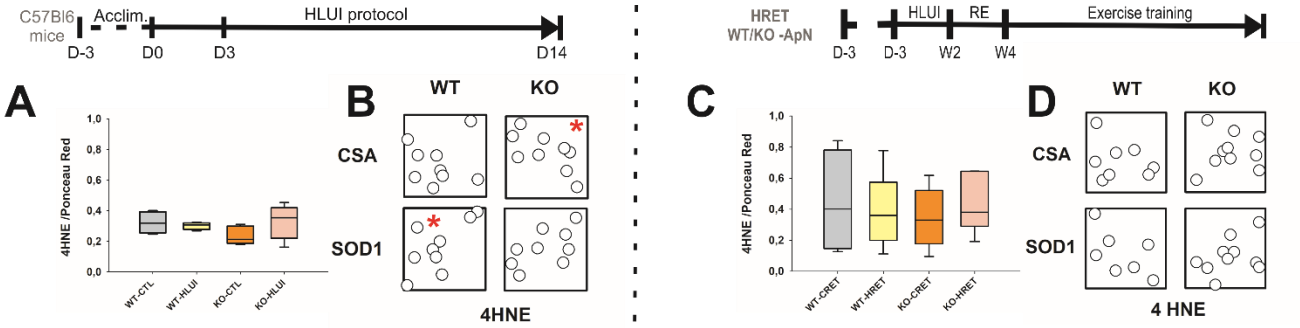

Fig 6. Lipids peroxidation product (4HNE) response to disuse (A-B) and reconditioning (C-D) in ApN-KO mice muscles. (A) and (C) 4HNE levels were determined using denaturant PAGE-SDS followed by a western blot. Densitometric analyses were performed with the *Image J* software. Signal was normalized on Ponceau Red. Data represented as boxplot; Two Way ANOVA, NS. **(B) and (D)** Associations between mean CSA, *Sod1* mRNA and 4-HNE levels were assessed with Pearson Product Moment correlation test following disuse **(B)** or reconditioning protocol **(D).** Correlations were considered as statistically significant with *p-values <0.05.

DISCUSSION

Skeletal muscle deconditioning occurs as a consequence of a prolonged period of hypoactivity (e.g. bed rest, limb immobilization, disease mediated sedentary behavior) which induces the development of a DMA at the tissue level (42, 43). ET remains the only effective therapeutic approach to reverse muscle deconditioning. However, such a therapeutic strategy is often constrained in patients by persistent muscle weakness and ET intolerance (7), particularly in patients with pre-existing chronic pathologies.

Since ApN was demonstrated to have myoprotective effects (reviewed by (20) and (44)) and to mediate ET beneficial effects (33), we previously interrogated ApN pathway key components response to disuse in an optimized DMA murine model (HLUI mice). In this model, we highlighted an elevation of ApN plasmatic level, disturbances in oligomeric form proportions, and muscle-type dependent alterations in adiporeceptor expression (at the mRNA and protein level). We thus hypothesized that such deregulations could reinforce the loss of muscle mass in DMA (36).

Here, we assessed whether the lack of ApN myoprotective effects in ApN-KO mice could (i) worsen the impact of HLUI-mediated skeletal muscle disuse and (ii) limit muscle rehabilitation consisting in 8 weeks of endurant ET protocol.

The HLUI murine model developed in our previous work (36) was designed to limit mouse stress and avoid related confounding factors. In this model, we showed that the experimental design and set-up successfully limited b.w loss in WT HLUI animals (C57BL/6 mice), as compared to other studies using unloading rodent models (45). Here, the same experimental design was maintained but the mouse strain differed (B6129SF2/J), as well as the diet. Indeed, while routine mouse breeding food usually contain large antioxidant excess, we limited their intake to the recommended amount. In those conditions, b.w. slight variations in WT mice were similar to our previous data obtained in C57BL/6 mice. However, we noticed that ApN-KO mice b.w was more affected by the HLUI protocol than WT, but remain similar to b.w loss observed in studies using unloading rodent devices (45). Likewise, b.w in mice lacking ApN was significantly lower than WT before (D-3), at the beginning (D0), and after (W2) the HLUI protocol. In accordance, lower b.w in ApN-KO animals was maintained after reloading and ET although the slight decrease in b.w slopes during the HLUI protocol was reversed during the reloading period in both WT and KO animals. Surprisingly, the study that generated those *Adipo*$^{-/-}$ mice strain did not reported any difference between WT and ApN-KO animals b.w (46). We also have to notice that

b.w measurements were neglected or not shown in most of the studies that used this ApN-KO mice strain.

As anticipated, ApN-KO animals presented undetectable levels of muscular *Adipoq* mRNA or plasmatic ApN but surprisingly, *Adipor1* expression in the *Soleus* muscle was also lowered in animals lacking ApN. Accordingly, *Adipor1* and *Adipor2* expression were reported to be inversely regulated by insulin in physiological conditions, via Phosphoinositide 3-kinase-dependent pathways (47). Such downregulation could therefore be attributed to an hyperinsulinemia linked to the loss of ApN insulino-sensitive effects. However, Ke Ma *et al.* who generated the ApN-KO mice, did not reported evidence of insulin-resistance in this model (46).
Furthermore, as expected from our previous work, *Adipor1* mRNA expression was found reduced by HLUI-mediated disuse in the *Soleus* muscle of WT mice. Accordingly, a similar *Adipor1* mRNA downregulation was observed in mouse *Soleus* muscle after 14 days of HLU without immobilization (35). In this study, Goto *et al.* further demonstrated that functional overloading and muscle reloading following HLU is concomitant with an *Adipor1* mRNA upregulation, highlighting a plausible link between mechanical loading in muscle and ApN pathway regulation (35). More surprisingly, our data highlighted that HLUI-mediated disuse also downregulated *Adipor1* mRNA in ApN-KO animals, providing new evidence for a possible regulation of this receptor by mechanical loading *per se* as suggested by (44, 48).

The evaluation of disuse-mediated alterations in the *Soleus* muscle indicates that the lack of ApN is associated with increased proportions of fast type IIa myofibers at the expense of slow type I myofibers. Such results fit with previous published data addressing myofiber changes in AdipoR1 KO mice (49). Those changes can be attributed to the reduction in the AMPK/SIRT1/PGC1α axis activation described in ApN or Adipor1 loss of function experiments (33, 49). Indeed, the activation of this axis by ApN enhances PGC1α expression and activation through its phosphorylation by active AMPK, thus increasing the number of type I myofiber by promoting mitochondrial biogenesis and oxidative metabolism (16, 49).

A slow-to-fast myofiber-type transition is commonly observed in unloading rodent models (50, 51). We previously showed this myofiber-type switch in the *Tibialis Anterior* muscle in our HLUI model. However, in the *Soleus* muscle, our results suggests that the kinetic of this transition is delayed, probably due to the stretched position of the *Soleus* muscle during the hindlimbs immobilization (52–54). Actually, muscle immobilization in a stretched position is associated with the persistence of isometric contractions (52–54) that may interfere with the slow-to-fast myofiber switch by inducing cytosolic Ca^{++} increases. Indeed, the increased Ca^{++} intracellular concentration stimulates the Ca^{++} Calmodulin-dependant Kinase (CaCMK). In its turn, CaCMK activates the Calcineurin (CaN) phosphatase involved in the translocation of the Nuclear Factor of Activated T-cells (NFAT) transcription factor into the nucleus where it activates the transcription of type I myofibers-related genes (55–58). The “protective effects” of isometric contractions on type I myofiber proportions seems to be maintained in lack of ApN as HLUI did not worsen the decrease in type I myofiber proportion in ApN-KO animals. The later result could be attributed to the reduced AMPK activity described in animals lacking ApN or Adipor1 (16, 19) as reported in hindlimb muscles of unloading rodent models (59). Regarding disuse-mediated morphometrical alterations, the HLUI procedure decreased mean myofiber CSA whatever mouse genotype, but DMA was more severe in ApN KO mice. Fiber type specific analyses revealed a similar effect in type IIa myofibers whereas type I myofibers appeared less affected by the lack of ApN or HLUI. In accordance, global, type I and type IIa myofiber CSA distribution in ApN-KO mice that underwent HLUI protocol were shifted towards smaller CSA clusters (<1500 μm^2) as compared to their matching controls. Importantly, in WT animals this effect

was only observed in type IIa myofibers, fitting with results we obtained in (36). According to our previous study (36) we showed here that the HLUI protocol induces a moderate atrophy in the *Soleus* muscle of WT animals. Importantly, the lack of ApN exacerbated the HLUI-mediated alterations in the slow-twitch muscle *Soleus*. This is probably the result of the loss of ApN myoprotective effects in those animals. Indeed, ApN pathway activation was reported to counteract excessive inflammation, oxidative stress and to support regeneration and oxidative metabolism in skeletal muscle (20).
On the other hand, the data presented here highlighted that, at baseline in animals having not encountered muscle deconditioning, the number of myofibers in higher CSA clusters is increased in ApN-KO animals as compared to WT, particularly for type I myofibers. To the best of our knowledge, only one study reported an increased CSA in type IIb myofibers from the *Tibialis Anterior* of ApN-KO mice (60). Given that type IIa fibers were described to have, in mean, a higher CSA as compared to type I fibres (61, 62), we can reasonably hypothesize that the increased global CSA observed for the *Soleus* muscle of ApN-KO mice may be attributed to the higher percentage of type IIa myofibers.
We then further investigated the consequences of the lack of ApN in muscle reconditioning process following disuse. As expected, type I myofiber proportion was still decreased after ET protocol in ApN-KO animals as compared to WT, indicating that the ET-mediated fast-to-slow myofiber switch in those mice is disturbed by the lack of ApN. Moreover, Inoue *et al.,* demonstrated that 2 months of ApN blockage with neutralizing primary antibodies reduced ET benefits on mice endurance (33), presumably by altering type I myofiber proportion.
Interestingly, WT animals that underwent a period of muscle disuse prior to RE and ET showed higher proportions of type I myofibers than the WT animals that have not encountered muscle deconditioning before ET. A similar effect was observed in the *Soleus* muscle of mice that underwent 4 weeks of hindlimb suspension followed by 60 days of reloading (63). The authors suggested that this effect is a compensatory mechanism to the loss of muscle endurance following disuse (63). Molecular actors mediating this effect remain to be identified but we showed here that this disuse-mediated "preconditioning" effect on type I myofiber proportion is ApN-dependent since it was not observed in ApN KO animals. Given that (i) ApN pathway activation in muscle promotes type I myofibers through the PGC1α phosphorylation and activation (that enhance in its turn mitochondrial biogenesis and homeostasis as well as key enzymes of the oxidative metabolism) (16, 19), that (ii) the ApN-mediated Ca^{++} influx triggers the CaCMK/CaN/NFAT signaling which positively acts on the slow MyHC1β promoter (56–58), and that (iii) the preconditioning-like effect was not observed in ApN-KO mice in this study; we hypothesize that ApN is a key effector required for this disuse-mediated preconditioning effect on myofibers.
Regarding morphometrical analyses, we noticed that ET successfully reversed the previously observed HLUI-induced muscle alterations in myofiber CSA and distribution. Moreover, we reported that the *Soleus* muscle of mice lacking ApN still presents myofiber with larger CSA than WT animals. Accordingly, CSA distribution analyses in animals devoid of ApN show increased proportions of myofibers in clusters characterized by a higher CSA as compared with WT and that this effect is particularly present in animals that underwent muscle deconditioning before ET. Different hypotheses may be suggested to explain this "hypertrophic-like" phenotype in ApN-KO mice. In addition to dysregulations in myofiber metabolism, an increase in intramyocellular lipids (IMCL) may be suggested in ApN-KO mice, as previously described in (60). Nevertheless, further investigations are required to decipher molecular mechanisms underlying *Soleus* muscle structural changes in ApK-KO mice.

Since excessive oxidative stress resulting from mitochondrial alterations in disused muscles was reported to contribute to the development of DMA (64, 65), we interrogated the consequences of the loss of ApN antioxidant properties on key actors of the redox homeostasis in HLUI *Soleus* muscles. HLUI upregulated *Nox2* and *Nox4* mRNA and downregulated *Sod2* mRNA in mice (whatever their genotype)

whereas *Sod1* mRNA was only downregulated in WT animals. Our results therefore indicate that HLUI triggered ROS production pathways while attenuating the expression of oxidative stress-detoxifying enzymes. However, we did not observe any significant modification in Sod1, Sod2 protein levels or 4-hydroxynoenenal (a lipid peroxidation product). The lack of ApN decreased *Sod2* mRNA levels at baseline, as expected (66) but HLUI effects on *Nox* and *Sod* mRNA levels were not amplified in ApN KO mice. Those observations could suggest that the exacerbation of DMA induced by the lack of ApN is not a consequence of an increased oxidative stress. However, correlation analyses shown in ApN-KO animals (but not in WT mice), that *Nox* expression, Sod1 protein levels and lipids peroxidation are higher in myofibres with smaller CSA, suggesting that DMA altered the redox status equilibrium in lack of ApN protection only. The exacerbation of DMA in ApN-KO animals may also be due to the suppression of other ApN myoprotective property. For instance, the more severe atrophy observed in ApN-KO animals could also be the result of the loss of ApN anti-inflammatory effects. Actually, ApN was shown to be secreted by skeletal muscle, in auto- and paracrine manners to locally counteract inflammation by repressing the Nuclear factor kappa B (NF-κB) activity (67, 68). A well, a recent study using RNA-sequencing analyses in unloaded rats *Soleus* reported for the first time in a model of unloading disuse, the upregulation of genes related to inflammation and oxidative stress (69). In addition, the lack of ApN could also alter the IGF/PI3K/Akt/mTOR signaling as ApN-mediated AMPK activation is known to reduce p70S6K1 inhibition on Insulin Receptor Substrate-1 (IRS-1) (70).

The alterations in the redox status equilibrium in ApN-KO animals were no longer observed after the ET protocol, except the *Nox2* mRNA downregulation in ApN-KO mice. Interestingly, *Sod1* mRNA is still downregulated in WT mice that underwent muscle deconditioning before ET whereas the *Sod2* downregulation in animals lacking ApN was reversed by ET, probably through an ApN-independent activation of PGC1α (66). Those results suggest that ET benefits are not drastically impaired in absence of ApN.

In conclusion, the loss of ApN protective properties aggravates atrophy and impairs compensatory mechanisms initiated during DMA, particularly fiber-type switches. This has persistent consequences in muscle plasticity during rehabilitation. However, ApN-independent mechanisms are likely involved in HLUI-mediated redox status perturbations and in ET benefits.

DATA AVAILABILITY

All data supporting the findings of this study are available within the article and its Supplementary Material.

SUPPLEMENTAL MATERIAL

Table 1. Primary and secondary antibody cocktails used in myofiber type immunofluorescence staining.

Table 2. Mouse primers used in RTqPCR analysis.

Suppl. Fig S1. Hindlimb Unloading and Immobilization (HLUI) protocol.

Suppl. Fig S2. Exercise training protocol (ET).

Suppl. Fig S3. Adiponectin receptors and co-receptor mRNA expression in the *Gastrocnemius* of WT and AdKO mice following CRET or HRET protocols.

Suppl. Fig S4. Pearson Product Moment correlations in CTL and HLUI mice.

Suppl. Fig S5. Pearson Product Moment correlations in CRET and HRET mice.

ACKNOWLEDGMENTS

We thank Bernard Blairon for his technical assistance during the conception and the optimization of the Hindlimb Unloading setup. We also thank Sarah Hennuy, Jérôme Francq and the Dv Sylviane Michel for their precious advice and suggestions regarding animal welfare during the optimization of the HLUI model and all through the protocols.

GRANTS

S.S., holds a FRIA doctoral fellowship (FC 41735) from the National Fund for Scientific Research (F.R.S-F.N.R. S), Belgium. The authors acknowledge funding from FRMH (Fonds pour la Recherche Médicale en Hainaut (Grant call 2015) and ABMM-téléthon (Grant call 2015).
DISCLOSURESThe authors declare they have no conflict of interest, financial or otherwise

AUTHOR CONTRIBUTIONS

A.T., A.L., A.E.D., and S.S., conceived and designed research; S.S., V.B., and V.J., performed the experiments; S.S. and V.B., analyzed data; A.T., and S.S., interpreted results of experiments; A.T., and S.S., prepared figures; A.T., and S.S drafted the manuscript; A.T., S.S., edited and revised manuscript; A.T., S.S., V .B, approved final version of manuscript.

REFERENCES

1. **Baehr LM**, **Hughes DC**, **Waddell DS**, **Bodine SC**. SnapShot: Skeletal muscle atrophy. *Cell* 185: 1618-1618.e1, 2022. doi: 10.1016/j.cell.2022.03.028.

2. **Puthucheary Z**, **Harridge S**, **Hart N**. Skeletal muscle dysfunction in critical care: Wasting, weakness, and rehabilitation strategies: *Critical Care Medicine* 38: S676–S682, 2010. doi: 10.1097/CCM.0b013e3181f2458d.

3. **Guitart M**, **Lloreta J**, **Mañas-Garcia L**, **Barreiro E**. Muscle regeneration potential and satellite cell activation profile during recovery following hindlimb immobilization in mice. *Journal of Cellular Physiology* 233: 4360–4372, 2018. doi: 10.1002/jcp.26282.

4. **Mañas-García L**, **Guitart M**, **Duran X**, **Barreiro E**. Satellite Cells and Markers of Muscle Regeneration during Unloading and Reloading: Effects of Treatment with Resveratrol and Curcumin. *Nutrients* 12: 1870, 2020. doi: 10.3390/nu12061870.

5. **Chen B**, **Shan T**. The role of satellite and other functional cell types in muscle repair and regeneration. *J Muscle Res Cell Motil* 40: 1–8, 2019. doi: 10.1007/s10974-019-09511-3.

6. **Bodine SC**. Disuse-induced muscle wasting. *The International Journal of Biochemistry & Cell Biology* 45: 2200–2208, 2013. doi: 10.1016/j.biocel.2013.06.011.

7. **Nakamura K**, **Ohsawa I**, **Masuzawa R**, **Konno R**, **Watanabe A**, **Kawano F**. Running training experience attenuates disuse atrophy in fast-twitch skeletal muscles of rats. *Journal of Applied Physiology* 123: 902–913, 2017. doi: 10.1152/japplphysiol.00289.2017.

8. **Boelens YFN**, **Melchers M**, **van Zanten ARH**. Poor physical recovery after critical illness: incidence, features, risk factors, pathophysiology, and evidence-based therapies. *Current Opinion in Critical Care* 28: 409–416, 2022. doi: 10.1097/MCC.0000000000000955.

9. **Amar D**, **Gay NR**, **Jean-Beltran PM**, **et al,.** Temporal dynamics of the multi-omic response to endurance exercise training. *Nature* 629: 174–183, 2024. doi: 10.1038/s41586-023-06877-w.

10. **Smith JAB**, **Murach KA**, **Dyar KA**, **Zierath JR**. Exercise metabolism and adaptation in skeletal muscle. *Nat Rev Mol Cell Biol* 24: 607–632, 2023. doi: 10.1038/s41580-023-00606-x.

11. **Delezie J**, **Handschin C**. Endocrine Crosstalk Between Skeletal Muscle and the Brain. *Front Neurol* 9: 698, 2018. doi: 10.3389/fneur.2018.00698.

12. **Krause MP**, **Liu Y**, **Vu V**, **Chan L**, **Xu A**, **Riddell MC**, **Sweeney G**, **Hawke TJ**. Adiponectin is expressed by skeletal muscle fibers and influences muscle phenotype and function. *Am J Physiol, Cell Physiol* 295: C203-212, 2008. doi: 10.1152/ajpcell.00030.2008.

13. **Liu Y**, **Palanivel R**, **Rai E**, **Park M**, **Gabor TV**, **Scheid MP**, **Xu A**, **Sweeney G**. Adiponectin stimulates autophagy and reduces oxidative stress to enhance insulin sensitivity during high-fat diet feeding in mice. *Diabetes* 64: 36–48, 2015. doi: 10.2337/db14-0267.

14. **Kadowaki T**, **Yamauchi T**, **Kubota N**, **Hara K**, **Ueki K**, **Tobe K**. Adiponectin and adiponectin receptors in insulin resistance, diabetes, and the metabolic syndrome. *J Clin Invest* 116: 1784–1792, 2006. doi: 10.1172/JCI29126.

15. **Tian L**, **Luo N**, **Zhu X**, **Chung B-H**, **Garvey WT**, **Fu Y**. Adiponectin-AdipoR1/2-APPL1 signaling axis suppresses human foam cell formation: Differential ability of AdipoR1 and AdipoR2 to regulate inflammatory cytokine responses. *Atherosclerosis* 221: 66–75, 2012. doi: 10.1016/j.atherosclerosis.2011.12.014.

16. **Yamauchi T**, **Nio Y**, **Maki T**, **Kobayashi M**, **Takazawa T**, **Iwabu M**, **Okada-Iwabu M**, **Kawamoto S**, **Kubota N**, **Kubota T**, **Ito Y**, **Kamon J**, **Tsuchida A**, **Kumagai K**, **Kozono H**, **Hada Y**, **Ogata H**, **Tokuyama K**, **Tsunoda M**, **Ide T**, **Murakami K**, **Awazawa M**, **Takamoto I**, **Froguel P**, **Hara K**, **Tobe K**, **Nagai R**, **Ueki K**, **Kadowaki T**. Targeted disruption of AdipoR1 and AdipoR2 causes abrogation of adiponectin binding and metabolic actions. *Nat Med* 13: 332–339, 2007. doi: 10.1038/nm1557.

17. **Yamauchi T**, **Iwabu M**, **Okada-Iwabu M**, **Kadowaki T**. Adiponectin receptors: a review of their structure, function and how they work. *Best Pract Res Clin Endocrinol Metab* 28: 15–23, 2014. doi: 10.1016/j.beem.2013.09.003.

18. **Yamauchi T**, **Iwabu M**, **Okada-Iwabu M**, **Kadowaki T**. Adiponectin receptors: A review of their structure, function and how they work. *Best Practice & Research Clinical Endocrinology & Metabolism* 28: 15–23, 2014. doi: 10.1016/j.beem.2013.09.003.

19. **Iwabu M**, **Yamauchi T**, **Okada-Iwabu M**, **Sato K**, **Nakagawa T**, **Funata M**, **Yamaguchi M**, **Namiki S**, **Nakayama R**, **Tabata M**, **Ogata H**, **Kubota N**, **Takamoto I**, **Hayashi YK**, **Yamauchi N**, **Waki H**, **Fukayama M**, **Nishino I**, **Tokuyama K**, **Ueki K**, **Oike Y**, **Ishii S**, **Hirose K**, **Shimizu T**, **Touhara K**, **Kadowaki T**. Adiponectin and AdipoR1 regulate PGC-1alpha and mitochondria by Ca(2+) and AMPK/SIRT1. *Nature* 464: 1313–1319, 2010. doi: 10.1038/nature08991.

20. **Abou-Samra M**, **Selvais CM**, **Dubuisson N**, **Brichard SM**. Adiponectin and Its Mimics on Skeletal Muscle: Insulin Sensitizers, Fat Burners, Exercise Mimickers, Muscling Pills … or Everything Together? *Int J Mol Sci* 21, 2020. doi: 10.3390/ijms21072620.

21. **Waki H**, **Yamauchi T**, **Kamon J**, **Kita S**, **Ito Y**, **Hada Y**, **Uchida S**, **Tsuchida A**, **Takekawa S**, **Kadowaki T**. Generation of Globular Fragment of Adiponectin by Leukocyte Elastase Secreted by Monocytic Cell Line THP-1. *Endocrinology* 146: 790–796, 2005. doi: 10.1210/en.2004-1096.

22. **Fiaschi T**, **Magherini F**, **Gamberi T**, **Modesti PA**, **Modesti A**. Adiponectin as a tissue regenerating hormone: more than a metabolic function. *Cell Mol Life Sci* 71: 1917–1925, 2014. doi: 10.1007/s00018-013-1537-4.

23. **Tanaka Y**, **Kita S**, **Nishizawa H**, **Fukuda S**, **Fujishima Y**, **Obata Y**, **Nagao H**, **Masuda S**, **Nakamura Y**, **Shimizu Y**, **Mineo R**, **Natsukawa T**, **Funahashi T**, **Ranscht B**, **Fukada S-I**, **Maeda N**, **Shimomura I**. Adiponectin promotes muscle regeneration through binding to T-cadherin. *Sci Rep* 9: 16, 2019. doi: 10.1038/s41598-018-37115-3.

24. **Abou-Samra M**, **Lecompte S**, **Schakman O**, **Noel L**, **Many MC**, **Gailly P**, **Brichard SM**. Involvement of adiponectin in the pathogenesis of dystrophinopathy. *Skeletal Muscle* 5: 25, 2015. doi: 10.1186/s13395-015-0051-9.

25. **Fiaschi T**, **Cirelli D**, **Comito G**, **Gelmini S**, **Ramponi G**, **Serio M**, **Chiarugi P**. Globular adiponectin induces differentiation and fusion of skeletal muscle cells. *Cell Res* 19: 584–597, 2009. doi: 10.1038/cr.2009.39.

26. **Fiaschi T**, **Giannoni E**, **Taddei ML**, **Chiarugi P**. Globular Adiponectin Activates Motility and Regenerative Traits of Muscle Satellite Cells. *PLoS ONE* 7: e34782, 2012. doi: 10.1371/journal.pone.0034782.

27. **Parker-Duffen JL**, **Walsh K**. Cardiometabolic effects of adiponectin. *Best Practice & Research Clinical Endocrinology & Metabolism* 28: 81–91, 2014. doi: 10.1016/j.beem.2013.09.001.

28. **Hug C**, **Wang J**, **Ahmad NS**, **Bogan JS**, **Tsao T-S**, **Lodish HF**. T-cadherin is a receptor for hexameric and high-molecular-weight forms of Acrp30/adiponectin. *Proc Natl Acad Sci USA* 101: 10308–10313, 2004. doi: 10.1073/pnas.0403382101.

29. **Fiaschi T**, **Tedesco FS**, **Giannoni E**, **Diaz-Manera J**, **Parri M**, **Cossu G**, **Chiarugi P**. Globular adiponectin as a complete mesoangioblast regulator: role in proliferation, survival, motility, and skeletal muscle differentiation. *Mol Biol Cell* 21: 848–859, 2010. doi: 10.1091/mbc.E09-04-0310.

30. **Ohashi K**, **Parker JL**, **Ouchi N**, **Higuchi A**, **Vita JA**, **Gokce N**, **Pedersen AA**, **Kalthoff C**, **Tullin S**, **Sams A**, **Summer R**, **Walsh K**. Adiponectin Promotes Macrophage Polarization toward an Anti-inflammatory Phenotype. *J Biol Chem* 285: 6153–6160, 2010. doi: 10.1074/jbc.M109.088708.

31. **Eming SA**, **Wynn TA**, **Martin P**. Inflammation and metabolism in tissue repair and regeneration. *Science* 356: 1026–1030, 2017. doi: 10.1126/science.aam7928.

32. **Pierard M**, **Conotte S**, **Tassin A**, **Boutry S**, **Uzureau P**, **Boudjeltia KZ**, **Legrand A**. Interactions of exercise training and high-fat diet on adiponectin forms and muscle receptors in mice. *Nutr Metab (Lond)* 13: 75, 2016. doi: 10.1186/s12986-016-0138-2.

33. **Inoue A**, **Cheng XW**, **Huang Z**, **Hu L**, **Kikuchi R**, **Jiang H**, **Piao L**, **Sasaki T**, **Itakura K**, **Wu H**, **Zhao G**, **Lei Y**, **Yang G**, **Zhu E**, **Li X**, **Sato K**, **Koike T**, **Kuzuya M**. Exercise restores muscle stem cell mobilization, regenerative capacity and muscle metabolic alterations via adiponectin/AdipoR1 activation in SAMP10 mice: Exercise ameliorate muscle regeneration. *Journal of Cachexia, Sarcopenia and Muscle* 8: 370–385, 2017. doi: 10.1002/jcsm.12166.

34. **Abou-Samra M**, **Selvais CM**, **Boursereau R**, **Lecompte S**, **Noel L**, **Brichard SM**. AdipoRon, a new therapeutic prospect for Duchenne muscular dystrophy. *Journal of Cachexia, Sarcopenia and Muscle* 11: 518–533, 2020. doi: 10.1002/jcsm.12531.

35. **Goto A**, **Ohno Y**, **Ikuta A**, **Suzuki M**, **Ohira T**, **Egawa T**, **Sugiura T**, **Yoshioka T**, **Ohira Y**, **Goto K**. Up-regulation of adiponectin expression in antigravitational soleus muscle in response to unloading followed by reloading, and functional overloading in mice. *PLoS ONE* 8: e81929, 2013. doi: 10.1371/journal.pone.0081929.

36. **Szczepanski S**, **Limpens M**, **Jenart V**, **Declèves A-E**, **Legrand A**, **Tassin A**. Muscle-type specific alterations and Adiponectin pathway characterization in a murine model of muscle disuse. (In preparation). [date unknown].

37. **Marzuca-Nassr GN**, **Vitzel KF**, **Murata GM**, **Márquez JL**, **Curi R**. Experimental Model of HindLimb Suspension-Induced Skeletal Muscle Atrophy in Rodents. *Methods Mol Biol* 1916: 167–176, 2019. doi: 10.1007/978-1-4939-8994-2_16.

38. **Hord JM**, **Garcia MM**, **Farris KR**, **Guzzoni V**, **Lee Y**, **Lawler MS**, **Lawler JM**. Nox2 signaling and muscle fiber remodeling are attenuated by losartan administration during skeletal muscle unloading. *Physiological Reports* 9, 2021. doi: 10.14814/phy2.14606.

39. **Lawler JM**, **Kunst M**, **Hord JM**, **Lee Y**, **Joshi K**, **Botchlett RE**, **Ramirez A**, **Martinez DA**. EUK-134 ameliorates nNOSμ translocation and skeletal muscle fiber atrophy during short-term mechanical unloading. *Am J Physiol Regul Integr Comp Physiol* 306: R470-482, 2014. doi: 10.1152/ajpregu.00371.2013.

40. **Cully TR**, **Rodney GG**. Nox4 – RyR1 – Nox2: Regulators of micro-domain signaling in skeletal muscle. *Redox Biol* 36: 101557, 2020. doi: 10.1016/j.redox.2020.101557.

41. **Powers SK**, **Lategan-Potgieter R**, **Goldstein E**. Exercise-induced Nrf2 activation increases antioxidant defenses in skeletal muscles. *Free Radical Biology and Medicine* 224: 470–478, 2024. doi: 10.1016/j.freeradbiomed.2024.07.041.

42. **Nunes EA**, **Stokes T**, **McKendry J**, **Currier BS**, **Phillips SM**. Disuse-induced skeletal muscle atrophy in disease and nondisease states in humans: mechanisms, prevention, and recovery strategies. *American Journal of Physiology-Cell Physiology* 322: C1068–C1084, 2022. doi: 10.1152/ajpcell.00425.2021.

43. **Atherton PJ**, **Greenhaff PL**, **Phillips SM**, **Bodine SC**, **Adams CM**, **Lang CH**. Control of skeletal muscle atrophy in response to disuse: clinical/preclinical contentions and fallacies of evidence. *Am J Physiol Endocrinol Metab* 311: E594-604, 2016. doi: 10.1152/ajpendo.00257.2016.

44. **Krause M**, **Milne K**, **Hawke T**. Adiponectin—Consideration for its Role in Skeletal Muscle Health. *IJMS* 20: 1528, 2019. doi: 10.3390/ijms20071528.

45. **Moustafa A**. Hindlimb unloading-induced reproductive suppression via Downregulation of hypothalamic Kiss-1 expression in adult male rats. *Reprod Biol Endocrinol* 19: 37, 2021. doi: 10.1186/s12958-021-00694-4.

46. **Ma K**, **Cabrero A**, **Saha PK**, **Kojima H**, **Li L**, **Chang BH-J**, **Paul A**, **Chan L**. Increased beta -oxidation but no insulin resistance or glucose intolerance in mice lacking adiponectin. *J Biol Chem* 277: 34658–34661, 2002. doi: 10.1074/jbc.C200362200.

47. **Tsuchida A**, **Yamauchi T**, **Ito Y**, **Hada Y**, **Maki T**, **Takekawa S**, **Kamon J**, **Kobayashi M**, **Suzuki R**, **Hara K**, **Kubota N**, **Terauchi Y**, **Froguel P**, **Nakae J**, **Kasuga M**, **Accili D**, **Tobe K**, **Ueki K**, **Nagai R**, **Kadowaki T**. Insulin/Foxo1 Pathway Regulates Expression Levels of Adiponectin Receptors and Adiponectin Sensitivity. *J Biol Chem* 279: 30817–30822, 2004. doi: 10.1074/jbc.M402367200.

48. **Goto A**, **Ohno Y**, **Ikuta A**, **Suzuki M**, **Ohira T**, **Egawa T**, **Sugiura T**, **Yoshioka T**, **Ohira Y**, **Goto K**. Up-Regulation of Adiponectin Expression in Antigravitational Soleus Muscle in Response to Unloading Followed by Reloading, and Functional Overloading in Mice. *PLoS ONE* 8: e81929, 2013. doi: 10.1371/journal.pone.0081929.

49. **Iwabu M**, **Yamauchi T**, **Okada-Iwabu M**, **Sato K**, **Nakagawa T**, **Funata M**, **Yamaguchi M**, **Namiki S**, **Nakayama R**, **Tabata M**, **Ogata H**, **Kubota N**, **Takamoto I**, **Hayashi YK**, **Yamauchi N**, **Waki H**, **Fukayama M**, **Nishino I**, **Tokuyama K**, **Ueki K**, **Oike Y**, **Ishii S**, **Hirose K**, **Shimizu T**, **Touhara K**, **Kadowaki T**. Adiponectin and AdipoR1 regulate PGC-1α and mitochondria by Ca2+ and AMPK/SIRT1. *Nature* 464: 1313–1319, 2010. doi: 10.1038/nature08991.

50. **Shenkman BS**. From Slow to Fast: Hypogravity-Induced Remodeling of Muscle Fiber Myosin Phenotype. *Acta Naturae* 8: 47–59, 2016.

51. **Wang J**, **Wang F**, **Zhang P**, **Liu H**, **He J**, **Zhang C**, **Fan M**, **Chen X**. PGC-1α over-expression suppresses the skeletal muscle atrophy and myofiber-type composition during hindlimb unloading. *Bioscience, Biotechnology, and Biochemistry* 81: 500–513, 2017. doi: 10.1080/09168451.2016.1254531.

52. **Baker JH**, **Matsumoto DE**. Adaptation of skeletal muscle to immobilization in a shortened position. *Muscle and Nerve* 11: 231–244, 1988. doi: 10.1002/mus.880110308.

53. **Fujita N**, **Fujimoto T**, **Tasaki H**, **Arakawa T**, **Matsubara T**, **Miki A**. Influence of muscle length on muscle atrophy in the mouse tibialis anterior and soleus muscles. *Biomed Res* 30: 39–45, 2009. doi: 10.2220/biomedres.30.39.

54. **Goldspink DF**. The influence of immobilization and stretch on protein turnover of rat skeletal muscle. *The Journal of Physiology* 264: 267–282, 1977. doi: 10.1113/jphysiol.1977.sp011667.

55. **Gundersen K**. Excitation-transcription coupling in skeletal muscle: the molecular pathways of exercise. *Biol Rev Camb Philos Soc* 86: 564–600, 2011. doi: 10.1111/j.1469-185X.2010.00161.x.

56. **Meissner JD**, **Umeda PK**, **Chang K**, **Gros G**, **Scheibe RJ**. Activation of the β myosin heavy chain promoter by MEF-2D, MyoD, p300, and the calcineurin/NFATc1 pathway. *Journal Cellular Physiology* 211: 138–148, 2007. doi: 10.1002/jcp.20916.

57. **Chin ER**, **Olson EN**, **Richardson JA**, **Yang Q**, **Humphries C**, **Shelton JM**, **Wu H**, **Zhu W**, **Bassel-Duby R**, **Williams RS**. A calcineurin-dependent transcriptional pathway controls skeletal muscle fiber type. *Genes Dev* 12: 2499–2509, 1998. doi: 10.1101/gad.12.16.2499.

58. **Parsons SA**, **Millay DP**, **Wilkins BJ**, **Bueno OF**, **Tsika GL**, **Neilson JR**, **Liberatore CM**, **Yutzey KE**, **Crabtree GR**, **Tsika RW**, **Molkentin JD**. Genetic loss of calcineurin blocks mechanical overload-induced skeletal muscle fiber type switching but not hypertrophy. *J Biol Chem* 279: 26192–26200, 2004. doi: 10.1074/jbc.M313800200.

59. **Vilchinskaya N**, **Krivoi I**, **Shenkman B**. AMP-Activated Protein Kinase as a Key Trigger for the Disuse-Induced Skeletal Muscle Remodeling. *IJMS* 19: 3558, 2018. doi: 10.3390/ijms19113558.

60. **Krause MP**, **Liu Y**, **Vu V**, **Chan L**, **Xu A**, **Riddell MC**, **Sweeney G**, **Hawke TJ**. Adiponectin is expressed by skeletal muscle fibers and influences muscle phenotype and function. *American Journal of Physiology-Cell Physiology* 295: C203–C212, 2008. doi: 10.1152/ajpcell.00030.2008.

61. **Zammit PS**. Function of the myogenic regulatory factors Myf5, MyoD, Myogenin and MRF4 in skeletal muscle, satellite cells and regenerative myogenesis. *Seminars in Cell & Developmental Biology* 72: 19–32, 2017. doi: 10.1016/j.semcdb.2017.11.011.

62. **Schiaffino S**, **Reggiani C**. Fiber Types in Mammalian Skeletal Muscles. *Physiological Reviews* 91: 1447–1531, 2011. doi: 10.1152/physrev.00031.2010.

63. **Feng H-Z**, **Chen X**, **Malek MH**, **Jin J-P**. Slow recovery of the impaired fatigue resistance in postunloading mouse soleus muscle corresponding to decreased mitochondrial function and a compensatory increase in type I slow fibers. *American Journal of Physiology-Cell Physiology* 310: C27–C40, 2016. doi: 10.1152/ajpcell.00173.2015.

64. **Hyatt H**, **Deminice R**, **Yoshihara T**, **Powers SK**. Mitochondrial dysfunction induces muscle atrophy during prolonged inactivity: A review of the causes and effects. *Archives of Biochemistry and Biophysics* 662: 49–60, 2019. doi: 10.1016/j.abb.2018.11.005.

65. **Hyatt HW**, **Powers SK**. Mitochondrial Dysfunction Is a Common Denominator Linking Skeletal Muscle Wasting Due to Disease, Aging, and Prolonged Inactivity. *Antioxidants* 10: 588, 2021. doi: 10.3390/antiox10040588.

66. **Kang C**, **Goodman CA**, **Hornberger TA**, **Ji LL**. PGC-1α overexpression by in vivo transfection attenuates mitochondrial deterioration of skeletal muscle caused by immobilization. *FASEB J* 29: 4092–4106, 2015. doi: 10.1096/fj.14-266619.

67. **Delaigle AM**, **Jonas J-C**, **Bauche IB**, **Cornu O**, **Brichard SM**. Induction of Adiponectin in Skeletal Muscle by Inflammatory Cytokines: *in Vivo* and *in Vitro* Studies. *Endocrinology* 145: 5589–5597, 2004. doi: 10.1210/en.2004-0503.

68. **Eisele PS**, **Salatino S**, **Sobek J**, **Hottiger MO**, **Handschin C**. The peroxisome proliferator-activated receptor γ coactivator 1α/β (PGC-1) coactivators repress the transcriptional activity of NF-κB in skeletal muscle cells. *J Biol Chem* 288: 2246–2260, 2013. doi: 10.1074/jbc.M112.375253.

69. **Cui Q**, **Yang H**, **Gu Y**, **Zong C**, **Chen X**, **Lin Y**, **Sun H**, **Shen Y**, **Zhu J**. RNA sequencing (RNA-seq) analysis of gene expression provides new insights into hindlimb unloading-induced skeletal muscle atrophy. *Annals of Translational Medicine* 8: 1595–1595, 2020. doi: 10.21037/atm-20-7400.

70. **Wang C**, **Mao X**, **Wang L**, **Liu M**, **Wetzel MD**, **Guan K-L**, **Dong LQ**, **Liu F**. Adiponectin Sensitizes Insulin Signaling by Reducing p70 S6 Kinase-mediated Serine Phosphorylation of IRS-1 *. *Journal of Biological Chemistry* 282: 7991–7996, 2007. doi: 10.1074/jbc.M700098200.

SUPPLEMENTAL MATERIAL

Table 1. Primary and secondary antibody cocktails used in myofiber type immunofluorescence staining.

Primary antibody cocktail				
	Antigen	**Host species/Isotype**	**Dilution**	**RRID**
ab 11575, Abcam	Laminin	Rabbit, IgG	1:50	RRID: AB_298179
BA-D5, DSHB	MyHC 7	Mouse, IgG2b	1:50	RRID: AB_2235587
SC-71, DSHB	MyHC2	Mouse, IgG1	1:100	RRID: AB_2147165
BF-F3, DSHB	MyHC4	Mouse, IgM	1:10	RRID: AB_2266724
Secondary antibody cocktail				
	Antigen	**Host species**	**Dilution**	**RRID**
Alexa 405, (ab175652) Abcam	Rabbit IgG	Goat	1:50	/
Alexa 647, (A-21242) Thermofisher	Mouse IgG2b	Goat	1:100	/
Alexa 488, (A-21121) Thermofisher	Mouse IgG1	Goat	1:100	/
Alexa 555, (A-21426) Thermofisher	Mouse IgM	Goat	1:50	/

Table S2. Mouse primers used in RTqPCR analysis.

Gene	**Sequence**	**Tm**
Rplp0	Fw: GGA-CCC-GAG-AAG-ACC-TCC-TT Rv: GCA-CAT-CAC-TCA-GAA-TTT-CAA-TGG	60°C
Adipoq	Fw: GTT-GCA-AGC-TCT-CCT-GTT-CC Rv: TCT-CCA-GGA-GTG-CCA-TCT-CT	58°C
Adipor1	Fw: TCT-TCG-GGA-TGT-TCT-TCC-TGG Rv: TTT-GGA-AAA-AGT-CCG-AGA-GAC-C	62°C
Adipor2	Fw: CCT-TTC-GGG-CCT-GTT-TTA-AGA Rv: GAG-TGG-CAG-TAC-ACC-GTG-TG	62°
Cdh13	Fw: GCC-CTC-GTG-AGC-CTT-CTT-C Rv: CAC-CCT-GAG-GTC-CGT-GAT-GT	58°
Nox2	Fw: TCCTATGTTCCTGTACCTTTGTG Rv: GTCCCACCTCCATCTTGAATC	58°C
Nox4	Fw: TCCAAGCTCATTTCCCACAG Rv: CGGAGTTCCATTACATCAGAGG	58°C
Sod1	Fw: CCA-GTG-CAG-GAC-CTC-ATT-TT Rv:	60°C
Sod2	Fw: CGC-GGC-CTA-CGT-GAA-CAA-T Rv: CCC-CAG-CAG-CGG-AAT-AAG	60°C
NrF2	Fw: AGA-GCA-ACT-CCA-GAA-GGA-ACA-G Rv: TGT-GGG-CAA-CCT-GGG-AGT-A	60°C

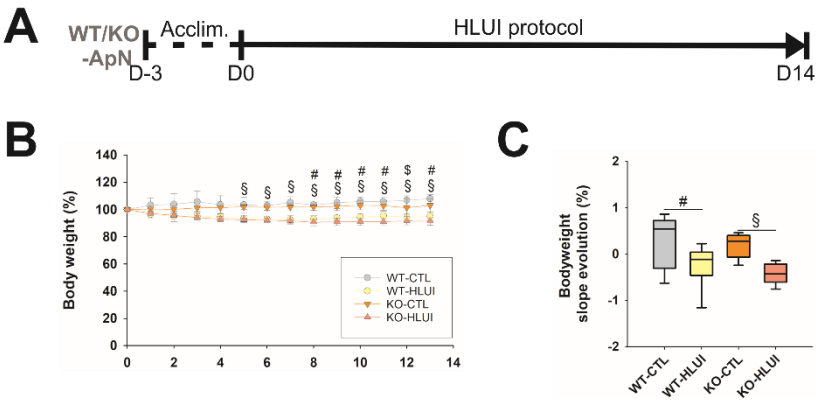

Suppl. Fig S1. Hindlimb Unloading and Immobilization (HLUI) protocol. (A) Timeline. (B) HLUI effect on body weight (b.w) evolution curve. B.w was measured daily and the first day of protocol (D0) was defined as a 100% baseline. Data represented as mean ± SEM, # p<0.05 (WT-CRET vs WT-HRET), § p<0.05 (KO-CRET vs KO-HRET), Two-way ANOVA repeated measures. (**C) Slope comparison.** B.w slope evolution was determined between D1 and D13. Data represented as boxplots; # p<0.05 (WT-CRET vs WT-HRET), § p<0.05 (KO-CRET vs KO-HRET), Two-way ANOVA, All Pairwise Multiple Comparison, Holm-Sidak method.

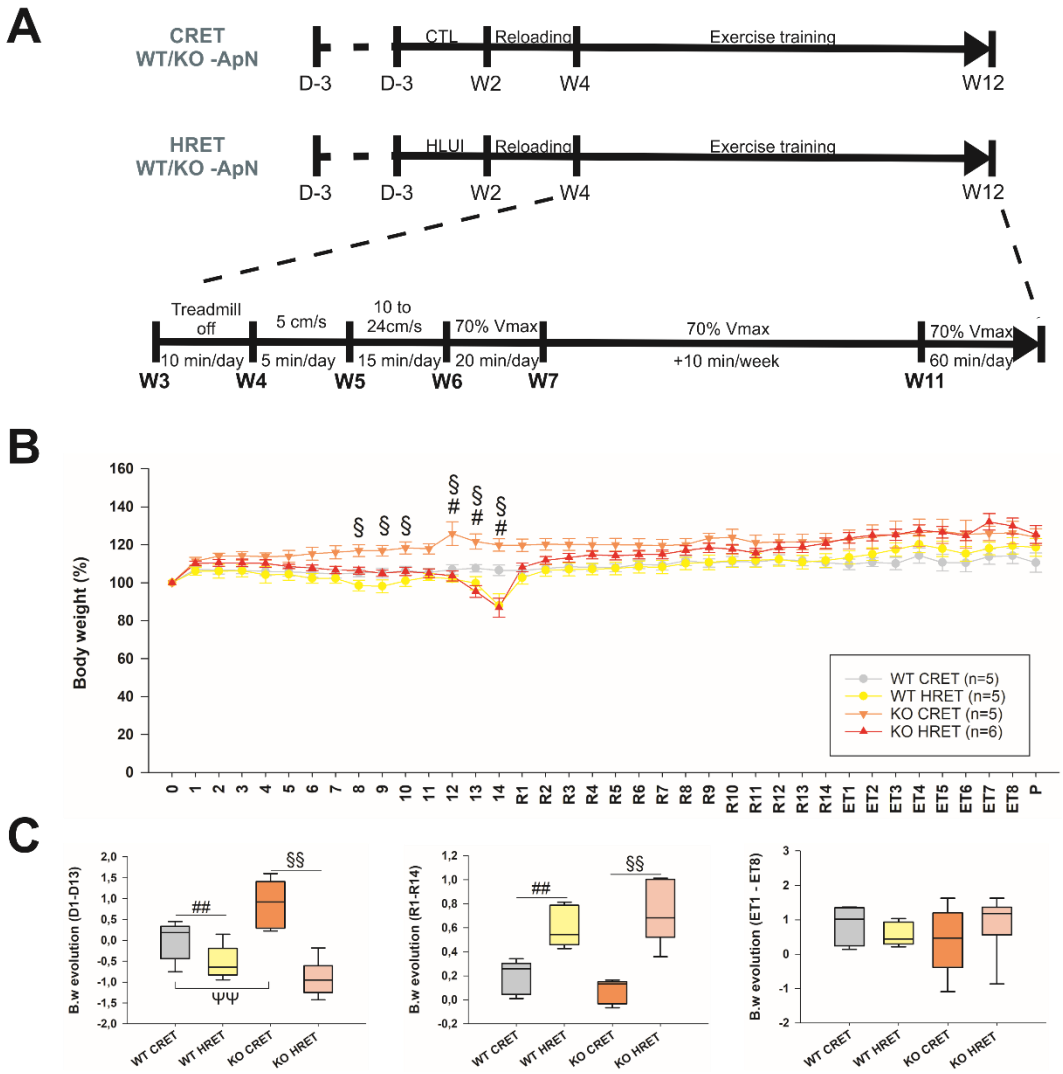

Suppl. Fig S2. Exercise training protocol (ET). (A) Timeline. Mice were acclimatized for 10 minutes to the treadmill room and device during the 2nd week of reloading. Then, the speed was fixed at 5cm/s during the first week of ET. In the 2nd week of ET, treadmill belt speed started at 10cm/s with a gradual speed increase of 2cm/s for 15 minutes. At the beginning of 3rd week of ET, an incremental speed test was performed. For each mouse, exercise was considered maximal, and the test was interrupted when the animal was unable to continue running at the belt speed despite receiving four electric stimulations in one minute. From 3rd week of ET to the last week, the belt speed during training was set at 70% of the maximal running velocity and exercise duration was increased by 10 min per week until a maximum of 60 min was reached. **(B) CRET and HRET effects on body weight (b.w) evolution curve.** B.w was measured daily and the first day of protocol (D0) was defined as a 100% baseline. Data represented as mean ± SEM, # $p<0.05$ (WT-CRET vs WT-HRET), § $p<0.05$ (KO-CRET vs KO-HRET), Two-way ANOVA repeated measures. **(C) Slope comparison.** B.w slope evolution was determined between D1 and D13, R1 and R14 and between ET1 and ET8. Data represented as boxplots; ## $p<0.01$ (WT-CRET vs WT-HRET), §§ $p<0.01$ (KO-CRET vs KO-HRET), Two-way ANOVA, All Pairwise Multiple Comparison, Holm-Sidak method.

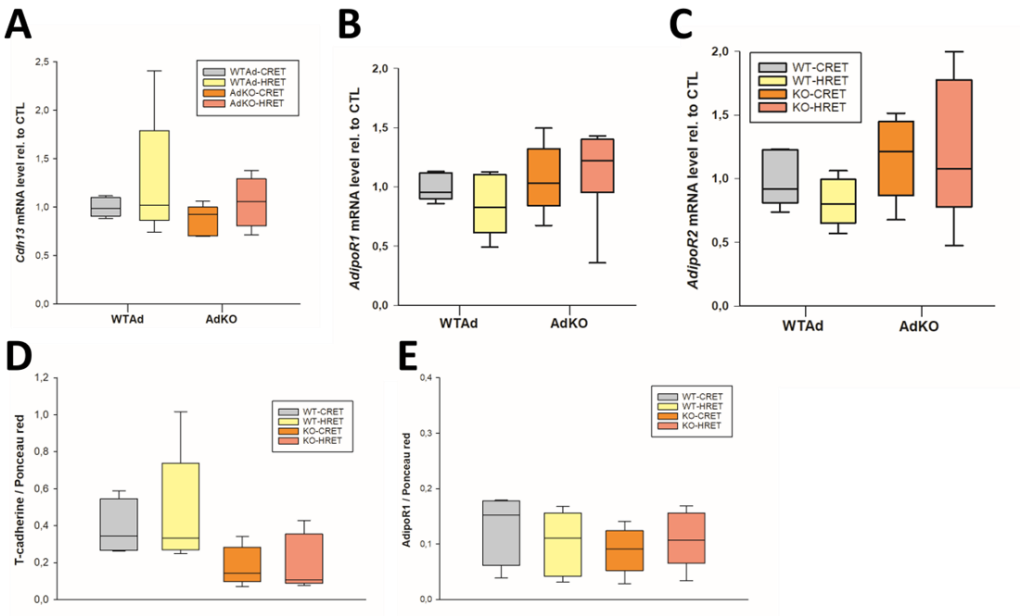

Suppl. Fig S3. Adiponectin receptors and co-receptor mRNA expression in the *Gastrocnemius* of WT and AdKO mice following CRET or HRET protocols. (A) *Cdh13* mRNA level was assessed in the *gastrocnemius* muscle of WT and AdKO mice following CRET or HRET protocol on 1µg of total RNA by RTqPCR (SYBR Green, LightCycler 96 SW1.1, ROCHE) with the ΔΔCt method (*RPLP0* as housekeeping gene) and normalised to WT-CRET (Control). Data represented as boxplot: Two-way ANOVA, NS. **(B) *Adipor1* mRNA level** was assessed in the *gastrocnemius* muscle of Ad and AdKO mice following CRET or HRET protocol on 1µg of total RNA by RTqPCR (SYBR Green, LightCycler 96 SW1.1, ROCHE) with the ΔΔCt method (RPLP0 as housekeeping gene) and normalised to WT-CRET (Control). Data represented as boxplot: Two-way ANOVA, NS. **(C) *Adipor2* mRNA level** was assessed in the gastrocnemius muscle of WT and AdKO mice following CRET or HRET protocol on 1µg of total RNA by RTqPCR (SYBR Green, LightCycler 96 SW1.1, ROCHE) with the ΔΔCt method (RPLP0 as housekeeping gene) and normalised to WT-CRET (Control). Data represented as boxplot: Two-way ANOVA, NS. **(D) T-Cadherin protein level** in *gastrocnemius* muscle was determined by SDS-PAGE electrophoresis followed by WB. Data represented as boxplot: Two-way ANOVA, NS **(E) AdipoR1 protein level** in *gastrocnemius* muscle was determined by SDS-PAGE electrophoresis followed by WB. Data represented as boxplot: Two-way ANOVA, NS

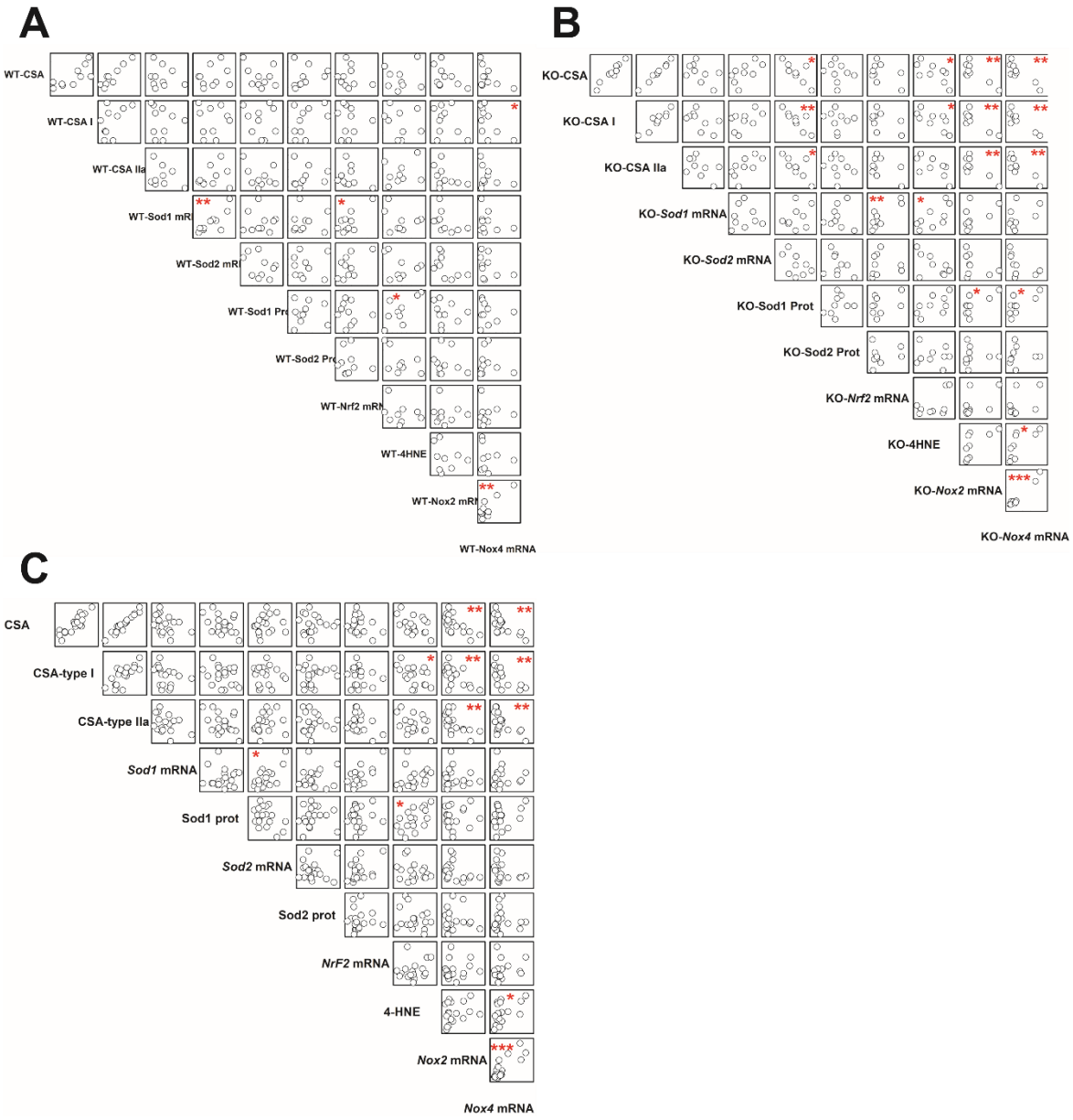

Suppl. Fig S4. Pearson Product Moment correlations in CTL and HLUI mice. (A) WT animals, (B) ApN-KO animals and **(c) All animals.** Correlations were considered as statistically significant with *p-values <0.05, ** p<0.01, ***p<0.001

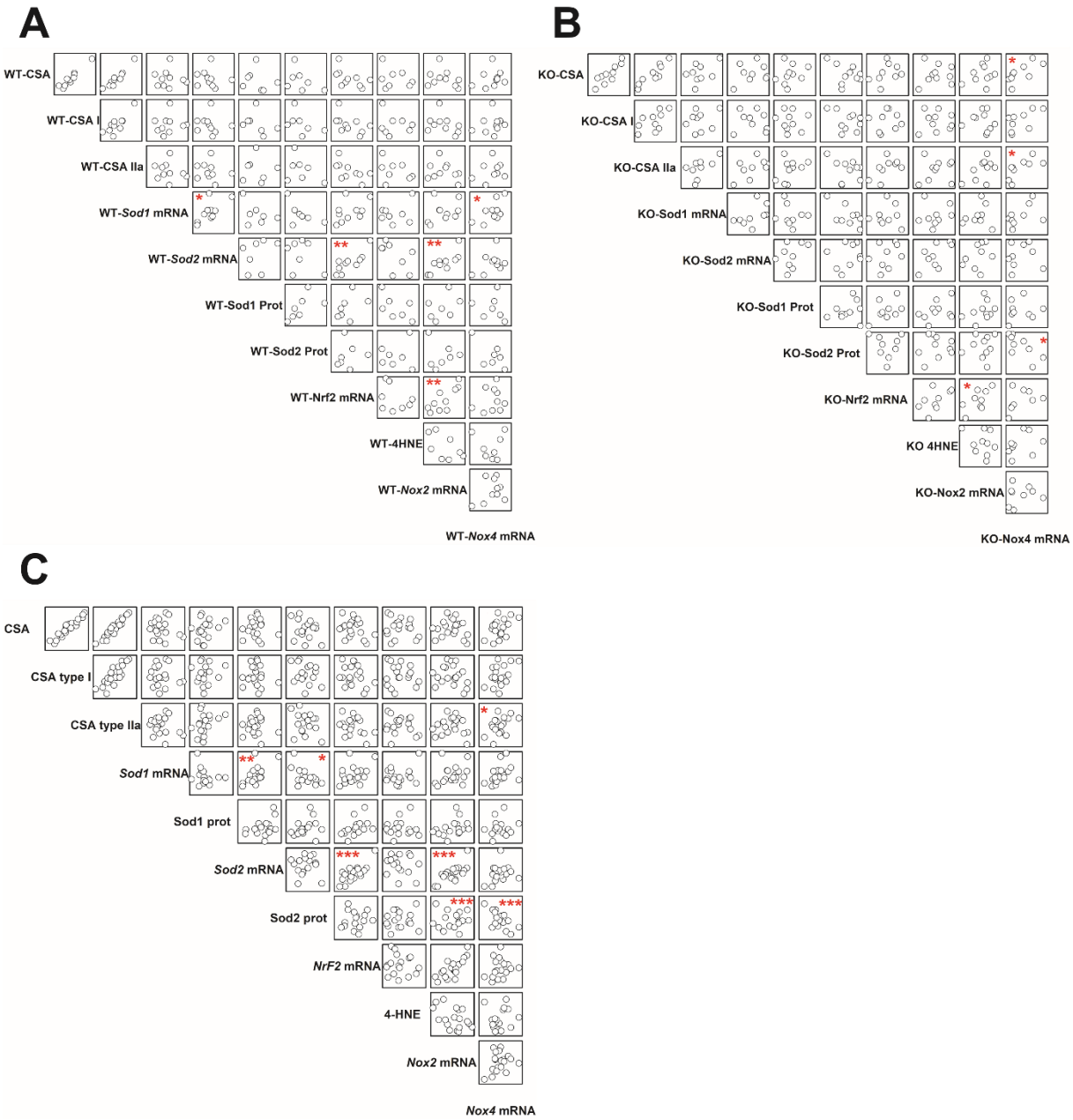

Suppl. Fig S5. Pearson Product Moment correlations in CRET and HRET mice. (A) WT animals, **(B) ApN-KO animals** and **(c) All animals.** Correlations were considered as statistically significant with *p-values <0.05, ** p<0.01, ***p<0.001

CONCLUSIONS

Conclusions

We optimized a murine model of Hindlimb Unloading and Immobilization (HLUI) mimicking DMA and limiting body weight loss and stress as confounding factors. In this model, comparing the slow-twitch *Soleus* and the fast-twitch *TA* muscles, we showed that HLUI induces a fibre-type-dependent atrophy whose severity is likely influenced by muscle positioning (stretched vs shortened) and myofibers type proportion during immobilization. HLUI causes a type I/IIa myofiber switch characterized by a different kinetic according to muscle type and positioning. Concomitantly, an elevation of ApN plasmatic level, disturbances in oligomeric form proportion, and muscle-type dependent alterations in adiporeceptor expression were observed.

Since we confirmed that DMA is associated with ApN pathway alterations, we then investigated whether the loss of ApN myoprotective properties during muscle deconditioning may exacerbate DMA or limit the benefits of muscle reconditioning. In ApN KO *Soleus* mouse muscle submitted to HLUI, we showed a more pronounced DMA severity and an increased proportion of type IIa myofibres. HLUI also has a "pre-conditioning-like effect" increasing, during ET, the type IIa/I myofibre transition. Importantly, this effect is prevented in the absence of ApN, suggesting that the loss of ApN protective properties impairs muscle plasticity during rehabilitation.

Finally, since ApN is known for its antioxidant properties, the *Soleus* muscle redox status has been investigated. Globally, ApN KO does not exacerbate HLUI-mediated changes in pro-oxidative/ antioxidant indicators, suggesting that additional ApN properties may be involved in the increased DMA severity observed in these animals. However, in ApN KO mice, correlation analyses showed that myofibers of smaller diameters exhibited higher *Nox* expression, Sod1 protein levels, and lipid peroxidation, indicating that DMA occurring in the absence of ApN is associated with redox equilibrium perturbations. These modifications are, globally, no longer observed after ET, even in ApN KO mice, suggesting that additional ApN-independent processes underline ET effects.

PROSPECTS

Prospects

Our analysis of hybrid I/IIa myofibres in the slow twitch *Soleus* and the fast twitch *Tibialis Anterior* (*TA*) muscles highlighted that the HLUI-mediated disuse induces a slow-to-fast myofibre switch. This switch is associated with increased proportions of type I myofibers that are also positive for type IIa marker. However, other hybrid myofibres combinations were described (e.g. hybrid I/IIx, IIa/IIx, IIx/IIb, …) (10, 53) and the response of these other hybrid myofiber types to HLUI-mediated disuse remains to be investigated to fully understand the myofibers type transitions occurring in the DMA model we optimized.
Moreover, the use of non-invasive methods such as Magnetic Resonance Imaging (MRI) could be used for limb muscle diameter and muscle alteration measurements all thorough the deconditioning, reloading, and reconditioning protocols. Furthermore, this strategy would allow to reduce the number of animals, in accordance with the "reduction" principle of the 3R rule (Reduce, Refine, Replace) (199).

After 14 days of HLUI, we observed ApN pathway alterations in the slow-twitch *Soleus* but not in the fast-twitch *TA* muscle suggesting that the disuse-mediated muscle alterations are muscle-type dependent. Moreover, we reported HLUI-mediated AdipoR dysregulations in the moderately affected *Soleus* which contains high amounts of type I myofibres. In contrast, AdipoR expression was unaffected in the *TA* muscle that contains less than 1% of type I myofibres and was more severely affected by disuse. In prospect, myofibre type immunofluorescence staining could be combined with AdipoR immunofluorescence detection to further investigate fiber-type dependant AdipoR modifications. Moreover, this type of experiment will give information about AdipoR location at the plasma membrane. Indeed, ApN biological effect could also be impaired by adiporeceptor internalization. AdipoR1/AdipoR2/T-Cadherin downstream signalling pathways (AMPK/SIRT1/PGC1a axis and PPARα expression and activity) remain to be investigated in the whole muscle and also specifically in slow and fast-type fibres by co-IF. This would allow to obtain a more complete vision of HLUI-mediated alterations of the ApN pathway.
Moreover, since ApN is known for its insulin-sensitizing effects, fasting glycemia, Insulin and IGF-1 plasmatic levels may be added as outcome measurement in our experimental conditions. As well, AkT/mTOR, AMPK and inflammation pathway responses to HLUI-mediated DMA can also be investigated as potential contributors to the more severe alterations observed in muscles from mice devoid of ApN. In parallel, investigations of the redox status in disused and reconditioned muscle should be continued by interrogating directly protein oxidation levels and ROS-mediated DNA damages with oxiblot assay and 8-hydroxy-2'-desoxyguanosine (8-OHdG) ELISA assay respectively, as we hypothesize those could contribute to the hypertrophic-like phenotype observed in mice lacking ApN
To further decipher the contribution of ApN protective role in DMA, gain-of-function studies have to be realized by using pharmacological agents either alone or in combination with ET. Pharmacological agents of interest are notably AdipoR activators (AdipoRON) and activators of AdipoR1-AMPK pathway (AICAR). Preventive and curative modalities should be tested.

On the other hand, given (i) ApN role in the regeneration process, (ii) the altered adult myogenesis described in DMA, ApN pathway needs to be further analyzed specifically in muscle satellite cells (SCs) and Fibro-adipogenic progenitors (FAP), two important cell types in the muscle regeneration process (200). SC and FAP muscle cell fractions can be isolated by Fluorescence-activated cell sorting (FACS) and it might be interesting to investigate myogenic and adipogenic markers by RT-qPCR, WB and ELISA in cells isolated *ex vivo*.
To further study whether ApN pathway dysregulations are involved in the impaired regeneration process associated with muscle deconditioning, (CTX 10 µM)-induced injury can be induce in HLUI mice to study the subsequent regeneration process. The regeneration potential following HLUI can then be deciphered by the measurement of (i) the number of quiescent $Pax7^+$ SC by IF (ii) gene and protein expression of myogenic (Pax7, MyoD1, Myogenin, Myostatin, Myosin Heavy Chain) and adipogenic markers (C/EBPα/β, PPAR-γ, PPARδ) by RTqPCR and WB.

Finally, our results suggest that ApN-independent processes underline ET effects. Among potential mechanisms, exerkines produced by skeletal muscle during ET are of great interest. Moreover, it remains unclear whether ApN can be considered as an exerkine. To clarify those points, it would be interesting to complete our *in vivo* approach with mechanistic experiments in reductionist models *in vitro*.
The electrical-pulse stimulation (EPS) model that can be applied both on murine and human myotubes. The use of this model would allow to induce muscle cell contractions to (i) study myofibre contraction impact *per se* on ApN pathway, and (ii) to obtain a media enriched in exerkines. Preliminary results have been obtained (**see preliminary results in Annexe 1**) but it remains necessary to improve the model through the testing of different kinetic of stimulation and resting periods, notably in the aim to maximise the amount of exerkines in the EPS-conditioned culture media. Once the model optimized, it should be interesting to assess the relative pro-myogenic contribution of ApN and exerkines on muscle cell differentiation. To this aim, the exerkine-enriched media can then be transferred on murine myoblasts to study the effect of exerkines on myoblasts proliferation (EdU) and myogenic differentiation by quantifying myogenin (MGN)-positive nuclei and the myosin heavy chain (MHC)-positive area. Myoblast fusion can also be assessed by the MFI (myogenic fusion index).
As well, the exerkine-enriched media can also be transferred on isolated murine myofibres (from HLUI mice for instance). In this model, myofibres are isolated with their associated quiescent SC, which remain in their niche under the surrounding basal lamina. Culturing isolated myofibers causes activation of their associated SC that co-express Pax7 and MyoD within 24h. SC divide after 36h and proliferate further before most of them down-regulate Pax7 and induce myogenin to differentiate. Others maintain Pax7 expression and return to a quiescent-like state, modeling SC self-renewal *ex vivo*.
Further ApN gain- and loss- of function experiments are planned in this EPS model. For instance, the effect of activators of ApN or downstream Ad pathway effectors could be compared with those of exerkines-enriched media. Finally, EPS will be applied on ApN-

deficient myotubes (shRNA or CRISPRCas9). The exerkine-enriched media will be tested on myobasts treated or not with shRNA against adiporeceptors or downstream pathway components to decipher ApN effects from other potential exerkines.

Bibliography

1. **Frontera W**, **Ochala J**. Skeletal Muscle: A Brief Review of Structure and Function. *Calcif Tissue Int* 3: 183–195, Mars. doi: DOI: 10.1007/s00223-014-9915-y.

2. **Gash MC**, **Kandle PF**, **Murray I**, **Varacallo M**. Physiology, Muscle Contraction [Online]. In: *StatPearls*. StatPearls Publishing http://www.ncbi.nlm.nih.gov/books/NBK537140/ [22 Feb. 2023].

3. **Zammit PS**, **Relaix F**, **Nagata Y**, **Ruiz AP**, **Collins CA**, **Partridge TA**, **Beauchamp JR**. Pax7 and myogenic progression in skeletal muscle satellite cells. *Journal of Cell Science* 119: 1824–1832, 2006. doi: 10.1242/jcs.02908.

4. **Chen B**, **Shan T**. The role of satellite and other functional cell types in muscle repair and regeneration. *J Muscle Res Cell Motil* 40: 1–8, 2019. doi: 10.1007/s10974-019-09511-3.

5. **Baghdadi MB**, **Tajbakhsh S**. Regulation and phylogeny of skeletal muscle regeneration. *Developmental Biology* 433: 200–209, 2018. doi: 10.1016/j.ydbio.2017.07.026.

6. **Zammit PS**. Function of the myogenic regulatory factors Myf5, MyoD, Myogenin and MRF4 in skeletal muscle, satellite cells and regenerative myogenesis. *Seminars in Cell & Developmental Biology* 72: 19–32, 2017. doi: 10.1016/j.semcdb.2017.11.011.

7. **Schiaffino S**, **Reggiani C**. Fiber Types in Mammalian Skeletal Muscles. *Physiological Reviews* 91: 1447–1531, 2011. doi: 10.1152/physrev.00031.2010.

8. **Pette D**. Skeletal muscle plasticity – history, facts and concepts. In: *Skeletal Muscle Plasticity in Health and Disease*, edited by Bottinelli R, Reggiani C. Springer Netherlands, p. 1–27.

9. **Kneppers A**, **Leermakers P**, **Pansters N**, **Backx E**, **Gosker H**, **Van Loon L**, **Schols A**, **Langen R**, **Verdijk L**. Coordinated regulation of skeletal muscle mass and metabolic plasticity during recovery from disuse. *The FASEB Journal* 33: 1288–1298, 2019. doi: 10.1096/fj.201701403RRR.

10. **Tobias IS**, **Galpin AJ**. Moving human muscle physiology research forward: an evaluation of fiber type-specific protein research methodologies. *American Journal of Physiology-Cell Physiology* 319: C858–C876, 2020. doi: 10.1152/ajpcell.00107.2020.

11. **Blaauw B**, **Schiaffino S**, **Reggiani C**. Mechanisms Modulating Skeletal Muscle Phenotype. In: *Comprehensive Physiology*, edited by Terjung R. Wiley, p. 1645–1687.

12. **Bodine SC**. The role of mTORC1 in the regulation of skeletal muscle mass. *Fac Rev* 11, 2022. doi: 10.12703/r/11-32.

13. **Schiaffino S**, **Reggiani C**, **Akimoto T**, **Blaauw B**. Molecular Mechanisms of Skeletal Muscle Hypertrophy. *JND* 8: 169–183, 2021. doi: 10.3233/JND-200568.

14. **Schultze SM**, **Hemmings BA**, **Niessen M**, **Tschopp O**. PI3K/AKT, MAPK and AMPK signalling: protein kinases in glucose homeostasis. *Expert Rev Mol Med* 14: e1, 2012. doi: 10.1017/S1462399411002109.

15. **Bodine SC**, **Stitt TN**, **Gonzalez M**, **Kline WO**, **Stover GL**, **Bauerlein R**, **Zlotchenko E**, **Scrimgeour A**, **Lawrence JC**, **Glass DJ**, **Yancopoulos GD**. Akt/mTOR pathway is a crucial regulator of skeletal muscle hypertrophy and can prevent muscle atrophy in vivo. *Nat Cell Biol* 3: 1014–1019, 2001. doi: 10.1038/ncb1101-1014.

16. **Liu GY**, **Sabatini DM**. mTOR at the nexus of nutrition, growth, ageing and disease. *Nat Rev Mol Cell Biol* 21: 183–203, 2020. doi: 10.1038/s41580-019-0199-y.

17. **Pullen N**, **Dennis PB**, **Andjelkovic M**, **Dufner A**, **Kozma SC**, **Hemmings BA**, **Thomas G**. Phosphorylation and activation of p70s6k by PDK1. *Science* 279: 707–710, 1998. doi: 10.1126/science.279.5351.707.

18. **Burnett PE**, **Barrow RK**, **Cohen NA**, **Snyder SH**, **Sabatini DM**. RAFT1 phosphorylation of the translational regulators p70 S6 kinase and 4E-BP1. *Proc Natl Acad Sci U S A* 95: 1432–1437, 1998. doi: 10.1073/pnas.95.4.1432.

19. **Chauvin C**, **Koka V**, **Nouschi A**, **Mieulet V**, **Hoareau-Aveilla C**, **Dreazen A**, **Cagnard N**, **Carpentier W**, **Kiss T**, **Meyuhas O**, **Pende M**. Ribosomal protein S6 kinase activity controls the ribosome biogenesis transcriptional program. *Oncogene* 33: 474–483, 2014. doi: 10.1038/onc.2012.606.

20. **Fumagalli S**, **Pende M**. S6 kinase 1 at the central node of cell size and ageing. *Front Cell Dev Biol* 10: 949196, 2022. doi: 10.3389/fcell.2022.949196.

21. **Gingras AC**, **Gygi SP**, **Raught B**, **Polakiewicz RD**, **Abraham RT**, **Hoekstra MF**, **Aebersold R**, **Sonenberg N**. Regulation of 4E-BP1 phosphorylation: a novel two-step mechanism. *Genes Dev* 13: 1422–1437, 1999. doi: 10.1101/gad.13.11.1422.

22. **Hara K**, **Horikoshi M**, **Yamauchi T**, **Yago H**, **Miyazaki O**, **Ebinuma H**, **Imai Y**, **Nagai R**, **Kadowaki T**. Measurement of the High-Molecular Weight Form of Adiponectin in Plasma Is Useful for the Prediction of Insulin Resistance and Metabolic Syndrome. *Diabetes Care* 29: 1357–1362, 2006. doi: 10.2337/dc05-1801.

23. **Salimi K**, **Alvandi M**, **Saberi Pirouz M**, **Rakhshan K**, **Howatson G**. Regulating eEF2 and eEF2K in skeletal muscle by exercise. .

24. **Baehr LM**, **Hughes DC**, **Waddell DS**, **Bodine SC**. SnapShot: Skeletal muscle atrophy. *Cell* 185: 1618-1618.e1, 2022. doi: 10.1016/j.cell.2022.03.028.

25. **Gordon BS**, **Kelleher AR**, **Kimball SR**. Regulation of muscle protein synthesis and the effects of catabolic states. *The International Journal of Biochemistry & Cell Biology* 45: 2147–2157, 2013. doi: 10.1016/j.biocel.2013.05.039.

26. **Zanchi NE**, **Lancha AHJ**. Mechanical stimuli of skeletal muscle: implications on mTOR/p70s6k and protein synthesis. *Eur J Appl Physiol* 102: 253–263, 2008. doi: 10.1007/s00421-007-0588-3.

27. **Shad BJ**, **Smeuninx B**, **Atherton PJ**, **Breen L**. The mechanistic and ergogenic effects of phosphatidic acid in skeletal muscle. *Appl Physiol Nutr Metab* 40: 1233–1241, 2015. doi: 10.1139/apnm-2015-0350.

28. **You J-S**, **Lincoln HC**, **Kim C-R**, **Frey JW**, **Goodman CA**, **Zhong X-P**, **Hornberger TA**. The Role of Diacylglycerol Kinase ζ and Phosphatidic Acid in the Mechanical Activation of Mammalian Target of Rapamycin (mTOR) Signaling and Skeletal Muscle Hypertrophy. *Journal of Biological Chemistry* 289: 1551–1563, 2014. doi: 10.1074/jbc.M113.531392.

29. **Bonaldo P**, **Sandri M**. Cellular and molecular mechanisms of muscle atrophy. *Disease Models & Mechanisms* 6: 25–39, 2013. doi: 10.1242/dmm.010389.

30. **Hyatt H**, **Deminice R**, **Yoshihara T**, **Powers SK**. Mitochondrial dysfunction induces muscle atrophy during prolonged inactivity: A review of the causes and effects. *Archives of Biochemistry and Biophysics* 662: 49–60, 2019. doi: 10.1016/j.abb.2018.11.005.

31. **Bell RAV**, **Al-Khalaf M**, **Megeney LA**. The beneficial role of proteolysis in skeletal muscle growth and stress adaptation. *Skelet Muscle* 6: 16, 2016. doi: 10.1186/s13395-016-0086-6.

32. **Atherton PJ**, **Greenhaff PL**, **Phillips SM**, **Bodine SC**, **Adams CM**, **Lang CH**. Control of skeletal muscle atrophy in response to disuse: clinical/preclinical contentions and fallacies of evidence. *Am J Physiol Endocrinol Metab* 311: E594-604, 2016. doi: 10.1152/ajpendo.00257.2016.

33. **Hyatt HW**, **Powers SK**. The Role of Calpains in Skeletal Muscle Remodeling with Exercise and Inactivity-induced Atrophy. *Int J Sports Med* 41: 994–1008, 2020. doi: 10.1055/a-1199-7662.

34. **Hyatt HW**, **Powers SK**. Mitochondrial Dysfunction Is a Common Denominator Linking Skeletal Muscle Wasting Due to Disease, Aging, and Prolonged Inactivity. *Antioxidants* 10: 588, 2021. doi: 10.3390/antiox10040588.

35. **Powers SK**, **Schrager M**. Redox signaling regulates skeletal muscle remodeling in response to exercise and prolonged inactivity. *Redox Biology* 54: 102374, 2022. doi: 10.1016/j.redox.2022.102374.

36. **Talbert EE**, **Smuder AJ**, **Min K**, **Kwon OS**, **Powers SK**. Calpain and caspase-3 play required roles in immobilization-induced limb muscle atrophy. *Journal of Applied Physiology* 114: 1482–1489, 2013. doi: 10.1152/japplphysiol.00925.2012.

37. **Smuder AJ**, **Kavazis AN**, **Hudson MB**, **Nelson WB**, **Powers SK**. Oxidation enhances myofibrillar protein degradation via calpain and caspase-3. *Free Radical Biology and Medicine* 49: 1152–1160, 2010. doi: 10.1016/j.freeradbiomed.2010.06.025.

38. **Sahoo G**, **Samal D**, **Khandayataray P**, **Murthy MK**. A Review on Caspases: Key Regulators of Biological Activities and Apoptosis. *Mol Neurobiol* 60: 5805–5837, 2023. doi: 10.1007/s12035-023-03433-5.

39. **Whidden MA**, **Smuder AJ**, **Wu M**, **Hudson MB**, **Nelson WB**, **Powers SK**. Oxidative stress is required for mechanical ventilation-induced protease activation in the diaphragm. *Journal of Applied Physiology* 108: 1376–1382, 2010. doi: 10.1152/japplphysiol.00098.2010.

40. **Huang J**, **Forsberg NE**. Role of calpain in skeletal-muscle protein degradation. *Proc Natl Acad Sci U S A* 95: 12100–12105, 1998. doi: 10.1073/pnas.95.21.12100.

41. **Goll DE**, **Thompson VF**, **Li H**, **Wei W**, **Cong J**. The calpain system. *Physiol Rev* 83: 731–801, 2003. doi: 10.1152/physrev.00029.2002.

42. **Vainshtein A**, **Sandri M**. Signaling Pathways That Control Muscle Mass. *Int J Mol Sci* 21: 4759, 2020. doi: 10.3390/ijms21134759.

43. **Smuder AJ**, **Sollanek KJ**, **Nelson WB**, **Min K**, **Talbert EE**, **Kavazis AN**, **Hudson MB**, **Sandri M**, **Szeto HH**, **Powers SK**. Crosstalk between autophagy and oxidative stress regulates proteolysis in the diaphragm during mechanical ventilation. *Free Radical Biology and Medicine* 115: 179–190, 2018. doi: 10.1016/j.freeradbiomed.2017.11.025.

44. **Rom O**, **Reznick AZ**. The role of E3 ubiquitin-ligases MuRF-1 and MAFbx in loss of skeletal muscle mass. *Free Radic Biol Med* 98: 218–230, 2016. doi: 10.1016/j.freeradbiomed.2015.12.031.

45. **Powell SR**. The ubiquitin-proteasome system in cardiac physiology and pathology. *Am J Physiol Heart Circ Physiol* 291: H1–H19, 2006. doi: 10.1152/ajpheart.00062.2006.

46. **Gomes MD**, **Lecker SH**, **Jagoe RT**, **Navon A**, **Goldberg AL**. Atrogin-1, a muscle-specific F-box protein highly expressed during muscle atrophy. *Proc Natl Acad Sci U S A* 98: 14440–14445, 2001. doi: 10.1073/pnas.251541198.

47. **Cohen S**, **Brault JJ**, **Gygi SP**, **Glass DJ**, **Valenzuela DM**, **Gartner C**, **Latres E**, **Goldberg AL**. During muscle atrophy, thick, but not thin, filament components are degraded by MuRF1-dependent ubiquitylation. *J Cell Biol* 185: 1083–1095, 2009. doi: 10.1083/jcb.200901052.

48. **Powers SK**, **Morton AB**, **Ahn B**, **Smuder AJ**. Redox control of skeletal muscle atrophy. *Free Radical Biology and Medicine* 98: 208–217, 2016. doi: 10.1016/j.freeradbiomed.2016.02.021.

49. **Sandri M**, **Sandri C**, **Gilbert A**, **Skurk C**, **Calabria E**, **Picard A**, **Walsh K**, **Schiaffino S**, **Lecker SH**, **Goldberg AL**. Foxo transcription factors induce the atrophy-related ubiquitin ligase atrogin-1 and cause skeletal muscle atrophy. *Cell* 117: 399–412, 2004. doi: 10.1016/s0092-8674(04)00400-3.

50. **Stitt TN**, **Drujan D**, **Clarke BA**, **Panaro F**, **Timofeyva Y**, **Kline WO**, **Gonzalez M**, **Yancopoulos GD**, **Glass DJ**. The IGF-1/PI3K/Akt Pathway Prevents Expression of Muscle Atrophy-Induced

Ubiquitin Ligases by Inhibiting FOXO Transcription Factors. *Molecular Cell* 14: 395–403, 2004. doi: 10.1016/S1097-2765(04)00211-4.

51. **Smith JAB**, **Murach KA**, **Dyar KA**, **Zierath JR**. Exercise metabolism and adaptation in skeletal muscle. *Nat Rev Mol Cell Biol* 24: 607–632, 2023. doi: 10.1038/s41580-023-00606-x.

52. **Schiaffino S**. Muscle fiber type diversity revealed by anti-myosin heavy chain antibodies. *FEBS J* 285: 3688–3694, 2018. doi: 10.1111/febs.14502.

53. **Medler S**. Mixing it up: the biological significance of hybrid skeletal muscle fibers. *Journal of Experimental Biology* 222: jeb200832, 2019. doi: 10.1242/jeb.200832.

54. **Shenkman BS**. From Slow to Fast: Hypogravity-Induced Remodeling of Muscle Fiber Myosin Phenotype. *Acta Naturae* 8: 47–59, 2016.

55. **Kammoun M**, **Cassar-Malek I**, **Meunier B**, **Picard B**. A simplified immunohistochemical classification of skeletal muscle fibres in mouse. *Eur J Histochem* 58, 2014. doi: 10.4081/ejh.2014.2254.

56. **Pette D**, **Peuker H**, **Staron RS**. The impact of biochemical methods for single muscle fibre analysis. *Acta Physiol Scand* 166: 261–277, 1999. doi: 10.1046/j.1365-201x.1999.00568.x.

57. **Wang J**, **Wang F**, **Zhang P**, **Liu H**, **He J**, **Zhang C**, **Fan M**, **Chen X**. PGC-1α over-expression suppresses the skeletal muscle atrophy and myofiber-type composition during hindlimb unloading. *Bioscience, Biotechnology, and Biochemistry* 81: 500–513, 2017. doi: 10.1080/09168451.2016.1254531.

58. **Feng H-Z**, **Chen X**, **Malek MH**, **Jin J-P**. Slow recovery of the impaired fatigue resistance in postunloading mouse soleus muscle corresponding to decreased mitochondrial function and a compensatory increase in type I slow fibers. *American Journal of Physiology-Cell Physiology* 310: C27–C40, 2016. doi: 10.1152/ajpcell.00173.2015.

59. **Handschin C**, **Chin S**, **Li P**, **Liu F**, **Maratos-Flier E**, **Lebrasseur NK**, **Yan Z**, **Spiegelman BM**. Skeletal muscle fiber-type switching, exercise intolerance, and myopathy in PGC-1alpha muscle-specific knock-out animals. *J Biol Chem* 282: 30014–30021, 2007. doi: 10.1074/jbc.M704817200.

60. **Chin ER**, **Olson EN**, **Richardson JA**, **Yang Q**, **Humphries C**, **Shelton JM**, **Wu H**, **Zhu W**, **Bassel-Duby R**, **Williams RS**. A calcineurin-dependent transcriptional pathway controls skeletal muscle fiber type. *Genes Dev* 12: 2499–2509, 1998. doi: 10.1101/gad.12.16.2499.

61. **Gundersen K**. Excitation-transcription coupling in skeletal muscle: the molecular pathways of exercise. *Biol Rev Camb Philos Soc* 86: 564–600, 2011. doi: 10.1111/j.1469-185X.2010.00161.x.

62. **Parsons SA**, **Millay DP**, **Wilkins BJ**, **Bueno OF**, **Tsika GL**, **Neilson JR**, **Liberatore CM**, **Yutzey KE**, **Crabtree GR**, **Tsika RW**, **Molkentin JD**. Genetic loss of calcineurin blocks mechanical overload-induced skeletal muscle fiber type switching but not hypertrophy. *J Biol Chem* 279: 26192–26200, 2004. doi: 10.1074/jbc.M313800200.

63. **Meissner JD**, **Umeda PK**, **Chang K**, **Gros G**, **Scheibe RJ**. Activation of the β myosin heavy chain promoter by MEF-2D, MyoD, p300, and the calcineurin/NFATc1 pathway. *Journal Cellular Physiology* 211: 138–148, 2007. doi: 10.1002/jcp.20916.

64. **Meissner JD**, **Freund R**, **Krone D**, **Umeda PK**, **Chang K-C**, **Gros G**, **Scheibe RJ**. Extracellular signal-regulated kinase 1/2-mediated phosphorylation of p300 enhances myosin heavy chain I/beta gene expression via acetylation of nuclear factor of activated T cells c1. *Nucleic Acids Res* 39: 5907–5925, 2011. doi: 10.1093/nar/gkr162.

65. **Raney MA**, **Turcotte LP**. Evidence for the involvement of CaMKII and AMPK in Ca2+-dependent signaling pathways regulating FA uptake and oxidation in contracting rodent muscle. *J Appl Physiol (1985)* 104: 1366–1373, 2008. doi: 10.1152/japplphysiol.01282.2007.

66. **Kang C**, **Li Ji L**. Role of PGC-1α signaling in skeletal muscle health and disease. *Ann N Y Acad Sci* 1271: 110–117, 2012. doi: 10.1111/j.1749-6632.2012.06738.x.

67. **Iwabu M**, **Yamauchi T**, **Okada-Iwabu M**, **Sato K**, **Nakagawa T**, **Funata M**, **Yamaguchi M**, **Namiki S**, **Nakayama R**, **Tabata M**, **Ogata H**, **Kubota N**, **Takamoto I**, **Hayashi YK**, **Yamauchi N**, **Waki H**, **Fukayama M**, **Nishino I**, **Tokuyama K**, **Ueki K**, **Oike Y**, **Ishii S**, **Hirose K**, **Shimizu T**, **Touhara K**, **Kadowaki T**. Adiponectin and AdipoR1 regulate PGC-1α and mitochondria by Ca2+ and AMPK/SIRT1. *Nature* 464: 1313–1319, 2010. doi: 10.1038/nature08991.

68. **Abou-Samra M**, **Selvais CM**, **Dubuisson N**, **Brichard SM**. Adiponectin and Its Mimics on Skeletal Muscle: Insulin Sensitizers, Fat Burners, Exercise Mimickers, Muscling Pills … or Everything Together? *IJMS* 21: 2620, 2020. doi: 10.3390/ijms21072620.

69. **Röckl KSC**, **Hirshman MF**, **Brandauer J**, **Fujii N**, **Witters LA**, **Goodyear LJ**. Skeletal muscle adaptation to exercise training: AMP-activated protein kinase mediates muscle fiber type shift. *Diabetes* 56: 2062–2069, 2007. doi: 10.2337/db07-0255.

70. **Hardie DG**, **Sakamoto K**. AMPK: a key sensor of fuel and energy status in skeletal muscle. *Physiology (Bethesda)* 21: 48–60, 2006. doi: 10.1152/physiol.00044.2005.

71. **Dos Santos M**, **Backer S**, **Auradé F**, **Wong MM-K**, **Wurmser M**, **Pierre R**, **Langa F**, **Do Cruzeiro M**, **Schmitt A**, **Concordet J-P**, **Sotiropoulos A**, **Jeffrey Dilworth F**, **Noordermeer D**, **Relaix F**, **Sakakibara I**, **Maire P**. A fast Myosin super enhancer dictates muscle fiber phenotype through competitive interactions with Myosin genes. *Nat Commun* 13: 1039, 2022. doi: 10.1038/s41467-022-28666-1.

72. **Almada AE**, **Wagers AJ**. Molecular circuitry of stem cell fate in skeletal muscle regeneration, ageing and disease. *Nat Rev Mol Cell Biol* 17: 267–279, 2016. doi: 10.1038/nrm.2016.7.

73. **Buckingham M**, **Relaix F**. PAX3 and PAX7 as upstream regulators of myogenesis. *Semin Cell Dev Biol* 44: 115–125, 2015. doi: 10.1016/j.semcdb.2015.09.017.

74. **Buckingham M**, **Rigby PWJ**. Gene regulatory networks and transcriptional mechanisms that control myogenesis. *Dev Cell* 28: 225–238, 2014. doi: 10.1016/j.devcel.2013.12.020.

75. **Fukada S-I**, **Akimoto T**, **Sotiropoulos A**. Role of damage and management in muscle hypertrophy: Different behaviors of muscle stem cells in regeneration and hypertrophy. *Biochim Biophys Acta Mol Cell Res* 1867: 118742, 2020. doi: 10.1016/j.bbamcr.2020.118742.

76. **Goldspink G**. MGF: a local growth factor or a local tissue repair factor?: Combining physiological and molecular biology methods have indicated how a factor expressed by stressed muscle induces local muscle fibre repair and adaptation. *PN* : 22–23, 2004. doi: 10.36866/pn.53.22.

77. **Tan Q**, **Li J**, **Yin Y**, **Shao W**. The Role of Growth Factors in the Repair of Motor Injury. *Front Pharmacol* 13: 898152, 2022. doi: 10.3389/fphar.2022.898152.

78. **Zöllner AM**, **Abilez OJ**, **Böl M**, **Kuhl E**. Stretching Skeletal Muscle: Chronic Muscle Lengthening through Sarcomerogenesis. *PLoS ONE* 7: e45661, 2012. doi: 10.1371/journal.pone.0045661.

79. **Peviani SM**, **Guzzoni V**, **Pinheiro-Dardis CM**, **Silva YPD**, **Fioravante ACR**, **Sagawa AH**, **Delfino GB**, **Durigan JLQ**, **Salvini TF**. Regulation of extracellular matrix elements and sarcomerogenesis in response to different periods of passive stretching in the soleus muscle of rats. *Sci Rep* 8: 9010, 2018. doi: 10.1038/s41598-018-27239-x.

80. **Hinks A**, **Hawke TJ**, **Franchi MV**, **Power GA**. The importance of serial sarcomere addition for muscle function and the impact of aging. *Journal of Applied Physiology* 135: 375–393, 2023. doi: 10.1152/japplphysiol.00205.2023.

81. **Nunes EA**, **Stokes T**, **McKendry J**, **Currier BS**, **Phillips SM**. Disuse-induced skeletal muscle atrophy in disease and nondisease states in humans: mechanisms, prevention, and recovery strategies. *American Journal of Physiology-Cell Physiology* 322: C1068–C1084, 2022. doi: 10.1152/ajpcell.00425.2021.

82. **Webster JM**, **Kempen LJAP**, **Hardy RS**, **Langen RCJ**. Inflammation and Skeletal Muscle Wasting During Cachexia. *Front Physiol* 11: 597675, 2020. doi: 10.3389/fphys.2020.597675.

83. **Bodine SC**. Disuse-induced muscle wasting. *The International Journal of Biochemistry & Cell Biology* 45: 2200–2208, 2013. doi: 10.1016/j.biocel.2013.06.011.

84. **De Santana FM**, **Premaor MO**, **Tanigava NY**, **Pereira RMR**. Low muscle mass in older adults and mortality: A systematic review and meta-analysis. *Experimental Gerontology* 152: 111461, 2021. doi: 10.1016/j.exger.2021.111461.

85. **Yin L**, **Li N**, **Jia W**, **Wang N**, **Liang M**, **Yang X**, **Du G**. Skeletal muscle atrophy: From mechanisms to treatments. *Pharmacological Research* 172: 105807, 2021. doi: 10.1016/j.phrs.2021.105807.

86. **Boelens YFN**, **Melchers M**, **van Zanten ARH**. Poor physical recovery after critical illness: incidence, features, risk factors, pathophysiology, and evidence-based therapies. *Current Opinion in Critical Care* 28: 409–416, 2022. doi: 10.1097/MCC.0000000000000955.

87. **Dos Santos C**, **Hussain SNA**, **Mathur S**, **Picard M**, **Herridge M**, **Correa J**, **Bain A**, **Guo Y**, **Advani A**, **Advani SL**, **Tomlinson G**, **Katzberg H**, **Streutker CJ**, **Cameron JI**, **Schols A**, **Gosker HR**, **Batt J**. Mechanisms of Chronic Muscle Wasting and Dysfunction after an Intensive Care Unit Stay. A Pilot Study. *Am J Respir Crit Care Med* 194: 821–830, 2016. doi: 10.1164/rccm.201512-2344OC.

88. **Cuthbertson BH**, **Roughton S**, **Jenkinson D**, **MacLennan G**, **Vale L**. Quality of life in the five years after intensive care: a cohort study. *Crit Care* 14: R6, 2010. doi: 10.1186/cc8848.

89. **Parry SM**, **Nalamalapu SR**, **Nunna K**, **Rabiee A**, **Friedman LA**, **Colantuoni E**, **Needham DM**, **Dinglas VD**. Six-Minute Walk Distance After Critical Illness: A Systematic Review and Meta-Analysis. *J Intensive Care Med* 36: 343–351, 2021. doi: 10.1177/0885066619885838.

90. **Ferrante LE**, **Pisani MA**, **Murphy TE**, **Gahbauer EA**, **Leo-Summers LS**, **Gill TM**. The Association of Frailty With Post-ICU Disability, Nursing Home Admission, and Mortality: A Longitudinal Study. *Chest* 153: 1378–1386, 2018. doi: 10.1016/j.chest.2018.03.007.

91. **Intiso D**, **Centra AM**, **Bartolo M**, **Gatta MT**, **Gravina M**, **Di Rienzo F**. Recovery and long term functional outcome in people with critical illness polyneuropathy and myopathy: a scoping review. *BMC Neurol* 22: 50, 2022. doi: 10.1186/s12883-022-02570-z.

92. **Heesakkers H**, **van der Hoeven JG**, **Corsten S**, **Janssen I**, **Ewalds E**, **Simons KS**, **Westerhof B**, **Rettig TCD**, **Jacobs C**, **van Santen S**, **Slooter AJC**, **van der Woude MCE**, **van den Boogaard M**, **Zegers M**. Clinical Outcomes Among Patients With 1-Year Survival Following Intensive Care Unit Treatment for COVID-19. *JAMA* 327: 559–565, 2022. doi: 10.1001/jama.2022.0040.

93. **Herridge MS**, **Tansey CM**, **Matté A**, **Tomlinson G**, **Diaz-Granados N**, **Cooper A**, **Guest CB**, **Mazer CD**, **Mehta S**, **Stewart TE**, **Kudlow P**, **Cook D**, **Slutsky AS**, **Cheung AM**, **Canadian Critical Care Trials Group**. Functional disability 5 years after acute respiratory distress syndrome. *N Engl J Med* 364: 1293–1304, 2011. doi: 10.1056/NEJMoa1011802.

94. **Kelleher AR**, **Kimball SR**, **Dennis MD**, **Schilder RJ**, **Jefferson LS**. The mTORC1 signaling repressors REDD1/2 are rapidly induced and activation of p70S6K1 by leucine is defective in skeletal muscle of an immobilized rat hindlimb. *American Journal of Physiology-Endocrinology and Metabolism* 304: E229–E236, 2013. doi: 10.1152/ajpendo.00409.2012.

95. **Glover EI**, **Phillips SM**, **Oates BR**, **Tang JE**, **Tarnopolsky MA**, **Selby A**, **Smith K**, **Rennie MJ**. Immobilization induces anabolic resistance in human myofibrillar protein synthesis with low and high dose amino acid infusion. *The Journal of Physiology* 586: 6049–6061, 2008. doi: 10.1113/jphysiol.2008.160333.

96. **Biolo G**, **Ciocchi B**, **Lebenstedt M**, **Barazzoni R**, **Zanetti M**, **Platen P**, **Heer M**, **Guarnieri G**. Short-term bed rest impairs amino acid-induced protein anabolism in humans. *The Journal of Physiology* 558: 381–388, 2004. doi: 10.1113/jphysiol.2004.066365.

97. **Ferrando B**, **Gomez-Cabrera MC**, **Salvador-Pascual A**, **Puchades C**, **Derbré F**, **Gratas-Delamarche A**, **Laparre L**, **Olaso-Gonzalez G**, **Cerda M**, **Viosca E**, **Alabajos A**, **Sebastiá V**,

Alberich-Bayarri A, **García-Castro F**, **Viña J**. Allopurinol partially prevents disuse muscle atrophy in mice and humans. *Sci Rep* 8: 3549, 2018. doi: 10.1038/s41598-018-21552-1.

98. **Phillips SM**, **McGlory C**. CrossTalk proposal: The dominant mechanism causing disuse muscle atrophy is decreased protein synthesis. *The Journal of Physiology* 592: 5341–5343, 2014. doi: 10.1113/jphysiol.2014.273615.

99. **Wall BT**, **Snijders T**, **Senden JMG**, **Ottenbros CLP**, **Gijsen AP**, **Verdijk LB**, **Van Loon LJC**. Disuse Impairs the Muscle Protein Synthetic Response to Protein Ingestion in Healthy Men. *The Journal of Clinical Endocrinology & Metabolism* 98: 4872–4881, 2013. doi: 10.1210/jc.2013-2098.

100. **Drummond MJ**, **Dickinson JM**, **Fry CS**, **Walker DK**, **Gundermann DM**, **Reidy PT**, **Timmerman KL**, **Markofski MM**, **Paddon-Jones D**, **Rasmussen BB**, **Volpi E**. Bed rest impairs skeletal muscle amino acid transporter expression, mTORC1 signaling, and protein synthesis in response to essential amino acids in older adults. *Am J Physiol Endocrinol Metab* 302: E1113-1122, 2012. doi: 10.1152/ajpendo.00603.2011.

101. **Puthucheary Z**, **Harridge S**, **Hart N**. Skeletal muscle dysfunction in critical care: Wasting, weakness, and rehabilitation strategies: *Critical Care Medicine* 38: S676–S682, 2010. doi: 10.1097/CCM.0b013e3181f2458d.

102. **Puthucheary Z**, **Montgomery H**, **Moxham J**, **Harridge S**, **Hart N**. Structure to function: muscle failure in critically ill patients. *J Physiol* 588: 4641–4648, 2010. doi: 10.1113/jphysiol.2010.197632.

103. **Cui Q**, **Yang H**, **Gu Y**, **Zong C**, **Chen X**, **Lin Y**, **Sun H**, **Shen Y**, **Zhu J**. RNA sequencing (RNA-seq) analysis of gene expression provides new insights into hindlimb unloading-induced skeletal muscle atrophy. *Annals of Translational Medicine* 8: 1595–1595, 2020. doi: 10.21037/atm-20-7400.

104. **Powers SK**, **Smuder A**, **Judge A**. Oxidative stress and disuse muscle atrophy: cause or consequence? *Curr Opin Clin Nutr Metab Care* 15: 240–245, 2012. doi: 10.1097/MCO.0b013e328352b4c2.

105. **Rudrappa SS**, **Wilkinson DJ**, **Greenhaff PL**, **Smith K**, **Idris I**, **Atherton PJ**. Human Skeletal Muscle Disuse Atrophy: Effects on Muscle Protein Synthesis, Breakdown, and Insulin Resistance—A Qualitative Review. *Front Physiol* 7: 361, 2016. doi: 10.3389/fphys.2016.00361.

106. **Biensø RS**, **Ringholm S**, **Kiilerich K**, **Aachmann-Andersen N-J**, **Krogh-Madsen R**, **Guerra B**, **Plomgaard P**, **van Hall G**, **Treebak JT**, **Saltin B**, **Lundby C**, **Calbet JAL**, **Pilegaard H**, **Wojtaszewski JFP**. GLUT4 and glycogen synthase are key players in bed rest-induced insulin resistance. *Diabetes* 61: 1090–1099, 2012. doi: 10.2337/db11-0884.

107. **Dirks ML**, **Wall BT**, **van de Valk B**, **Holloway TM**, **Holloway GP**, **Chabowski A**, **Goossens GH**, **van Loon LJC**. One Week of Bed Rest Leads to Substantial Muscle Atrophy and Induces Whole-Body Insulin Resistance in the Absence of Skeletal Muscle Lipid Accumulation. *Diabetes* 65: 2862–2875, 2016. doi: 10.2337/db15-1661.

108. **Cannavino J**, **Brocca L**, **Sandri M**, **Bottinelli R**, **Pellegrino MA**. PGC1-α over-expression prevents metabolic alterations and soleus muscle atrophy in hindlimb unloaded mice. *J Physiol* 592: 4575–4589, 2014. doi: 10.1113/jphysiol.2014.275545.

109. **Kang C**, **Goodman CA**, **Hornberger TA**, **Ji LL**. PGC-1α overexpression by in vivo transfection attenuates mitochondrial deterioration of skeletal muscle caused by immobilization. *FASEB J* 29: 4092–4106, 2015. doi: 10.1096/fj.14-266619.

110. **Walsh CJ**, **Batt J**, **Herridge MS**, **Dos Santos CC**. Muscle Wasting and Early Mobilization in Acute Respiratory Distress Syndrome. *Clinics in Chest Medicine* 35: 811–826, 2014. doi: 10.1016/j.ccm.2014.08.016.

111. **Baek K-W**, **Jung Y-K**, **Kim J-S**, **Park JS**, **Hah Y-S**, **Kim S-J**, **Yoo J-I**. Rodent Model of Muscular Atrophy for Sarcopenia Study. *J Bone Metab* 27: 97–110, 2020. doi: 10.11005/jbm.2020.27.2.97.

112. **Feng H**, **Yang L**, **Liang YY**, **Ai S**, **Liu Y**, **Liu Y**, **Jin X**, **Lei B**, **Wang J**, **Zheng N**, **Chen X**, **Chan JWY**, **Sum RKW**, **Chan NY**, **Tan X**, **Benedict C**, **Wing YK**, **Zhang J**. Associations of timing of physical activity with all-cause and cause-specific mortality in a prospective cohort study. *Nat Commun* 14: 930, 2023. doi: 10.1038/s41467-023-36546-5.

113. **Bull FC**, **Al-Ansari SS**, **Biddle S**, **Borodulin K**, **Buman MP**, **Cardon G**, **Carty C**, **Chaput J-P**, **Chastin S**, **Chou R**, **Dempsey PC**, **DiPietro L**, **Ekelund U**, **Firth J**, **Friedenreich CM**, **Garcia L**, **Gichu M**, **Jago R**, **Katzmarzyk PT**, **Lambert E**, **Leitzmann M**, **Milton K**, **Ortega FB**, **Ranasinghe C**, **Stamatakis E**, **Tiedemann A**, **Troiano RP**, **Van Der Ploeg HP**, **Wari V**, **Willumsen JF**. World Health Organization 2020 guidelines on physical activity and sedentary behaviour. *Br J Sports Med* 54: 1451–1462, 2020. doi: 10.1136/bjsports-2020-102955.

114. **Howard EE**, **Pasiakos SM**, **Fussell MA**, **Rodriguez NR**. Skeletal Muscle Disuse Atrophy and the Rehabilitative Role of Protein in Recovery from Musculoskeletal Injury. *Adv Nutr* 11: 989–1001, 2020. doi: 10.1093/advances/nmaa015.

115. **Joyner MJ**, **Coyle EF**. Endurance exercise performance: the physiology of champions. *The Journal of Physiology* 586: 35–44, 2008. doi: 10.1113/jphysiol.2007.143834.

116. **Chen J**, **Zhou R**, **Feng Y**, **Cheng L**. Molecular mechanisms of exercise contributing to tissue regeneration. *Signal Transduct Target Ther* 7: 383, 2022. doi: 10.1038/s41392-022-01233-2.

117. **Egan B**, **Sharples AP**. Molecular responses to acute exercise and their relevance for adaptations in skeletal muscle to exercise training. *Physiological Reviews* 103: 2057–2170, 2023. doi: 10.1152/physrev.00054.2021.

118. **Konopka AR**, **Suer MK**, **Wolff CA**, **Harber MP**. Markers of Human Skeletal Muscle Mitochondrial Biogenesis and Quality Control: Effects of Age and Aerobic Exercise Training. *The Journals of Gerontology: Series A* 69: 371–378, 2014. doi: 10.1093/gerona/glt107.

119. **Konopka AR**, **Harber MP**. Skeletal muscle hypertrophy after aerobic exercise training. *Exerc Sport Sci Rev* 42: 53–61, 2014. doi: 10.1249/JES.0000000000000007.

120. **Walton RG**, **Kosmac K**, **Mula J**, **Fry CS**, **Peck BD**, **Groshong JS**, **Finlin BS**, **Zhu B**, **Kern PA**, **Peterson CA**. Human skeletal muscle macrophages increase following cycle training and are associated with adaptations that may facilitate growth. *Sci Rep* 9: 969, 2019. doi: 10.1038/s41598-018-37187-1.

121. **Shefer G**, **Rauner G**, **Stuelsatz P**, **Benayahu D**, **Yablonka-Reuveni Z**. Moderate-intensity treadmill running promotes expansion of the satellite cell pool in young and old mice. *FEBS J* 280: 4063–4073, 2013. doi: 10.1111/febs.12228.

122. **Murach KA**, **Fry CS**, **Dupont-Versteegden EE**, **McCarthy JJ**, **Peterson CA**. Fusion and beyond: Satellite cell contributions to loading-induced skeletal muscle adaptation. *The FASEB Journal* 35, 2021. doi: 10.1096/fj.202101096R.

123. **Furrer R**, **Handschin C**. Molecular aspects of the exercise response and training adaptation in skeletal muscle. *Free Radical Biology and Medicine* 223: 53–68, 2024. doi: 10.1016/j.freeradbiomed.2024.07.026.

124. **D'Hulst G**, **Palmer AS**, **Masschelein E**, **Bar-Nur O**, **De Bock K**. Voluntary Resistance Running as a Model to Induce mTOR Activation in Mouse Skeletal Muscle. *Front Physiol* 10: 1271, 2019. doi: 10.3389/fphys.2019.01271.

125. **Ogasawara R**, **Suginohara T**. Rapamycin-insensitive mechanistic target of rapamycin regulates basal and resistance exercise-induced muscle protein synthesis. *FASEB j* 32: 5824–5834, 2018. doi: 10.1096/fj.201701422R.

126. **Masschelein E**, **D'Hulst G**, **Zvick J**, **Hinte L**, **Soro-Arnaiz I**, **Gorski T**, **Von Meyenn F**, **Bar-Nur O**, **De Bock K**. Exercise promotes satellite cell contribution to myofibers in a load-dependent manner. *Skeletal Muscle* 10: 21, 2020. doi: 10.1186/s13395-020-00237-2.

127. **Laurens C**, **Bergouignan A**, **Moro C**. Exercise-Released Myokines in the Control of Energy Metabolism. *Front Physiol* 11: 91, 2020. doi: 10.3389/fphys.2020.00091.

128. **Piccirillo R**. Exercise-Induced Myokines With Therapeutic Potential for Muscle Wasting. *Front Physiol* 10: 287, 2019. doi: 10.3389/fphys.2019.00287.

129. **Legård GE**, **Pedersen BK**. Muscle as an Endocrine Organ. In: *Muscle and Exercise Physiology*. Elsevier, p. 285–307.

130. **Bilski J**, **Brzozowski T**. Special Issue "Adipokines, Myokines, and Physical Exercise in Health and Disease 2.0." *IJMS* 25: 940, 2024. doi: 10.3390/ijms25020940.

131. **Kirk B**, **Feehan J**, **Lombardi G**, **Duque G**. Muscle, Bone, and Fat Crosstalk: the Biological Role of Myokines, Osteokines, and Adipokines. *Curr Osteoporos Rep* 18: 388–400, 2020. doi: 10.1007/s11914-020-00599-y.

132. **Li F**, **Li Y**, **Duan Y**, **Hu C-AA**, **Tang Y**, **Yin Y**. Myokines and adipokines: Involvement in the crosstalk between skeletal muscle and adipose tissue. *Cytokine & Growth Factor Reviews* 33: 73–82, 2017. doi: 10.1016/j.cytogfr.2016.10.003.

133. **Pedersen BK**, **Åkerström TCA**, **Nielsen AR**, **Fischer CP**. Role of myokines in exercise and metabolism. *Journal of Applied Physiology* 103: 1093–1098, 2007. doi: 10.1152/japplphysiol.00080.2007.

134. **Safdar A**, **Saleem A**, **Tarnopolsky MA**. The potential of endurance exercise-derived exosomes to treat metabolic diseases. *Nat Rev Endocrinol* 12: 504–517, 2016. doi: 10.1038/nrendo.2016.76.

135. **García-Hermoso A**, **Ramírez-Vélez R**, **Díez J**, **González A**, **Izquierdo M**. Exercise training-induced changes in exerkine concentrations may be relevant to the metabolic control of type 2 diabetes mellitus patients: A systematic review and meta-analysis of randomized controlled trials. *Journal of Sport and Health Science* 12: 147–157, 2023. doi: 10.1016/j.jshs.2022.11.003.

136. **Chow LS**, **Gerszten RE**, **Taylor JM**, **Pedersen BK**, **van Praag H**, **Trappe S**, **Febbraio MA**, **Galis ZS**, **Gao Y**, **Haus JM**, **Lanza IR**, **Lavie CJ**, **Lee C-H**, **Lucia A**, **Moro C**, **Pandey A**, **Robbins JM**, **Stanford KI**, **Thackray AE**, **Villeda S**, **Watt MJ**, **Xia A**, **Zierath JR**, **Goodpaster BH**, **Snyder MP**. Exerkines in health, resilience and disease. *Nat Rev Endocrinol* 18: 273–289, 2022. doi: 10.1038/s41574-022-00641-2.

137. **Schäffler A**, **Buechler C**. CTRP family: linking immunity to metabolism. *Trends in Endocrinology & Metabolism* 23: 194–204, 2012. doi: 10.1016/j.tem.2011.12.003.

138. **Vester SK**, **Beavil RL**, **Lynham S**, **Beavil AJ**, **Cunninghame Graham DS**, **McDonnell JM**, **Vyse TJ**. Nucleolin acts as the receptor for C1QTNF4 and supports C1QTNF4-mediated innate immunity modulation. *Journal of Biological Chemistry* 296: 100513, 2021. doi: 10.1016/j.jbc.2021.100513.

139. **Krause MP**, **Liu Y**, **Vu V**, **Chan L**, **Xu A**, **Riddell MC**, **Sweeney G**, **Hawke TJ**. Adiponectin is expressed by skeletal muscle fibers and influences muscle phenotype and function. *American Journal of Physiology-Cell Physiology* 295: C203–C212, 2008. doi: 10.1152/ajpcell.00030.2008.

140. **Berner HS**, **Lyngstadaas SP**, **Spahr A**, **Monjo M**, **Thommesen L**, **Drevon CA**, **Syversen U**, **Reseland JE**. Adiponectin and its receptors are expressed in bone-forming cells. *Bone* 35: 842–849, 2004. doi: 10.1016/j.bone.2004.06.008.

141. **Nishida M**, **Funahashi T**, **Shimomura I**. Pathophysiological significance of adiponectin. *Med Mol Morphol* 40: 55–67, 2007. doi: 10.1007/s00795-007-0366-7.

142. **Peake PW**, **Kriketos AD**, **Campbell LV**, **Shen Y**, **Charlesworth JA**. The metabolism of isoforms of human adiponectin: studies in human subjects and in experimental animals. *eur j endocrinol* 153: 409–417, 2005. doi: 10.1530/eje.1.01978.

143. **Krause M**, **Milne K**, **Hawke T**. Adiponectin—Consideration for its Role in Skeletal Muscle Health. *IJMS* 20: 1528, 2019. doi: 10.3390/ijms20071528.

144. **Nakano Y**, **Tobe T**, **Choi-Miura N-H**, **Mazda T**, **Tomita M**. Isolation and Characterization of GBP28, a Novel Gelatin-Binding Protein Purified from Human Plasma. *Journal of Biochemistry* 120: 803–812, 1996. doi: 10.1093/oxfordjournals.jbchem.a021483.

145. **Hu E**, **Liang P**, **Spiegelman BM**. AdipoQ Is a Novel Adipose-specific Gene Dysregulated in Obesity. *Journal of Biological Chemistry* 271: 10697–10703, 1996. doi: 10.1074/jbc.271.18.10697.

146. **Scherer PE**, **Williams S**, **Fogliano M**, **Baldini G**, **Lodish HF**. A Novel Serum Protein Similar to C1q, Produced Exclusively in Adipocytes. *Journal of Biological Chemistry* 270: 26746–26749, 1995. doi: 10.1074/jbc.270.45.26746.

147. **Maeda K**, **Okubo K**, **Shimomura I**, **Funahashi T**, **Matsuzawa Y**, **Matsubara K**. cDNA Cloning and Expression of a Novel Adipose Specific Collagen-like Factor, apM1 (AdiposeMost Abundant Gene Transcript 1). *Biochemical and Biophysical Research Communications* 221: 286–289, 1996. doi: 10.1006/bbrc.1996.0587.

148. **Kadowaki T**, **Yamauchi T**, **Kubota N**, **Hara K**, **Ueki K**, **Tobe K**. Adiponectin and adiponectin receptors in insulin resistance, diabetes, and the metabolic syndrome. *J Clin Invest* 116: 1784–1792, 2006. doi: 10.1172/JCI29126.

149. **Liu Y**, **Palanivel R**, **Rai E**, **Park M**, **Gabor TV**, **Scheid MP**, **Xu A**, **Sweeney G**. Adiponectin Stimulates Autophagy and Reduces Oxidative Stress to Enhance Insulin Sensitivity During High-Fat Diet Feeding in Mice. *Diabetes* 64: 36–48, 2015. doi: 10.2337/db14-0267.

150. **Wang Y**, **Lam KSL**, **Yau M**, **Xu A**. Post-translational modifications of adiponectin: mechanisms and functional implications. *Biochem J* 409: 623–633, 2008. doi: 10.1042/BJ20071492.

151. **Shapiro L**, **Scherer PE**. The crystal structure of a complement-1q family protein suggests an evolutionary link to tumor necrosis factor. *Current Biology* 8: 335–340, 1998. doi: 10.1016/S0960-9822(98)70133-2.

152. **Richards AA**, **Stephens T**, **Charlton HK**, **Jones A**, **Macdonald GA**, **Prins JB**, **Whitehead JP**. Adiponectin Multimerization Is Dependent on Conserved Lysines in the Collagenous Domain: Evidence for Regulation of Multimerization by Alterations in Posttranslational Modifications. *Molecular Endocrinology* 20: 1673–1687, 2006. doi: 10.1210/me.2005-0390.

153. **Simpson F**, **Whitehead JP**. Adiponectin—It's all about the modifications. *The International Journal of Biochemistry & Cell Biology* 42: 785–788, 2010. doi: 10.1016/j.biocel.2009.12.021.

154. **Tsao T-S**, **Tomas E**, **Murrey HE**, **Hug C**, **Lee DH**, **Ruderman NB**, **Heuser JE**, **Lodish HF**. Role of Disulfide Bonds in Acrp30/Adiponectin Structure and Signaling Specificity. *Journal of Biological Chemistry* 278: 50810–50817, 2003. doi: 10.1074/jbc.M309469200.

155. **Pajvani UB**, **Hawkins M**, **Combs TP**, **Rajala MW**, **Doebber T**, **Berger JP**, **Wagner JA**, **Wu M**, **Knopps A**, **Xiang AH**, **Utzschneider KM**, **Kahn SE**, **Olefsky JM**, **Buchanan TA**, **Scherer PE**. Complex Distribution, Not Absolute Amount of Adiponectin, Correlates with Thiazolidinedione-mediated Improvement in Insulin Sensitivity. *Journal of Biological Chemistry* 279: 12152–12162, 2004. doi: 10.1074/jbc.M311113200.

156. **Basu R**, **Pajvani UB**, **Rizza RA**, **Scherer PE**. Selective downregulation of the high molecular weight form of adiponectin in hyperinsulinemia and in type 2 diabetes: differential regulation from nondiabetic subjects. *Diabetes* 56: 2174–2177, 2007. doi: 10.2337/db07-0185.

157. **Waki H**, **Yamauchi T**, **Kamon J**, **Kita S**, **Ito Y**, **Hada Y**, **Uchida S**, **Tsuchida A**, **Takekawa S**, **Kadowaki T**. Generation of Globular Fragment of Adiponectin by Leukocyte Elastase Secreted by Monocytic Cell Line THP-1. *Endocrinology* 146: 790–796, 2005. doi: 10.1210/en.2004-1096.

158. **Abe Y**, **Eto S**, **Matsumae T**, **Ogahara S**, **Murata T**, **Watanabe M**, **Nakashima H**, **Saito T**. The proportion and metabolic effects of adiponectin multimeric isoforms in patients with chronic kidney disease on maintenance hemodialysis. *Renal Failure* 32: 849–854, 2010. doi: 10.3109/0886022X.2010.494804.

159. **Beltowski J**, **Jamroz-Wisniewska A**, **Widomska S**. Adiponectin and its Role in Cardiovascular Diseases. *CHDDT* 8: 7–46, 2008. doi: 10.2174/187152908783884920.

160. Adipor1 - Adiponectin receptor protein 1 - Mus musculus (Mouse) - Adipor1 gene & protein [Online]. [date unknown]. https://www.uniprot.org/uniprot/Q91VH1 [29 Aug. 2019].

161. ADIPOR1 - Adiponectin receptor protein 1 - Homo sapiens (Human) | UniProtKB | UniProt [Online]. [date unknown]. https://www.uniprot.org/uniprotkb/Q96A54/entry [19 Nov. 2024].

162. Adipor2 - Adiponectin receptor protein 2 - Mus musculus (Mouse) - Adipor2 gene & protein [Online]. [date unknown]. https://www.uniprot.org/uniprot/Q8BQS5 [29 Aug. 2019].

163. ADIPOR2 - Adiponectin receptor protein 2 - Homo sapiens (Human) - ADIPOR2 gene & protein [Online]. [date unknown]. https://www.uniprot.org/uniprot/Q86V24 [29 Aug. 2019].

164. **Yamauchi T**, **Kamon J**, **Ito Y**, **Tsuchida A**, **Yokomizo T**, **Kita S**, **Sugiyama T**, **Miyagishi M**, **Hara K**, **Tsunoda M**, **Murakami K**, **Ohteki T**, **Uchida S**, **Takekawa S**, **Waki H**, **Tsuno NH**, **Shibata Y**, **Terauchi Y**, **Froguel P**, **Tobe K**, **Koyasu S**, **Taira K**, **Kitamura T**, **Shimizu T**, **Nagai R**, **Kadowaki T**. Cloning of adiponectin receptors that mediate antidiabetic metabolic effects. *Nature* 423: 762–769, 2003. doi: 10.1038/nature01705.

165. **Yamauchi T**, **Nio Y**, **Maki T**, **Kobayashi M**, **Takazawa T**, **Iwabu M**, **Okada-Iwabu M**, **Kawamoto S**, **Kubota N**, **Kubota T**, **Ito Y**, **Kamon J**, **Tsuchida A**, **Kumagai K**, **Kozono H**, **Hada Y**, **Ogata H**, **Tokuyama K**, **Tsunoda M**, **Ide T**, **Murakami K**, **Awazawa M**, **Takamoto I**, **Froguel**

P, **Hara K**, **Tobe K**, **Nagai R**, **Ueki K**, **Kadowaki T**. Targeted disruption of AdipoR1 and AdipoR2 causes abrogation of adiponectin binding and metabolic actions. *Nat Med* 13: 332–339, 2007. doi: 10.1038/nm1557.

166. **Yamauchi T**, **Iwabu M**, **Okada-Iwabu M**, **Kadowaki T**. Adiponectin receptors: A review of their structure, function and how they work. *Best Practice & Research Clinical Endocrinology & Metabolism* 28: 15–23, 2014. doi: 10.1016/j.beem.2013.09.003.

167. **Hug C**, **Wang J**, **Ahmad NS**, **Bogan JS**, **Tsao T-S**, **Lodish HF**. T-cadherin is a receptor for hexameric and high-molecular-weight forms of Acrp30/adiponectin. *Proc Natl Acad Sci USA* 101: 10308–10313, 2004. doi: 10.1073/pnas.0403382101.

168. **George SJ**, **Beeching CA**. Cadherin:catenin complex: A novel regulator of vascular smooth muscle cell behaviour. *Atherosclerosis* 188: 1–11, 2006. doi: 10.1016/j.atherosclerosis.2005.12.017.

169. **Fukuda S**, **Kita S**, **Obata Y**, **Fujishima Y**, **Nagao H**, **Masuda S**, **Tanaka Y**, **Nishizawa H**, **Funahashi T**, **Takagi J**, **Maeda N**, **Shimomura I**. The unique prodomain of T-cadherin plays a key role in adiponectin binding with the essential extracellular cadherin repeats 1 and 2. *Journal of Biological Chemistry* 292: 7840–7849, 2017. doi: 10.1074/jbc.M117.780734.

170. **Matsuda K**, **Fujishima Y**, **Maeda N**, **Mori T**, **Hirata A**, **Sekimoto R**, **Tsushima Y**, **Masuda S**, **Yamaoka M**, **Inoue K**, **Nishizawa H**, **Kita S**, **Ranscht B**, **Funahashi T**, **Shimomura I**. Positive Feedback Regulation Between Adiponectin and T-Cadherin Impacts Adiponectin Levels in Tissue and Plasma of Male Mice. *Endocrinology* 156: 934–946, 2015. doi: 10.1210/en.2014-1618.

171. **Tanaka Y**, **Kita S**, **Nishizawa H**, **Fukuda S**, **Fujishima Y**, **Obata Y**, **Nagao H**, **Masuda S**, **Nakamura Y**, **Shimizu Y**, **Mineo R**, **Natsukawa T**, **Funahashi T**, **Ranscht B**, **Fukada S**, **Maeda N**, **Shimomura I**. Adiponectin promotes muscle regeneration through binding to T-cadherin. *Sci Rep* 9: 16, 2019. doi: 10.1038/s41598-018-37115-3.

172. **Zhou L**, **Deepa SS**, **Etzler JC**, **Ryu J**, **Mao X**, **Fang Q**, **Liu DD**, **Torres JM**, **Jia W**, **Lechleiter JD**, **Liu F**, **Dong LQ**. Adiponectin activates AMP-activated protein kinase in muscle cells via APPL1/LKB1-dependent and phospholipase C/Ca2+/Ca2+/calmodulin-dependent protein kinase kinase-dependent pathways. *J Biol Chem* 284: 22426–22435, 2009. doi: 10.1074/jbc.M109.028357.

173. **Eisele PS**, **Salatino S**, **Sobek J**, **Hottiger MO**, **Handschin C**. The peroxisome proliferator-activated receptor γ coactivator 1α/β (PGC-1) coactivators repress the transcriptional activity of NF-κB in skeletal muscle cells. *J Biol Chem* 288: 2246–2260, 2013. doi: 10.1074/jbc.M112.375253.

174. **Boursereau R**, **Abou-Samra M**, **Lecompte S**, **Noel L**, **Brichard SM**. New targets to alleviate skeletal muscle inflammation: role of microRNAs regulated by adiponectin. *Sci Rep* 7: 43437, 2017. doi: 10.1038/srep43437.

175. **Okada-Iwabu M**, **Yamauchi T**, **Iwabu M**, **Honma T**, **Hamagami K**, **Matsuda K**, **Yamaguchi M**, **Tanabe H**, **Kimura-Someya T**, **Shirouzu M**, **Ogata H**, **Tokuyama K**, **Ueki K**,

Nagano T, **Tanaka A**, **Yokoyama S**, **Kadowaki T**. A small-molecule AdipoR agonist for type 2 diabetes and short life in obesity. *Nature* 503: 493–499, 2013. doi: 10.1038/nature12656.

176. **Yamauchi T**, **Kamon J**, **Waki H**, **Terauchi Y**, **Kubota N**, **Hara K**, **Mori Y**, **Ide T**, **Murakami K**, **Tsuboyama-Kasaoka N**, **Ezaki O**, **Akanuma Y**, **Gavrilova O**, **Vinson C**, **Reitman ML**, **Kagechika H**, **Shudo K**, **Yoda M**, **Nakano Y**, **Tobe K**, **Nagai R**, **Kimura S**, **Tomita M**, **Froguel P**, **Kadowaki T**. The fat-derived hormone adiponectin reverses insulin resistance associated with both lipoatrophy and obesity. *Nat Med* 7: 941–946, 2001. doi: 10.1038/90984.

177. **Yamauchi T**, **Kamon J**, **Waki H**, **Terauchi Y**, **Kubota N**, **Hara K**, **Mori Y**, **Ide T**, **Murakami K**, **Tsuboyama-Kasaoka N**, **Ezaki O**, **Akanuma Y**, **Gavrilova O**, **Vinson C**, **Reitman ML**, **Kagechika H**, **Shudo K**, **Yoda M**, **Nakano Y**, **Tobe K**, **Nagai R**, **Kimura S**, **Tomita M**, **Froguel P**, **Kadowaki T**. The fat-derived hormone adiponectin reverses insulin resistance associated with both lipoatrophy and obesity. *Nat Med* 7: 941–946, 2001. doi: 10.1038/90984.

178. **Liu Y**, **Turdi S**, **Park T**, **Morris NJ**, **Deshaies Y**, **Xu A**, **Sweeney G**. Adiponectin corrects high-fat diet-induced disturbances in muscle metabolomic profile and whole-body glucose homeostasis. *Diabetes* 62: 743–752, 2013. doi: 10.2337/db12-0687.

179. **Abou-Samra M**, **Selvais CM**, **Boursereau R**, **Lecompte S**, **Noel L**, **Brichard SM**. AdipoRon , a new therapeutic prospect for Duchenne muscular dystrophy. *Journal of Cachexia, Sarcopenia and Muscle* 11: 518–533, 2020. doi: 10.1002/jcsm.12531.

180. **Balasubramanian P**, **Schaar AE**, **Gustafson GE**, **Smith AB**, **Howell PR**, **Greenman A**, **Baum S**, **Colman RJ**, **Lamming DW**, **Diffee GM**, **Anderson RM**. Adiponectin receptor agonist AdipoRon improves skeletal muscle function in aged mice. *eLife* 11: e71282, 2022. doi: 10.7554/eLife.71282.

181. **Delaigle AM**, **Jonas J-C**, **Bauche IB**, **Cornu O**, **Brichard SM**. Induction of Adiponectin in Skeletal Muscle by Inflammatory Cytokines: *in Vivo* and *in Vitro* Studies. *Endocrinology* 145: 5589–5597, 2004. doi: 10.1210/en.2004-0503.

182. **Delaigle AM**, **Senou M**, **Guiot Y**, **Many M-C**, **Brichard SM**. Induction of adiponectin in skeletal muscle of type 2 diabetic mice: in vivo and in vitro studies. *Diabetologia* 49: 1311–1323, 2006. doi: 10.1007/s00125-006-0210-y.

183. **Jortay J**, **Senou M**, **Abou-Samra M**, **Noel L**, **Robert A**, **Many M-C**, **Brichard SM**. Adiponectin and Skeletal Muscle. *The American Journal of Pathology* 181: 245–256, 2012. doi: 10.1016/j.ajpath.2012.03.035.

184. **Jortay J**, **Senou M**, **Delaigle A**, **Noel L**, **Funahashi T**, **Maeda N**, **Many MC**, **Brichard SM**. Local Induction of Adiponectin Reduces Lipopolysaccharide-Triggered Skeletal Muscle Damage. *Endocrinology* 151: 4840–4851, 2010. doi: 10.1210/en.2009-1462.

185. **Abou-Samra M**, **Boursereau R**, **Lecompte S**, **Noel L**, **Brichard SM**. Potential Therapeutic Action of Adiponectin in Duchenne Muscular Dystrophy. *The American Journal of Pathology* 187: 1577–1585, 2017. doi: 10.1016/j.ajpath.2017.02.018.

186. **Fiaschi T**, **Giannoni E**, **Taddei ML**, **Chiarugi P**. Globular Adiponectin Activates Motility and Regenerative Traits of Muscle Satellite Cells. *PLoS ONE* 7: e34782, 2012. doi: 10.1371/journal.pone.0034782.

187. **Abou-Samra M**, **Lecompte S**, **Schakman O**, **Noel L**, **Many MC**, **Gailly P**, **Brichard SM**. Involvement of adiponectin in the pathogenesis of dystrophinopathy. *Skeletal Muscle* 5: 25, 2015. doi: 10.1186/s13395-015-0051-9.

188. **Ohashi K**, **Parker JL**, **Ouchi N**, **Higuchi A**, **Vita JA**, **Gokce N**, **Pedersen AA**, **Kalthoff C**, **Tullin S**, **Sams A**, **Summer R**, **Walsh K**. Adiponectin Promotes Macrophage Polarization toward an Anti-inflammatory Phenotype. *Journal of Biological Chemistry* 285: 6153–6160, 2010. doi: 10.1074/jbc.M109.088708.

189. **Goto A**, **Ohno Y**, **Ikuta A**, **Suzuki M**, **Ohira T**, **Egawa T**, **Sugiura T**, **Yoshioka T**, **Ohira Y**, **Goto K**. Up-Regulation of Adiponectin Expression in Antigravitational Soleus Muscle in Response to Unloading Followed by Reloading, and Functional Overloading in Mice. *PLoS ONE* 8: e81929, 2013. doi: 10.1371/journal.pone.0081929.

190. **Ciciliot S**, **Rossi AC**, **Dyar KA**, **Blaauw B**, **Schiaffino S**. Muscle type and fiber type specificity in muscle wasting. *The International Journal of Biochemistry & Cell Biology* 45: 2191–2199, 2013. doi: 10.1016/j.biocel.2013.05.016.

191. **Nakamura K**, **Ohsawa I**, **Masuzawa R**, **Konno R**, **Watanabe A**, **Kawano F**. Running training experience attenuates disuse atrophy in fast-twitch skeletal muscles of rats. *Journal of Applied Physiology* 123: 902–913, 2017. doi: 10.1152/japplphysiol.00289.2017.

192. **Inoue A**, **Cheng XW**, **Huang Z**, **Hu L**, **Kikuchi R**, **Jiang H**, **Piao L**, **Sasaki T**, **Itakura K**, **Wu H**, **Zhao G**, **Lei Y**, **Yang G**, **Zhu E**, **Li X**, **Sato K**, **Koike T**, **Kuzuya M**. Exercise restores muscle stem cell mobilization, regenerative capacity and muscle metabolic alterations via adiponectin/AdipoR1 activation in SAMP10 mice: Exercise ameliorate muscle regeneration. *Journal of Cachexia, Sarcopenia and Muscle* 8: 370–385, 2017. doi: 10.1002/jcsm.12166.

193. **O'Leary VB**, **Jorett AE**, **Marchetti CM**, **Gonzalez F**, **Phillips SA**, **Ciaraldi TP**, **Kirwan JP**. Enhanced adiponectin multimer ratio and skeletal muscle adiponectin receptor expression following exercise training and diet in older insulin-resistant adults. *Am J Physiol Endocrinol Metab* 293: E421-427, 2007. doi: 10.1152/ajpendo.00123.2007.

194. **Zeng Q**, **Isobe K**, **Fu L**, **Ohkoshi N**, **Ohmori H**, **Takekoshi K**, **Kawakami Y**. Effects of exercise on adiponectin and adiponectin receptor levels in rats. *Life Sci* 80: 454–459, 2007. doi: 10.1016/j.lfs.2006.09.031.

195. **Chang S-P**, **Chen Y-H**, **Chang W-C**, **Liu I-M**, **Cheng J-T**. Increase of adiponectin receptor gene expression by physical exercise in soleus muscle of obese Zucker rats. *Eur J Appl Physiol* 97: 189–195, 2006. doi: 10.1007/s00421-006-0163-3.

196. **Pierard M**, **Conotte S**, **Tassin A**, **Boutry S**, **Uzureau P**, **Boudjeltia KZ**, **Legrand A**. Interactions of exercise training and high-fat diet on adiponectin forms and muscle receptors in mice. *Nutrition & Metabolism* 13, 2016. doi: 10.1186/s12986-016-0138-2.

197. **Ma K**, **Cabrero A**, **Saha PK**, **Kojima H**, **Li L**, **Chang BH-J**, **Paul A**, **Chan L**. Increased beta -oxidation but no insulin resistance or glucose intolerance in mice lacking adiponectin. *J Biol Chem* 277: 34658–34661, 2002. doi: 10.1074/jbc.C200362200.

198. **Ouedraogo R**, **Gong Y**, **Berzins B**, **Wu X**, **Mahadev K**, **Hough K**, **Chan L**, **Goldstein BJ**, **Scalia R**. Adiponectin deficiency increases leukocyte-endothelium interactions via upregulation of endothelial cell adhesion molecules in vivo. *J Clin Invest* 117: 1718–1726, 2007. doi: 10.1172/JCI29623.

199. **Russell WMS**, **Burch RL**. *The principles of humane experimental technique*. Special ed., [Nachdr. der Ausg.] London 1959. Potters Bar, Herts: Universities Federation for Animal Welfare, 1992.

200. **Wosczyna MN**, **Konishi CT**, **Perez Carbajal EE**, **Wang TT**, **Walsh RA**, **Gan Q**, **Wagner MW**, **Rando TA**. Mesenchymal Stromal Cells Are Required for Regeneration and Homeostatic Maintenance of Skeletal Muscle. *Cell Reports* 27: 2029-2035.e5, 2019. doi: 10.1016/j.celrep.2019.04.074.

201. **Bettadapur A**, **Suh GC**, **Geisse NA**, **Wang ER**, **Hua C**, **Huber HA**, **Viscio AA**, **Kim JY**, **Strickland JB**, **McCain ML**. Prolonged Culture of Aligned Skeletal Myotubes on Micromolded Gelatin Hydrogels. *Sci Rep* 6: 28855, 2016. doi: 10.1038/srep28855.

Additional publications

- Szczepanski, S., M., Bloemmart, V., Jenart, V., Decleves, A.-E., Legrand, A., & Tassin, A. “Effect of Adiponectin knockout in a context of skeletal muscle deconditioning and reconditioning in mice.
- ”. (Currently in preparation. Submission expected in 2025).
- Szczepanski, S., Limpens, M., V., Jenart, V., Decleves, A.-E., Legrand, A., Tassin, A., " Muscle-type specific alterations and Adiponectin pathway characterization in a murine model of muscle disuse ". (Accepted by co-authors. Submitted in January 2025 in Physiological Reports).
- Szczepanski, S., Limpens, M., Bloemmart, V., Jenart, V., Decleves, A.-E., Legrand, A., & Tassin, A. « Adiponectin pathway in murine models of skeletal muscle deconditioning and reconditioning”. PhysPhar Automn Meeting (2024), Bruxelles, Belgium. Oral communication.
- Szczepanski, S., Limpens, M., Bloemmart, V., Jenart, V., Decleves, A.-E., Legrand, A., & Tassin, A. « Adiponectin pathway in murine models of skeletal muscle deconditioning and reconditioning”. 8th International Myology Congress (2024), Paris, France. Poster presentation.
- Szczepanski, S., Limpens, M., Decleves, A.-E., Legrand, A., & Tassin, A. Adiponectin pathway in a murine model of disuse muscle atrophy: an in vivo study. 7th International Myology Congress (2022), Nice, France. Poster presentation.
- Szczepanski, S., Limpens, M., Decleves, A.-E., Legrand, A., & Tassin, A. Adiponectin pathway in a murine model of disuse muscle atrophy: an in vivo study. Physphar Spring Meeting (2022). Poster presentation.

Annexes

ANNEXE 1. Supplementary data.

A.1.1. Background & Aims

Exercise training (ET) is the only effective strategy to counteract DMA. Among processes involved in ET benefits, ET-induced myokines, named **exerkines** (e.g. Irisin, IL6, …) have been highlighted. Here, we conduct a pilot study to implement and optimize a reductionist ET-like model *in vitro*, allowing investigations of molecular mechanisms underlying the effect of muscle cell contraction. The model of Electrical-Pulse Stimulation (EPS) on myotubes (**Figure A1**) was previously shown to recapitulate key properties of skeletal muscle contraction *in vivo* (201). In prospect of my thesis, and by using this model, we want to determine the specific effects of muscle contraction on ApN pathway as well as the respective pro-myogenic effects of ApN and exerkines by using ApN gain and loss-of-function experiments.

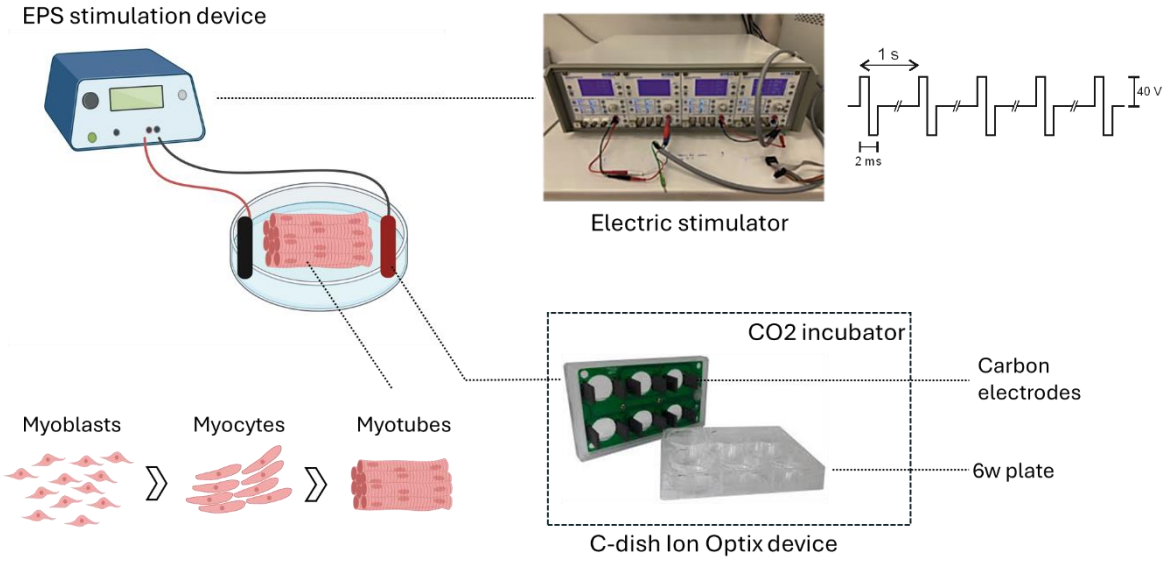

Figure A1. Device implemented for Electrical-Pulse-Stimulation (EPS) on myotubes. Myotubes at 6 days of differentiation were stimulated at low frequency (Square Biphasic Pulses; 1Hz;40V/60mm; 2ms) thanks to the device "C-dish Ion Optix" (USA) linked to an electric stimulator (EMKA Technologies, STM-B01). Original illustrations.

A.1.2. Material and methods

Cell culture

Immortalized murine myoblasts (C2C12, ATCC CRL-1772) were cultured in a proliferation medium composed of DMEM high glucose supplemented with 10% FBS (VWR, S181B 500) and 1% Penicillin/Streptomycin (P/S, Thermofisher) at 37°C with 5% CO_2 and 21% O_2. Specifically for subsequent EPS stimulation, myoblasts were seeded on 6 well plates self-coated with Collagen I (Collagen R, 0.2%, Labconsult, SERV.4725402) until 100% confluence in the proliferation medium. Cells were then washed with PBS and differentiated for 7 days (D7) in DMEM High Glucose supplemented with human insulin 10µg/ml (Sigma), bovine apo-transferrin 100µg/ml (Sigma) and 1% P/S.

Electrical-Pulse stimulation (EPS)

After optimal differentiation (D7), medium was refreshed, and EPS was applied on myotubes (Square biphasic pulse; 1Hz; 40V/60mm; 2ms) to initiate contraction while unstimulated myotubes were kept with electrodes without stimulation as control. This was performed for 6 hours by using the C-Dish device (IonOptix) linked to an electric stimulator (EMKA Technologies, STM-B01). Myotubes were then either directly collected (EPS 6h) or left on the plate for a 4h resting period (EPS 6h +4h). In the latter case, the medium was replaced between the EPS protocol and the 4h resting period. The effects of EPS-mediated myotube contraction on ApNn pathway were then evaluated through the investigation of AdipoR1 and AdipoR2 expression at the mRNA (RTqPCR) and protein levels (Western blot). AMPK activity was interrogated by western blot as an indicator of myotube contraction.

EPS-conditioned culture medium collection and transfer

To allow EPS-conditioned medium transfer experiments, the medium was collected either directly after EPS stimulation (EPS 6h medium) or after 4h of resting period (EPS 6h + 4h medium). Medium from unstimulated myotubes was also collected (Unstimulated medium). EPS-conditioned media were then transferred either (i) on C2C12 myoblasts for 24h or (ii) on C2C12 myotubes at day 2 of differentiation. In (i) myoblast proliferation was assessed by using an EdU staining. In (ii) *Myog* mRNA level was measured as an marker of early differentiation.

A.1.3. Preliminary data

According to our pilot study, the adhesion of myotubes to the support was found to be a limiting step during EPS. Collagen coating helps to delay myotubes detachment for up to 6 hours (**Figure A2**). At this stage, as well as 4h after EPS, ApN pathway components are not significantly modified as compared to unstimulated myotubes (**Figure A3)**.

We then performed preliminary experiments on the EPS-conditioned medium (**Figure A4)**. Our first data showed that ApN concentration in the culture medium is likely at the limit of ELISA Kit sensitivity, both in EPS-stimulated and unstimulated myotubes. Interestingly, Irisin

concentration tends to be higher in the EPS-conditioned medium than in the control, 4h after EPS.

The EPS-conditioned culture medium was then transferred to myoblast cultures. We observed that the culture medium harvested immediately after the 6h of EPS induced myoblast mortality (data not shown). One hypothesis to explain this effect is the release of toxic molecules by electrodes. Lactate release by myotubes during their contraction is also to consider. However, the culture medium harvested 4h after EPS does not induce mortality. This medium does not appear to impact myoblast proliferation or early differentiation (**Figure A4)**. Further investigations are now needed to optimize the model and particularly, to increase exerkine concentration in the EPS-conditioned medium. To this aim, additional stimulation/resting kinetics will be envisaged. Moreover, we initiated the development of gelatin hydrogels with "micropatterns" to promote the maturation and alignment of myotubes during EPS protocols (**Figure A5**).

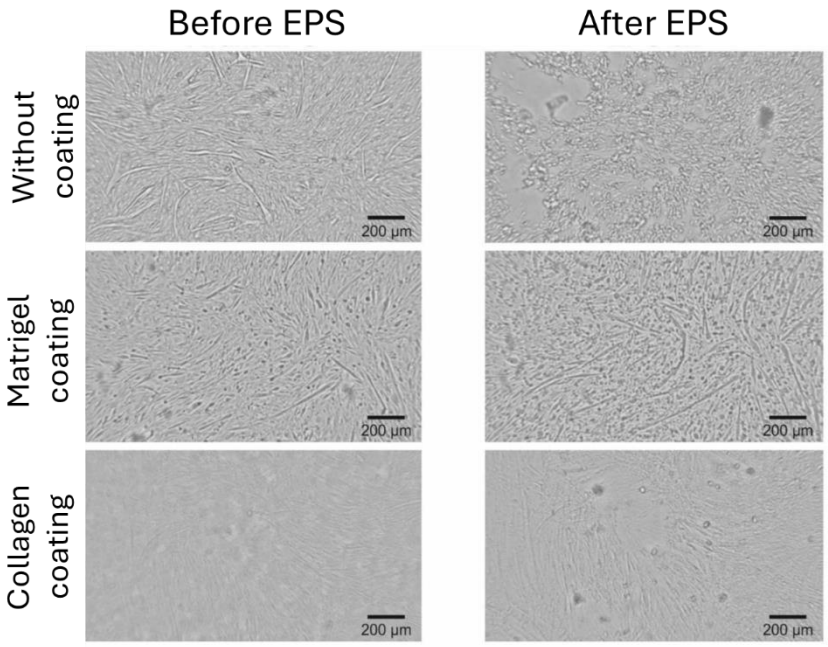

Figure A2. Effect of Electrical-Pulse-Stimulation (EPS) on cell adherence according to different plate coating. C2C12 myoblasts were differentiated during 7 days. Cells adherence was monitored thanks to a Cytosmart microscope.

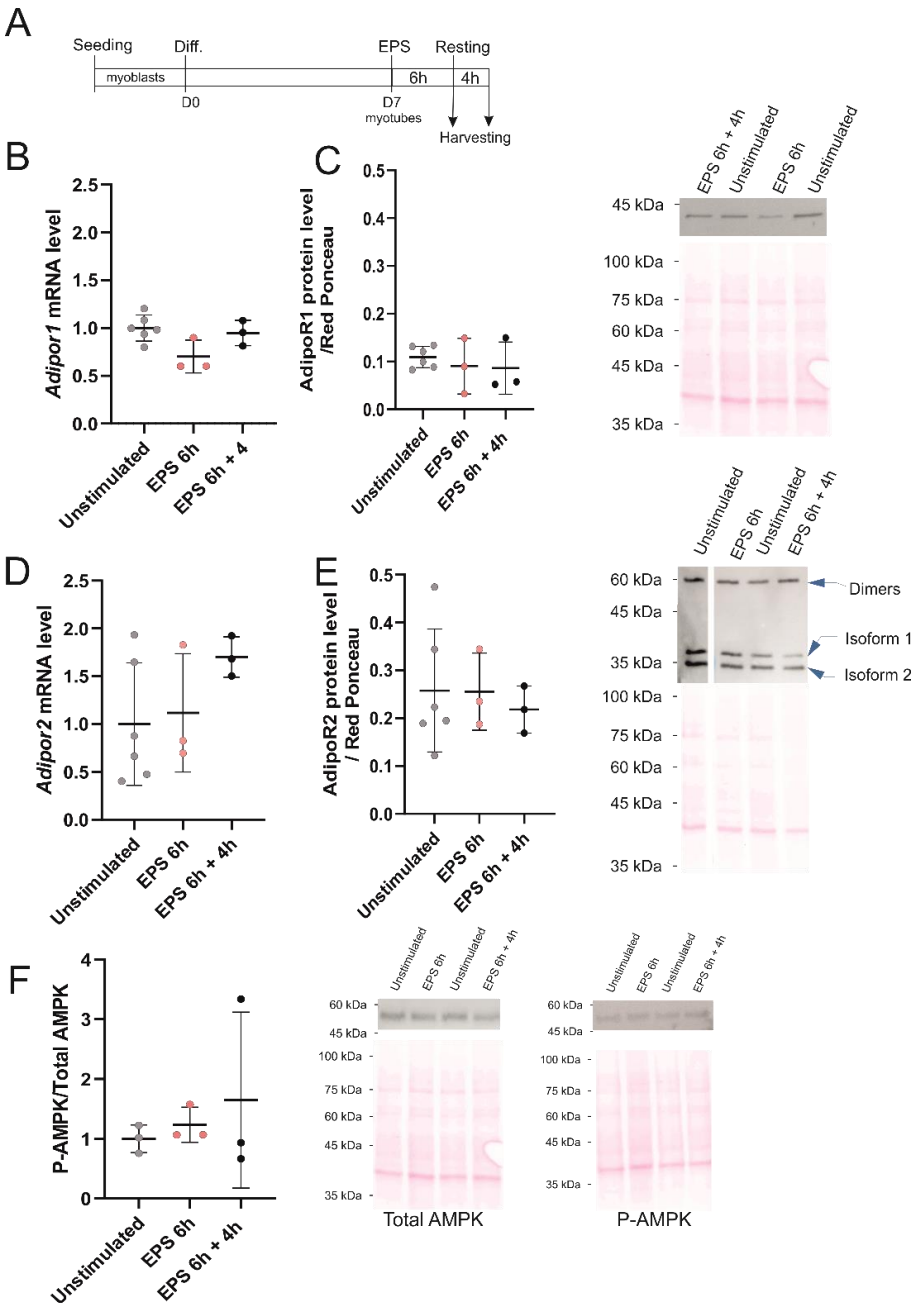

Figure A3. Effect of Electrical-Pulse-Stimulation (EPS) on Adiponectin pathway components in myotubes: preliminary results (A) Timeline. Murine C2C12 myoblasts were seeded in a 6-well plate and differentiated for 7 days (D7). EPS was then applied on myotubes for 6h. The medium was first harvested at this time point (6h). After medium renewal, cells were maintained in a resting state for 4h and the medium was harvested at this time point (6h+4h). **(B-D) Relative *Adipor1* and *Adipor2* expressions** determined by RTqPCR (SYBR Green) and normalized to *Rplp0* (ΔΔCt method). **(C-E) AdipoR1 and AdipoR2 protein levels** determined by a SDS-PAGE followed by Western Blot. Red Ponceau was used as a loading control. **(F) AMPK activity** was evaluated through the phosphorylated AMPK(P-AMK) to total AMPK ratio (SDS-PAGE followed by a Western Blot)**.** ANOVA One Way: NS. Data presented as Mean ± SD. The experiment was realized in technical triplicates and on 3 independent cultures. Collaboration with. L. Paprzycki, Master student, PhRR.

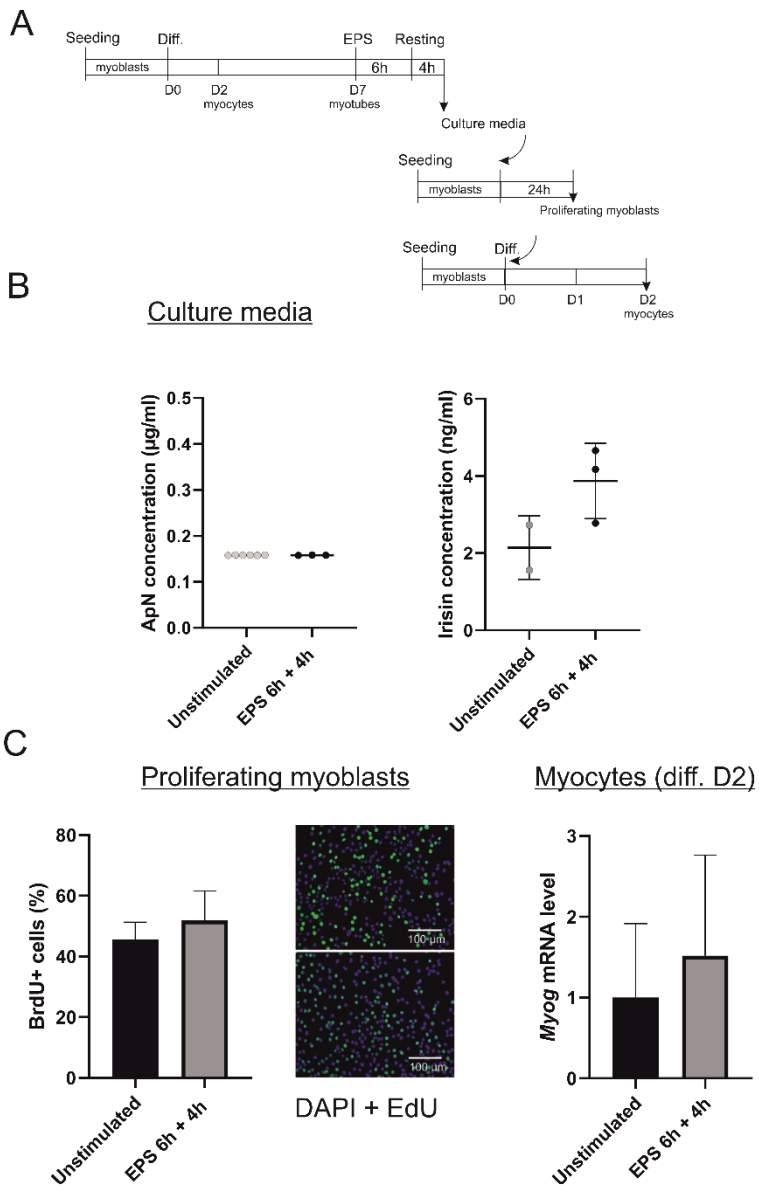

Figure A4. Effect of Electrical-Pulse-Stimulation (EPS) on myotube culture medium. (A) Experimental design. (B) Adiponectin (ApN) and Irisin concentrations were determined by ELISA (Adiponectin/Acrp Quantikine ELISA kit, R&D ; Irisin: EK-067-29, Phoenix Pharmaceuticals, inc.). Data presented as Mean ± SD. ApN: T-test: NS, n=3 independent culture; irisin: Mann Whitney: NS, n=3 technical triplicate. **(C) Effect of the medium conditioned by EPS-myotubes on myoblast proliferation**, determined through fluorescence staining and counting of EdU cells (*Image J software*) **(D) Effect of the medium conditioned by EPS-myotubes on early differentiation** evaluated through the expression of the gene encoding Myogenin (*MyoG*) by RTqPCR (SYBR Green) and normalized to *Rplp0* (ΔΔCt method) **(C-D)** Data presented as Mean ± SD. N=3 independent cultures. T-test: NS. Collaboration with. L. Paprzycki, Master student, and A. Delpierre, PhD student, PhRR, UMONS.

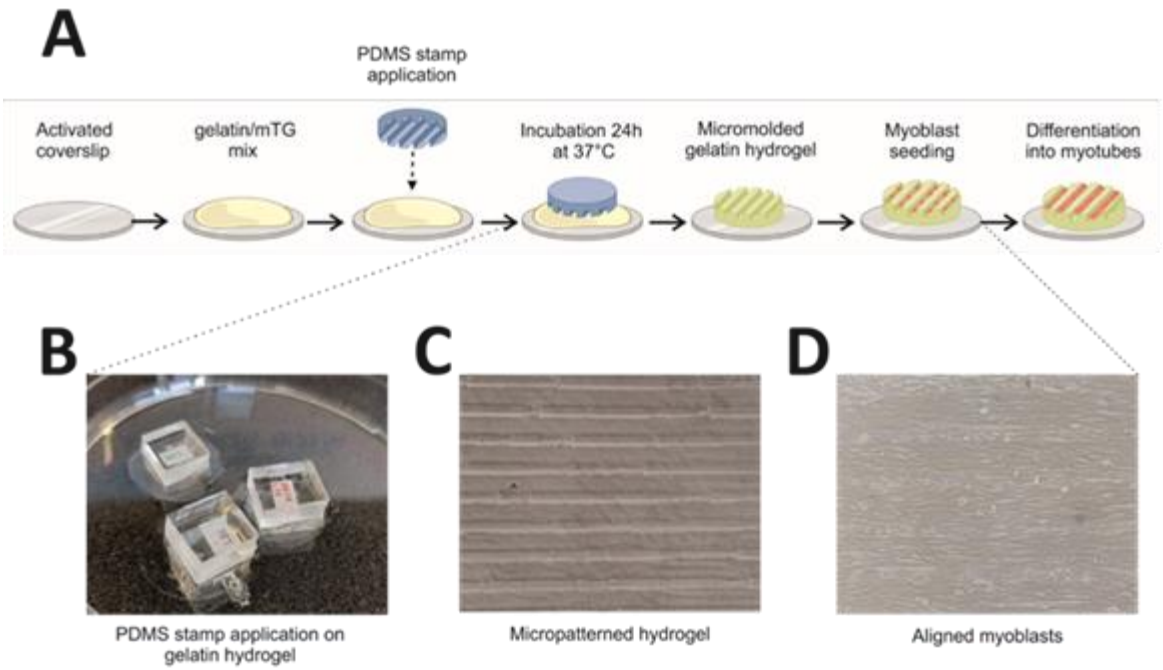

Figure A5. Electrical-Pulse-Stimulation (EPS) on myotubes growth on Micromolded Gelatin Hydrogel. (A) Protocol of micromolded gelatin hydrogels manufacturing, adapted from (201). Briefly, one drop of gelatin (10%w/v)/ microbian transglutaminase (mTG, 8%w/v) was placed on an activated coverslip. A PDMS stamp produced by lithography (coll. Pr. S. Gabriele) was then applied on the hydrogel drop and incubated 24h to allow micropattern printing (parallel lines of 10µm depth and length). After stamp removal, the hydrogel is sterilized by UV exposure and myoblasts were then seeded. **(B)** PDMS stamp application on the gelatin hydrogel: photography. **(C)** Microscopic picture of micropatterned hydrogel. **(D**) Microscopic picture of C2C12 murine myoblasts aligned on the micropatterned hydrogel.